Control of Rotor Vibrations Using Hybrid Squeeze Film Dampers

PRINCIPAL INVESTIGATOR

A. El-Shafei

Faculty of Engineering
Cairo University
Giza, Egypt

Grant No. F49620-92-J-0512

30 September 1992 - 29 March 1997

REPORT DOCUMENTATION PAGE

Form Approved
OMB No. 0704-0188

1. AGENCY USE ONLY (Leave blank)	2. REPORT DATE	3. REPORT TYPE AND DATES COVERED
	November, 1997	Final Technical 30 Sep.92-29 Mar.97

4. TITLE AND SUBTITLE

Control of Rotor Vibrations Using Hybrid Squeeze Film Dampers

5. FUNDING NUMBERS

G

F49620-92-J-0512

6. AUTHOR(S)

A. El-Shafei, A.T. Massoud, M. El-Hakim, J.P. Hathout, R. Youssef

7. PERFORMING ORGANIZATION NAME(S) AND ADDRESS(ES)

Faculty of Engineering
Cairo University
Giza, Egypt

8. PERFORMING ORGANIZATION REPORT NUMBER

MDP-EOARD-1/97

9. SPONSORING/MONITORING AGENCY NAME(S) AND ADDRESS(ES)

EOARD
PSC 802 Box 14
EPO AE 09499-0200

10. SPONSORING/MONITORING AGENCY REPORT NUMBER

11. SUPPLEMENTARY NOTES

12a. DISTRIBUTION/AVAILABILITY STATEMENT

Approved for Public Release; Distribution Unlimited

12b. DISTRIBUTION CODE

13. ABSTRACT (Maximum 200 words)

This report covers the development of the Hybrid Squeeze Film Damper (HSFD) for use as an active control device for controlling rotor vibrations. In particular, the work done included the automation and design of the HSFD, the elaborate modeling of the HSFD, the development of the control algorithms, and finally the experimental verification of the performance and control of the HSFD.

This extensive research project confirmed the capabilities of the HSFD as an efficient and powerful controlling element for high speed rotors, particularly of aircraft engines and rocket turbopumps. Specifically, the results of this research project establish that the HSFD:

1) improves the vibration isolation capability of the rotor support,
2) reduces the amplitude of vibration of the rotor at all speeds, and
3) results in a rotating machine that is capable of operating under varying and adverse conditions.

It is the opinion of the research team that the HSFD is now ready for engine testing. The device is reliable, the control algorithms are sufficiently developed, the laboratory experimentation and verification were extensive and illustrate the strengths and adaptability of HSFDs. It is thus appropriate to expect that this work should lead to full-scale engine testing of the active control of rotor vibrations using HSFDs.

14. SUBJECT TERMS

Rotordynamics-Control of Rotor Vibrations-Squeeze Film Dampers
Active Control - Aircraft Engine Vibrations

15. NUMBER OF PAGES

264

16. PRICE CODE

17. SECURITY CLASSIFICATION OF REPORT	18. SECURITY CLASSIFICATION OF THIS PAGE	19. SECURITY CLASSIFICATION OF ABSTRACT	20. LIMITATION OF ABSTRACT
Unclassified	Unclassified	Unlimited	

CONTENTS

PART I

SUMMARY AND PREVIOUS WORK

CONTENTS

EXECUTIVE SUMMARY

This report summarizes the effort expended and the results achieved from the project "Control of Rotor Vibrations Using Hybrid Squeeze Film Dampers", grant no. F49620-92-J-0512. The objective of the work done was to investigate the active control of rotating machinery vibration using the newly developed hybrid squeeze film dampers (HSFDs). In particular, the work done included the automation of the hybrid damper, the development of the design of the hybrid damper, the elaborate modeling of the hybrid damper, the development of the control algorithms for the hybrid damper, and finally the experimental verification of the performance and control of the HSFD.

The work in this project was successful in attaining all of these objectives. The hybrid damper control circuit was automated by an electronically controlled proportional pressure control valve with the associated hydraulic circuit. Computer control of the HSFD was achieved. The hybrid damper was completely redesigned to allow for its automation, including instrumenting the damper, adding retainer springs, adding feedback springs and redesigning for compactness. A complete mathematical model was developed for the damper and its control elements. The λ-model was used for finite damper modeling. Simulation of the behavior of the open-loop control system was performed.

A complete test rig was designed with multi-modes. The test rig was well-instrumented and computer-controlled. The test rig consisted of the rotor supported by two HSFDs and driven by a variable speed electric motor.

Simulation of the behavior of the open-loop and closed-loop control system of the test rig was performed for the multi-mode rotor. Several control algorithms were developed and applied to the rotor system. The on-off basic control algorithm with feedback on speed was developed to act as long damper at critical speeds and short damper away from critical speeds. It was shown that this control algorithm is quite effective but requires pre-knowledge of the behavior of the rotor system and is not able to accommodate variable operating conditions. A PI control algorithm was developed and also shown to be effective. The enhancement of the PI-controller by gain scheduling provides one of the best control alternatives, both in controlling resonant conditions and sudden unbalance. The LQR controller was not as effective as the PI-controller. The developed adaptive controller, with a unique nonlinear model, was also extremely effective both for controlling resonant conditions and sudden unbalance.

Experimentally, the on-off controller, the PI-controller (with and without gain scheduling), and the model reference adaptive controller were all applied. In addition a nonlinear-proportional controller was also developed and applied, and was shown to be the best overall controller of the HSFD. The experimental results, which involved elaborate set-up and verification and identification, confirmed the results of the theory and simulation and illustrated the power and utility of the developed algorithms, and of the HSFD itself as a robust controlling element of rotor vibrations.

It is the opinion of the research team that this extensive research project confirmed the capabilities of the Hybrid Squeeze Film Damper, as an efficient and powerful

controlling element for high speed rotors, particularly of aircraft engines and rocket turbopumps. Specifically the results of this research project establish that the HSFD:

1) improves the vibration isolation capability of the rotor support,
2) reduces the amplitude of vibration of the rotor at all speeds,
3) enhances the stability of the rotating machine,
4) allows the rotor and damper to operate at high loads, and
5) results in a rotating machine that is capable of operating under varying and adverse conditions.

It is also the opinion of the research team that the HSFD is now ready for engine testing. The control algorithms are sufficiently developed, the laboratory experimentation and verification were extensive and illustrate the strengths and adaptability of HSFDs. In addition, the concept of HSFDs relies on a reliable and robust device that has been used extensively in aircraft engines for over than thirty years as a passive vibration controller. It is thus the belief of the research team that the results of this work should lead to full-scale engine testing for the active control of rotor vibrations using HSFDs.

The research team consisted of several people who were involved in the work reported in this report. They include:

Aly El-Shafei	Associate Professor and Principal Investigator
Atef T. Massoud	Assistant Professor
Medhat M. El-Hakim	Doctoral Candidate
Jean-Pierre Hathout	Graduate Student
Refaat Youssef	Graduate Student
Ramadan M. Aly	Lab Technician

Also several papers were written and published from the work performed in this project. These papers are:

1 - El-Shafei, A. and Hathout, J.P., "Modeling and Control of HSFDs for Active Control of Rotor-Bearing Systems", ASME Journal of Engineering for Gas Turbine and Power, Vol.117, No.4, October 1995, pp. 757-766.

2 - El-Shafei, A. and El-Hakim, M., "Development of a Test Rig and Experimental Verification of the Performance of HSFDs for Active Control of Rotors", Presented at the International Gas Turbine Congress and Exposition, Houston, TX, June 1995, ASME paper 95-GT-256.

3 - Hathout, J.P. and El-Shafei, A., "Adaptive Control of Rotor-Bearing Systems Using Hybrid Squeeze Film Dampers", Proceedings of Sixth International Conference on Vibration in Rotating Machinery, Oxford England, September 1996, pp. 671-690.

4 - Hathout, J.P., El-Shafei, A. and Youssef, R., "Active Control of Multi-Mode Rotor-Bearing Systems Using HSFDs", ASME Journal of Tribology, Vol. 119, No. 1, January 1997, pp. 49-56.

5 - Hathout, J.P. and El-Shafei, A., "PI Control of HSFDs for Active Control of Rotor-Bearing Systems", ASME Journal of Engineering for Gas Turbine and Power, Vol. 119, No. 3, July 1997, pp. 658-667.

Additional papers are planned particularly on the recent experimental results, including:

6 - "On-Off Control of HSFDs".

7 - "Experimental Control of HSFD Using PID Controllers".

8 - "Application of Adaptive Controller to HSFD".

9 - "Comparison of Control Algorithms for Active Control of HSFDs".

CHAPTER 1
INTRODUCTION

In the quest for improved performance of rotating machinery, particularly aircraft engines and rocket turbopumps, it is desirable to increase the rotor speed beyond several criticals, and yet minimize the rotor vibration and ensure the engine's proper operation in adverse conditions. It is thus desirable to actively control the vibration of rotating machinery because of its effectiveness in wide speed ranges and its adaptability to changing operating conditions.

Active vibration control of rotors of aircraft jet engines, rocket turbopumps and high speed compressors has been investigated in the past. Passive vibration control has been used for over thirty years, namely using squeeze film dampers. However, active vibration control is sought because of its effectiveness in wide speed ranges and its adaptability to changing operating conditions. Three active vibration control devices have been suggested: (1) Magnetic Bearings, (2) Lateral Force Actuators, and (3) Active Squeeze Film Dampers.

Magnetic Bearings have been investigated for actively controlling the vibration of rotating machinery (Schweitzer and Ulbrich, 1980, and Bradfield et al., 1989). Yet, as far as aircraft engines are concerned, magnetic bearings are still at a developmental stage and have not been used in aircraft engines for several reasons, including : (1) the inability of magnetic bearings to withstand high temperatures, (2) the control algorithms for magnetic bearings are still under development, and most importantly (3) magnetic bearings have still to prove their reliability. In fact the recent work on catcher bearings (Swanson et al., 1996) illustrates the reliability issues with magnetic bearings. Lateral force actuators have also been suggested as active vibration controllers (Palazzolo et al., 1989, and Nonami et al., 1989) and also are still at a developmental stage (Tang et al., 1994). Their shortcomings include: (1) possible coupling of motion in orthogonal directions, (2) they require large size actuators, and (3) they also have still to prove their reliability.

Squeeze film dampers (SFDs), on the other hand, have a proven track record. They have been used successfully for the last twenty years to passively damp rotating machinery, in particular aircraft engines (White, 1972, Gunter et al., 1977, and Holmes and Dogan, 1985). They provide the primary source of damping in aircraft engines since the rolling element bearings on which these engines are mounted provide very little damping. Thus, because of their reliability, it seems natural to develop SFDs to actively control rotor vibrations. Burrows et al., (1983) investigated the possibility of controlling rotating machinery vibration by controlling the pressure in a SFD, and they point out that control of rotors using active SFDs is much cheaper than using magnetic bearings, and is more simple and reliable. Adams and Zahloul (1987) studied the control of rotors by controlling the pressure in hydrostatic SFDs. Mu et al. (1991) and Bonneau and Frene (1994) proposed a movable conical SFD. El-Shafei (1991b) proposed using Hybrid Squeeze Film Dampers (HSFDs) for active vibration control of rotors (El-Shafei, 1993). The performance of HSFDs was verified experimentally, and it was shown that HSFDs are effective in controlling the amplitude of rotor vibrations and in reducing the force transmitted to the support. Also it was shown that the hybrid damper is much more effective in controlling rotor vibrations than the previous strategies of controlling the pressure in a conventional squeeze film damper.

Because of its demonstrated capability and excellent performance in controlling rotor vibrations and because of the reliability of SFDs it was decided to develop the Hybrid Squeeze Film Damper. This work is concerned with the development of the HSFD for actively controlling rotating machinery vibration. Before starting this project the development of the HSFD (El-Shafei, 1993) was that it has been used in the laboratory in a manually controlled configuration as an on-off controller. However, the controller was to be automated, and different control strategies to be developed for optimum system performance. This, in fact, is the crucial phase in the development of the HSFD (Akin, 1990). Thus the work in this project was designed to automate the HSFD, develop control strategies for the HSFD-rotor system and demonstrate the results experimentally.

1.1.1 BASIC THEORY OF HSFD

Most of the analyses of SFDs consider the short bearing approximation to Reynolds equation, which is justified if the damper is short in the axial direction such that the flow in the damper is axial rather than circumferential. On the other hand, the long bearing approximation to Reynolds equation, which is justified if the damper is long in the axial direction such that the flow in the damper is circumferential, has attracted comparatively verly little attention (e.g. Feder et al., 1978; Holmes and Dogan, 1985; El-Shafei, 1991a). Usually open-ended dampers are considered short dampers and tightly sealed dampers are considered long dampers regardless of the actual physical length of the damper (which is usually short with respect to the diameter of the damper).

Short dampers and long dampers have very different characteristics (El-Shafei, 1989). In general, long dampers are better at attenuating the amplitude response of the rotor, while short dampers are better at reducing the force transmitted to the support. Recently a hybrid damper that can act as a long damper or as a short damper based on the instructions of a controller was developed (El-Shafei, 1991b and 1993). Its performance was experimentally verified, and it was shown that in the long damper mode the HSFD is effective in controlling the amplitude of rotor vibrations and in the short damper mode the HSFD is effective in reducing the force transmitted to the support.

Also it was shown that the long damper provides more damping than a short damper. Thus if it is required to stabilize a rotor, then the long damper will remove more energy than the short damper. Also, because of the larger forces that are transmitted through a long damper, the long damper can be considered as a high load damper, i.e., it will be able to sustain high loads without executing large orbits (El-Shafei, 1991a), and thus the possibility of jump resonance is reduced.

From previous analyses, it can be shown that the short damper is better at decreasing the force transmitted to the engine frame above the critical speed, while the long damper is better at attenuating the amplitude of the whirl at the critical speed. Also the

long damper rarely exhibits the jump resonance phenomenon while the short damper rarely exhibits the additional critical speeds due to fluid inertia. Thus, if a squeeze film damper is designed to operate as a short damper when a small force transmitted to the support is desired, and to operate as a long damper when a small amplitude of vibration is desired; this would lead to a more effective squeeze film damper, and would allow rotors to operate safely at higher speeds. This can be accomplished by actively controlling the squeeze film damper to change its characteristics to either the long damper or the short damper. This implies that the control algorithm for such a hybrid damper would be as simple as just switching from long to short dampers and vice versa.

This suggested that it is possible to develop an actively controlled hybrid squeeze film damper which can operate as a long damper near critical speeds, such that it effectively attenuates the amplitude response of the engine and avoids the possibility of a jump resonance, and it also can operate as a short damper at the operating speed region, such that it effectively reduces the force transmitted to the engine frame. This is possible by designing the sealing on the damper, such that the damper becomes tightly sealed (i.e., long damper) or open-ended (i.e., short damper) according to the instructions of the controller.

1.1.2 DESIGN OF THE HYBRID DAMPER

Tecza et al., (1983) examined two dampers, and the results of their experiments showed that the so-called globally sealed damper simulated a short damper and the locally sealed damper simulated a long damper. In the globally sealed damper they had two grooves: a feed groove and a drain groove at each end of the damper with no end seals. The only sealing was by quad rings on the journal face to prevent oil leakage. The locally sealed damper had two end holes: a feed hole and a drain hole. Piston rings were used to seal the ends of the damper. Thus, both the oil feed and drain and the sealing method affect the performance of the damper.

In the design of the hybrid damper, it was decided on feeding the oil by three feed holes distributed circumferentially at the center of the damper. The three holes would

ensure continuous oil feed to the damper and would have minimum effect on the flow pattern in the damper. The feed holes were provided with check valves to prevent back flow through the feed holes (El-Shafei, 1993).

Several sealing methods were investigated for the hybrid damper. The sealing had to be both controllable and effective, i.e., it had to be an effective seal for the long damper mode, and it had to be controllable in order to have no end seal in the short damper mode. It was decided to use two movable sealing rings with sliding fit both to the end caps and to the housing, one on each end of the damper as shown in Figure 1 (El-Shafei, 1993). The principle of the seals' operation is simple. The damper oil film and the hydraulically actuated seals are supplied from independently variable sources. In order for the damper to operate as a long damper, the pressure to the seal chambers is elevated above the internal pressure of the damper. The seal rings will move in axially and seal the oil film inside the damper clearance. In order to return to the short damper configuration, the seal pressure is lowered until it is less than the internal pressure of the damper. This causes the seal rings to return to their original positions.

This was the basic concept of the HSFD at the onset of the work reported herein. The HSFD was further developed as shown in the work performed during the project.

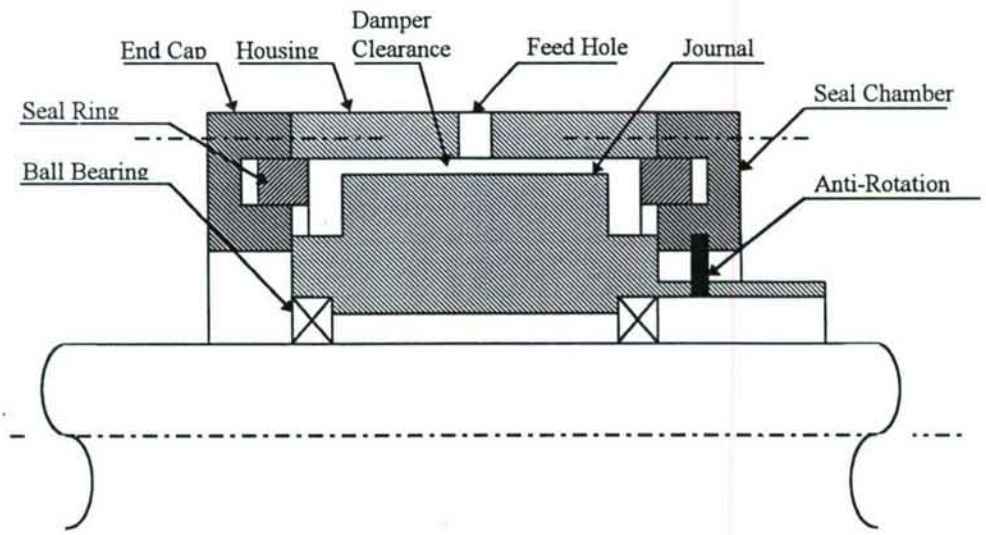

Figure 1 Schematic of HSFD

1.1.3 SUMMARY

It was shown that the long and short dampers have very different characteristics. The long damper: (1) is better at attenuating the amplitude response at the critical speed; (2) is less susceptible to the jump resonance phenomenon; (3) removes more energy to stabilize a rotor; and (4) can be considered as a high load damper. However, the long damper is susceptible to the effects of fluid inertia and transmits a large force to the support. On the other hand, the short damper transmits a small force to the support and has negligible fluid inertia effect, but is susceptible to the jump resonance phenomenon. Table 1 summarizes the differences between short and long dampers.

Table 1. Short Versus Long Dampers

	Short Dampers	**Long Dampers**
Flow	Axial	Circumferential
Damping	Low	High
Amplitude Response	Higher	Low at Critical Speed
Transmissibility	Low at Running Speed	Higher
Fluid Inertia	Minimal	Considerable
Load	Low	High
Stability	Fair	Better
Jump Resonance	Possible	Less Probable

The differences between the short and long dampers were exploited in developing a hybrid damper that can act as a short damper or as a long damper based on the instructions of a controller. Experimentally, the hybrid damper was manually controlled, and it was demonstrated that in the long damper mode the hybrid damper was extremely efficient at reducing the orbit size, and in the short damper mode the hybrid damper was efficient at reducing the force transmitted to the support. Thus both the experimental and theoretical findings, illustrate that the hybrid damper can be used effectively to control rotating machinery vibrations.

The hybrid damper's characteristics were demonstrated as an on-off controller, i.e. it operates in either the long damper mode or the short damper mode, which may be sufficient. However, there are an infinite number of configurations of finite dampers that can be obtained by placing the sealing rings in intermediate positions. Thus, an

adaptive controller needs to be developed to exploit these possibilities and continuously adapt the hybrid damper to the continuously varying operating conditions.

The objectives of this work were to improve the performance of rotating machinery, particularly aircraft engines and rocket turbopumps, by minimizing the rotor vibration at all speeds, and ensuring the engine's proper operation in adverse conditions. This was achieved by actively controlling the rotor vibration, and in particular by using the newly developed hybrid squeeze film damper as a controller, which was demonstrated to be an extremely effective device in controlling rotor vibration.

To achieve the objectives of this research work, there was a need to develop the control algorithm for the hybrid damper, and to verify the control scheme experimentally. In order to do so, the design of the hybrid damper and the associated fluid control circuit were both automated and perfected. Developing the control algorithm is the crucial step in the development of the hybrid damper. In fact, Akin (1990) specifically stated that: "the reliability of the control system will probably govern the applicability of the concept". He also added that the hybrid damper "certainly has potential for certain designs" of aircraft engines and rocket turbopumps.

In the work done reported herein, it is shown that, the development of the control algorithm for the hybrid squeeze film damper resulted in an efficient control system for the vibration of rotating machinery. In particular, it is shown that the actively controlled hybrid squeeze film damper :

(1) improves the vibration isolation capability of the support,
(2) reduces the amplitude of vibration of the rotor,
(3) enhances the stability of the rotating machine,
(4) allows the rotor and damper to operate at high loads, and
(5) results in a rotating machine that is capable of operating under varying and adverse conditions.

which should lead to overall improved performance and safety of rotating machinery.

CHAPTER 2
SUMMARY OF PREVIOUS REPORTS

This chapter summarizes the work reported in previous reports under this project. The objective is to provide a complete development of the HSFD in this final report, and to provide a comprehensive picture of the HSFD, and of the development effort that resulted in its current state.

The previous reports presented the two-track work progress in the project. One track was the theoretical model, and the other track was the experimental work. A good part of the theoretical development was included in the Master's thesis of Jean-Pierre Hathout, who worked on the development of the control algorithms. Hathout's thesis is included in this final report in its entirety because of its completeness and because it represents a significant portion of the work done in this project. It is thus not necessary to include in this chapter the theoretical development presented by previous reports, since it is included in Hathout's thesis. The only exception to this is the modal analysis of multi-mode rotors with HSFDs, which is included at the end of this chapter.

1.2.1 THEORETICAL DEVELOPMENT

The theoretical development, presented in Hathout's thesis, included development of a model for the modified hybrid squeeze film damper, including the modeling of the long and short damper modes by the λ-model, modeling the sealing ring dynamics, modeling of the automated hydraulic circuit, modeling of the proportional control valve, and modeling of the rotor dynamics. This model was presented in previous reports on the work done in this project.

This developed model constituted a set of nonlinear differential equations, that were put in non-dimensional form, and thus represented a complete dynamical model of the open-loop system. This open-loop system was simulated using MATLAB and SIMNON software packages, as well as in-house software, and the results of the simulation were reported previously. Details of the mathematical model and of the

nonlinear simulations are included in Hathout's thesis, Part II of this report. These simulations illustrated the behavior of the open-loop system, as well as the HSFD, under transient conditions, and emphasized the utility of the HSFD as an efficient control device that is able to adapt effectively to various controlling signals.

The other point in Hathout's thesis that was reported previously is the development of the on-off controller. The basic idea is to exploit the differences between long and short dampers to provide a controller that forces the HSFD to be a long damper at critical speeds and a short damper away from critical speeds. This controller was developed based on the feedback of speed and required the preknowledge of the critical speeds. This was not considered a drawback in the design of the on-off controller since a critical speed analysis is always performed during the design of high speed rotating machinery. However, this controller cannot adapt to varying operating conditions. The summary of the work for the on-off controller is presented in Hathout's thesis, and illustrates the effective control of the critical speeds and of the forces transmitted to the support during run-up/run-down conditions and during operation.

The other work in Hathout's thesis concentrated on the control systems development, and was not included in previous reports. Thus, it is deemed necessary as new contributions to this project's work.

1.2.2 DEVELOPMENT OF TEST RIG AND EXPERIMENTATION WITH HSFDs

In this section, the development of a test rig for the experimental investigation of the HSFD-rotor system is presented. The design of the test rig, the HSFD and the rotor system are discussed. The experimental set-up consisted of the rotor-HSFD system controlled through a pressure control servovalve for controlling the pressure in the sealing chambers. The hydraulic circuit was controlled through a digital computer with a data acquisition and control system. The on-off control strategy with feedback on speed was implemented on the computer control system and is shown to be quite effective in controlling the first mode of vibration of the rotor system. Most of the

work discussed here was presented in previous reports except for the on-off control. However, it was decided to be included in this section because a complete redesign of the test rig was necessary and is reported in Part III.

1.2.2.1 Design of the Hybrid Squeeze Film Damper

The original design of the HSFD (El-Shafei, 1993) used two movable sealing rings with sliding fit both to the end caps and to the housing, one on each end of the damper as shown in Figure 1. The principle of the seals' operation is simple. The damper oil film and the hydraulically actuated seals are supplied from independently variable sources. In order for the damper to operate as a long damper, the pressure to the seal chambers is elevated above the internal pressure of the damper. The seal rings will move in axially and seal the oil film inside the damper clearance. In order to return to the short damper configuration, the seal pressure is lowered until it is less than the internal pressure of the damper. This causes the seal rings to return to their original positions.

For the automated HSFD, it may be required to locate the sealing rings in intermediate positions, other than those for the short or long dampers, to provide for the required rotor control. Thus controlling the pressure is not enough to accurately control the position of the sealing rings. It was decided that the sealing rings should be connected to springs that would act to restrain their motion versus the applied pressure in the sealing chambers. As later illustrated by the computer simulations of the system (El-Shafei et al., 1993), this turned out to be an effective method of controlling the position of the sealing rings.

To physically incorporate the springs in the design of the HSFD, 3 measuring rods were connected to each sealing ring, and would protrude through the sealing chambers and the end caps, as shown in Figure 2. Springs, resting on the surfaces of the end caps, can be connected to the measuring rods to provide spring action restraining the motion of the sealing rings versus the applied pressure in the sealing chamber. The measuring rods have an additional benefit, they could be directly connected to a position transducer (e.g. an LVDT) to accurately measure the position of the sealing

rings. In order to accommodate the measuring rods into the HSFD design several changes needed to be made, including increasing the width of the seal rings to allow for the connection with the measuring rods, providing outlet ports for the measuring rods in the end caps, and sealing these outlet ports against oil leakage.

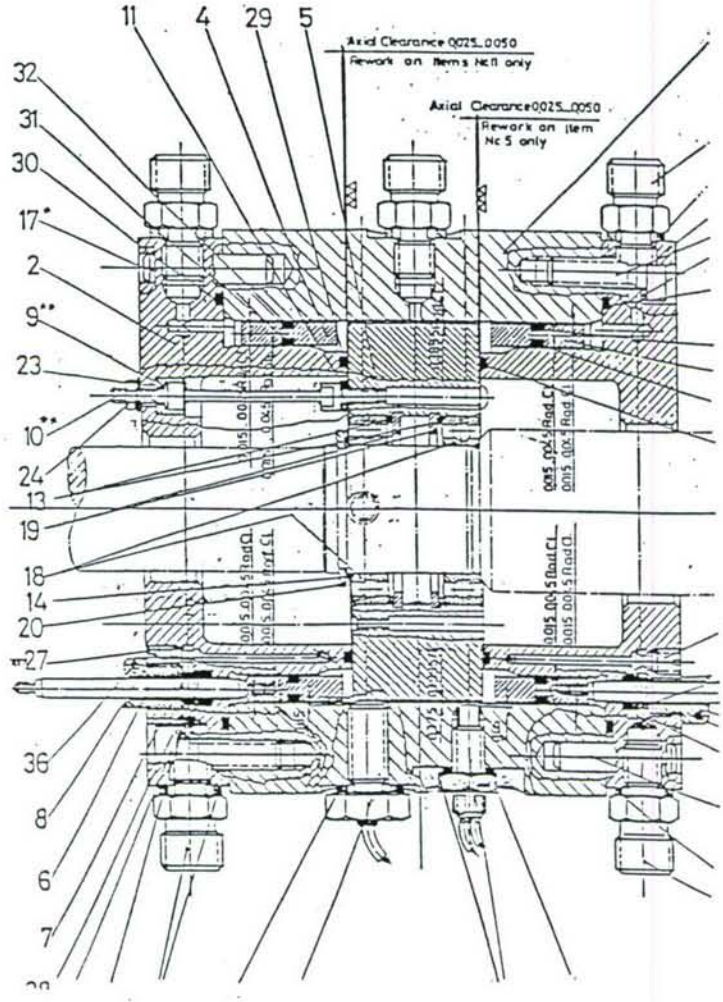

Figure 2 Cut-Out In The Manufactured HSFD

The original design of the HSFD prevented the rotation of the journal using an anti-rotation pin (Figure 1). However, in order to center the journal in the damper, a centering spring is usually used, which also prevents the journal from rotation while allowing it to precess. The spring rods shown in Figure 2 allow for centering the journal in the damper, in addition to preventing the damper from rotation. The centering spring action provided by the spring rods can be an important factor in the dynamics of the rotor bearing system (El-Shafei, 1990) and will be investigated carefully later on. To accommodate the spring rods, the journal diameter was increased.

An additional problem that existed with the original design of the HSFD is that the outer surface of the sealing ring had to slide with very close tolerances on two surfaces: the damper housing and the end cap. This was a burden on the machining process since the same tolerances had to be maintained between the sealing ring and the housing and between the sealing ring and the end cap. In order to eliminate this machining problem, the housing was extended to cover all of the sealing chamber, and the end cap now covers the ends of the sealing chambers only (Figure 2). Nevertheless, the end cap needs to be in contact with the journal (as shown in Figure 2) to prevent oil leakage onto the shaft in the short damper mode.

As in the previous design, the oil feed to the damper is provided by three feed holes distributed circumferentially at the center of the damper. The damper oil drain in the short damper mode is through the end caps. No damper drain is required in the long damper mode. The oil port for the seal chambers is located now on the extended housing. This is the port connecting the seal chambers with the pressure control electrohydraulic servovalve. This port provides for both the feed and drain to the seal chamber and is the only port required.

It should be pointed out that only two supply ports will be used as supply ports to the damper, while the third port can be used either as a supply to or a drain from the damper. This is useful in the long damper configuration, since in the long damper mode the fluid is trapped in the damper, and the heat generated will cause an increase in the fluid temperature thus decreasing the viscosity of the fluid. This is highly undesirable, and the fluid drained from the center of the damper through a small feed hole will aid in cooling the fluid. However, this may not be sufficient, and in the complete computer controlled test rig we have made arrangements (through temperature feedback) to momentarily change to the short damper mode, thus flooding the damper and cooling it, if needed.

1.2.2.2 Design of a Rotor Test Rig

It is required to test the HSFD concept on a rotor test rig in order to evaluate the performance of the HSFD and to investigate the interaction of the control system with

the HSFD-rotor-bearing system. The rotor test rig should be able to pass several critical speeds, to investigate the capability of the damper of controlling more than one mode, and the damper should be able to control these critical speeds and their associated modes.

The design objectives of the rotor were set for the rotor to cross two or more critical speeds in a speed range about 12.000 rpm, which is a speed deemed possible to attain with a speed-controlled DC motor. Moreover, the location of the hybrid damper on the rotor had to be such that the damper can control the associated modes, i.e. for the critical speeds traversed by the rotor, the damper has to be located at a point on the rotor which exhibits high modal activity for all modes traversed. The ideal situation would be to have large amplitudes for each of the modes at the bearing locations. This is advantageous since the dampers are normally located at the bearings, and thus it will not be necessary to add a new location on the rotor for the damper implementation.

Thus the objectives of the design of the rotor test rig can be summarized in traversing two or more critical speeds and the associated modes should exhibit large amplitude at the bearing locations. A critical speed analysis was initiated using the available program CRITSPD developed by RODYN, Inc. The program provides the undamped critical speeds and the associated mode shapes, given the rotor dimensions, the disk and bearing locations, and the bearing and support stiffnesses.

Since two or more critical speeds were required, a three mass rotor was initially investigated as a possible rotor for the test rig. However, we faced a problem of having small modal activity at the bearing location for some of the modes. This meant that the damper had to work even harder to control this mode. Alternatively, the modal activity at the bearing location would be very sensitive to the value of the bearing stiffness and the support stiffness used. These two parameters (the bearing stiffness and the support stiffness) are the two most uncertain parameters in the design of the rotor test rig, since they depend heavily on the manufacturing and assembly of the test rig. Thus because of this uncertainty and the possibility of not controlling the modes by the HSFD, the three mass rotor was disregarded.

Further investigations and trials led to the consideration of the one mass rotor of Figure 3. This rotor exhibited three critical speeds in the speed range under consideration and appreciable modal activity at the bearing locations, thus satisfying the design requirements. In addition, further investigations revealed that the modal shapes are not sensitive to small changes in the bearing or support stiffness, only the critical speeds change, thus ensuring high modal activity for the three modes at the bearing locations irrespective of the actual stiffness of the bearing or the support.

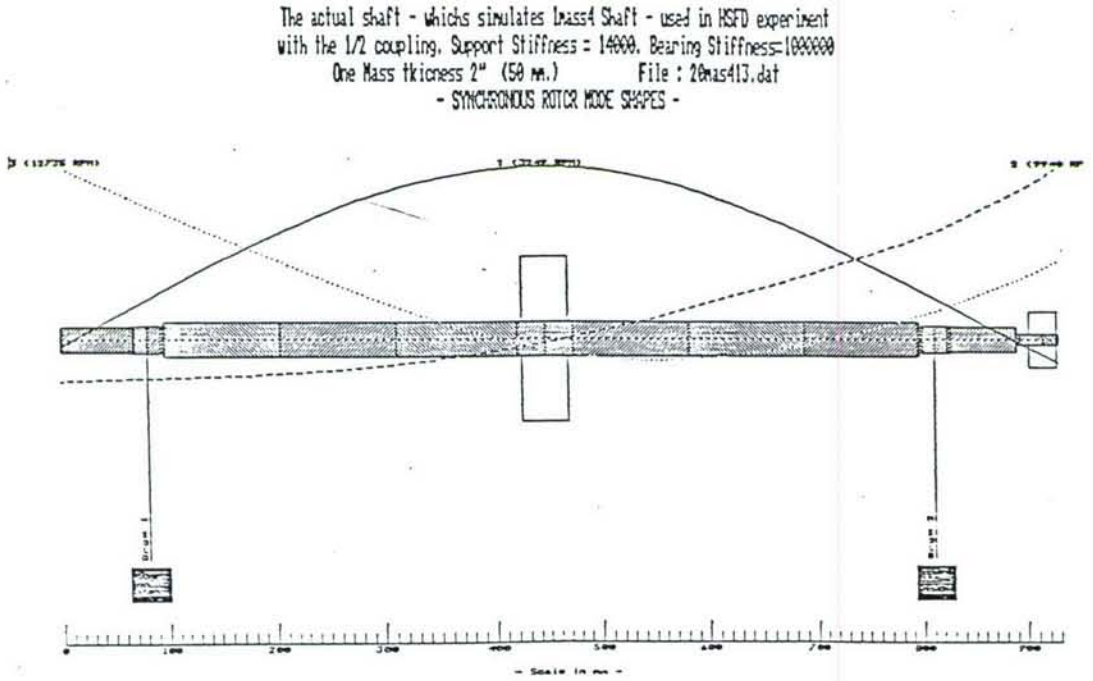

Figure 3 The Rotor-Bearing System And Its Modes

The one mass rotor of Figure 3 was chosen as the rotor for the HSFD test rig since it satisfies the design requirements of the rotor test rig. Moreover, it is relatively insensitive to the uncertainties in the support and bearing stiffness. In addition, the one mass rotor of Figure 3 resembles the Jeffcott rotor, so often studied, in fact the theory of the HSFD was first investigated on a Jeffcott rotor (El-Shafei, 1993). This makes the one mass rotor simpler to model particularly because of its symmetrical characteristics (El-Shafei and Hathout, 1995).

The one mass rotor of Figure 3 exhibits three flexible modes. The first mode at 3249 rpm is a bending mode. The second mode at 9940 rpm is nearly a conical mode with much activity due to the weight of the coupling. This mode would be hard to excite by

an unbalance at the disk location. The third mode is a second bending critical and is at 12735 rpm. The total rotor weight is 11.57 Kg and the disk weight is 6.12 Kg. In this analysis the bearings are assumed to be rigid and the support stiffness at each bearing was assumed to be 2452 N/mm. This would ensure that to carry the rotor weight, the support deflection (of the spring rods of Figure 2) would be about 0.023 mm.

The damper for the test rig had to be designed to accommodate the design of the rotor. Since the theory of the HSFD was based on a one mode rotor, it was decided to design the HSFD for the first mode of the rotor of Figure 3. In addition, in order to manifest the differences between long and short dampers, and to stress the versatility of the HSFD, it was decided that the bearing parameter B, and the inertia parameter M, would be chosen such that there would be a major difference in the behavior of the damper in each mode of operation. Studying the work of El-Shafei (1990) and (1991a) where a parametric study of the behavior of SFD supported rotors was conducted, and using these parametric studies as a guidance in choosing the values of B and M, it was decided to choose a value of B equal to about 0.01, and the value of M about 0.2. Furthermore, in order for the open-ended configuration of the HSFD to operate as a short damper the L/D ratio should be less than 0.4. These criteria were chosen as the design criteria for the HSFD. In essence, the approach taken here was to design the HSFD as an effective long damper to attenuate the amplitude of vibration at the first mode of the rotor of Figure 3, and to observe the resulting short damper characteristics. This design strategy was confirmed by El-Shafei et al. (1994), where different design approaches were investigated, and the simulation results indicated the superiority of the approach described above.

The journal of the HSFD of Figure 2, has a radius R=37.5mm to accommodate the rotor of Figure 3, the bearings and the centering springs. Thus the radius of the damper is dictated by the design configuration. However, the length L and radial clearance c of the HSFD have to be designed according to the above criteria. For the first rotor mode the natural frequency = 3249 rpm, and the modal mass 2m = 8.7 Kg (from the results of CRITSPD). Thus ω_n = 340 rad/s, and m = 4.35 Kg. In addition choosing L/D = 1/3, thus L = 25 mm. The oil chosen for our test rig is Shell Tellus 46

with viscosity μ = 0.014 Ns/m^2 at 70°C, the oil density ρ = 917 Kg/m^3, then choosing c= 750 μm, the bearing parameter for the short damper becomes B_s = 0.013, and the inertia parameter for the short damper becomes M_s = 0.165, while with this damper design the bearing parameter for the long damper becomes B_l = 0.029, and the inertia parameter for the long damper becomes M_l = 0.37. These data for the inertia and bearing parameters satisfy the design requirements.

1.2.2.3 Automation of the HSFD Control Circuit

In the previous testing of the HSFD, the objective of controlling the pressure in the sealing chambers was achieved through manually controlling the flow in the hydraulic circuit through needle valves (El-Shafei, 1993). Redundancy was an objective in the design of this circuit.

In order to achieve the objectives of active control of rotor vibration, the hydraulic circuit needed to be automated, in the sense that electrically controlled valves are required for the circuit control. Moreover, at this stage of development of the HSFD, redundancy in the hydraulic circuit was not required and needed to be eliminated. The automated hydraulic control circuit of Figure 4 fulfilled these objectives. An electrohydraulic pressure control valve 2 was used to control the pressure in the sealing chambers. The servovalve was normally closed, however when it received a current signal, it connected the supply line, through an orifice, to the sealing chamber, thus increasing the pressure in the sealing chamber. If, on the other hand, a reduction in pressure was required, the servovalve connected the drain, also through an orifice, to the sealing chamber, thus reducing the pressure in the sealing chamber. When the required pressure was achieved the valve was closed.

The pressure control servovalve was chosen over the more common flow control servovalve, since the associated hydraulic circuit is simpler in this particular application, and in addition continuous flow would be required to maintain a constant pressure with the flow control servovalve which is an unnecessary energy loss.

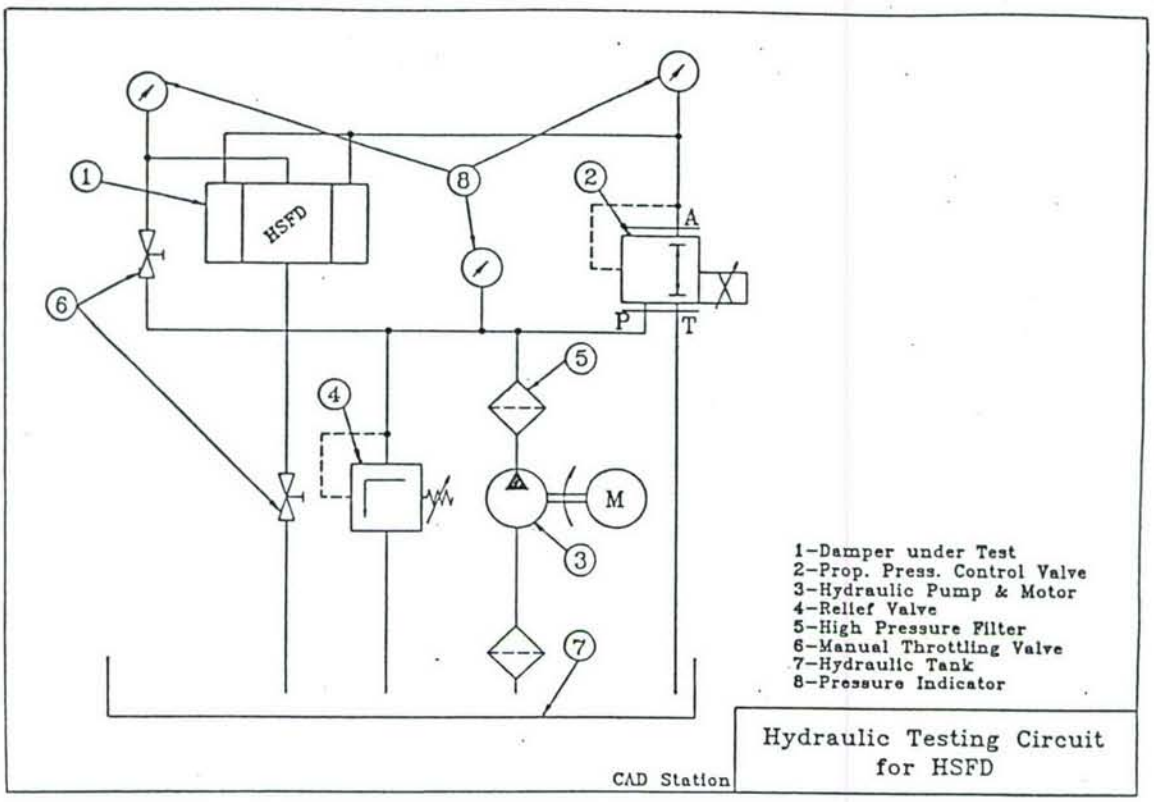

Figure 4 Automated Hydraulic Circuit

Several important features of the automated hydraulic circuit of Figure 4 need to be discussed. Firstly, the supply to the damper is still the same, only a manual throttling valve was added to the circuit to reduce the supply pressure to that required by the damper. The damper drain is also through a needle valve as before. Secondly, the sealing chamber, in this design, has only one port. This port is used to both supply and drain the sealing chamber. Thirdly, the pressure control servovalve is the only component required to control the pressure in the sealing chambers. The feed and drain of the seal chamber is provided through the pressure control servovalve. This simple design of the automated pressure control circuit provides for an efficient control loop. Moreover, because of the current control of the servovalve, it can be easily interfaced to a computer to provide computer control.

1.2.2.4 Complete Computer-Controlled Test Rig

Figure 5 shows the complete computer controlled test rig. The test rig consisted of the rotor of Figure 3 supported on two HSFDs as shown in Figure 2 driven by a high speed DC motor through a flexible coupling. The oil feed and drain into and out of the

dampers were controlled by the hydraulic circuit of Figure 4. The hydraulic circuit was controlled by the pressure control valve signal which is generated from the computer.

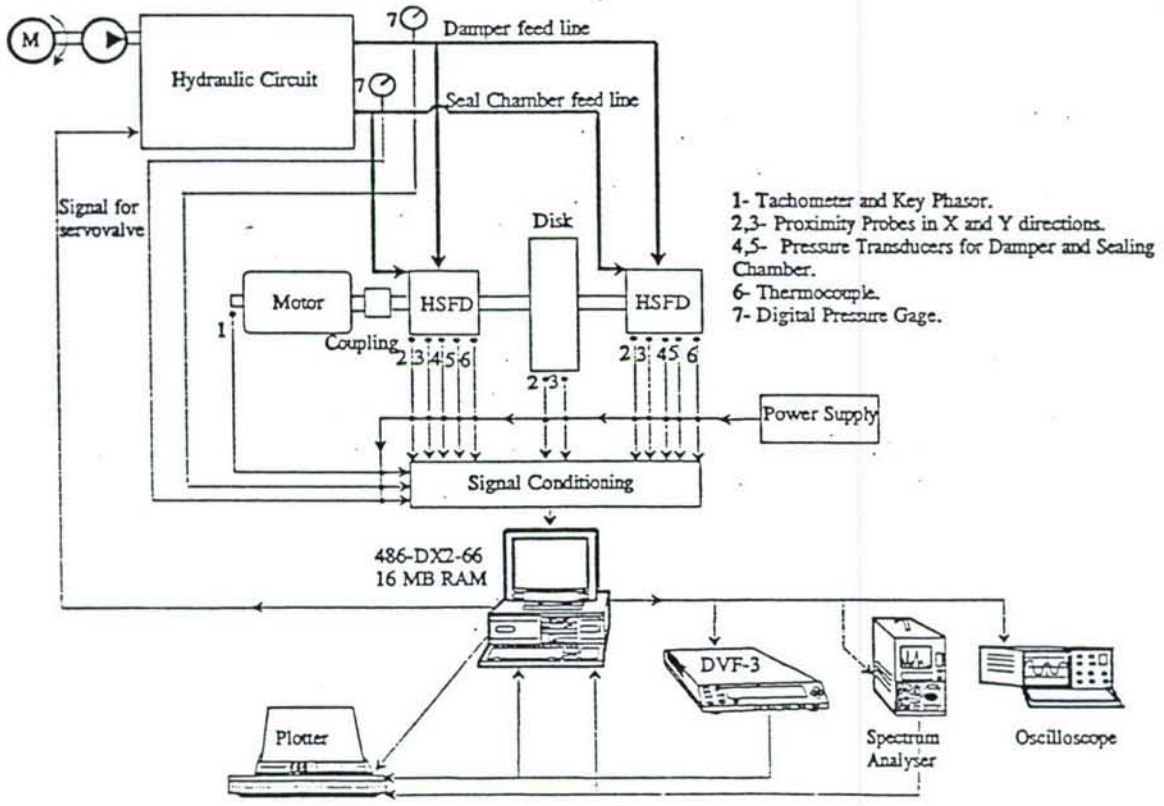

Figure 5 Complete Computer-Controlled Test Rig

The computer was a 486 DX2-66 PC compatible with 16 MB and 660 MB hard disk. Two cards are installed into the computer. A GPIB card based on the IEEE 488.2 standard is used to control the instruments in the test rig. The other card is a 16 channel 12-bit data acquisition card with two channel control. Both cards are from National Instruments.

The GPIB card is a National Instruments PC II/IIA, and was used to control and acquire data from the Bently Nevada DVF-3 tracking filter and the Brüel & Kjær 2033 single channel spectrum analyzer. The DVF-3 is a two channel tracking filter to which the signal from two of the proximity probes are routed and filtered according to the speed of the shaft, which was also fed into the DVF-3 by another proximity probe monitoring a key-way. The spectrum analyzer was used to view both the time and

frequency domain signals from the pressure transducers, or the acceleration signal measured on the damper housing. Both the DVF-3 and the B&K 2033 could either download the data into the computer or directly onto a plotter. Two plotters were available: a Tektronix HC-100 and a Brüel & Kjær 2308.

The data acquisition card is a National Instruments AT-MIO-16F-5 card with 200 KHz sampling rate. The card is 16 channels Analog-to-Digital conversions for data acquisition and 2 channels Digital-to-Analog conversions for control. All channels are 12-bit. Both the GPIB and data acquisition and control cards were controlled by the National Instruments LabView software, which is a versatile and powerful software system that is capable of performing a wealth of functions including a variety of signal processing functions.

In addition to the proximity probe monitoring the key-way for speed information, each of the HSFDs and the central disk are monitored by two proximity probes each, 90° apart, for a total of seven eddy current proximity probes (Bently Nevada series 7200, 5 mm) monitoring the rotor. The proximity probes within the dampers were located in a very tight space. In order to avoid interference from adjacent material, and to reduce the possibility of disturbing the flow within the damper, a Teflon adapter was manufactured to isolate the probes and allowing them only to view the journal motion. Figure 6 shows two photographs of the test rig and the instrumentation used.

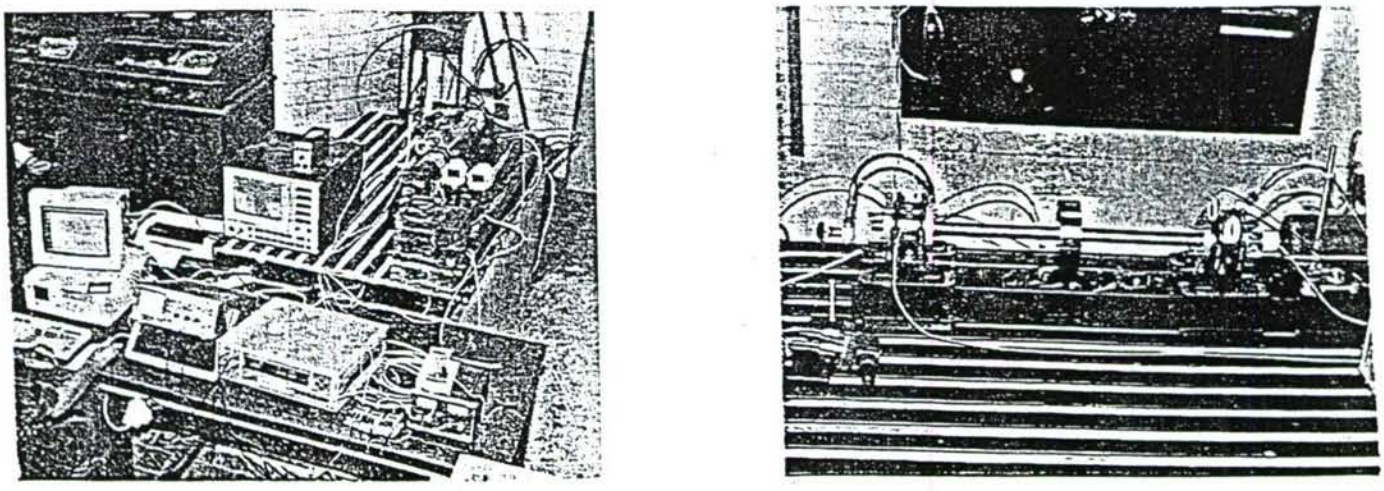

Figure 6 Test Rig And Instrumentation

Each of the dampers is monitored by two Kulite XT-190 pressure transducers for monitoring the dynamic pressure in the damper and the pressure in the sealing chambers. These signals were either fed to the spectrum analyzer or directly to the computer or both. The hydraulic circuit lines were also monitored by Digital Pressure Gages HBM Digibar type PE200/20 bar and are also fed into the computer. In addition, two thermocouples were inserted within the HSFD to monitor the temperature in the damper, both for viscosity determination and for possible use in feedback.

1.2.2.5 Static Testing of HSFD

The developed damper shown in Figure 2, though very simple in concept, yet there are various issues pertaining to its performance that needed to be addressed. First and foremost, the type of sealing that is used needed to be evaluated carefully for leakage, particularly that we have moving parts within the damper. Second, it was required to find the minimum pressure difference that would move the sealing ring. Finally, the spring stiffness required to position the sealing ring in intermediate positions and its characteristics needed to be evaluated. To address these issues for the damper with moving parts, a series of static testing was conducted.

For leakage, the damper and the sealing chamber were tested with relatively high supply pressures up to 20 bar (about 297 psi). This was done for each chamber independently and for the damper itself. The tests were successful and were repeated several times to verify the sealing even during the motion of the sealing ring. No leakage was detected.

Several tests were performed to find the minimum pressure difference that would move the sealing rings. This was done with no springs attached to the sealing rings. The results were consistent whether there was pressure in the damper or not. A pressure difference of 2 bar was sufficient to overcome stiction and change from short mode to long mode or vice-versa.

Finally, the last set of tests were performed to test the possibility of locating the sealing ring in intermediate positions between the short and long damper modes. This was

done with the aid of a set of 3 springs acting against the supply pressure to the sealing chamber, and were mounted in parallel on each side of the damper. These experiments of the finiteness of the damper were quite satisfactory and show the capability of this design of the HSFD to give any required position of the sealing ring, resulting in the appropriate damping needed to dampen the rotor vibration.

We chose to test with a random set of soft springs with stiffness of 4.406 N/mm per spring. The test procedure was as follows. The damper is set in the short damper mode (fully open) by supplying pressure into the damper at 3 bar, while connecting the sealing chamber to the drain. Then the pressure in the sealing chamber is gradually increased manually through a throttle valve, and the pressure is recorded, while the position of the sealing ring is recorded with the aid of a dial gage mounted on one of the measuring rods (see Figure 7). The test is carried out until the long damper position is attained (fully closed). The differential pressure is evaluated and is plotted against the sealing ring travel (see Figure 8). The test is repeated several times to check repeatability, and was also repeated for each side of the two dampers.

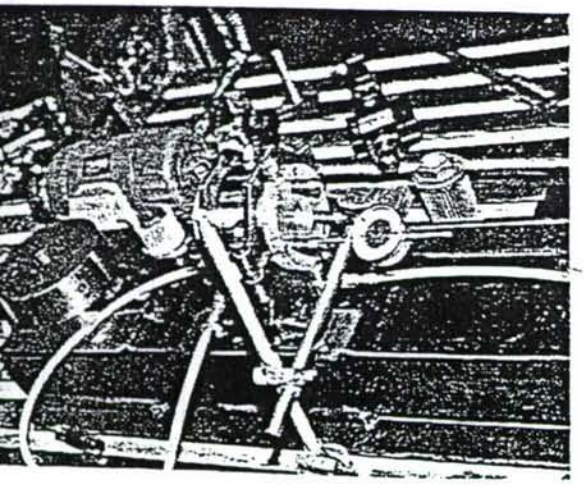

Figure 7 Static testing of the HSFD

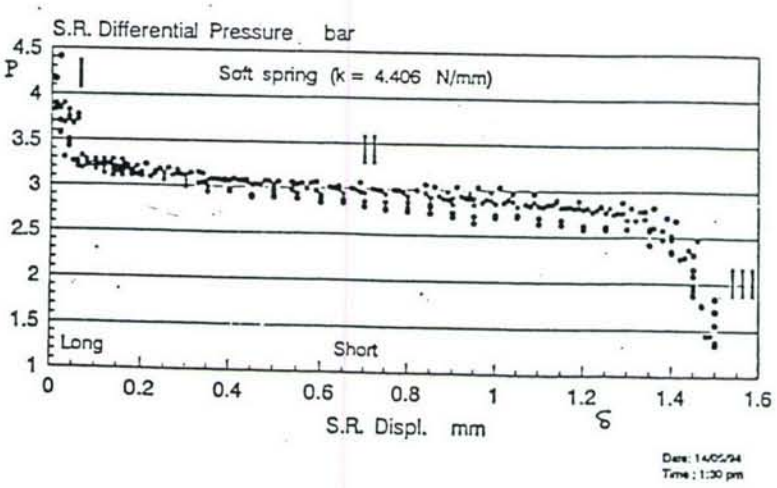

Figure 8 Test results for the static testing of HSFD

Figure 8 shows the experimentally measured relationship between the differential pressure and the sealing ring travel for a spring stiffness of 4.406 N/mm. The Figure shows three distinct regions. In each region we can represent the relationship between the differential pressure and the displacement by a linear relationship. Region I is for a spring totally compressed with contact between the coils. Region II is the region with

the widest displacement and would be the region of actual control of the sealing ring travel. Region III is the region of loss of control from the spring, and is probably due to the travel of the sealing ring resulting in the spring not being in compression. Actually Figure 8 represents the nonlinear spring stiffness of the sealing ring spring. We were planning another set of tests to determine the amount of damping provided by the friction acting on the sealing ring, if necessary. This could be performed by a sinusoidal test, where a shaker is used to move the sealing ring with variable frequencies, and obtain the stiffness and damping from the impedance characteristics.

We have tested the damper with different sets of springs and the effect of stiffer springs is to move the whole curve in Figure 8 upwards. This is not desirable since a larger supply pressure would be required to the sealing chamber in this case. In essence, the spring stiffness should be chosen to be the lowest stiffness that would control the position of the sealing ring.

The static testing showed the direct relationship between the differential pressure on the sealing ring and its position, thus allowing the accurate positioning of the sealing ring in any position between the short and long modes. Moreover, the results were repeatable and were essentially consistent between all four sides of the two dampers manufactured. The relationship thus obtained experimentally can be used directly in the implementation of the control algorithm for the finite damper.

1.2.2.6 Preliminary Dynamic Testing of HSFD

To investigate the on-off control algorithm based on speed feedback suggested by El-Shafei and Hathout (1995) as a means for active rotor vibration control using HSFDs, a series of dynamic tests were planned. These tests involved running the rotor to a high speed and then allowing it to shut-down freely, and observing the behavior of the HSFD as the rotor traverses through the critical speeds.

The on-off control algorithm based on speed feedback, calls for an accurate determination of the critical speeds, and programming the HSFD to operate in the long damper mode at the critical speed and in the short damper mode away from the critical speed. Our plan called for the control of the rotor of Figure 3, which has critical

speeds of 3249 rpm, 9940 rpm and 12735 rpm. However, by running a critical speed test we found that the test rig exhibited only one critical speed at about 3600 rpm. Going back to CRITSPD, we found that this could have happened because of a large change of support stiffness from 2452 N/mm (14000 lb/in) for the rotor of Figure 3, to 12259 N/mm (70000 lb/in) for the rotor of Figure 9, with critical speeds 3593 rpm, 19298 rpm and 24175 rpm. This explains why we only observed a single critical speed at 3600 rpm in our test rig. Our concern was that our design of the HSFD caused this additional stiffening of the support, so we repeated the tests without the HSFDs and only with the retainer springs. The same critical speed was attained, and we concluded that the analytical design of the retainer springs as if they were cantilevered supports was the reason for underestimating their stiffness by a factor of 5.

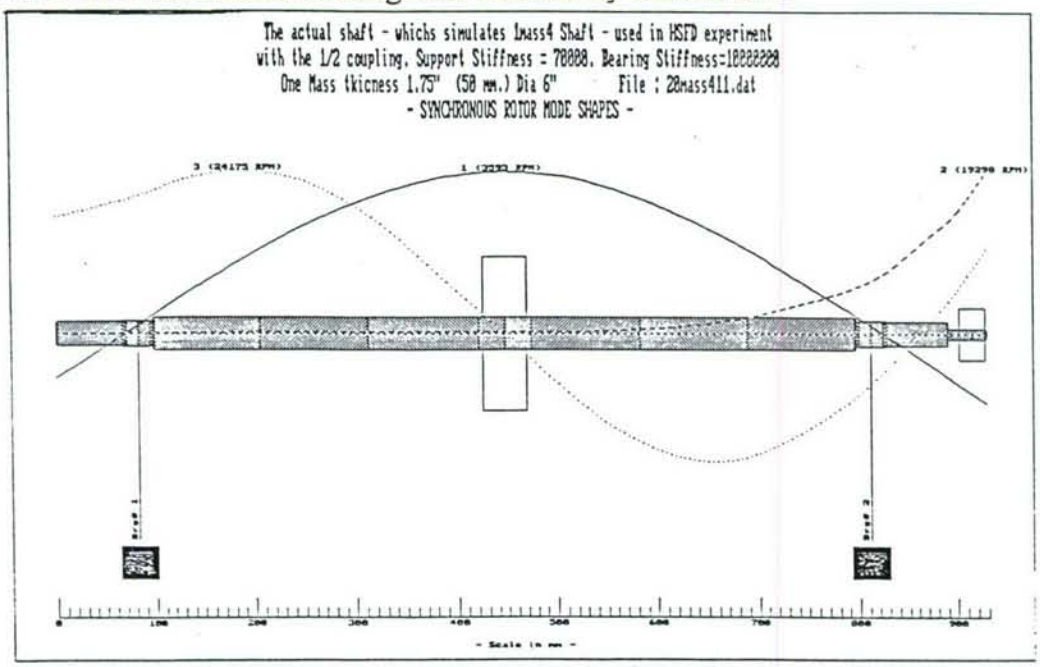

Figure 9 Actual Rotor-Bearing System Modes

Pending the change of the retainer springs, we decided to conduct the coast-down tests with the current rotor with retainer spring stiffness of 12259 N/mm (70000 lb/in) and critical speed of 3593 rpm. The difference of the spring stiffness is a rotor dynamics problem, and it does not affect the basic concept of the HSFD.

To plan the coast-down test, we decided to change between short and long damper modes for the speed feedback at 5500 rpm. The results for the shutdown test are shown in Figure 10 (a) for the short damper and the long damper modes, and it is clear the larger damping capacity obtained from the long damper mode at this critical

speed. Away from the critical speed, we did not measure the force transmitted to the support, however it can be shown that for an uncavitated damper with the amplitude response shown in Figure 10 (a) the short damper mode attenuates the force transmitted to the support by as much as 27 times the long damper transmitted forces. And this is for a case where the rotor of Figure 9 exhibits small modal activity and thus small amplitude response at the damper location.

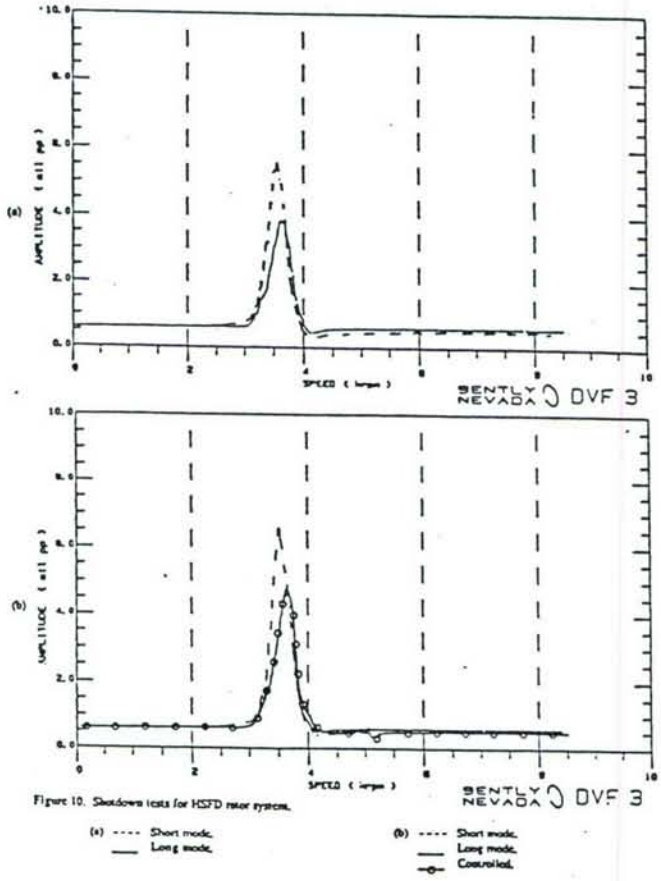

Figure 10 Shutdown Tests for HSFD-Rotor System

The control algorithm is implemented in the shut-down tests shown in Figure 10 (b). This test is superimposed on two shut-down tests one for a long damper mode, and the other is for short damper mode. It can be seen that the actively controlled rotor followed the short damper response from above 8000 rpm to about 5500 rpm. And then after a brief transient followed the long damper response very closely (thus achieving attenuation of the amplitude response). The results are impressive, particularly the fact that the results of the controlled rotor followed closely either the short or long damper response, which shows the repeatability of the results. In

addition, the small transient after application of the control action indicates the fast and stable action of the HSFD.

The results shown in Figure 10 were obtained directly from the DVF-3 and plotted on the Tektronix HC-100 plotter. These are the first published experimental results for the active control of HSFDs and demonstrate the effective application of the speed control feedback algorithm developed by El-Shafei and Hathout (1995).

1.2.3 MODAL ANALYSIS OF MULTI-MODE ROTORS USING HSFDS

In order to evaluate the performance of the HSFD and to investigate the interaction of the control system with the HSFD rotor system, it is required to test the HSFD and the proposed speed feedback algorithm in controlling multiple resonances. To achieve this, the rotor was remodeled to manifest multiple critical speeds and their associated modes. This section is concerned with the development of an entirely new model for the rotor based on the modal analysis technique. Previously, efforts have been done in the modal analysis of linear rotor models (Childs, 1974a and b, Gunter *et al.*, 1978). The analysis performed in this section is the use of modal analysis for a nonlinear rotor based on linear undamped critical speed analysis (Bonneau *et al.*, 1989). This is the basic approximation that proves to be quite useful for developing a control algorithm for the HSFD since a simple model is always needed for the development of controllers. This approximation involves the consideration of the modes of concern and the neglect of other modes. In addition, fluid inertia forces were taken into consideration in the modeling of the HSFD which showed to have great influence in the performance of the long damper, but in the contrary, have little effects on the short damper mode. The open-loop steady state behavior of the system is studied for both the short damper and the long damper configurations. The on-off control algorithm based on the running speed attained by the rotor was performed on this multiple mode rotor. Both the transient and steady state closed-loop behaviors were studied and showed again that the HSFD is a powerful and reliable device for active control of rotating machinery.

1.2.3.1 Development of a model for the HSFD-rotor-control system

The purpose of this section is to introduce a multi-mode rotor model and to illustrate the behavior of the HSFD system with multi-mode rotors. The complete model developed in Hathout's thesis is used for all of the rotor-HSFD system, except for the rotor which is modeled using modal analysis, as discussed below.

Modal analysis is generally implemented to linear systems (Childs, 1974a and b, Gunter et al., 1978), but as discussed before our system is nonlinear because of the nonlinearity of SFDs. Modal analysis is performed on the linear part of the rotor model and all nonlinearities are transferred to the right-hand side of the equations as will be shown later. This allowed us to perform modal analysis for a nonlinear rotor system. The major advantage of modal analysis is that we are able to obtain a limited set of equations describing the behavior of the designed continuous system with the required number of modes manifested.

The modal analysis is performed based on the rotor data and critical speed results. The equations of motion of the shaft-disk-bearings assembly can be written as

$$[M]\{\ddot{x}\} + [K]\{x\} = \{f_x\} \tag{1}$$

$$[M]\{\ddot{y}\} + [K]\{y\} = \{f_y\} \tag{2}$$

where [M] represents the mass matrix containing the masses of the 30 stations of our designed rotor, [K] is the stiffness matrix, {x}and {y}are vectors of the rotor positions at the left journal center, the disk center, and the right journal center, and the vectors $\{f_x\}$ and $\{f_y\}$ comprise the damping forces F_{Dli} and F_{Dri}, the inertia forces F_{Ili} and F_{Iri} acting respectively on the left and right journals, and the unbalance force F_{Ui} acting on the disk, i takes the values of either x or y.

Using the modal transformation:

$$\{x\} = [U]\{q_x\} \tag{3}$$

$$\{y\} = [U]\{q_y\} \tag{4}$$

where [U] is the modal matrix comprising the five planar mode shapes obtained from the critical speed analysis, and $\{q_X\}$ and $\{q_Y\}$are the generalized modal vectors in the x and y directions. By substituting equations (3) and (4) for {x} and {y} into equations (1) and (2) respectively, and by multiplying both equations by $[U]^T$ which is the transpose of the modal matrix, the uncoupled equations of motion then become

$$\{\ddot{q}_i\}+[\omega^2]\{q_i\}=\{N_i\} \tag{5}$$

and

$$\{N_i\}=[U]^T\{f_i\} \tag{6}$$

where i takes the values of either x or y, $[\omega^2]$ is a diagonal matrix with elements as the system five natural frequencies squared, and $\{N_i\}$ is the modal force vector.

The forces acting on both the left and right damper can be described as

$$\sum F_{damper_{ji}} = F_{Dji} + F_{Iji} \tag{7}$$

where j takes the values of l and r for left and right damper respectively, and i takes the values of x and y. The damping forces acting at both the left and right journals are given by

$$\begin{Bmatrix} F_{Djx} \\ F_{Djy} \end{Bmatrix} = \begin{bmatrix} -C_{xxj} & -C_{xyj} \\ -C_{yxj} & -C_{yyj} \end{bmatrix} \begin{Bmatrix} \dot{x}_j \\ \dot{y}_j \end{Bmatrix} \tag{8}$$

The damping coefficients C_{xx}, C_{xy}, C_{yx} and C_{yy} for the HSFD should reduce to those of the short damper at one extreme and to those of the long damper at the other extreme. To incorporate the effect of a finite damper in the HSFD model, a simple model is used. It consists of a linear combination of the short damper model and the long damper model and is due to Holmes and Dogan (1985), such that

$$C_{ij} = \lambda C_{ijs} + (1-\lambda) C_{ijl} \tag{9}$$

where i and j take the values x and y. λ is a measure of the finiteness of the damper, in the sense that if λ=1, at one extreme, the damper behaves as a short damper, and if λ=0, at the other extreme, the damper behaves as a long damper. Nevertheless, λ can take any value between 0 and 1, thus it will behave as a finite damper. Holmes and Dogan (1985) obtained experimentally the appropriate value of λ the damper they were studying, and they were able to show that a damper with an end seal at a distance

from the end equal to the radial clearance c approaches the short damper, and a damper with a closed end will approach the long damper. Thus, in our model we take the factor λ to be equal to the ratio a/c, where a is the distance of the sealing ring from the end of the damper.

It should be stressed that the damping coefficients are taken as for uncavitated dampers in cartesian frame (El-Shafei and Eranki, 1994). The dampers are assumed uncavitated for two main reasons. The first reason is that simplicity in modeling is necessary at the development stage in the design of the control algorithm. The second reason is that cavitation has already been introduced in our recent models (El-Shafei et al., 1994) and showed very slight difference with the uncavitated case except for jump resonance at high levels of unbalance (El-Shafei, 1990).

It should be pointed out that our main interest is the effect of the damper on the rotor dynamics. Vapor cavitation can be important only at high levels of unbalance which results in the jump-up phenomenon. Otherwise, gaseous cavitation can also affect the response of the rotor (sometimes it is claimed to result in a jump-down phenomenon) however, with the supply pressure common in aircraft engines, aeration and gaseous cavitation can be reduced, and in our test results (El-Shafei and El-Hakim, 1995) the effect of gaseous cavitation was not observed for a supply pressure of 3 bar (45 psi). Actually our test-rig showed that an uncavitated model was sufficient for the supply pressure we used which is about half the supply pressure commonly used in aircraft engine dampers today.

Up to this point in modeling, the set of equations of motion for the rotor-bearing system taking into consideration the damping effect as nonlinear forces acting externally upon the system can be described using modal coordinates, as in equation (5). By this formulation, we have managed to transfer all nonlinearities due to the nonlinear damping coefficients of the damper to the right-hand side of the equations and thus performed modal analysis on the linear part of the model. This allowed us to carry out approximately the modal analysis for a nonlinear rotor system.

Thus, the model is now consisting of a set of uncoupled second order differential equations that can be easily integrated numerically.

In effect, the approach we have taken can be thought of as a complete modal analysis of the rotor alone, which is perfectly legitimate since the rotor is linear, and after obtaining the uncoupled modal equations, the nonlinear damper is introduced directly in the modal coordinates, thus we obtain a set of uncoupled nonlinear differential equations representing the continuous rotor system. This set of nonlinear differential equations can be used both for the simulation of the multi-mode rotor, and for the development of the control algorithm.

The fluid inertia forces acting on the journals were evaluated before by El-Shafei and Crandall (1991) and were shown to be proportional to the usual radial, centripetal, tangential, and Coriolis accelerations of the journal plus an additional nonlinear acceleration. These five components, which form the inertia forces, have coupled the system again since they are proportional to the acceleration of system in both x and y directions. The fluid inertia forces are given by

$$\begin{Bmatrix} F_{Ijx} \\ F_{Ijy} \end{Bmatrix} = \begin{bmatrix} \cos\psi & -\sin\psi \\ \sin\psi & \cos\psi \end{bmatrix} \begin{Bmatrix} F_{I,radial} \\ F_{I,tangential} \end{Bmatrix} \tag{10}$$

where

$$F_{I,radial} = -M_{rrad}\ddot{e} - M_{rnon}\frac{\dot{e}^2}{e} - M_{rtan}e\ddot{\psi} - M_{rcor}2\dot{e}\dot{\psi} + M_{rcen}e\dot{\psi}^2 \tag{11}$$

$$F_{I,tangential} = -M_{trad}\ddot{e} - M_{tnon}\frac{\dot{e}^2}{e} - M_{ttan}e\ddot{\psi} - M_{tcor}2\dot{e}\dot{\psi} - M_{tcen}e\dot{\psi}^2 \tag{12}$$

where ψ is the angle of circular whirl at the damper. M_{rad}, M_{non}, M_{tan}, M_{cor}, and M_{cen} are the inertial coefficients in both radial and tangential directions (El-Shafei and Crandall, 1991). These inertial coefficients are dependent on the inertia parameter of the damper M which can take the value M_s in the short damper case at one extreme, M_l in the long damper case at the other extreme, or any finite value between both M_s and M_l. As discussed before for the case of damping coefficients in equation (9), the damper can act between two extremes which are the long damper and short damper modes. A simple linear relationship can permit the damper to act as a finite damper

and sense the right amount of inertia according to the position of the sealing ring (i.e. the value of λ). This linear relationship can be written as

$$M = \lambda M_s + (1-\lambda) M_l \tag{13}$$

The introduction of the inertia forces has coupled the set of modal equations (5), since these forces are proportional to the acceleration of the system in both q_x and q_y directions. The set of equations will have the form

$$[M_i]\{\ddot{q}_i\} + [\omega^2]\{q_i\} = \{N_i\} \tag{14}$$

To overcome the coupling introduced by the inertia forces parameters in the matrix $[M_i]$, we thought of transferring the inertia forces to the right-hand side as done before in the case of the damping forces, but we encountered some difficulties since the values of the accelerations of q_x and q_y are not evaluated at each integration step. Therefore, in order to perform modal analysis on the linear part of the system and transfer all nonlinearities due to inertia forces to the right-hand side, we had to solve the set of equations (14) for the vector $\{\ddot{q}_i\}$ algebraically at each integration step. Hence, equation (14) is put in the form

$$[M_i]\{\ddot{q}_i\} = \{b_i\} \tag{15}$$

where $\{b_i\}$ denotes the right-hand side known vector. Equation (15) consists of a set of linear algebraic equations that are solved for $\{\ddot{q}_i\}$ at each step of integration and hence the values of the nonlinear inertia forces can be evaluated. Thus again, as in the damping forces case, modal analysis is performed on the linear part of the system.

The unbalance forces acting on the disk in both the x and y directions are

$$F_{Ux} = mu\Omega^2 \cos\Omega t - mu\alpha \sin\Omega t \tag{16}$$

$$F_{Uy} = mu\Omega^2 \sin\Omega t + mu\alpha \cos\Omega t \tag{17}$$

where u denotes the unbalance of the disk, m is the mass of the disk, Ω is the rotational speed, α is the rotor angular acceleration, and t is the time in seconds.

It is desirable to nondimensionalize the above equations before adding them to the rest of the model developed by El-Shafei and Hathout (1995) that describes the rest of the system comprising the sealing ring dynamics and the servovalve characteristics. To nondimensionalize the governing equations of the rotor-disk-bearings system, the same nondimensionalized parameters used by El-Shafei and Hathout (1995) are implemented. Nondimensionalization is preferred, because nondimensional equations are less prone to numerical difficulties since the parameters and variables are scaled, and also the nondimensionalization results in a reduced number of parameters and generalizes the analysis.

1.2.3.2 Simulation of the Behavior of the Open-Loop Control System

To simulate the behavior of the open-loop system, the equations developed in the previous section describing the dynamics of the complete open-loop system are implemented on a digital computer. In order to simulate this model, the most convenient and robust integration technique is the Runge-Kutta 4 method. An in-house package developed by the authors is used in the simulations described in this section. The step used is 0.005 and showed to be suitable. It should be emphasized that in order to overcome the coupling in the equations of motion (14) caused by the introduction of the fluid inertia forces which are proportional to both accelerations in x and y directions as explained in the previous section, we solved the set of linear equations (15) by the Gaussian Elimination method at each integration step. This solution was performed using the LSARG routine from the IMSL library. This allowed us to perform modal analysis on a nonlinear system by transferring all nonlinearities to the right-hand side of the set of equations and perform modal analysis on the linear part.

The parameter values for the HSFD and the servovalve used in the simulations are taken as in El-Shafei and Hathout (1995). In addition, the inertia parameter for the

short damper mode M_S is taken 0.1266 and simulations are performed for a nondimensional unbalance of $U = 0.1$. These nondimensional parameters correspond to the rotor, the HSFD and the test rig built at Cairo University. The HSFD parameters were chosen such that the long damper will be effective in suppressing the critical speeds. For the same dimensions, a short damper will be much less effective since it induces less damping to the system than the long damper and thus gives a wide range of damping to the HSFD. This is a good design methodology and will result in a quite large clearance for the damper. This is not a drawback since the damper will be effective as a high load damper too. In all simulations shown in this section, the initial conditions were taken as: $\lambda = 1$, $q_i = 0.01$ (i takes the values of x and y), and all other variables equal to zero.

The open-loop steady state behavior of the system is performed. The eccentricity ratio for both right and left dampers ε_r and ε_l respectively, the vibration amplitude of the rotor center r, and the transmitted damper force at both right and left bearings F_r and F_l (which is defined as the ratio of the damping force to the unbalance force) are studied versus the nondimensional rotational speed Ω^* (which is defined as the ratio of the rotational speed Ω to the first natural frequency). Figure 11 shows the steady state behavior of both the short damper and the long damper for an unbalance $U = 0.1$. It can be clearly seen from both Figures 11 (a) and (b), which describe respectively the steady state behavior of ε_r and ε_l, that the short damper and the long damper exhibit completely distinct behaviors. Also, it can be easily seen that there are obvious differences in the profiles of the curves between the left and the right dampers for the same damper mode. This is because the rotor is unsymmetric.

The short damper mode exhibits mainly five modes as judged from both Figures 11 (a) and (b). Mainly three modes are accentuated in both damper sides and are at nondimensional rotational speeds of $\Omega^* = 1$, 4 and 11 approximately. These modes correspond to the first, the third and the fourth mode of the critical speed analysis

performed before. The second mode is well damped and can be clearly evidenced in both Figures 11 (a) and (b) at $\Omega^* = 2.1$ approximately, while the fifth mode which should appear at $\Omega^* = 12.4$ approximately is highly attenuated in both sides.

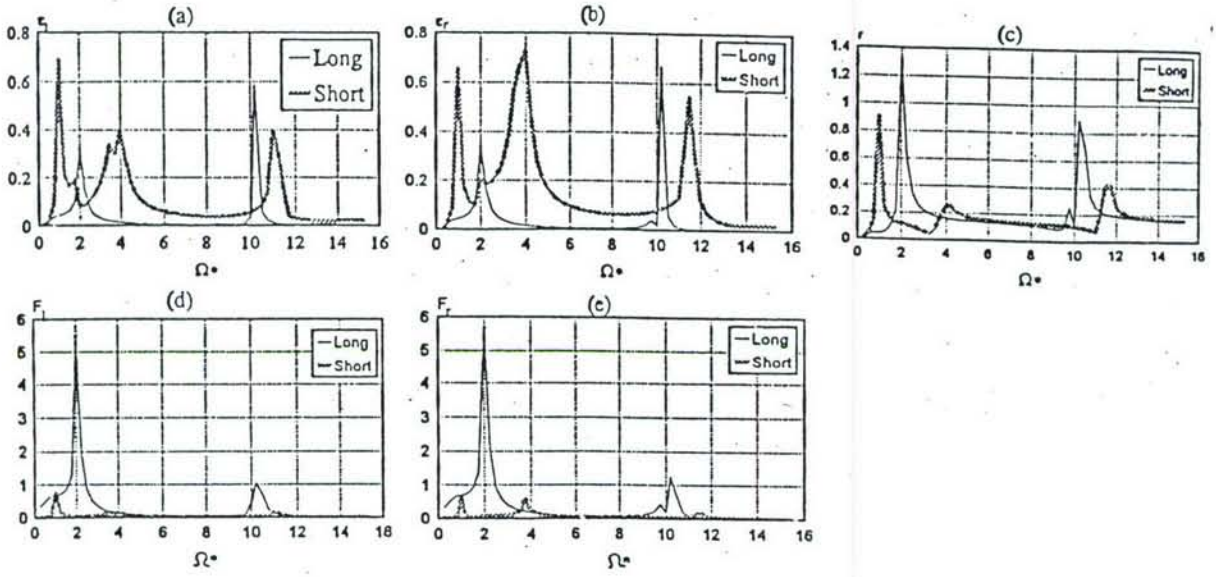

Figure 11 The open-loop behavior of the left, right damper, disk center and the transmitted force

The long damper mode, as illustrated in Figure 11, reveals a drastic change in the profile of the curve. The first mode is shifted to $\Omega^* = 0.9$ approximately and is highly damped, the second mode is highly damped too. The third mode is shifted to $\Omega^* = 2$ approximately and is accentuated due to fluid inertia. Both the fourth and fifth modes are well damped, and an additional very accentuated mode is seen at $\Omega^* = 10.2$ approximately, and is probably caused by the shifting of higher modes due to fluid inertia effects. These sensitive changes in the long damper configuration are due to the relatively high long damper inertia parameter, $M_l = 0.285$ (El-Shafei, 1991a). No significant effects appeared in the short damper mode due to the relatively low short damper inertia parameter, $M_s = 0.1266$ (El-Shafei, 1990).

Figures 11 (a) and (b) show that the eccentricity behavior is always better in the long damper mode except when the spikes appear due to fluid inertia in the long mode.

Figure 11 (c) shows the same behavior. On the other hand, Figures 11 (d) and (e) show that the transmitted short damper force is always less than the long damper force.

1.2.3.3 Control Algorithm Development based on Rotor Speed Feedback

As shown before by El-Shafei and Hathout (1995), simplicity is a major advantage in control system development and we would like to compliment the investigation of the previously proposed algorithm that relied on two levels of damping: the short damper configuration and the long damper configuration. Depending only on two modes of damping, an on-off controller was designed to actively switch between them and give the required level of damping at the required time. This algorithm, despite its simplicity, showed to be very efficient and gave an overall enhanced behavior of the steady-state history of the rotor. Moreover, It can be shown (Burrows et al., 1983) that for some rotors, only two damping levels are sufficient to control the behavior of the rotor-bearings system.

Basically, the control algorithm proposed herein requires the accurate determination of the critical speeds of the rotor before the implementation of the algorithm. The controllable HSFD is then designed to provide distinctly different damping capacities for the rotor bearing system based on extensive simulation. A proposed HSFD design procedure is discussed by El-Shafei and Hathout (1995). The nonlinear unbalance responses for the two levels of damping provided by the HSFD are also required. In this case the basic assumption is the validity of the modal analysis approach as presented for the nonlinear system. It is also assumed that the unbalance force is the only force applied to the system. Based on the unbalance response, the speeds at which it is desirable to use the short damper mode and those for which the long damper mode is desirable, are determined. The control algorithm is then simply based on measuring the rotor speed and controlling the HSFD to provide the long damper mode at the critical speeds and the short damper mode away from the critical speeds.

This algorithm was implemented experimentally by El-Shafei and El-Hakim (1995) and proved to be successful in demonstrating the concept of the on-off control for a single mode rotor.

It can be seen from Figure 11 which illustrates the steady state behavior of the open-loop system that the behavior of the rotor system is speed dependent, and that both modes, the short damper and the long damper, are behaving distinctly different. Thus, it is proposed that in order to design a good on-off controller, the best feedback law deduced for the closed-loop system is based on the feedback of rotor speed. This active on-off controller can thus be activated at specific rotor speeds at the desired damping level and for the necessary speed range. This algorithm is quite attractive due to its ease in application since only one variable is needed for feedback which is the rotor speed, and according to Figure 11 it is clear that the feedback on speed would be quite effective in improving rotor behavior. However, this feedback law would require the pre-knowledge of the system behavior. This is not considered to be a serious drawback since usually a meticulous analysis of the system critical speeds is performed beforehand, and thus can be easily programmed into the on-off controller.

To apply the simple active control algorithm based on speed feedback to the system described in this paper, let us study the behavior of the steady state response in Figure 11. To overcome the first critical speed which is quite large in the short damper case, the damper is chosen to operate in the long damper mode from rest until $\Omega^*= 1.5$, thus benefiting from the larger damping provided by the long damper in this region. At $\Omega^*= 1.5$, the system is switched to the short damper mode to take advantage of the smaller damping force of the short damper mode in a region of mild vibration. Note that the damping force is always greater in the long damper mode than in the short damper mode, especially in two regions from rest to $\Omega^*= 3.5$ approximately, and from $\Omega^*= 9.5$ to $\Omega^*= 11$ approximately, thus in non-resonant regions one should benefit from the smaller force of the short damper mode. The system is chosen to run in the

short damper mode until a speed of $\Omega^* = 3$ beyond which an increase in the amplitude of vibration occurs as shown in Figures 11 (a) and (b). Thus, at $\Omega^* = 3$ the system is switched to the long damper mode to overcome the region of high vibration which extends until $\Omega^* = 6$ with the penalty of having a slightly higher damping force than in the short damper. Once the high amplitudes of vibration are bypassed and replaced by the smaller amplitudes of the long damper mode, the system is preferred to act in the short damper to avoid excess damping force on the bearings. Therefore, the system runs in the short damper mode in the region from $\Omega^* = 6$ to $\Omega^* = 10.8$ to decrease the damping force on the bearings while in a region of moderate vibration and also to overcome the serious spike induced from inertia effects, at $\Omega^* = 10$ approximately, in the long damper mode. At $\Omega^* = 10.8$, once again the system is switched to the long damper mode to overcome the last critical speed until $\Omega^* = 13$ and then the system is switched to the short damper mode. Figure 12 shows the closed-loop steady state behavior of the controlled system. There is no doubt that the closed- loop shows a remarkably improved behavior and this shows the power of the proposed on-off controller based on speed feedback.

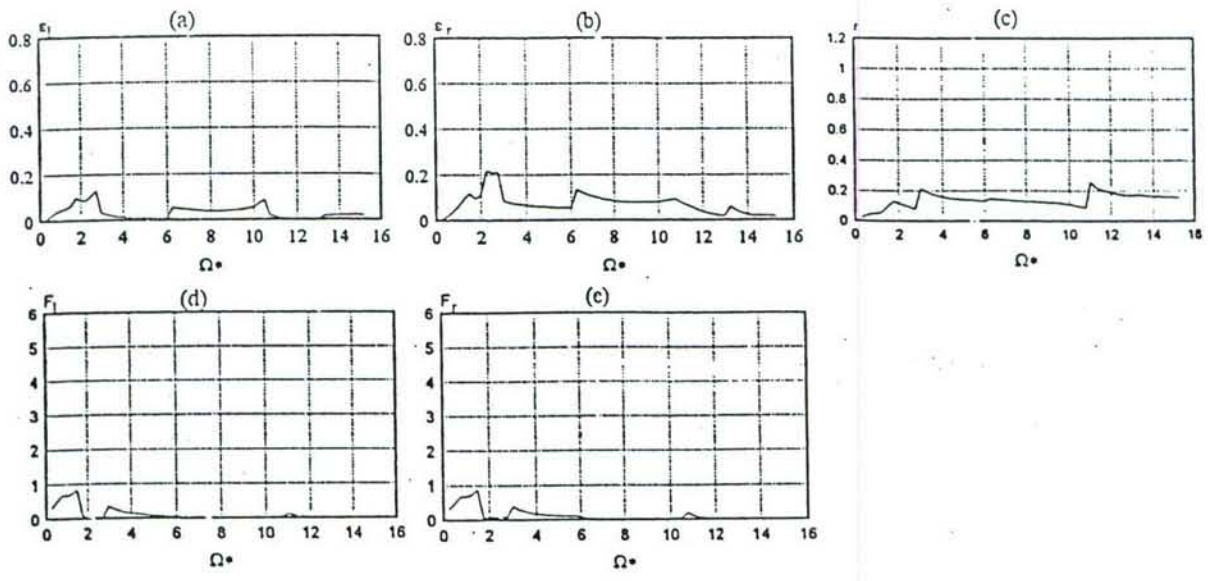

Figure 12 The closed-loop behavior of the left, right damper, disk center and the transmitted force

The transient behavior of the closed-loop system is also investigated to fully evaluate the capabilities of the proposed control strategy. The transient behavior in the control action is studied for ε_r, ε_l, r, F_r and F_l at each switching speed. Figures 13, 14, 15, 16 and 17 illustrate the transient response during the control action at Ω^*= 1.5, 3, 6, 10.8 and 13 respectively. It should be noted that the time scale in all the time simulations is in nondimensional time τ which is defined as the product $\omega_n t$, where ω_n is the rotor first natural frequency and t is the time in seconds. Thus a unity on the time axis in the plots will represent 5.3 milliseconds. An overall study of the transient response of the closed-loop system shows that our system is quite a success since the response is fast, stable and accurate. While switching from the long mode to the short mode at Ω^*=1.5, in Figure 13, some oscillations persist for a small time of about 0.95 seconds for ε_l, ε_r and r due to low damping of the short damper mode. While in switching from short to long at Ω^*= 3, in Figure 14, the system immediately switches to the long damper mode in less than 0.13 seconds with no sensitive oscillations, and shows a well-behaved response due to larger damping in the long damper mode. The rest of the Figures from 15 to 17 show a graphical display of the transient behavior of the system at the different switching speeds which compliment the issues discussed in both Figures 13 and 14, in showing a fast, stable, and well-behaved transient response of the closed-loop system. Therefore, the active on-off control algorithm based on rotor speed feedback results in an enhanced performance both in its transient and steady state responses.

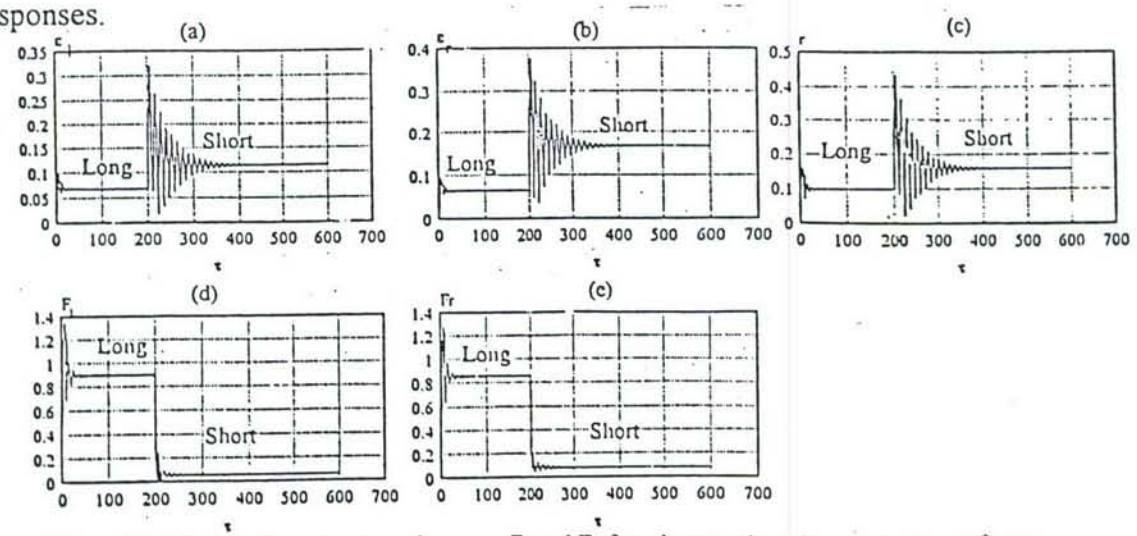

Figure 13 The transient response of ε_l, ε_r, r, F_l and F_r from long to short damper mode at Ω^*=1.5

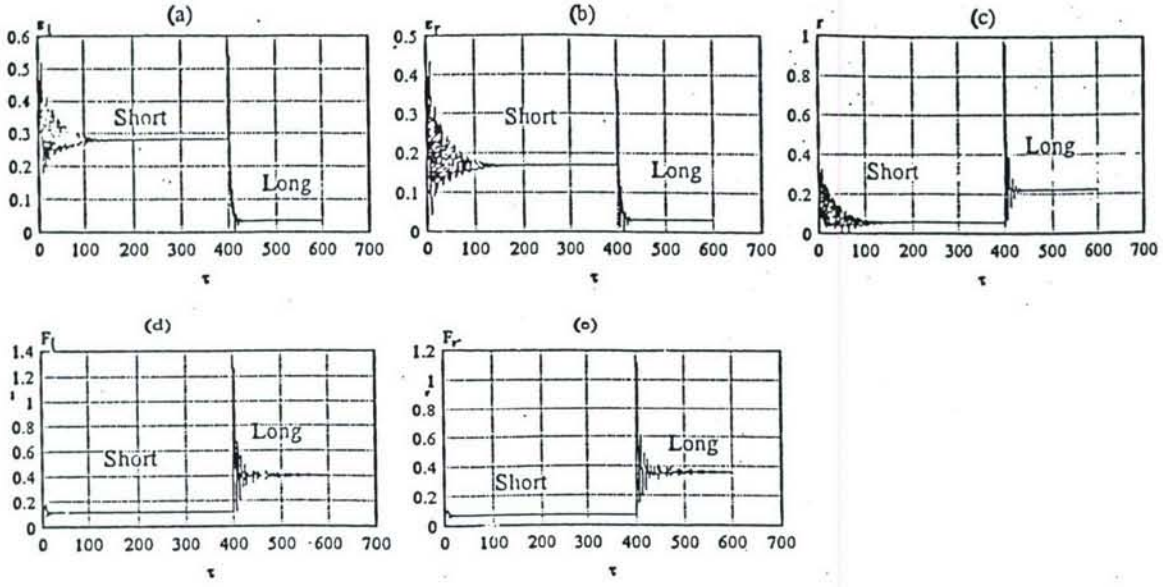

Figure 14 The transient response of ε_l, ε_r, r, F_l and F_r from short to long damper mode at Ω^*=3.0

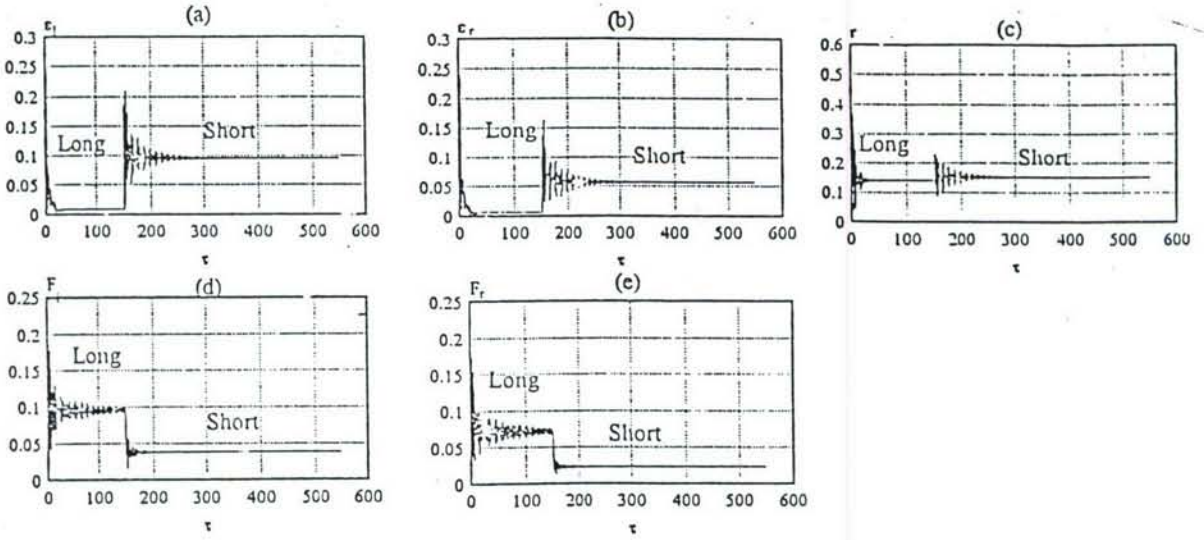

Figure 15 The transient response of ε_l, ε_r, r, F_l and F_r from long to short damper mode at Ω^*=6

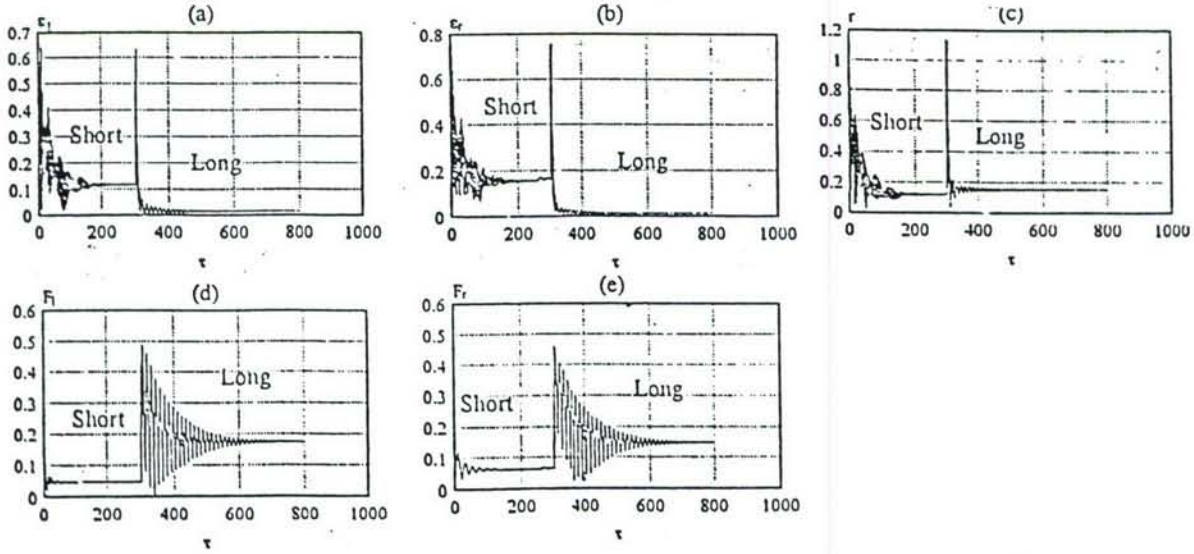

Figure 16 The transient response of ε_l, ε_r, r, F_l and F_r from short to long damper mode at Ω^*=10.8

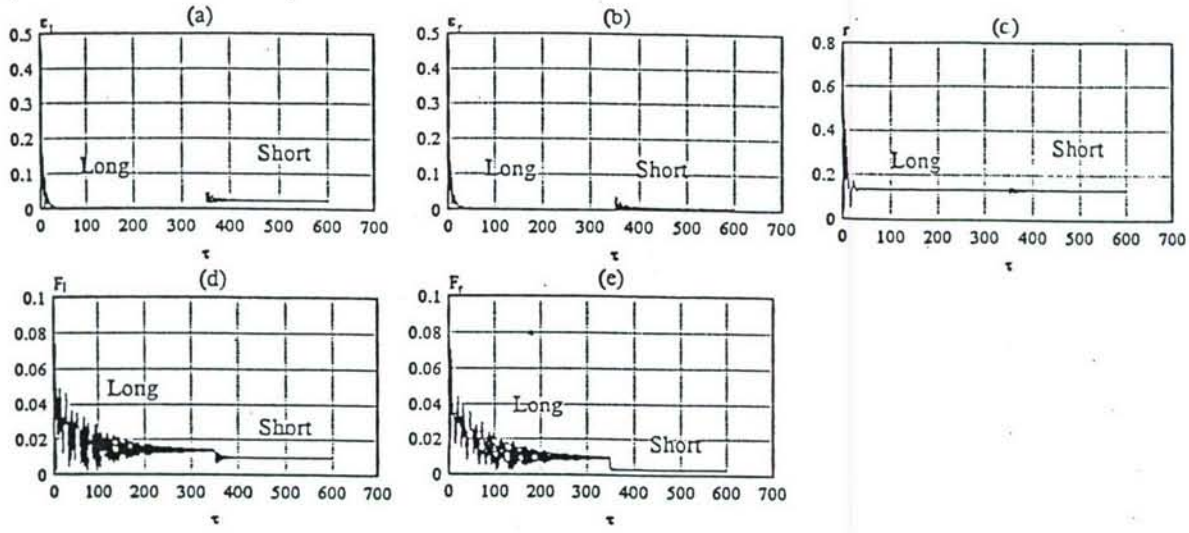

Figure 17 The transient response of ε_l, ε_r, r, F_l and F_r from long to short damper mode at Ω^*=13

1.2.4 SUMMARY

The work presented in this chapter represents the work reported previously and included:

a) Theoretical development for the HSFD and the automated circuit, including simulations of the open-loop system, and on-off-controller.

b) Development of test rig and experimental verification of the performance of HSFDs, both statically and dynamically in a single mode, on-off controller.

c) Modal analysis of multi-mode rotors using HSFDs, and particular application of the on-off controller to multi-mode rotors.

The new work, not reported previously, is included in Parts II and III. Part II represents the control development in Hathout's thesis, while Part III represents the experimental control application.

REFERENCES

Adams, M.L., and Zahloul, H., 1987, "Attenuation of Rotor Vibration Using Controlled-Pressure Hydrostatic Squeeze-Film Dampers", presented at the Eleventh Biennial ASME Vibrations Conference, Boston, MA, September 1987.

Akin, J.T., 1990, private communication, Pratt & Whitney, copy of letter included as appendix.

Bonneau, O., and Frene, J., 1994, "Numerical Study of a Flexible Rotor Mounted in an Active Squeeze Film Damper", Proc. Fourth International Conference on Rotor Dynamics, Chicago IL, pp. 341-350.

Bonneau, O., Kassai, A., Frene, J., and Der Hagopian, J., 1989, "Dynamical Behavior of an Elastic Rotor with Squeeze Film Damper" Eurotrib 89, Helsinki, Finland, Proceedings Vol. 4, pp. 145-149.

Bradfield, C.D., Roberts, J.B., and Karunendiran, S., 1989, "A Programmable Electromagnetic Bearing for Vibration Control of a Flexible Shaft", in Rotating Machinery Dynamics, T.S. Sankar et al. editors, ASME publication DE-Vol. 18-1, pp.335-343.

Burrows, C.R., Sahinkaya, M.N., and Turkay, O.S., 1983, "An Adaptive Squeeze-Film Bearing", ASME paper No. 83-Lub-23.

Childs, D.W., 1974a, "A Rotor-Fixed Modal Simulation Model for Flexible Rotating Equipment", J. Engng. Industry, Trans. ASME, series B, Vol. 96, No. 2, pp. 659-669, May 1974.

Childs, D.W., 1974b, "Two Jeffcott-Based Modal Simulation Models for Flexible Rotating Equipment", J. Engng. Industry, ASME Paper No. 74-WA/DE-17, 1974.
CRITSPD-PC, Version 1.04, 1987, User's Manual, by RODYN-Vibration, Inc., Charlottesville, VA, USA.

El-Shafei, A., 1989, "Long and Short Bearing Approximations for Squeeze Film Dampers", Proceedings of the Vibration Institute, pp. 145-151.

El-Shafei, A., 1990, "Unbalance Response of a Jeffcott Rotor Incorporating Short Squeeze Film Dampers", Journal of Engineering for Gas Turbine and Power, Trans. ASME, Vol. 112, No. 4, pp. 445-453.

El-Shafei, A., 1991a, "Unbalance Response of Jeffcott Rotor Incorporating Long Squeeze Film Dampers", Journal of Vibration and Acoustics, Trans. ASME, Vol. 113, No. 1, pp. 85-94.

El-Shafei, A., 1991b, "Hybrid Squeeze film Damper for Active Control of Rotors", U.S. Patent number 5,058,452, October.

El-Shafei, A., 1993, "Experimental and Analytical Investigation of Hybrid Squeeze Film Dampers", Journal of Engineering for Gas Turbine and Power, Trans. ASME, Vol. 115, No. 2, pp. 353-359.

El-Shafei, A., and Crandall, S.H., 1991, "Fluid Inertia Forces in Squeeze Film Dampers", presented at the 13th Biennial ASME Vibration Conference, Miami, FL, September, published in Rotating Machinery and Vehicle Dynamics, T.C. Huang et al. editors, ASME DE-Vol. 35, pp. 219-228.

El-Shafei, A., and El-Hakim, M., 1995, "Development of a Test Rig and Experimental Verification of the Performance of HSFDs for Active Control of Rotors", presented at the International Gas Turbine and Aeroengine Congress and Exposition, Houston, Texas - June 5-8, 1995, ASME paper 95-GT-256.

El-Shafei, A., and Eranki, R.V., 1994, "Dynamic Analysis of Squeeze Film Damper Supported Rotors Using Equivalent Linearization", ASME Journal of Engineering for Gas Turbine and Power, vol. 116, No. 3, pp. 682-691.

El-Shafei, A., and Hathout, J.P., 1995, "Modeling and Control of HSFDs for Active Control of Rotor-Bearing Systems", ASME Journal of Engineering for Gas Turbine and Power, Vol. 117, No. 4, pp. 757-766.

El-Shafei, A., El-Hakim, M., and Hathout, J.P., 1993, "Control of Rotor Vibrations Using Hybrid Squeeze Film Dampers", Report MDP-EOARD-1/93, Cairo University.

El-Shafei, A., El-Hakim, M., Hathout, J.P., and Youssef, R., 1994, "Control of Rotor Vibrations Using Hybrid Squeeze Film Dampers", Report MDP-EOARD-2/94, Cairo University.

Feder, E., Bansal, P.N., and Blanco, A., 1978, "Investigation of Squeeze Film Damper Forces Produced by Circular Centered Orbits", Journal of Engineering for Power, Trans. ASME, Vol. 100, pp. 15-21.

Gunter, E.J., Barrett, L.E., and Allaire, P.E., 1977, "Design of Nonlinear Squeeze Film Dampers for Aircraft Engines", Journal of Lubrication Technology, Trans. ASME, Vol. 99, No. 1, pp. 57-64.

Gunter, E.J., Choy, K.C., and Allaire, P.E., 1978, "Modal Analysis of Turborotors Using Planar Modes-Theory", Journal of the Franklin Institute, Vol. 305, No. 4, pp.221-243.

Holmes, R., and Dogan, M., 1985, "The Performance of a Sealed Squeeze-Film Bearing in a Flexible Support Structure", Proc. I. Mech. E., Vol. 199, No. C1.

Mu, C., Darling, J., and Burrows, C.R., 1991, "An Appraisal of a Proposed Active Squeeze Film Damper", Journal of Tribology, Trans. ASME, Vol. 113, No. 4, pp.750-754.

Nonami, K., DiRusso, E., and Fleming, D.P., 1989, "Active Vibration Control for Flexible Rotor by Optimal Direct-Output Feedback Control", in Rotating Machinery Dynamics, T.S. Sankar et al. editors, ASME publication DE-Vol. 18-1, pp. 327-334.

Palazzolo, A.B., Lin, R.R., Kascak, A.F., Montague, J., and Alexander, R.M., 1989, "Test and Theory for Piezoelectric Actuator - Active Vibration Control of Rotating Machinery", in Rotating Machinery Dynamics, T.S. Sankar et al. editors, ASME publication DE-Vol. 18-1, pp. 367-374.

Schweitzer, G., and Ulbrich, H., 1980, "Magnetic Bearings - A Novel Type of Suspension", Proceedings of the Second International Conference on Vibrations in Rotating Machinery, I. Mech. E., pp. 151-156.

Swanson, E.E., Raju, K.V.S., and Kirk, R.G., 1996, "Test Results and Numerical Simulation of AMB Rotor Drop", Proc. I. Mech. E. Sixth International Conference on Vibrations in Rotating Machinery, Oxford, pp. 119-132.

Tang, P., Palzzolo, A.B., Kascak, A.F., and Montague, G.T., 1995, "Active Vibration Control of Rotating Machinery With a Hybrid Piezohydraulic Actuator System", ASME Journal of Engineering for Gas Turbine and Power, Vol. 117, No. 4, pp.767-776.

Tecza, J.A., Giordano, J.C., Zorzi, E.S., and Drake, S.K., 1983, "Squeeze Film Damper Technology: Part 2 - Experimental Verification Using a Controlled Orbit Test Rig", ASME paper No. 83-GT-248.

White, D.C., 1972, "The Dynamics of a Rigid Rotor Supported on Squeeze Film Dampers", Conference on Vibrations of Rotating Machinery, Proc. I. Mech. E., pp.213-229.

UNITED
TECHNOLOGIES
PRATT&WHITNEY

P.O. Box 109600
West Palm Beach, FL 33410-9600
(407) 796-2000

Government Engine Business

Appendix

June 18, 1990

Dr. Aly El-Shafei
Department of Mechanical Design and Production
Cairo University
Giza, Egypt

Dear Dr. El-Shafei,

Thank-you for taking the time to send the videotape of your hybrid damper experiments. I found the results interesting and we are also actively pursuing active viscous dampers for controlling vibration.

I view the concept of varying the damper between long and short damper modes as a matter of design practicality. In other words, the reliability of the control system will probably govern the applicability of the concept. It certainly has potential for certain designs.

Good luck in your new position.

Sincerely,

J. T. (Tony) Akin
Pratt & Whitney Aircraft

JTA/lmf

PART II

HATHOUT'S MASTER'S THESIS

ACTIVE CONTROL OF ROTOR VIBRATIONS USING HYBRID SQUEEZE FILM DAMPERS

by

Jean-Pierre Y. Hathout

Thesis

Submitted in Partial Fulfillment of the Requirements for the Degree of Master of Science in Mechanical Engineering in the Department of Mechanical Design and Production, Faculty of Engineering, Cairo University

Supervised by

Prof. Dr. M. E. Elaraby

and

Dr. A. El-Shafei

Department of Mechanical Design and Production

Faculty of Engineering

Cairo University

1995

DEDICATION

This thesis is dedicated to my parents Virginia and Youssef, who always sacrificed their happiness for the welfare of their children, to my sister Nathalie who is always of great support to me and to the memory of my grand mother Ida.

ACKNOWLEDGMENT

I wish to express my deepest gratitude to Professor M.E. Elaraby for supervising my thesis, and for his fruitful debates as he was the first one to introduce me to Automatic Control.

I am also very lucky to have my thesis done under the supervision of Dr. A. El-Shafei. Not only for his scientific assessment throughout the progression of this thesis, but also for his guidance, patience, and continual support. I am grateful for learning a lot from him; particularly how to be "professional" in my work. Above all, I appreciate the family atmosphere he created in our "team".

Thanks are also merited for the "team" that works in the Vibration Lab at Cairo University which contributed a lot both to my academic and social lives, and whom I consider my second family. Thanks a lot for the team members: Mr. M. El-Hakim, Mr. H. Bayoumi, Mr. R. Youssef and Mr. Ramadan.

I also would like to thank Dr. Ahmed S. Zaki from the Aeronautical Department, at Cairo University and Dr. Jeff Shamma from the Aeronautical Department at the University of Texas at Austin for productive discussions that gave me further insight into the problems at hand.

The work presented in this thesis is supported by EOARD, US Air Force Office of Scientific Research, Grant No. F49620-92-J-0512. This support is gratefully acknowledged.

Finally, major credit goes to my family. My father, mother and sister have continuously provided me with love, care and support. To all of them this thesis is dedicated.

ABSTRACT

The work presented in this thesis is concerned with the modeling and control of hybrid squeeze film dampers(HSFDs) for active control of rotor vibrations. Previously, it was shown both theoretically and experimentally that HSFDs can be used for controlling rotor vibrations [1]*. This is done by controlling the flow in a SFD through movable end seals, thus achieving the ability to change the damper from a short damper to a long damper and vice-versa. However, the control of the HSFD was manual. In this study, an automatically controlled circuit is developed for the HSFD, incorporating a pressure control servovalve for controlling the pressure in the sealing chambers. A complete mathematical model of this open-loop system is developed and is implemented on a digital computer. A new design is proposed to use the HSFD as a finite damper, thus it could achieve any amount of damping between the short and long damper modes through the accurate positioning of the movable seals. The simulation results of the open-loop system illustrate that the automatically controlled HSFD can be a very useful device for the active control of rotors.

Several closed-loop control theories are investigated. First, an on-off active closed-loop control strategy based on rotor speed feedback is considered both in the steady-state and transient points of view. This on-off control strategy results in a much improved behavior of the rotor system in attenuating high amplitude vibration at critical speeds, however it could not compensate for sudden transient imbalance such as through sudden blade-loss. A proportional integral (PI) controller is proposed and shows to

[ ]* number between brackets designates reference at the end of the thesis.

compensate well for sudden transients as well as transient run-up through critical speeds. A gain scheduling technique (GS) is examined to enhance the performance of the PI controller. Optimal control theory is also investigated through a linear quadratic regulator (LQR) with an incorporated state observer which allows full-state feedback. Moreover, a model reference adaptive controller (MRAC) is tested. Insights into these several control strategies with a comparative approach, helps in choosing the appropriate regulator for our system that would give the enhanced performance sought after.

TABLE OF CONTENTS

NOMENCLATURE

a = distance of sealing ring from the end of the journal, m
A = system matrix
A_r = area of the sealing ring exposed to the pressure, m^2
B = input control vector
$B_e = \mu R^3/m_r\omega_n c^2$ = end force coefficient
$B_S = \mu R^3/m\omega_n c^3$ = bearing parameter for the short damper
$B_l = B_S\,(R^2/L^2)$ = bearing parameter for the long damper
c = radial clearance of damper, m
C = half damping coefficient at rotor center, Ns/m
C_1 = damping coefficient of sealing ring, Ns/m
C_{ijn} = damping coefficients, i and j take the values of x and y in the (x,y) frame or r and t in the (rr,tt) frame, n = s for short damper and n = l for long damper Ns/m.
$\overline{C}_{ij\,n}$ = nondimensional damper coefficient, Ns/m.
ΔC = increase of damping, Ns/m.
$\Delta \overline{C}$ = increase of damping, nondimensional.
D = output vector connecting input to output directly
$e = \sqrt{x_E^2 + y_E^2}$ = damper eccentricity, m.
$F = \sqrt{F_{dx}^2 + F_{dy}^2}\ /U\Omega^{*2}$ = transmitted damping force, defined as the ratio of the damping to the unbalance force, nondimensional.
F_d = force acting on the sealing ring, N
F_{di} = damping force in the x (i=x) and y (i=y) directions, N
$F_d^* = F_d/m_r c\omega_n^2$ = nondimensional force at journal end
$G(s)$ = plant transfer function
$G_m(s)$ = reference model transfer function
i = current supplied to servovalve, mA.
I = Identity matrix
i_{max} = maximum current input to the servovalve, (≅ 10 mA)
$i_O = i/i_{max}$ = nondimensional current.
J, J_m = performance index for LQR and MRAC cases respectively
k_i = integral controller gain, nondimensional.
k_p = proportional controller gain, nondimensional.
K = half rotor stiffness, N/m.
K_{opt} = LQR vector of gains
K_r = retainer spring stiffness, N/m
K_s = spring stiffness, N/m
K_I = valve's gain, MPa/mA
$K^* = K/m\omega_n^2$ = nondimensional rotor stiffness.
$K_r^* = K_r/m\omega_n^2$ = nondimensional retainer spring stiffness.

$K_s^* = K_S/m_r\omega_n^2$ = nondimensional spring stiffness

$K^*_I = K_I\, i_{max} Ar/m_r\omega_n^{\,2}\, c$ = nondimensional valve gain

L = damper length, m

L = estimator dynamics matrix

m = half disk mass, kg

m_b = rotor journal mass, kg

$m_o = m/mb$ = mass ratio

m_r = mass of sealing ring, kg

N_x, N_u = State Command Matrices for reference and control input respectively

p = pressure in sealing chamber, N/m^2

$p^* = pA_r/m_r c\omega_n^2$ = nondimensional pressure in sealing chambers

P = positive definite matrix obtained from the solution of the Riccati equation

Q = performance measure weighting matrix

$r = \sqrt{x_S^2 + y_S^2}\ /c$ = the vibration amplitude at rotor center, nondimensional

ref = reference input, nondimensional

R = damper radius, m

R_c = cost of control weighting matrix

$R_k = K_r^*/K^*$ = stiffness ratio

s = Laplace operator.

t = time, s

u_c = nondimensional control input.

$U = u/c$ = nondimensional unbalance

u = unbalance, m

x = state vector

$\hat{x}$ = vector of estimated states

x_e = error of the estimate

x_i = x-displacement at the journal center E ($i = E$), or at the disk center S ($i = S$), m

x_r = reference input vector

x_{ss} = steady state behavior of the system

y_i = y-displacement at the journal center E ($i = E$), or at the disk center S ($i = S$), m

$\bar{x}_i = x_i/c$ = nondimensional x-displacement

y = output vector

$\bar{y}_i = y_i/c$ = nondimensional y-displacement

α = rotor angular acceleration

α_o = angle (Figure 7), rad.

$\alpha^* = \alpha/\omega_n^2$ = nondimensional rotor angular acceleration

β = angle (Figure 7), rad.

$\varepsilon = e/c$ = eccentricity ratio, nondimensional

ε_m = model reference eccentricity ratio, nondimensional

ε_r = eccentricity reference input, nondimensional

γ = adaptation gain rate

$\eta = C/m\omega_n$ = damping loss factor

$\eta_1 = C_1/m_r\omega_n$ = damping loss factor at sealing ring

θ_o = oil film angle, rad.

θ = adaptation parameter

λ = a/c = measure of the finiteness of the HSFD, nondimensional
μ = fluid dynamic viscosity coefficient, Ns/m^2
π = 3.14159265....
$\tau = \omega_n t$ = nondimensional time, a unity is equivalent to 5.3 milliseconds
ω_n = fundamental natural frequency of the rotor, rev/min
ω_{nl} = valve's apparent natural frequency, Hz
$\omega_r = \omega_{nl}/\omega_n$ = nondimensional ratio of natural frequencies
Ω = rotor speed, rad/s
$\Omega^* = \Omega/\omega_n$ = nondimensional rotor speed (frequency ratio)
ψ = angle (Figure 7), rad.
ζ_l = valve's apparent damping ratio
$\dot{(\,)}$ = denotes differentiation w.r.t. t
$(\,)'$ = denotes differentiation w.r.t. τ

LIST OF ABBREVIATIONS

CAD = Computer Aided Design
GS = Gain Scheduling technique
GS-PI = Gain Scheduling technique on PI
HSFD = Hybrid Squeeze Film Damper
LQR = Linear Quadratic Regulator
LP = Low Pressure Turbine
MIMO = Multiple Input Multiple Output
MRAC = Model Reference Adaptive Controller
MRAS = Model Reference Adaptive System
SIMO = Single Input Single Output
SISO = Single Input Single Output
PI = Proportional Integral Controller
PID = Proportional Integral Derivative Controller

LIST OF FIGURES

CHAPTER 1

INTRODUCTION

Squeeze film dampers (SFDs) are damping devices used essentially in aircraft gas turbine engines to damp the whirling vibrations of rotors. Their ability to attenuate the amplitude of engine vibrations and to decrease the magnitude of the force transmitted to the engine frame makes them an attractive rotor support.

Simplicity and reliability afforded in the design of SFDs, that were usually used as passive devices, have enticed researchers to use SFDs as active devices. Active control of rotor-bearing systems vibrations is still in progress and many active devices as magnetic bearings, lateral force actuators are still in their developmental stage and have to prove their reliability. Hybrid Squeeze Film Dampers (HSFDs), first proposed by El-Shafei [2], have already undergone a big step in proving their reliability, effectiveness and simplicity. Simplicity of the HSFDs makes them very attractive devices for active control of rotor vibrations. Finding a robust controller for the HSFD is the decisive phase that would enable the HSFD to be an effective active controller for rotor-bearing systems.

1.1 Background and Literature Survey

Active vibration control of rotors of aircraft engines, rocket turbopumps and high speed compressors has been investigated in the last decade or so. Passive vibration control has been used for over twenty years, namely using squeeze film dampers (SFDs). However, active vibration control is sought because of its effectiveness in wide speed ranges and its adaptability to changing operating conditions.

Three active vibration control devices have been suggested in the literature: (1) Magnetic Bearings, (2) Lateral Force Actuators, and (3) Active Squeeze Film Dampers.

Magnetic Bearings [3] and [4] have been investigated for actively controlling the vibration of rotating machinery. Yet, as far as aircraft engines are concerned, magnetic bearings are still at a developmental stage and have not been used in aircraft engines for several reasons, including: (1) the inability of magnetic bearings to withstand high temperatures, (2) the control algorithms for magnetic bearings are still under development, and most importantly (3) magnetic bearings have still to prove their reliability.

Lateral Force Actuators have recently been suggested as active vibration controllers, [5] and [6], and also are still under development. Their shortcomings include: (1) possible coupling of motion in orthogonal directions, (2) they require

large size actuators, and (3) they also have still to prove their reliability for using them in aircraft engines.

Squeeze Film Dampers (SFDs), on the other hand, have a proven track record. They have been used successfully for the last twenty years to passively damp rotating machinery, in particular aircraft engines [7], [8] and [9]. They provide the primary source of damping in aircraft engines since the rolling element bearings on which those engines are mounted provide very little damping. Thus, because of their reliability, it seems natural to develop SFDs to actively control rotor vibrations.

Burrows *et al.* [10] investigated the possibility of controlling rotating machinery vibration by controlling the pressure in a SFD, and they point out that control of rotors using active SFDs is much cheaper than using magnetic bearings, and is more simple and reliable. Adams and Zahloul [11] studied the control of rotors by controlling the pressure in hydrostatic SFDs. Mu *et al.* [12] proposed an active SFD by using a movable conical damper ring.

El-Shafei [1] and [2] proposed using Hybrid Squeeze Film Dampers (HSFDs) for active vibration control of rotors. The basic idea behind the HSFD is to control the flow in the SFD through movable metallic end seals, thus achieving the ability to change the damper from a short damper to a long damper and vice-versa. The performance of the HSFDs was verified experimentally, and it was shown that HSFDs are effective in controlling the amplitude of rotor vibrations and in reducing the force transmitted to the support [2]. Also, it was shown that the HSFD is much more

effective in controlling rotor vibrations than the previous strategies of controlling the pressure in a conventional SFD.

Because of its demonstrated capability and excellent performance in controlling rotor vibrations and because of the reliability of SFDs, it is desirable to develop the Hybrid Squeeze Film Damper and develop an active control algorithm that would exploit its capabilities at maximum.

Significant efforts have been made to apply active vibration control devices to rotating machinery such as aircraft jet engines, rocket turbopumps and high speed compressors. Implementing active vibration control on rotating machinery is expected to give advantages such as the adaptability of the controller to a myriad of load conditions, the attenuation of vibration amplitude while run-up and coast-down through the critical speeds, and the reaction of the controller to minimize sudden transient vibration such as sudden imbalance, e.g., through blade loss.

Active vibration control of rotors has been studied using different types of devices such as electromagnetic bearings and lateral force actuators. In the majority of the active control strategies research for vibration control mentioned in the literature, electromagnetic bearings have the largest share. Schweitzer [13] and Ulbricht *et al.* [14] examined the stability and observability of rotor-bearing systems with active vibration control. Weise [15] proposed a proportional, integral, derivative (PID) control of rotor vibrations using magnetic bearings which force the rotor to spin about its inertial axis. Keith *et al.* [16] and Allaire *et al.* [17] have implemented analog and digital PD controllers with magnetic bearings. Zhu *et al.* [18] proposed the use of optimal control strategies for magnetic bearings. Several efforts using optimal control

methods were also investigated for lateral force actuators like the work of Palazzolo *et al.* [19] and [20].

As a first attempt for active control of rotors using HSFDs, El-Shafei and Hathout [21] proposed an on-off control algorithm based on feedback of rotor speed and it was shown by simulation to be quite powerful in controlling rotor vibrations while passing through a critical speed. The same algorithm based on feedback of rotor speed was tested experimentally and was shown to be quite successful [22]. Moreover, this algorithm showed by simulation to be quite effective in suppressing multi-modes of more complicated rotor models incorporating fluid inertia effects [23]. The feedback on rotor speed is quite attractive for its simplicity and efficiency, but it requires a pre-knowledge of the system critical speeds which are usually known beforehand while the rotor is designed. This feedback on rotor speed algorithm will not be able to compensate for sudden rotor imbalance, our current goal is to design an active controller capable of overcoming such sudden transient behavior and in addition capable of reacting while passing through critical speeds.

1.2 Thesis Goals and Outline

The literature articles surveyed in the previous section indicate the need to find an appropriate controller for the HSFD for actively controlling rotor-bearing systems. The development of the control system is, in fact, the crucial phase in the development of the HSFD.

This thesis presents the development of the HSFD for actively controlling rotating machinery vibration. The last state of development of the HSFD [1] is that it has been used in the laboratory in a manually controlled configuration as an on-off controller.

The thesis goals are to develop an adaptive damper that could give the appropriate damping to damp a myriad of operating conditions with different disturbances. The development of an automatically controlled circuit to control the HSFD is of primary importance since it is envisioned that the control will be through a digital computer. A complete mathematical model which emulates the system behavior is required for simulations. Also, the study of the behavior of the open-loop system is very helpful in determining the algorithms to be used for the control. Last but not least, Controllers of different control theories are investigated in depth since no research on the adequate controller for the HSFD has been done yet.

To achieve these goals, we start in Chapter 2 with enhancing the design of the HSFD to make it an adaptive device. Some development has been achieved in the design of the HSFD to change it from a two mode damper (short and long damper modes) to a finite damper that can achieve any amount of damping between the short damper and the long damper configurations through the accurate positioning of the sealing rings.

In this research specifically in Chapter 2, an automatically controlled circuit is developed for the HSFD, incorporating a pressure control servovalve for controlling the pressure in the sealing chambers. The aim is to develop a simple hydraulic control circuit that would eliminate the redundancy in the previous manual system and moreover to have access to control the HSFD via a digital computer, and this was achieved by the use of an electrically operated pressure control servovalve.

A complete mathematical model of this open-loop system is developed and is implemented on a digital computer. This mathematical model of the rotor-HSFD-control system includes the proposed model of the HSFD that emulates the behavior of the HSFD for various finite positions of the sealing rings. This issue is discussed in

Chapter 3. Simulations of the behavior of the open-loop system both in the steady state and transient view points are studied and analyzed in Chapter 4.

The control development through an On-Off controller is presented in Chapter 5. Modern control theories are investigated further on, complete re-modeling of the system is needed to be manipulated in MATLAB™ [24] and SIMULAB™ [25]. Chapters from 6 to 9, include the modeling, the different regulators design, and the simulations of several controllers to investigate their capability of controlling both transient run-up through critical speeds and sudden imbalance. Chapter 6 deals with the conventional control theory through a Proportional Integral (PI) controller. Chapter 7 proposes an enhancement for the behavior of the PI regulator by introducing the Gain Scheduling Technique (GS), the GS-PI nonlinear control system proves to be more efficient than the PI regulator alone.

Chapter 8 investigates the Optimal Control theory through a Linear Quadratic Regulator (LQR), the design of the LQR is based on a state-space analysis of the rotor-HSFD-control system. This requires the linearization of the nonlinear model of our system presented in Chapter 3. The controller gain matrix is obtained through selecting the weighting matrices which minimize the value of the performance index for best trade-off between performance and cost of control and hence solving the Ricatti equation [26]. The control law requires complete knowledge of the states, and since not all states are measured, thus a continuous Kalman estimator is designed based on the state-space model to reconstruct full-state feedback.

Chapter 9 investigates the adaptive control theory through Model Reference Adaptive Control (MRAC). The gradient approach is used as a regulator through the MIT rule [27]. Also, a selected reference model is accurately chosen to design a good

model following algorithm that would result in a behavior as close as possible to the ideal required behavior of the reference model.

Finally, in Chapter 10, insights into all the control algorithms presented in the thesis with a comparative approach, helps us choose the appropriate regulator for our system that would give the enhanced performance sought after.

CHAPTER 2

DEVELOPMENT OF THE DAMPER AND THE CONTROL CIRCUIT

2.1 Adaptive Hybrid Squeeze Film Damper

In previous studies [28], [29] and [30], it was shown that there are two distinct kinds of SFDs, namely short dampers and long dampers. In short dampers the oil flow is primarily axial and thus the pressure gradient in the axial direction dominates and consequently the short bearing approximation to Reynolds equation applies. In long dampers, on the other hand, the oil flow is primarily circumferential and thus the pressure gradient in the circumferential direction dominates and consequently the long bearing approximation to Reynolds applies. Usually open-ended dampers are considered short dampers [29] and tightly sealed dampers are considered long dampers regardless of the actual physical length of the damper which is usually short with respect to the diameter of the damper [30].

Short dampers and long dampers have very different characteristics [28]. In general, because of their larger damping capacity, long dampers are better at attenuating the amplitude response of the rotor-bearing system; while the short dampers are better at reducing the force transmitted to the support.

The concept of having a damper that would change its characteristics and behave either in the short damper configuration or in the long damper configuration is very attractive. El-Shafei [1] proposed a new concept for actively controlling high speed rotating machinery. The proposed controlling mechanism consists of a hybrid squeeze film damper (HSFD) that can be adaptively controlled to change its characteristics according to the instructions of a controller. In an extreme case the HSFD can act as a long damper which is known to be effective in reducing the amplitude of vibration of rotating machinery. In the other extreme, the HSFD acts as a short damper which is shown to be effective in reducing the force transmitted to the bearings. The design proposed then, was tested experimentally on a Bently Nevada Rotor Kit [1] and showed to be very efficient in controlling the amplitude of vibration and the short damper configuration in reducing the transmitted force.

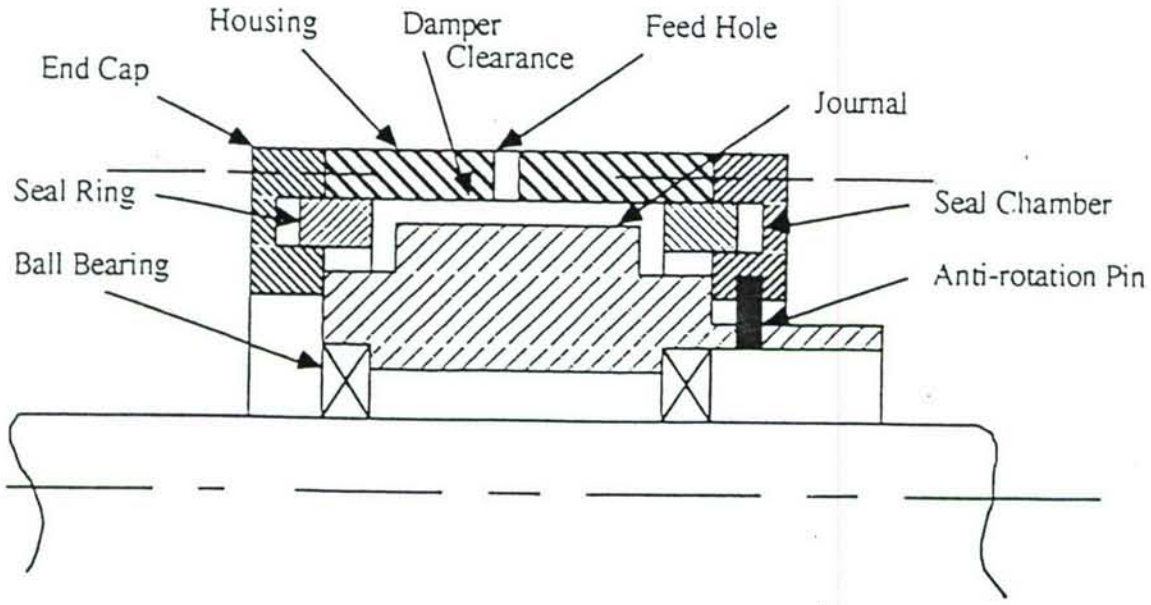

Figure 1 Schematic of the Original HSFD

The original design of the HSFD [1] used two movable metal sealing rings with sliding fit both to the end caps and to the housing, one on each end of the damper as shown in Figure 1. The principle of the seals' operation is simple. The damper oil film and the hydraulically actuated seals are supplied from independently variable sources. In order for the damper to operate as a long damper, the pressure to the seal chambers is elevated above the internal pressure of the damper. The seal rings will move in axially and seal the oil film inside the damper clearance. In order to return the to the short damper configuration, the seal pressure is lowered until it is less than the internal pressure of the damper. This causes the seal rings to return to their original positions.

The design an adaptive HSFD that would give the appropriate amount of damping according to the level of vibration needed to be suppressed is our goal. Thus, we thought of designing an adaptive HSFD that would give several possibilities of finite dampers behaving somewhere in the middle of both the short damper and long damper configurations. Thus, any amount of damping can be achieved from the HSFD provided that the sealing rings can be accurately positioned between the two damper modes. However, when we started the current development stage of the HSFD, we were not able to accurately position the sealing rings with the HSFD design of El-Shafei [1] shown in Figure 1. Therefore, the new design of the adaptive HSFD incorporates a spring that aids in locating the seal ring at any required position.

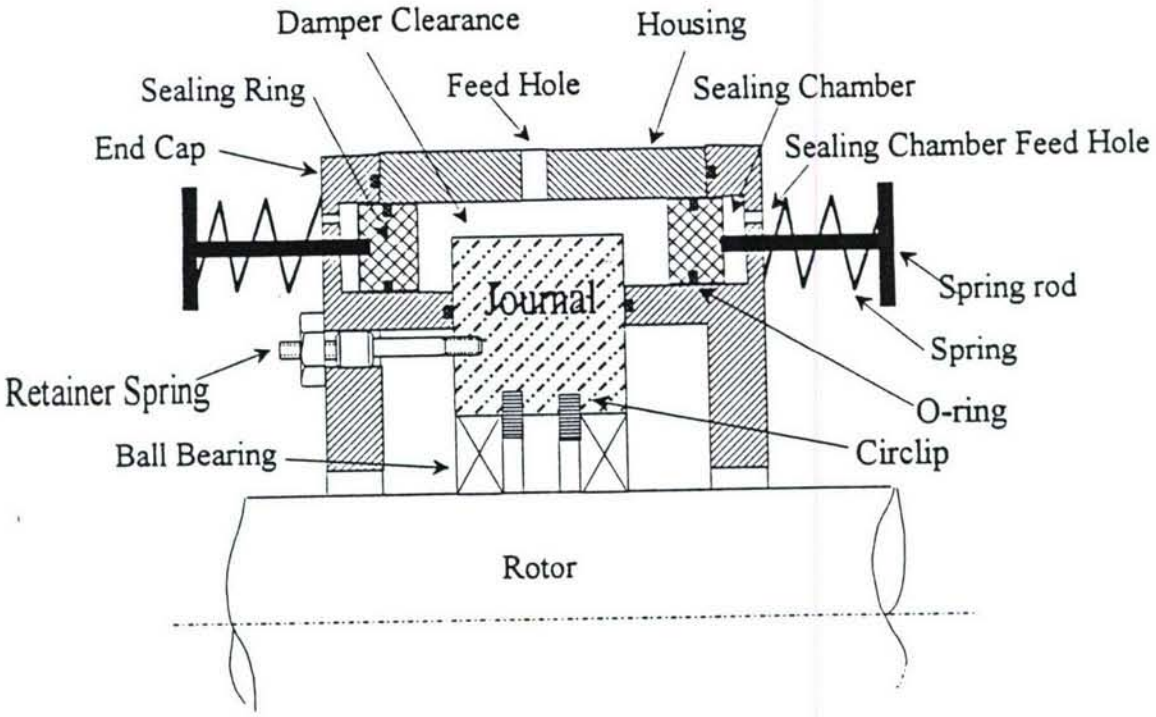

Figure 2. Schematic of the HSFD

Figure 2 shows a schematic of the newly proposed design incorporating springs to achieve the finite damper configuration. The spring is off-load when the damper is acting in the short damper mode. With the help of the spring which is connected to the sealing ring, while the pressure in the sealing chamber is increased, the force exerted on the seal is counteracted by the spring force and hence the accurate positioning of the seal is possible. It should be noted that the design incorporates also retainer springs that center the journal in the casing, i.e. hold the static load of the rotor, and moreover impede the outer race of the bearing to rotate. Thus, the spinning of the rotor does not reach the oil. Only when the rotor whirls, does the oil film act to damp the whirling motion.

2.2 AUTOMATION OF THE HSFD CONTROL CIRCUIT

In the previous testing of the HSFD, the objective of controlling the pressure in the sealing chambers was achieved through manually controlling the flow in the hydraulic circuit (Figure 3) through needle valves [1]. Redundancy was an objective in the design of this circuit.

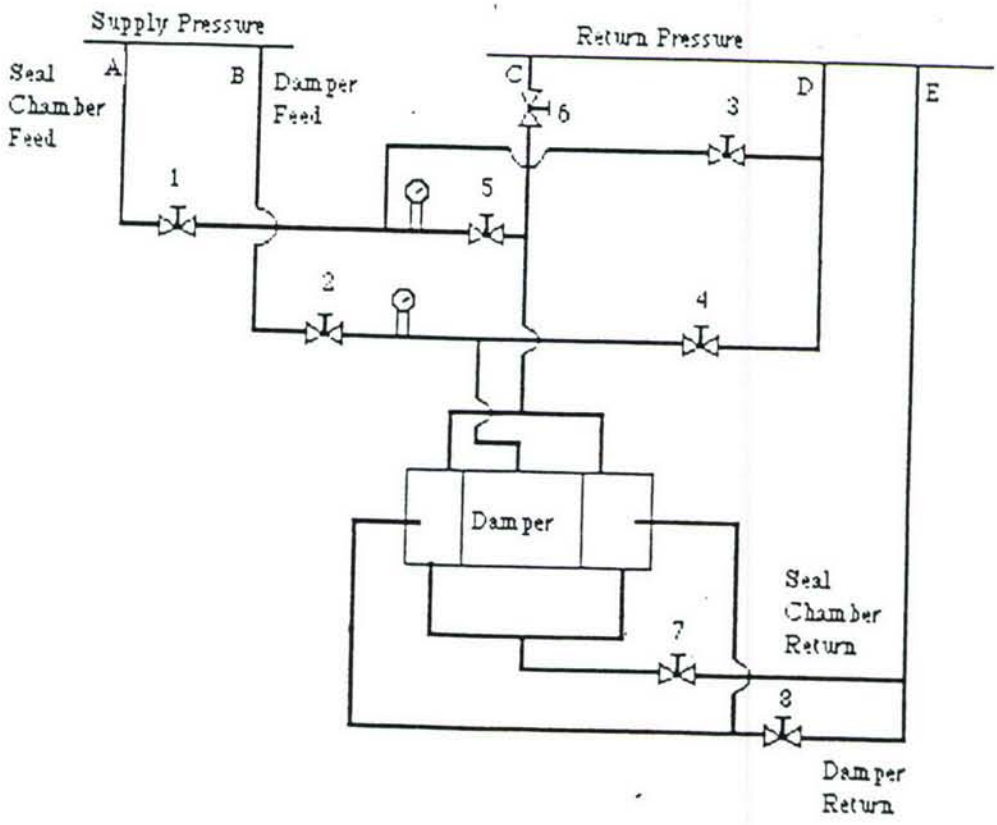

Figure 3 Manual Hydraulic Circuit

In order to achieve the objectives of active control of rotor vibration, the hydraulic circuit needs to be automated, in the sense that electrically controlled valves will be required for the circuit control. Moreover, at this stage of development of the

HSFD, redundancy in the hydraulic circuit is not required and needs to be eliminated. The automated hydraulic circuit of Figure 4 fulfills these objectives. An electrohydraulic pressure control servovalve is used to control the pressure in the sealing chambers. The servovalve is normally closed, however when it receives a current signal (through digital computer control), it connects the supply line, through an orifice, to the sealing chamber, thus increasing the pressure in the sealing chamber. If, on the other hand, a reduction in pressure is required, the servovalve connects the drain, also through an orifice, to the sealing chamber. When the required pressure is achieved the valve is closed.

The pressure control servovalve was chosen over the more common flow control servovalve, since the associated hydraulic circuit is simpler in this particular application, and in addition continuous flow would be required to maintain a constant pressure with the flow control servovalve which is an unnecessary energy loss.

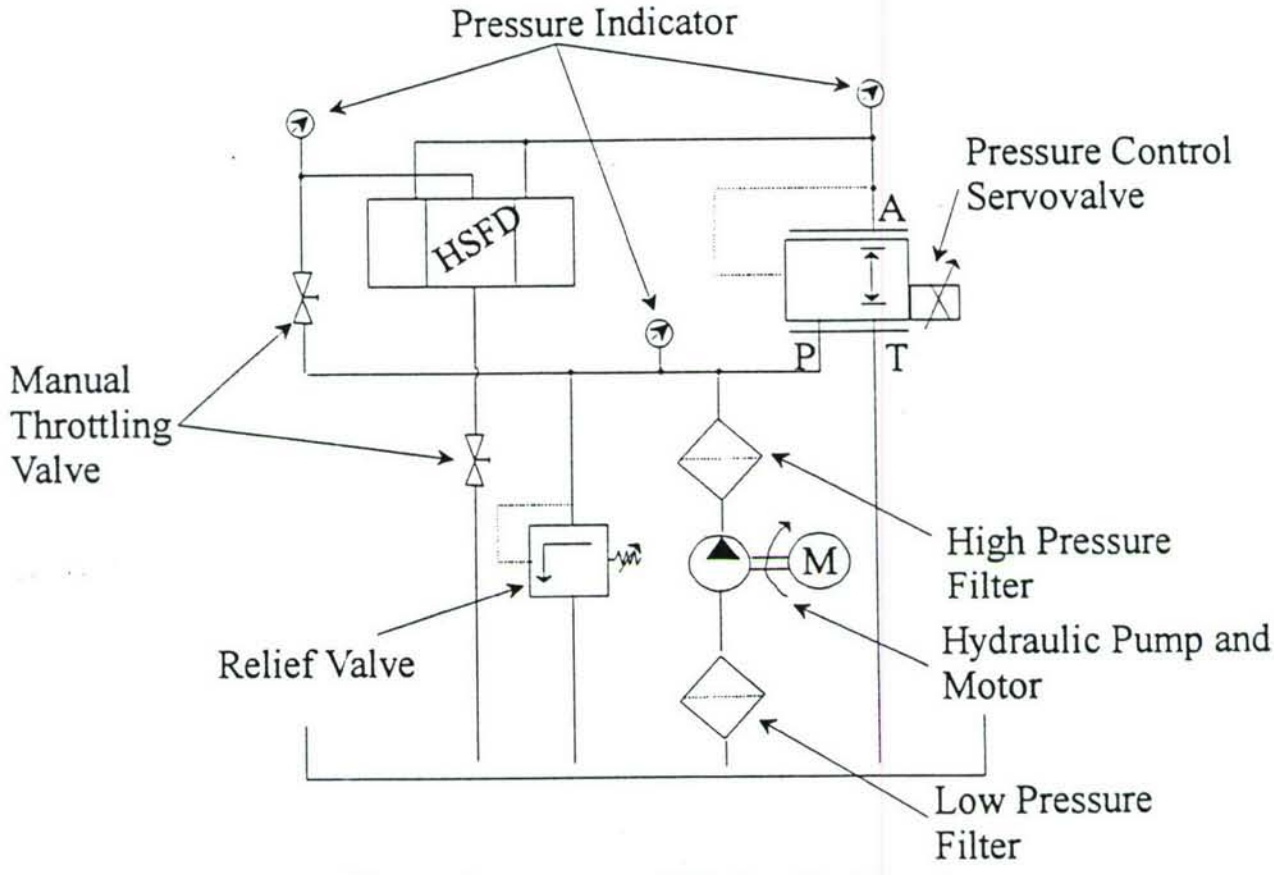

Figure 4. Automated Hydraulic Circuit

Several important features of the automated hydraulic circuit of Figure 4 need to be discussed. Firstly, the supply to the damper is still the same, only a manual throttling valve was added to the circuit to reduce the supply pressure to that required by the damper. The damper drain is also through a needle valve as before. Also, a pressure reducing valve is connected in the damper line to reduce the pressure in the damper to the necessary amount required in the damper. Secondly, the sealing chamber, in this design, has only one port. This port is used to both supply and drain the sealing chamber. Thirdly, the pressure control servovalve is the only component required to control the pressure in the sealing chambers. The feed and drain of the seal

chamber is provided through the pressure control servovalve. This simple design of the automated pressure control circuit provides for an efficient control loop. Moreover, because of the current control of the servovalve, it can be easily interfaced to a computer to provide computer control.

It should be pointed out that there are three supply holes to the damper distributed circumferentially at the center of the damper. It is anticipated that only two ports will be used as supply ports to the damper, while the third port can be used either as a supply to or a drain for the damper. This is useful in the long damper configuration, since in the long damper mode the fluid is trapped in the damper, and the heat generated will cause an increase in the fluid temperature thus decreasing the viscosity of the fluid. This is highly undesirable, and the fluid drained from the center of the damper through a small feed hole will aid in cooling the fluid. However, this may not be sufficient, and in our test rig at Cairo University we have made arrangements (through temperature feedback) to momentarily change to the short damper mode, thus flooding the damper and cooling it, if needed.

CHAPTER 3

COMPLETE MATHEMATICAL MODELING OF THE OPEN-LOOP SYSTEM

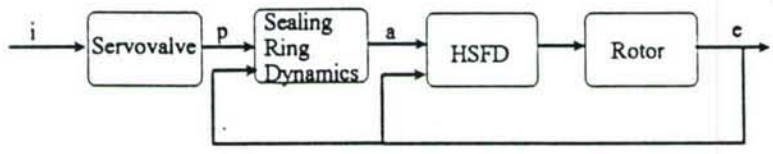

Figure 5. Simplified Block Diagram of the Open-Loop.

The previous sections in this thesis illustrate the development of the design of the HSFD and its associated control circuit. In this section, a mathematical model suitable for implementation on a digital computer, is developed for the HSFD, the control circuit and the rotor. This system was modeled recently by El-Shafei and Hathout [21] and is presented in the thesis for completeness. The HSFD-rotor-control system consists of a pressure control servovalve, the HSFD and the rotor. This system can be considered as an open-loop system, where the current i actuates the servovalve, which in turn controls the pressure p in the sealing chamber, thus controlling the position of the sealing rings, which control the amount of damping applied to the rotor. Figure 5 shows a block diagram of the open-loop system.

It should be emphasized that, as shown in Figure 5, the sealing ring dynamics depend both on the pressure in the sealing chamber p and the pressure in the damper which depends on the eccentricity e of the journal in the damper. In addition, the damping provided by the HSFD depends both on the position of the sealing ring and the eccentricity e. Thus, there is an unmistakable coupling between the whole system in the sense that the rotor behavior depends on the HSFD and the sealing ring dynamics, yet the sealing ring dynamics and the HSFD depend on the rotor behavior. Moreover, it should be stressed that the system under investigation is nonlinear in nature because of the nonlinearity of squeeze film dampers.

In the following paragraphs a complete nonlinear dynamic model of the system shown in Figure 5 will be developed. The differential equations will then be nondimensionalized to scale the variables thus reducing the possibility of numerical difficulties when implementing the model on a digital computer.

The Rotor

It was decided to use the Jeffcott rotor as a model for the first two modes of a test rig, built at Cairo University, both because of the simplicity of the Jeffcott rotor and its resemblance to the test rig rotor. Figure 6 shows a Jeffcott rotor mounted on two identical ball bearings, each of which is surrounded by an HSFD. The outer race of each ball bearing, which is assumed rigid and massless, is constrained from rotating by a retainer spring of stiffness K_r, which also acts to center the journal in the clearance of the oil film. The rotor is assumed massless with a stiffness 2K, the disk is assumed

rigid with mass 2m, and the damping acting on the rotor center has a damping coefficient of 2C.

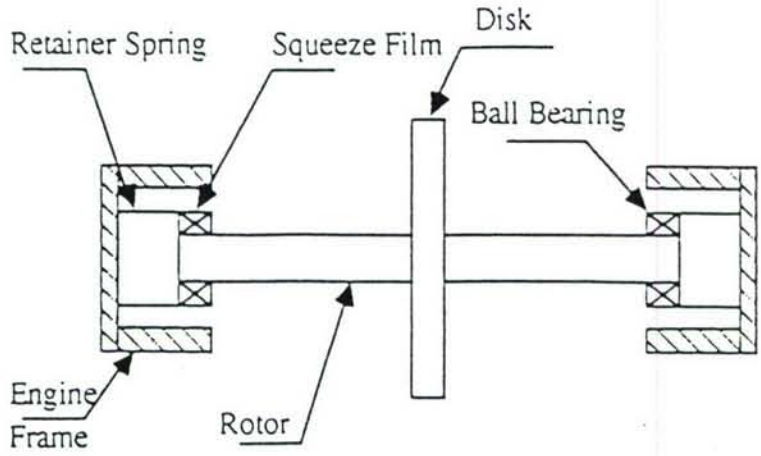

Figure 6 Jeffcott Rotor on HSFDs

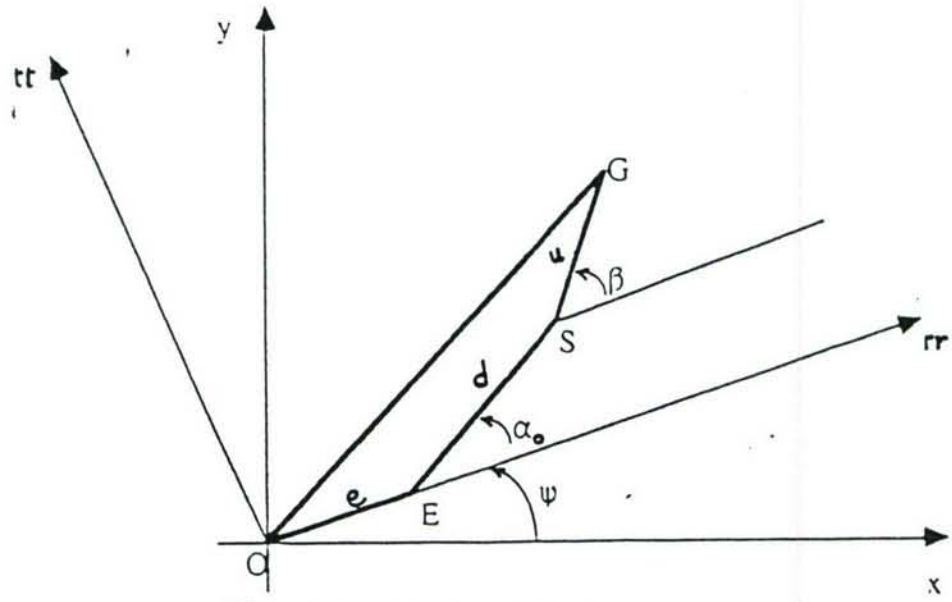

Figure 7 Side View of the Rotor

Figure 7 shows the side view of the Jeffcott rotor of Figure 6. The mass of the disk is centered at the center of gravity G, the geometric center of the disk is at S and the center of the journal is at E, while the center of the damper is O. It can be seen from Figure 7 that due to the unbalance u, the rotor deflects a distance d and the journal has an eccentricity e with respect to the damper. (rr,tt) is the whirling coordinate system and (x,y) represents the stationary coordinate system. For a steady circular whirl $\psi = \omega t$, where ω is the whirling frequency of the journal and t is time. It should be noted that because of the symmetry of the Jeffcott rotor, both ends of the rotor will exhibit similar behavior.

The equations of motion of the center of the disk S are

$$m\ddot{x}_S + C\dot{x}_S + K(x_S - x_E) = m\Omega^2 u\cos\Omega t - m\alpha u\sin\Omega t \qquad (1)$$

$$m\ddot{y}_S + C\dot{y}_S + K(y_S - y_E) = m\Omega^2 u\sin\Omega t + m\alpha u\cos\Omega t \qquad (2)$$

where x_S, y_S, x_E, and y_E are the positions of the center of the disk S and the center of the journal E, respectively, in the (x,y) frame of Figure 7, u is the unbalance at the disk, t is the time in seconds, Ω is the rotational speed, and α is the rotational acceleration of the rotor.

Assuming that the rotor journal has a mass m_b, (which would include the part of the rotor lumped at the damper location), the equations of motion of the journal center E are

$$m_b\ddot{x}_E + C_{xx}\dot{x}_E + C_{xy}\dot{y}_E + K(x_E - x_S) + K_r x_E = 0 \quad (3)$$

$$m_b\ddot{y}_E + C_{yx}\dot{x}_E + C_{yy}\dot{y}_E + K(y_E - y_S) + K_r y_E = 0 \quad (4)$$

where C_{xx}, C_{xy}, C_{yx}, and C_{yy} are the damping coefficients of the HSFD. A model of the HSFD that does not include fluid inertia is used. This is a simplifying assumption that is deemed necessary at the development stage of the control algorithm because of the simplicity afforded. It should be noted that the effect of fluid inertia can be approximately introduced by judiciously increasing m_b [31]. In addition it is assumed that the damper is pressurized and operates uncavitated. The main effect of cavitation is to reduce the damping, by as much as a factor of 2, and to possibly introduce undesirable nonlinear vibrations such as jump resonance [29]. Usually, aircraft engines have a supply pressure of 4 bar to 5.5 bar. In some applications this may be adequate in suppressing cavitation. In order to develop a robust controller a simple model will be needed and we chose to follow an uncavitated model in the control development. Cavitation can be avoided experimentally by using a supply pressure to the damper as high as 14 bar in our test rig. The damping coefficients for uncavitated short and long dampers are well known and are used here in a stationary cartesian frame [32].

It should be noted that in equations (3) and (4) we have neglected the effect of friction of the metallic sealing rings on the journal face in the long damper mode. This may be an important consideration, however, communication with aircraft engine manufacturers indicated that such an effect is minimal in SFD applications in aircraft

engines. We intend to investigate this effect experimentally, but all the results that are shown in this thesis rely on a model that does not include the effect of the friction of the sealing ring on the journal, and the results show that the HSFD can be very effective in controlling rotor vibrations.

The Hybrid Squeeze Film Damper

The damping coefficients where C_{xx}, C_{xy}, C_{yx}, and C_{yy} for the HSFD should reduce to those of the short damper at one extreme and to those of the long damper at the other extreme. To incorporate the effect of a finite damper in the HSFD model, a simple model due to Holmes and Dogan [9] is used, which is simply a linear combination of the short damper model and the long damper model. Thus

$$C_{ij} = \lambda C_{ijs} + (1-\lambda) C_{ijl} \tag{5}$$

where λ is a measure of the finiteness of the damper, and C_{ijs} and C_{ijl} represent the short and long damper coefficients, respectively, and i and j take the values x and y. This model simply says that if λ is equal to zero, then we have the long damper model, and if λ is equal to one, then we have the short damper model. For any intermediate value for λ between 0 and 1 we obtain the corresponding finite damper.

Holmes and Dogan [9] obtained experimentally the appropriate value of λ for the damper they were studying. Moreover, they were able to show that a damper with an end seal at a distance from the end equal to the radial clearance c approaches the

short damper, and a damper with a closed end will approach the long damper. Thus in our model of the HSFD we take the factor λ to be equal to the ratio a/c, where a is the distance of the seal ring from the end of the damper.

It is customary to obtain the damping coefficients for short and long dampers in the (rr,tt) frame shown in Figure 7. In order to use the damping coefficients with the (x,y) coordinate system, to be used in equations (3), (4) and (5), then we need to make a transformation from the (rr,tt) frame to the (x,y) frame. Thus [32],

$$C_{xx} = [C_{rr}\cos^2\psi - C_{rt}\sin\psi\cos\psi - C_{tr}\sin\psi\cos\psi + C_{tt}\sin^2\psi]$$

$$C_{xy} = [C_{rr}\sin\psi\cos\psi + C_{rt}\cos^2\psi - C_{tr}\sin^2\psi - C_{tt}\sin\psi\cos\psi]$$

$$C_{yx} = [C_{rr}\sin\psi\cos\psi - C_{rt}\sin^2\psi + C_{tr}\cos^2\psi - C_{tt}\sin\psi\cos\psi]$$

$$C_{yy} = [C_{rr}\sin^2\psi + C_{rt}\sin\psi\cos\psi + C_{tr}\sin\psi\cos\psi + C_{tt}\cos^2\psi]$$

The above transformation equations are valid for both the short and long damper coefficients [32] and hence for the HSFD. The damping coefficients in the (rr,tt) frame for the short and long dampers are well known (see, for example, [31]). However, a minor complication occurs in determining the cavitation boundaries in SFDs. The Gumbel boundary conditions are usually used in analytical work because of their simplicity, but even then the instantaneous position and extent of the film will depend

on the instantaneous position and velocity of the journal [32]. To avoid this complication, many investigators assume a circular centered orbit for the journal in the damper in the steady state, for which the cavitated film reduces to a π–film. However, this is not valid here since we are interested in the behavior of the control system and the rotor, thus the transient behavior is equally important in addition to the steady state behavior.

To avoid this complication and to simplify the modeling, we are going to assume an uncavitated damper. This assumption is justified by the simplicity in modeling and the need to obtain results representative of the system behavior in a short period of time. Moreover, the essential behavior of the system is retained with the uncavitated damper and thus the performance of the control system can be adequately anticipated with such a model. For an uncavitated damper, the damping coefficients for the short and long damper are given by [31]

$$C_{rrs} = \frac{\pi(1+2\varepsilon^2)}{(1-\varepsilon^2)^{5/2}} \qquad C_{tts} = \frac{\pi}{(1-\varepsilon^2)^{3/2}}$$

$$C_{rrl} = \frac{12\pi}{(1-\varepsilon^2)^{3/2}} \qquad C_{ttl} = \frac{24\pi}{(2+\varepsilon^2)(1-\varepsilon^2)^{1/2}}$$

and C_{rt} and C_{tr} are equal to zero for both the short and long dampers. The damping coefficients are function of the eccentricity ratio ε and their behavior with different ε value is well known and illustrated in [31].

The Sealing Rings Dynamics

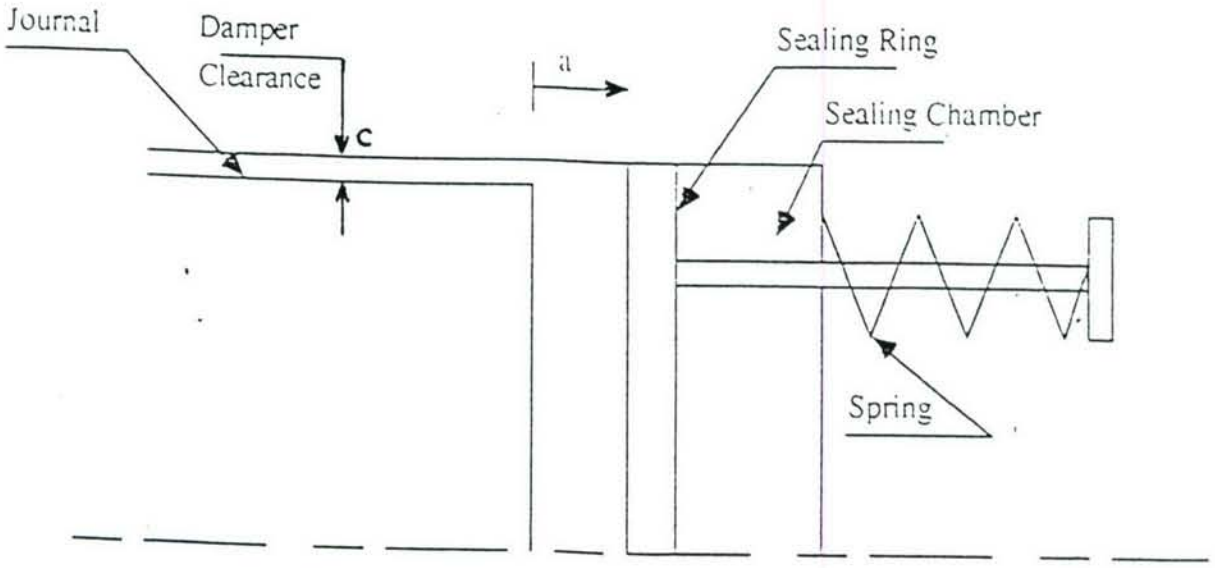

Figure 8 Schematic of the Sealing Rings

Figure 8 shows a schematic of the sealing ring. The position of the sealing ring from the journal end is the distance a. The forces acting on the ring are those due to the pressure in the sealing chamber, the pressure at the journal end, the spring stiffness, and possibly some damping acting on the sealing ring. Thus the equation of motion of the sealing ring becomes

$$m_r\ddot{a} + C_1\dot{a} + K_s(a - a_{max}) = F_d - pA_r \tag{6}$$

where m_r is the mass of the sealing ring, F_d is the force at the journal end, p is the pressure in the sealing chamber, A_r is the area of the sealing ring exposed to the pressure p, K_s is the spring stiffness, and C_1 is the damping coefficient on the sealing ring. The maximum travel of the sealing ring a_{max} can be taken equal to the radial clearance c, since the HSFD achieves the short damper mode by placing the sealing ring at a distance equal c [9].

To obtain the force F_d acting on the sealing ring due to the pressure in the damper, the pressure at the end of the journal is integrated over the exposed area of the sealing ring. Thus

$$F_d = \int_{\theta_1}^{\theta_2} \int_{R+c-h}^{R+c} p_d r dr d\theta \tag{7}$$

where $\theta_1$and θ_2 equal respectively 0 and 2π for an uncavitated damper, p_d is the damper pressure at the journal end, R is the journal radius, and h is the film thickness given by

$$h = c - e\cos\theta$$

The pressure at the journal end is assumed to have the same behavior as the damping coefficients, equation (5), in the sense that it is assumed to be a linear combination of the pressure at the journal end for the short damper case and that for the long damper case [21]. However, for the short damper case the pressure at the journal end is assumed to be zero gage, since it is directly connected to the drain. Thus, the pressure at the journal end for the HSFD is given by

$$p_d = (1-\lambda)p_{dl}$$

where P_{dl} is the pressure in the long damper which is given by [33]

$$p_{dl} = \left(\frac{6\mu R^2}{c^3}\right)\left(\left[\frac{1}{\varepsilon(1-\varepsilon\cos\theta)^2} - \frac{1}{\varepsilon(1+\varepsilon)^2}\right]\dot{e} + \left[\frac{2\sin\theta(2-\varepsilon\cos\theta)}{(2+\varepsilon^2)(2-\varepsilon\cos\theta)}\right]e\dot{\psi}\right)$$

where ε is the eccentricity ratio e/c, and $\dot{e}$ and $e\dot{\psi}$ are the radial and tangential velocities of the journal, respectively. The journal velocities in the (x,y) are related to the frame radial and tangential velocities of the journal by

$$\begin{Bmatrix}\dot{x}_E\\ \dot{y}_E\end{Bmatrix} = \begin{bmatrix}\cos\psi & -\sin\psi\\ \sin\psi & \cos\psi\end{bmatrix}\begin{Bmatrix}\dot{e}\\ e\dot{\psi}\end{Bmatrix}$$

Substituting the above equations into equation (7), and performing the integrations neglecting terms O(c/R) and assuming an uncavitated film in the damper as before, the force F_d becomes

$$F_d = \frac{6\mu R^3(1-\lambda)}{c^2}\frac{2\pi}{\varepsilon}\left[\frac{1}{(1-\varepsilon^2)^{0.5}} - \frac{1}{(1+\varepsilon)^2}\right]\{\dot{x}_E\cos\psi + \dot{y}_E\sin\psi\} \qquad (8)$$

where ε = e/c and

$$e = \sqrt{x_E^2 + y_E^2} \qquad \text{and} \qquad \psi = \tan^{-1}\frac{y_E}{x_E}$$

Servovalve

The pressure control electrohydraulic servovalve provides a pressure increase or decrease in response to a current input. Thayer [34] reports that the dynamic characteristics of the pressure control servovalve can be adequately represented by

$$\frac{\ddot{p}}{\omega_{n1}^2} + \frac{2\zeta_1}{\omega_{n1}}\dot{p} + p = K_1 i \tag{9}$$

where p is the controlled pressure, i is the input current (which usually has a maximum value of 10 mA), K_1 is the valve's static gain (usually of the order 0.9 MPa/mA), ζ_1 is the valve's apparent damping ratio (usually between 0.3 and 0.5), and ω_{n1} is the valve's apparent natural frequency (usually of the order of 250 Hz).

Equations (1) to (6), (8) and (9) constitute a complete model of the open loop control system for the hydraulic-HSFD-rotor system. It is desirable to nondimensionalize the governing equations before implementing them on a digital computer. This is because the nondimensional equations are less prone to numerical difficulties since the parameters and variables are scaled, and also the nondimensionalization results in a reduced number of parameters and generalizes the analysis.

To nondimensionalize the system equations we define the following nondimensional quantities:

$\varepsilon = e/c$ = eccentricity ratio

$\bar{x}_i = x_i/c$ = nondimensional x-displacement at the journal center E ($i = E$), or at the disk center S ($i = S$)

$\bar{y}_i = y_i/c$ = nondimensional y-displacement at the journal center E ($i = E$), or at the disk center S ($i = S$)

$U = u/c$ = nondimensional unbalance

$K^* = K/m\omega_n^2$ = nondimensional rotor stiffness

$K^*_r = K_r/m\omega_n^2$ = nondimensional retainer spring stiffness

$\Omega^* = \Omega/\omega_n$ = nondimensional rotor speed

$\alpha^* = \alpha/\omega_n^2$ = nondimensional rotor angular acceleration

$\eta = C/m\omega_n$ = damping loss factor for the rotor

$R_k = K_r^*/K^*$ = stiffness ratio

$m_o = m/m_b$ = mass ratio

$\lambda = a/c$ = measure of the finiteness of the HSFD

$\bar{C}_{ij} = C_{ij}/m\omega_n$ = nondimensional damping coefficients.

$B_S = \mu R^3/m\omega_n c^3$ = bearing parameter for the short damper

$B_l = B_S\,(R^2/L^2)$ = bearing parameter for the long damper

$\eta_1 = C_1/m_r\omega_n$ = damping loss factor at sealing ring

$K^*_S = K_S/m_r\omega_n^2$ = nondimensional spring stiffness

$F_d^* = F_d/m_r c\omega_n^2$ = nondimensional force at journal end.

$B_e = \mu R^3/m_r\omega_n c^2$ = end force coefficient

$p^* = pA_r/m_r c\omega_n^2$ = nondimensional pressure in sealing chambers

$\omega_r^* = \omega_{n1}/\omega_n$ = nondimensional ratio of natural frequencies

$K^*_I = K_I i_{max} A_r / m_r \omega_n^2$ = nondimensional valve gain

$i_O = i / i_{max}$ = nondimensional current.

$\tau = \omega_n t$ = nondimensional time

and ( )′ = denotes differentiation w.r.t. τ.

where i_{max} is the maximum current at the servovalve, $\omega_n^2 = (K_{eq}/m)$ is the first natural frequency of the rotor-bearing system and $K_{eq} = K_r K/(K_r+K)$ is the equivalent stiffness of the rotor and the retainer spring. The damper effect on the stiffness of the rotor system is due to its nonlinearity, and is included in our model within the nonlinear damping coefficients. It should be noted that since we chose to nondimensionalize the parameters by using the natural frequency ω_n, then K^* and K_r^* are determined completely by knowledge of R_k, since $K_{eq}^* = 1$, then

$$K^* = 1 + 1/R_k$$

and $$K_r^* = 1 + R_k$$

The nondimensional form of equations (1) and (2) is obtained by dividing through by $m\omega_n^2 c$, thus (1) and (2) become

$$\bar{x}_S'' + \eta \bar{x}_S' + K^*(\bar{x}_S - \bar{x}_E) = \Omega^{*2} U \cos\Omega^* \tau - \alpha^* U \sin\Omega^* \tau \qquad (10)$$

$$\bar{y}_S'' + \eta \bar{y}_S' + K^*(\bar{y}_S - \bar{y}_E) = \Omega^{*2} U \sin\Omega^* \tau + \alpha^* U \cos\Omega^* \tau \qquad (11)$$

Similarly, dividing equations (3) and (4) by $m\omega_n{}^2c$, we get

$$\bar{x}_E'' + m_o\bar{C}_{xx}\bar{x}_E' + m_oC_{xy}\bar{y}_E' + m_oK^*(\bar{x}_E - \bar{x}_S) + m_oK_r^*\bar{x}_E = 0 \qquad (12)$$

$$\bar{y}_E'' + m_o\bar{C}_{yx}\bar{x}_E' + m_o\bar{C}_{yy}\bar{y}_E' + m_oK^*(\bar{y}_E - \bar{y}_S) + m_oK_r^*\bar{y}_E = 0 \qquad (13)$$

Dividing equation (5) by $m\omega_n$, we get

$$\bar{C}_{ij} = B_s[\lambda C_{ijs}^* + (1-\lambda)\frac{R^2}{L^2}C_{ijl}^*] \qquad (14)$$

where C_{ijs}^* and C_{ijl}^* are the nondimensional short and long damper coefficients. Also, dividing equation (6) by $m_r\omega_n{}^2c$, we get

$$\lambda'' + \eta_1\lambda' + K_S^*(\lambda - 1) = F_d^* - p^* \qquad (15)$$

To obtain F_d^*, we divide equation(8) also by $m_r\omega_n{}^2c$, thus

$$F_d^* = \frac{12\pi}{\varepsilon}B_e(1-\lambda)\left[\frac{1}{(1-\varepsilon^2)^{0.5}} - \frac{1}{(1+\varepsilon)^2}\right]\{\bar{x}_E'\cos\psi + \bar{y}_E'\sin\psi\} \qquad (16)$$

Finally, multiplying equation (9) by $A_r/\ m_r\omega_n{}^2c$, we get

$$p^{*''} + 2\zeta_1\omega_r^*p^{*'} + \omega_r^{*2}p^* = \omega_r^{*2}K_1^*i_o \qquad (17)$$

Equations (10) to (17) constitute the complete nondimensional nonlinear mathematical model for the open loop system of Figure 5. This model is used in the simulations described in the next chapter.

CHAPTER 4

SIMULATION OF THE BEHAVIOR OF THE OPEN-LOOP CONTROL SYSTEM

To simulate the behavior of the open-loop system, the equations developed in the previous chapter describing the dynamics of the complete open-loop system are implemented on a digital computer. The purpose of the simulations is to illustrate the transient behavior of the open-loop system, in particular the response of the system to a current signal at the servovalve and its effect on the dynamics of the rotor and the sealing ring in the HSFD. Moreover, simulations on the open-loop control system were used to select appropriate values for some of the system parameters that were not selected in the design of the rotor and the HSFD, and were left to be determined from the simulation of the dynamical behavior of the system. Also, simulations would investigate the behavior of the system in the stability point of view. Since the modeling and the simulation of the system were done in parallel with the design of the rotor and the HSFD, the initial simulations were done with parameter values that were perceived appropriate for the application at hand. However, the later simulations, which are the only ones reported in this thesis, are based on the actual parameter values selected for the rotor and the HSFD on our test rig in Cairo University.

An in-house package is developed to integrate the set of differential equations describing the open-loop system. Simulations were carried out by using the Runge-

Kutta 4 integration technique which is known for its robustness in handling nonlinear dynamic systems. The step size used was 0.001 and showed to be suitable. In order to perform the integration on the system's differential equations, the differential equations (10) to (13), (15) and (17) are first transformed to a set of 12 first order differential equations (i.e. they are put in state variable format). These 12 differential equations along with equations (14) and (16) are implemented in a system model suitable for numerical integration. In all simulations presented in this work, the initial conditions were taken as:

$$\bar{x}_E = \bar{y}_E = 0.001, \lambda = 1, \text{and all other values equal to zero.}$$

Early simulations indicated that the value of λ can become negative. Since this is impossible, because when $\lambda = 0$ the sealing ring is in contact with journal and cannot go beyond that, it was decided to modify the model in order to restrict λ in the positive range only. Thus if λ becomes negative, the modified model automatically sets it equal to zero.

The parameter values used in the simulations are as follows:

$m_o = 9.9,$

$\eta = 0.01,$

$K^* = 3.6,$

$K_r^* = 1.384,$

$R^2/L^2 = 2.25,$

$B_s = 0.01295,$

$B_e = 0.09881,$

$\zeta_1 = 0.5,$

$\omega_r^* = 8.278,$

$K_1^* = 10528,$

and $U = 0.1.$

The above nondimensional parameters correspond to the rotor design parameters at the first critical speed, and the design parameters of the HSFD.

While performing early simulations, the nondimensional valve's gain parameter K_1^* taken to be 10528 showed to be quite inappropriate for our control system. It was quickly realized that with such a high gain, the valve supplies pressure to the sealing chambers that would cause the damper to be in the long damper mode in response to even the smallest of servovalve's input current. The simulations showed that acceptable behavior can be achieved by choosing K_1^* to be 105, that's a hundred times smaller than the original value. It was decided to continue simulations using this value, since it would be possible to place an attenuator in the control circuit to significantly lower the circuit gain.

The servovalve's parameters were selected from Moog's technical bulletin [32]. A closer investigation revealed that $K_1^* = 10528$ corresponds to a valve's gain $K_1 = 0.861$ MPa/mA (125 psi/mA) for a 6.89 Mpa (1000 psi) supply pressure servovalve. Since we certainly do not need a 6.89 MPa servovalve (a 1.4 MPa servovalve will suffice, if available) it is conceivable that the valve's gain could be

considerably lower. This point was investigated further with our valve's manufacturers [32], and a pressure control servovalve of gain approximately equal to the one chosen for simulations was found and currently working on our experimental test rig.

In addition, the rotor was assumed to be running steadily at its fundamental critical speed, thus

$\Omega^* = 1.0$

$\alpha^* = 0$

This leaves only two parameters yet to be determined. These are K_s^* and η_1, the nondimensional stiffness and loss factor at the sealing rings. These parameters were left to be determined by trial and error, based on the simulation of the dynamic behavior of the system. It should be pointed out that the spring and the damping at the sealing rings are only being used to accurately position the sealing ring at intermediate positions against the pressure in the sealing chambers, as discussed earlier in Chapter 2.

The control algorithm sought for requires us to have for the same short damper mode of the HSFD, a long damper that will be effective in suppressing the critical speeds. The HSFD parameters were chosen such that the long damper will be effective in suppressing the critical speeds. For the same long damper dimensions, a short damper will provide much less damping and thus allows a flexibility in providing damping to the rotor system. Therefore, we chose to decrease the damping in the HSFD. The decrease of damping in the HSFD is achieved by increasing the clearance

c of the damper. In general, the design of the HSFD should be optimized for suppressing the critical speeds in the long damper mode. This is a good design methodology, that will also result in a relatively large clearance damper which would allow the HSFD to be effective in attenuating the high amplitudes in the long damper mode, and moreover to be an effective high load damper.

Several simulations were performed in order to find the appropriate values of K_s^* and η_1. It was finally decided to use the values $K_s^* = 31$ and $\eta_1 = 0.08$. These values of the nondimensional spring stiffness and the loss factor correspond to Ks = 50 N/mm and a damping ratio of 0.007 approximately. With these values it is possible to place the sealing ring anywhere in the sealing chamber. An example that illustrates the ability to position the sealing ring in any intermediate position is shown in Figure 11 and will be discussed later.

It should be noted that the time scale in all the time simulations is in nondimensional time τ, and thus a unity in the time axis in the plots will represent 5.3 milliseconds.

Figure 9 illustrates the transient behavior of the open-loop control system during operation. The simulation is started with zero input current to the servovalve, i.e. short damper mode. At $\tau = 75$, the current is suddenly switched to $i_o = 0.31$ (Figure 9(a)), which is enough to change from the short damper mode to the long damper mode, i.e. a step change in the current is applied at $\tau = 75$. Figures 9 (b) and (c) illustrate the behavior of the pressure in the sealing chambers p^* and λ to the step

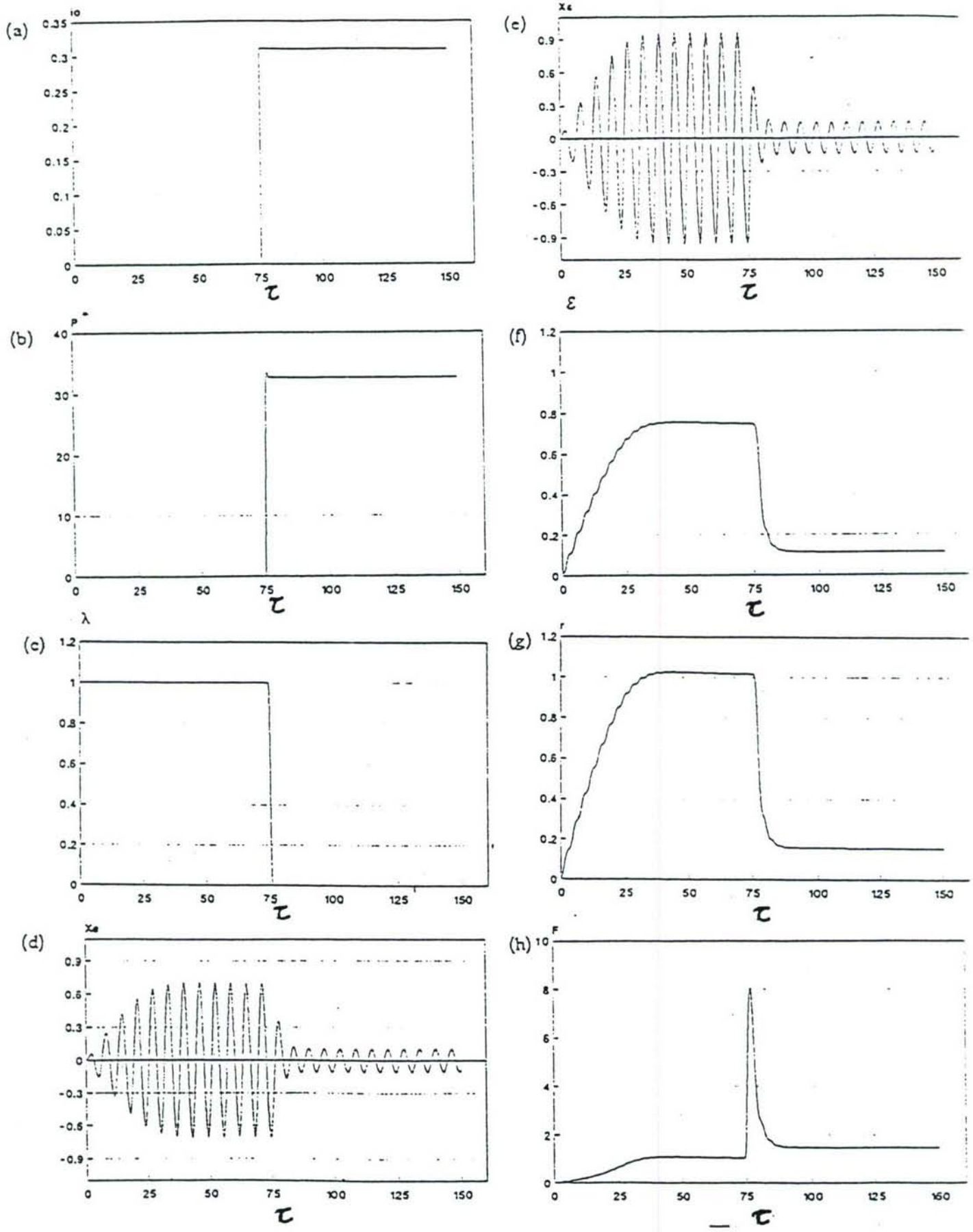

Figure 9 Simulation of the Transient Behavior of the Open-Loop Control System while Switching from the Short Damper Mode to the Long Damper Mode

change in the input current. It can be seen that both p^* and λ respond almost immediately with a step in their magnitudes. There is a little transient spike in p^* that quickly disappears. The long damper mode is thus achieved in very little time. Figures 9 (d) and (e) illustrate the displacements of the journal and the disk at the change from short to long damper modes for U = 0.1. Also, Figures 9 (f), (g) and (h) show the transient behavior from short damper to long damper modes of the eccentricity ratio ε, the amplitude at the disk center r, and the transmitted damping force F to the bearings. These Figures show a graphic display of the power and usefulness of the HSFD. The large amplitude oscillations in the short damper mode are replaced by the small oscillations in the long damper mode, after a short transient time of about τ = 5 to 10, which corresponds to about 0.0265 to 0.053 seconds. In addition, Figure 9 shows that the transient response of the open-loop system is fast, stable, generally well behaved and achieves the required behavior.

An additional simulation was performed to study the behavior of the change from the long damper mode to the short damper mode. This simulation was done to see if the pressure in the damper and the spring action would be enough to drive the sealing ring to the short damper position (λ = 1). Hence, an input current of i_o = 0.31 is entered to the pressure control servovalve at τ = 0, this obliges the HSFD to switch to the long damper mode, then the current is shut to zero at τ = 75 to switch the HSFD to the short damper mode. Figure 10 shows the transient behavior of the system in response to this change of current. The response is very fast, and the sealing ring motion λ (Figure 10 (c)) reaches the short damper position, i.e. λ = 1, without oscillation but rather in a decayed motion after a small transient spike. The decay

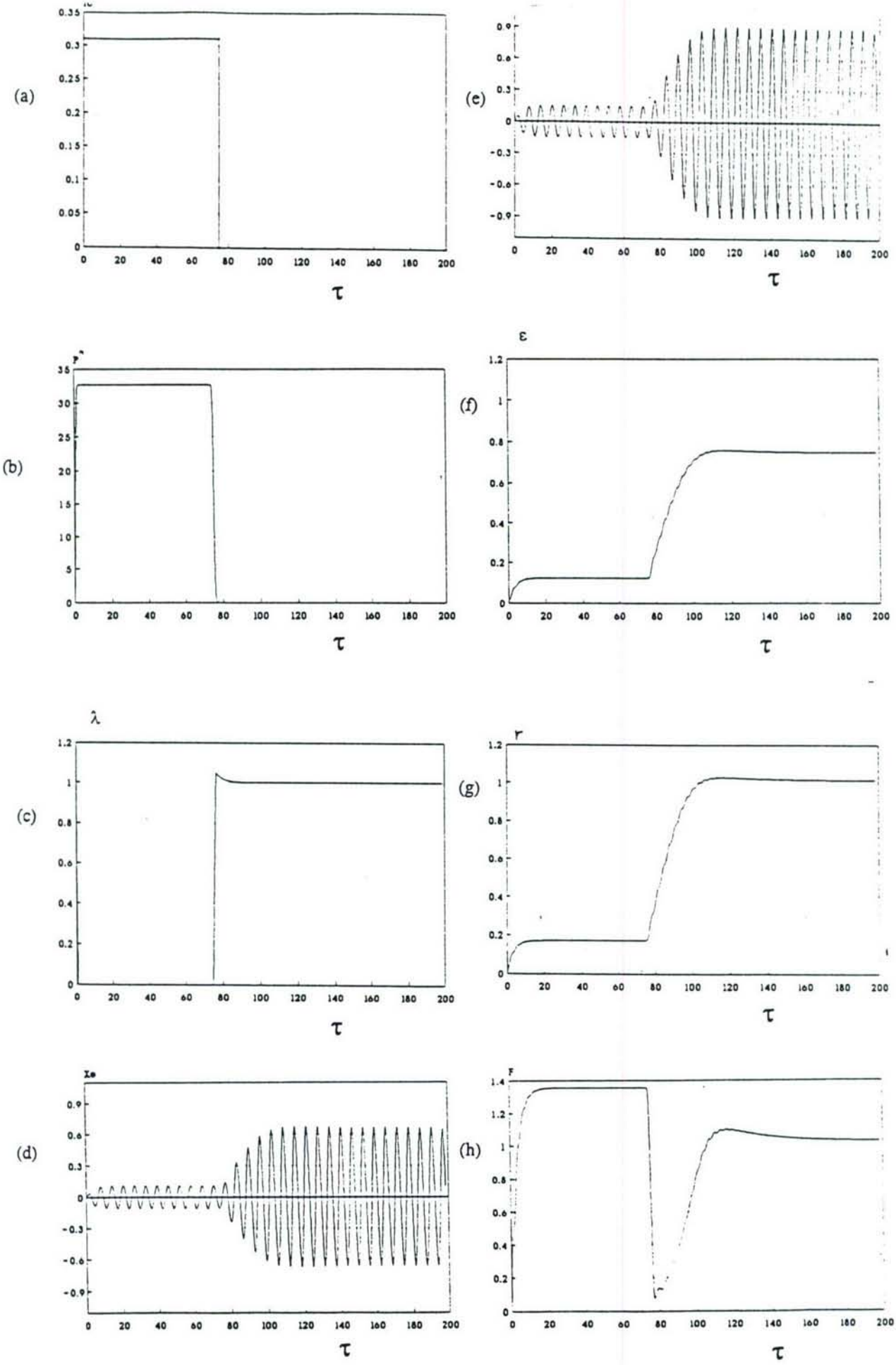

Figure 10 Simulation of the Transient Behavior of the Open-Loop Control System while Switching from the Long Damper Mode to the Short Damper Mode

transient time takes about $\tau = 20$, i.e. 0.106 seconds, for the sealing ring to reach the short damper mode position.

The above two simulations for a step change in current resulting in a step change in amplitude response are quite dramatic and are in fact the objective of this investigation, in the sense that it is required to change the rotor behavior by actively controlling it. This has been achieved in the open-loop sense. The next step is to use feedback in order to investigate the various methods of achieving this on-off control automatically.

Furthermore, the finiteness of the damper, i.e. the capability of the HSFD to behave as a finite damper between the short and the long damper configuration, is investigated. Thus, this would allow us to design other control techniques that would depend primarily on the adaptability of the HSFD. The simulation shown in Figure 9 is repeated in Figure 11, but with a smaller step change in current, resulting in a step change in λ equal to 0.5 approximately, i.e. a finite damper, among many others possible, is achieved rather than either long or short damper modes. In the work of El-Shafei [1], the HSFD operated only as a short damper or as a long damper and it was suggested that any amount of damping can be achieved from the HSFD provided that the sealing rings can be accurately positioned between the two damper modes. However, when we started the current developmental stage of the HSFD, we were not able to accurately position the sealing rings with the HSFD design of El-Shafei [1] shown in Figure 1. Alternatively, we have added a spring connected to each sealing ring such that the spring acts against the applied pressure in the sealing chamber, as

shown in Figure 2, thus providing a means of controlling the sealing rings' position. Figure 11 illustrates that the finite damper can be achieved actively with this configuration, and as expected provides more damping than the short damper, but less damping than the long damper as compared with previous simulations. This means that the controller can provide any amount of damping to the rotor that is needed to achieve the required behavior under any operating conditions, provided that the amount of damping required is between the short and the long damper modes.

Figure 11 (c) shows that λ, i.e. the seal ring, oscillates for time $\tau = 25$ i.e. for 0.1325 seconds about its equilibrium position before stopping at $\lambda = 0.5$. This oscillation is caused by the spring attached to the sealing ring. This is an undesirable oscillation, that can affect the performance of the system, thus additional damping at the sealing rings will be required to dampen this oscillation. However, because of the uncertainty of the amount of damping in our test rig, this point will be investigated experimentally further on. However, this bad oscillation can be compensated when control techniques will be used as it will be shown in coming chapters concerned with the development stages of different control algorithms.

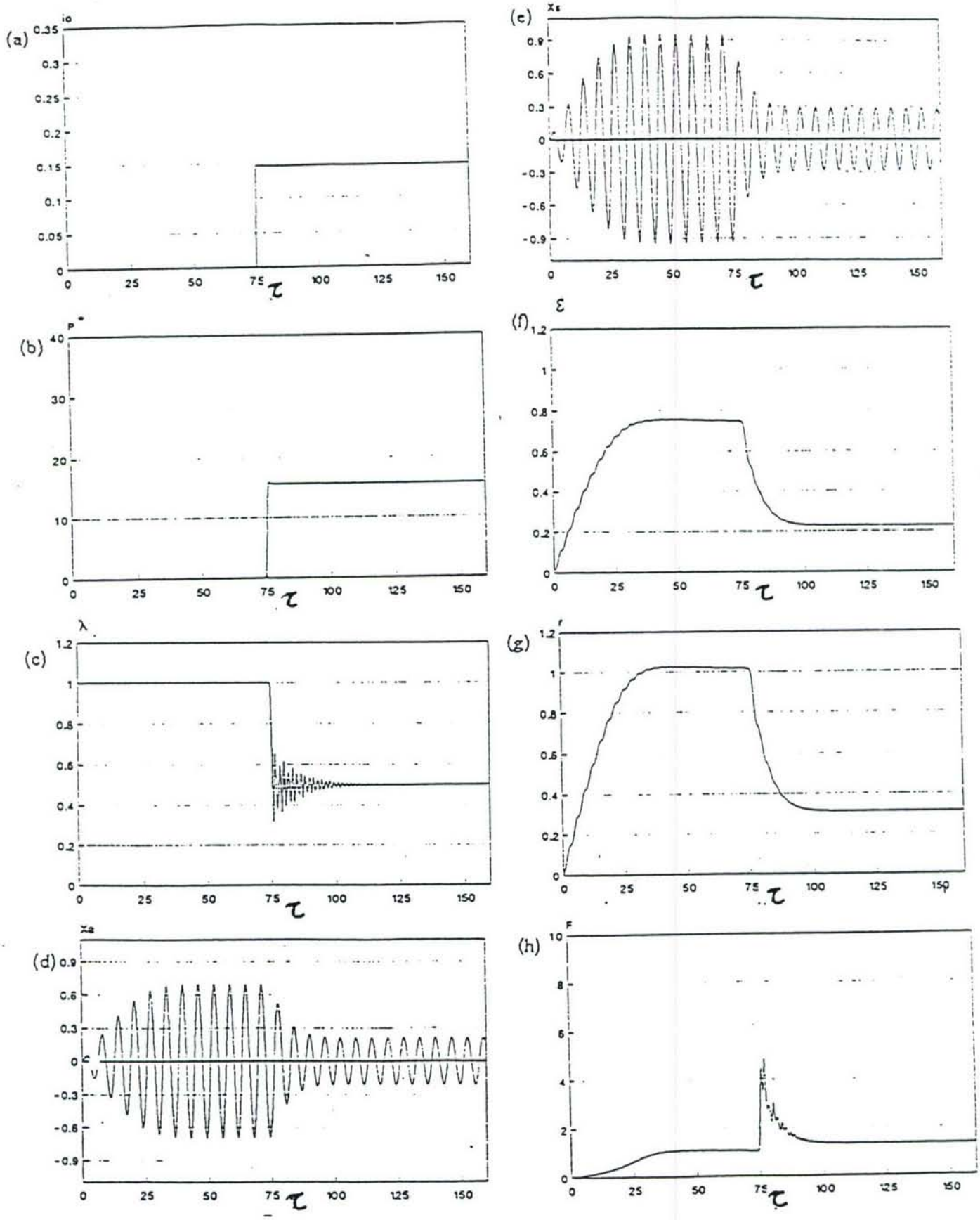

Figure 11 Simulation of the Transient Behavior of the Open-Loop Control System while Switching from the Short Damper Mode to the Finite Damper Mode

CHAPTER 5

CONTROL DEVELOPMENT THROUGH AN ON-OFF CONTROLLER

It is required to develop an active control algorithm for the HSFD to exploit its capabilities in providing changeable amounts of damping to the rotor-bearings system. It is anticipated that an adaptive control algorithm will be required to achieve the full capabilities of the adaptive HSFD.

In the following chapters, the main concern is to investigate several different control theories and make a judgment on the most appropriate algorithm for controlling the HSFD. First, it was clear that a bang bang on-off controller would be useful as a first tackle on control. The purpose of attacking first the on-off active control will be explained in depth later in this chapter. This chapter is also involved in the tasks we expect our controller to achieve and in the problems the controller should react to and compensate for.

The first task required from the controller is to overcome the high amplitudes of vibration while passing through critical speeds. This control action would enhance the behavior of the rotor-bearing system through run-up and shut-down. A trade-off will be taken into consideration while designing the control algorithm between lowering both the amplitude of vibration of the rotor-bearing system and the

transmitted damping force on the bearings. This will show to be the crucial idea that would permit damping the rotor system only when it is deemed necessary.

Rotating machinery may experience dangerously high dynamic loading due to the sudden imbalance associated with blade-loss, for instance. Many cases of the destruction of turbomachinery were blamed on excessive bearing loads due to blade loss. Although considerable efforts are put into the steady state vibration control, there are few methods applicable to transient vibration control of rotor-bearing systems [19] and [35] . The objective of this research is to investigate the capability of the controller to suppress rotor vibrations caused by sudden mass imbalance; this is regarded as the second task required from our controller.

The first algorithm we undertook was based on only two levels of damping, the short damper mode and the long damper mode. Although we are aware of the capability of the HSFD to act as adaptive device capable of giving a wide choice of finite dampers between the short damper and the long damper configurations, as discussed earlier in Chapter 5, we limited ourselves in testing first an active bang bang control. The basic idea behind this limitation, which will be removed in further development of the HSFD controller in the next chapters, is to start with the most simple algorithm in the control of the rotor system.

Simplicity is a major advantage in control system development. In addition, it can be shown [10] that for some rotor systems only two levels of damping will be required to control the behavior of the rotor-bearing system. Thus an on-off controller that can actively change between the short and long damper modes can be sufficient for the control of some classes of rotor systems.

5.1 On-Off Controller Design

To develop an on-off controller that changes between short and long damper modes of operation, the steady state behavior of the system was first studied. The eccentricity ratio ε, the vibration amplitude at the rotor center r, and the transmitted damper force F are studied for the short and long damper modes versus the rotational speed Ω^*. The amplitude at the rotor center r is defined by

$$r = \sqrt{x_S^2 + y_S^2} \ /c$$

and the transmitted damping force F can be written as

$$F = \sqrt{F_{dx}^2 + F_{dy}^2} \ /U\Omega^{*2}$$

the damping forces in the x and y directions are respectively

$$F_{dx} = -\overline{C}_{xx}\overline{x}'_E - \overline{C}_{xy}\overline{y}'_E$$

$$F_{dy} = -\overline{C}_{yx}\overline{x}'_E - \overline{C}_{yy}\overline{y}'_E$$

Figure 12 shows the short and long damper steady state behavior for an unbalance of U = 0.1. It can be seen from Figure 12 (a), that the short damper system exhibits two critical speeds: the first at approximately $\Omega^* = 1$, i.e at 1800 rpm, and the second at approximately at $\Omega^* = 7.2$, i.e. 12960 rpm. The second critical speed is due to the mass of the rotor journal m_b included in our model. On the other hand, the long damper system exhibits only one critical speed at approximately $\Omega^* = 1.2$, i.e. at 2160 rpm. At all frequencies the long damper mode journal eccentricity ε is lower than that of the short damper mode. Figure 12 (b) reveals that the second critical speed for the short damper mode is well damped for this flexible rotor. Figure 12 (c) shows that the

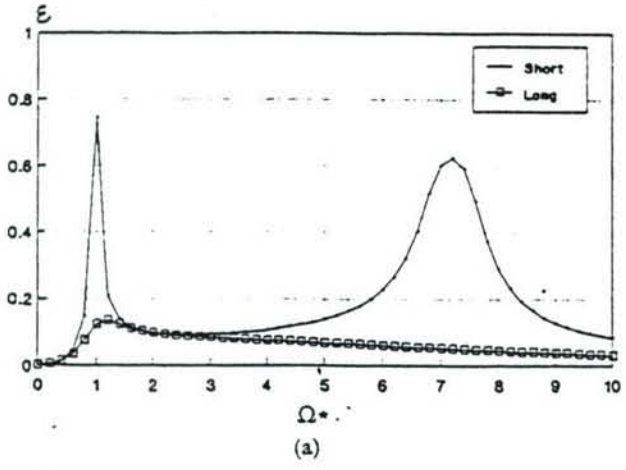

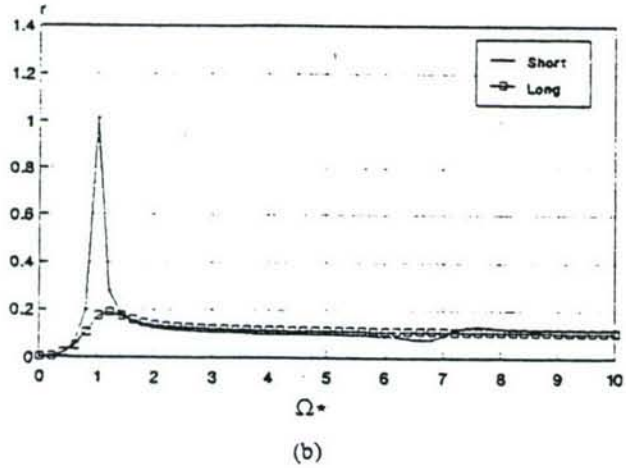

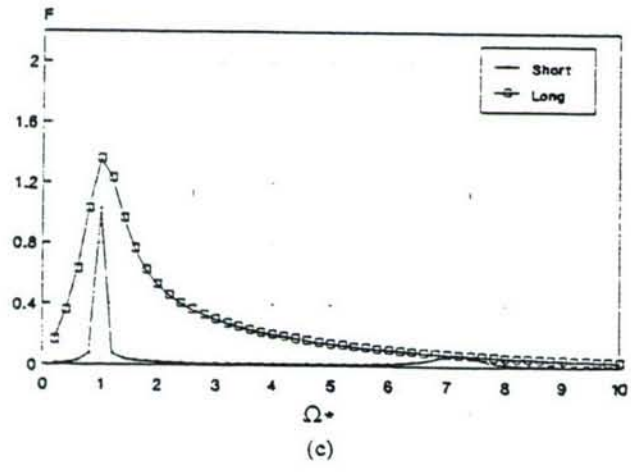

Figure 12 Steady State Behavior of the Open-Loop System.

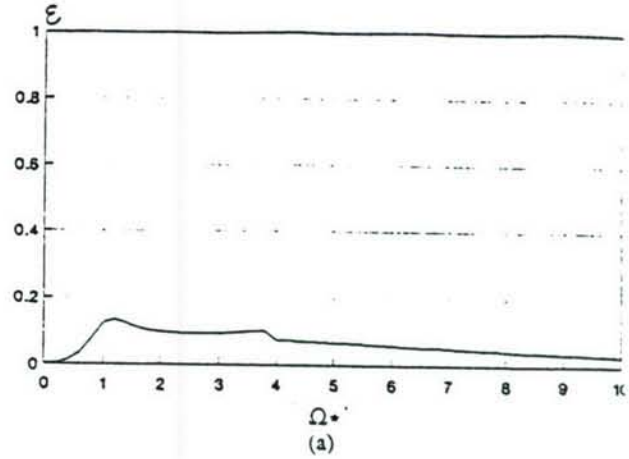

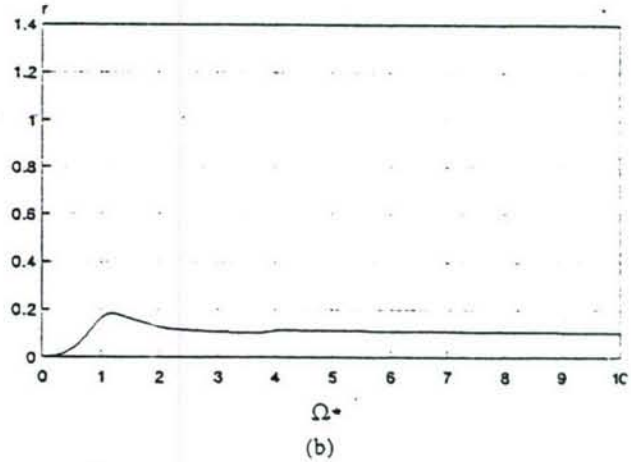

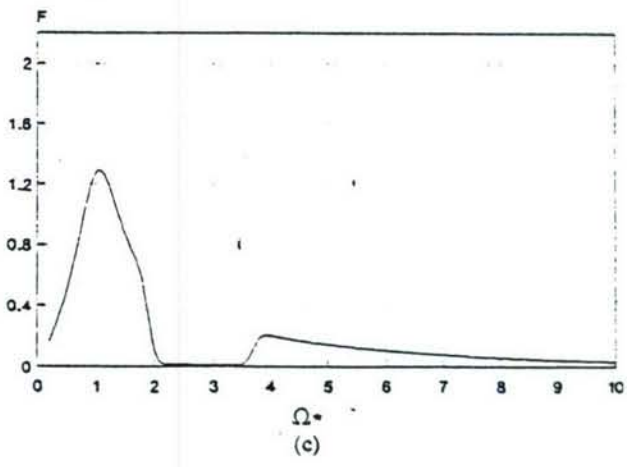

Figure 13 Steady State Behavior of the Closed-Loop Syster

transmitted damper force in the short damper mode is always less than that of the long damper.

It can be seen from Figure 12 that the behavior of the rotor is speed dependent, and the long damper and short damper modes exhibit distinctly different behavior. It is thus proposed that a simple closed-loop system would rely on the feedback of the rotor speed. Other feedback laws could be based on the feedback of the eccentricity ratio and/or the transmitted damper force (and will be used in next chapters), however it is quite clear from Figure 12 that the feedback on speed is quite effective in controlling rotor vibrations. On the other hand, this feedback law would rely on the knowledge of the rotor behavior at various damping levels and at various speeds. This active on-off controller can thus be actuated at specific rotational speeds to achieve the desired damping level for that particular speed range. It is realized that such a controller will rely on the pre-knowledge of the system behavior, however this is not considered to be a serious drawback since usually an elaborate analysis of the system critical speeds is done beforehand, and the results can be easily programmed into the controller. The simplicity afforded by the proposed active control strategy based on rotational speed feedback renders it quite attractive.

As an example consider the system behavior of Figure 12. The simple active control algorithm based on feedback of speed is applied such that the system operates in the long damper from rest until $\Omega^* = 1.8$, thus benefiting from the large damping provided by the long damper mode while the rotor traverses the first critical speed. At $\Omega^* = 1.8$ the system switches to the short damper mode, hence the first critical speed in the short damper is avoided. Noting that the damping force of the short mode is quite small with respect to the long mode in nonresonant regions, we benefit from the short damper till a speed of $\Omega^* = 3.6$; in this region the short damping force is dramatically less. At $\Omega^* = 3.6$, the system is switched to the long damper mode. The large amplitudes, associated with the second critical in the short mode, are bypassed

and replaced with the smaller values of the long damper mode with a penalty of increase in the damping force. The steady state behavior of the closed-loop system is illustrated in Figure 13, which shows quite an improvement in the behavior for the closed-loop system. This illustrates the power of the proposed control strategy based on speed feedback.

To fully assess the capabilities of the proposed control strategy the transient behavior of the closed-loop system during control action is studied and is shown in Figures 14 and 15. The transient response of the rotor system when switching to the short damper mode at $\Omega^* = 1.8$ exhibits some oscillations which persist for about 1 second and are due to the low damping in the short damper mode as shown in Figure 14. However, the transient response of the rotor system is generally well behaved when switching to the high damping value at the long damper mode for the case $\Omega^* = 3.6$, as shown in Figure 15. It can be seen that the transient response of the closed-loop system is fast, stable and achieves the required behavior. Thus, the active on-off control algorithm based on speed feedback exhibits satisfactory behavior in both its transient control action and the steady state response.

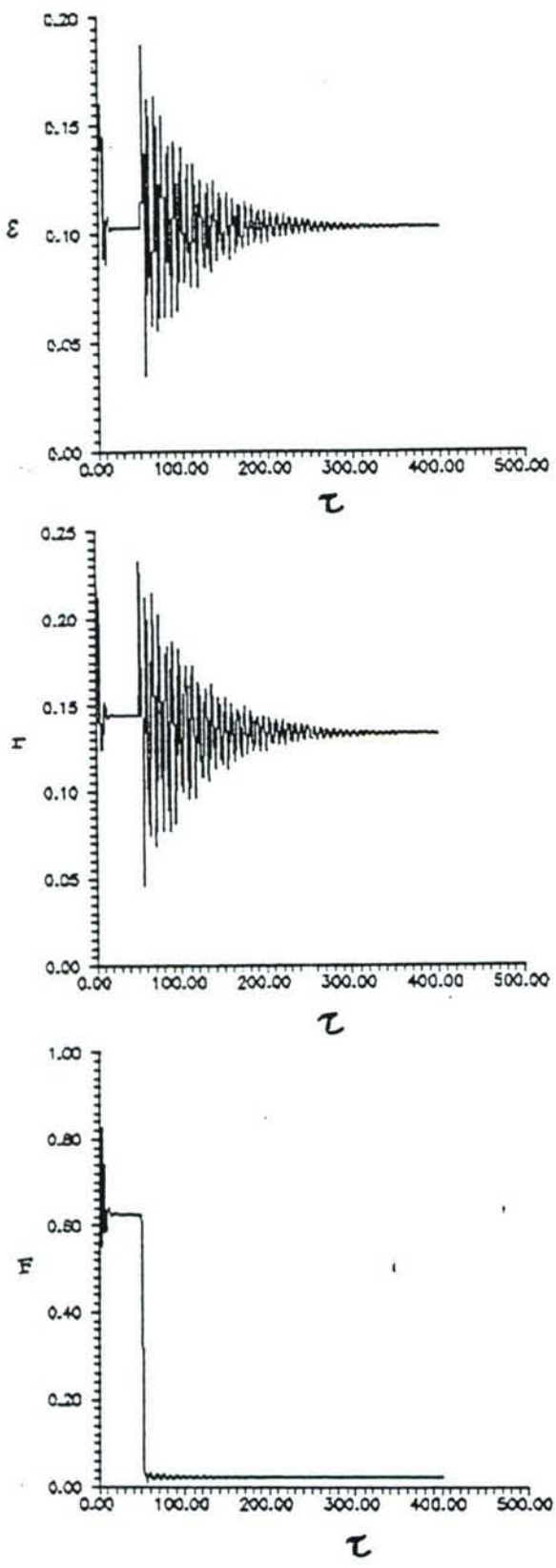

Figure 14 Transient Behavior of Closed Loop System while switching from Long Damper Mode to Short Damper Mode at $\Omega^*=1.8$.

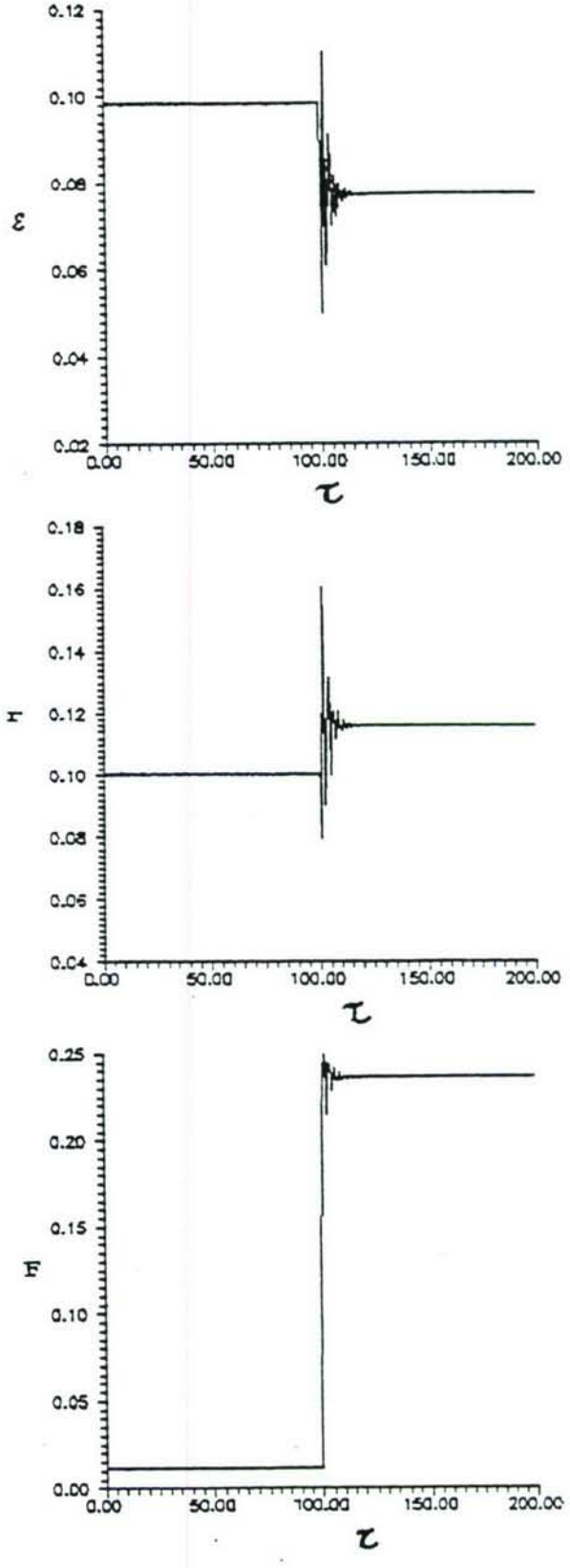

Figure 15 Transient Behavior of Closed Loop System while switching from Short Damper Mode to Long Damper Mode at $\Omega^*=3.6$.

5.2 On-Off Control Of Transient Run-Up through Critical Speeds

The design of the controller for the HSFD is mainly for controlling the system in its transient behavior. Transient run-up and coast-down through critical speeds when starting-up or shutting-down rotating machinery induces excessive bearing loads at criticals.

Figure 16 shows the open-loop behavior to transient run-up of the rotor. The uncontrolled system, i.e. while the HSFD behaves in the short damper mode, is speeded up linearly from rest to a nondimensional speed Ω^* of 12 (equivalent to 21590 rpm approximately) in nondimensional time equal 1200 and equivalent to about 7 seconds approximately. The uncontrolled run-up of the rotor is done for an unbalance of U = 0.1. The eccentricity ratio ε, the vibration amplitude at the rotor center r, and the transmitted damper force F are studied again for the uncontrolled open-loop system versus the nondimensional run-up time τ. It can be clearly seen from Figure 16 (a), that the short damper mode exhibits mainly two modes at speeds of Ω^* = 1 and 7.2 approximately as acknowledged before while studying the steady state open-loop behavior of the short damper mode. The first and second modes are quite accentuated and some transient oscillations persist after the first mode is surpassed. Figure 16 (b) shows that the second mode is well damped for the vibration amplitude of he rotor center r.

The same run-up discussed above is proceeded for the on-off controlled system based on the rotational speed feedback. Figure 17 shows the controlled system behavior through transient run-up. The switching speeds preprogrammed into the controller are chosen to give the best compromise possible between attenuating the high peaks of vibration at critical speeds and giving the minimum damping in regions of

mild vibration. The system is chosen to run in the long damper mode from rest to a speed $\Omega^* = 2.2$, hence the first mode is surpassed. Then, in the region from $\Omega^* = 2.2$ to 5 the system is chosen to run in the short damper mode to benefit with the considerably lower damping force at a region of low vibration. Again from $\Omega^* = 5$ to 9, the system is switched to the long damper mode to overcome the second peak. Finally at $\Omega^* = 9$, the system is switched off to the short mode. Figure 17 shows how the controlled HSFD based on speed feedback can be a powerful device for rotor-bearing control.

Despite the excellent performance of the on-off active controller based on speed feedback, this controller would not compensate for a sudden imbalance occurrence due, for example, to a sudden blade-loss. This is because of the incapacity of the controller to compensate for unpredictable events. The controller is based on the pre-knowledge of the rotordynamics of the rotor-bearing system. This means that the controller is pre-programmed with the speeds at which to switch to or from a certain damper mode. The capability of a controller to sense high vibration amplitude and to compensate for it in both transient run-up and sudden imbalance is highly required, since it is of prime importance that such controllers be capable of controlling the rotor in normal working conditions, but also in preventing disasters like in sudden blade-loss from a rotating machine. For that reason, it was indispensable for us to investigate more "intelligent" control algorithms that would allow such control action.

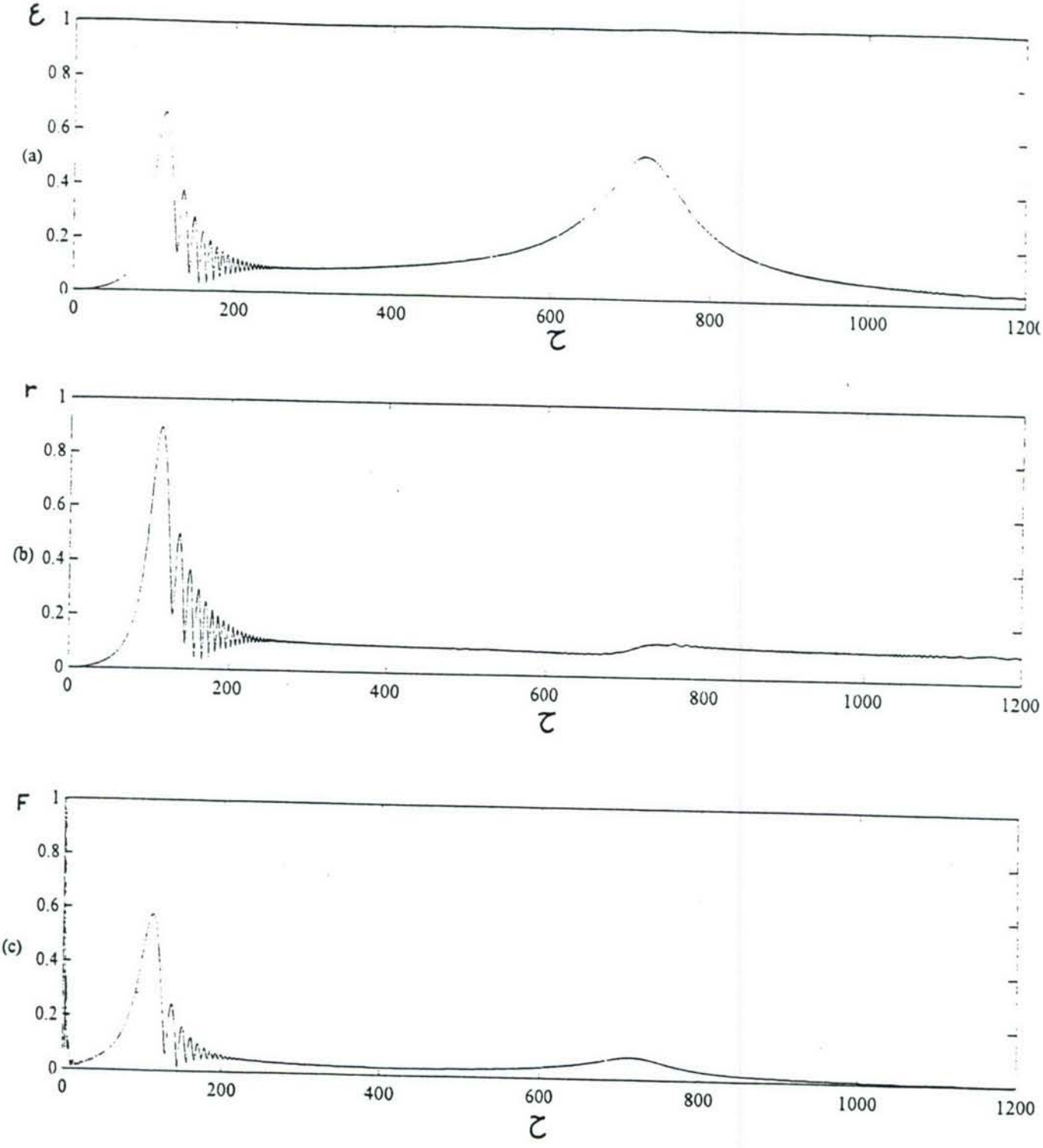

Figure 16 Uncontrolled (Short Damper Mode) Transient Run-Up of the Rotor

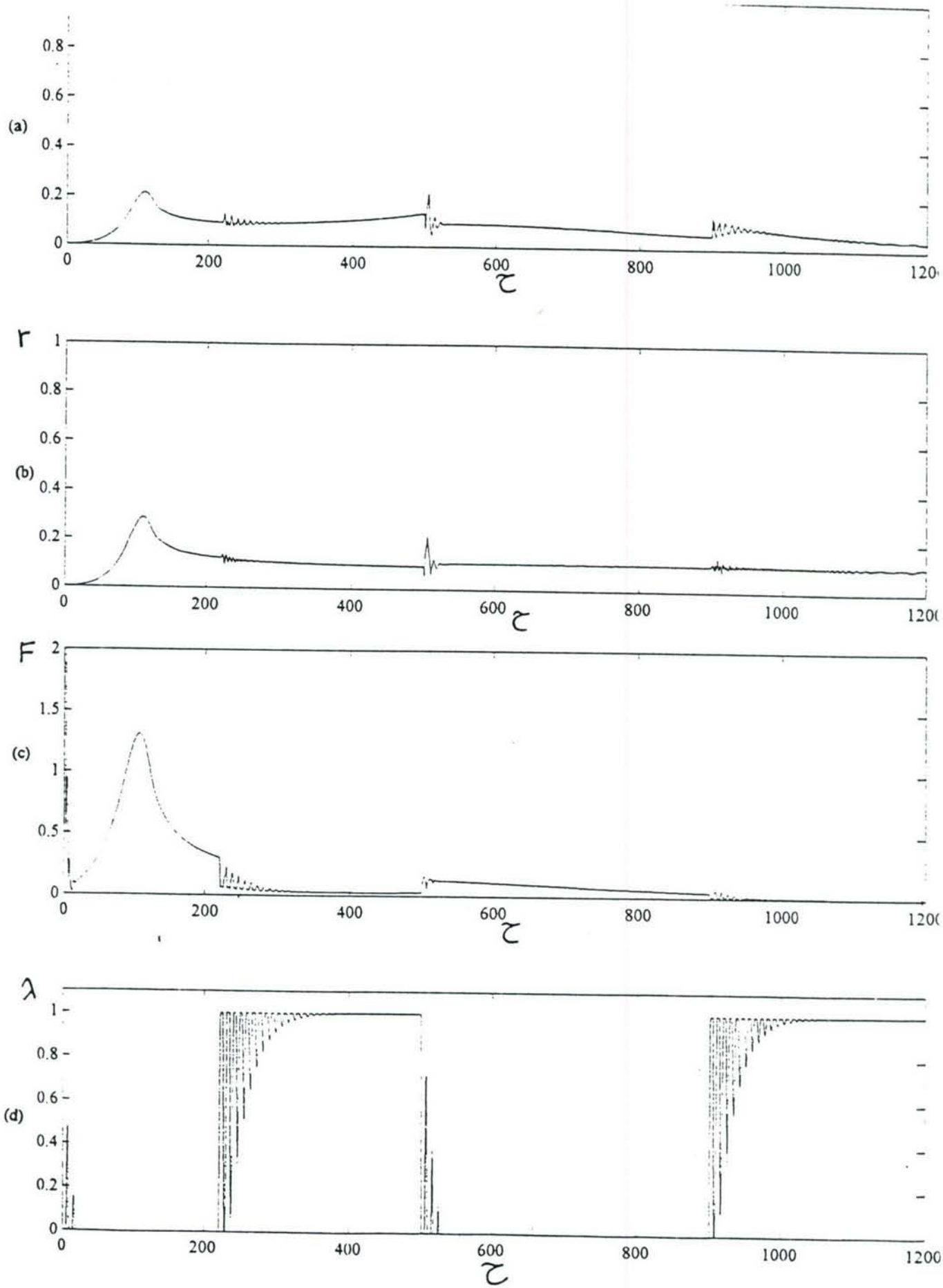

Figure 17 Controlled Transient Run-Up, On-Off Controller

CHAPTER 6

PROPORTIONAL PLUS INTEGRAL CONTROLLER (PI)

This chapter is concerned with the development of a conventional controller through proportional plus integral control for the HSFD. The full remodeling of the system to be incorporated in MATLAB™ [24] and SIMULAB™ [25] was necessary and will be discussed in details. A very large number of simulations were indispensable for the choice of the controller gains as will be shown later. Finally, a last section in this chapter is concerned with testing the controller for both controlling rotor-bearing system while run-up through criticals and compensating for sudden imbalance, i.e. through blade-loss.

6.1 Theory and Modeling

The system is chosen to behave in the short damper mode in its normal condition, which gives the least amount of damping to the rotor in our system, and any deviation of λ from the short damper mode position (i.e. λ=1) towards the long damper mode position would translate into an increase in the damping of the HSFD. This increase in damping ΔC is the effective control input to the rotor. The controlled damping increase ΔC can be deducted from equation (5), thus

$$\Delta C = (1 - \lambda)(C_s - C_l) \qquad (18)$$

and hence the equations of motion of the journal center in both x and y directions, equations (12) and (13) respectively, can be changed in the form shown below where the right-hand side represents the effective control input to the system, i.e. the damping force causes the increase of damping to the system ΔC. In nondimensional form:

$$\bar{x}_E'' + m_o \bar{C}_{xx_s} \bar{x}_E' + m_o K^* (\bar{x}_E - \bar{x}_S) + m_o K_r^* \bar{x}_E = -m_o \Delta \bar{C} \bar{x}_E' \qquad (19)$$

$$\bar{y}_E'' + m_o \bar{C}_{yy_s} \bar{y}_E' + m_o K^* (\bar{y}_E - \bar{y}_S) + m_o K_r^* \bar{y}_E = -m_o \Delta \bar{C} \bar{y}_E' \qquad (20)$$

It should be noted that the coupling damping terms C_{xy} and C_{yx} were neglected with respect to C_{xx} and C_{yy}, due to their lower order and primarily for having a simpler system while building its block diagram.

Equation (18) describing the increase of damping and the equations of motion of the journal center (19) and (20) are added to the rest of the nondimensional model developed in Chapter 4 and the whole model is transformed to the Laplace-domain, and is put in a block diagram format.

Figure 18 shows the block diagram of our open-loop plant consisting of the servovalve transfer function, the sealing ring dynamics, the HSFD, and the rotordynamics in both the x and y directions. The servovalve reacts to the input current i, and causes an increase in the sealing chamber pressure P which pushes the sealing ring to move with a displacement λ and hence controls the amount of damping

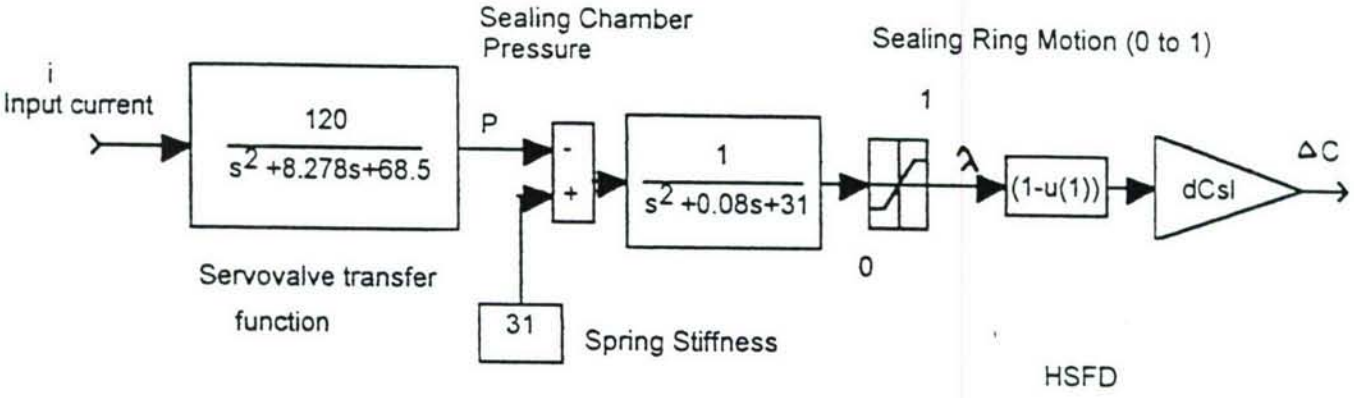

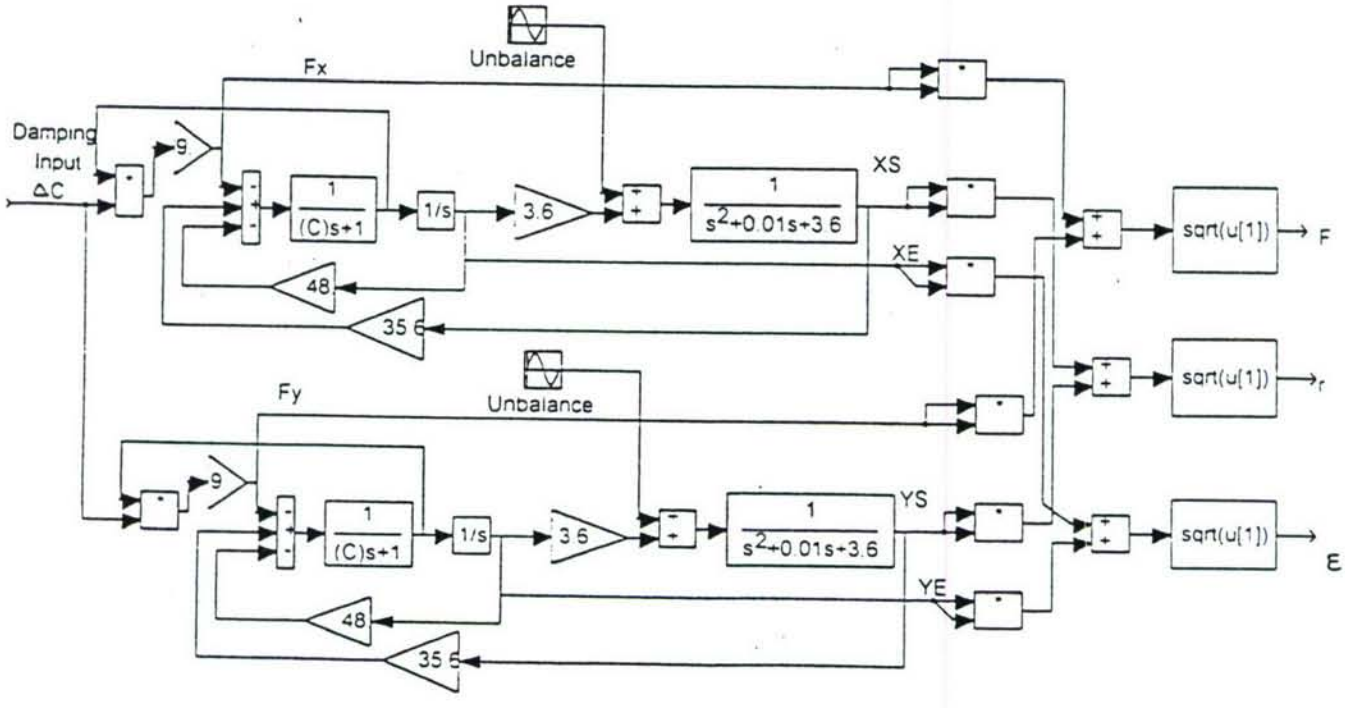

Figure 18 Block Diagram of the Open-Loop Plant for SIMULAB™ Manipulation

input ΔC to the rotordynamics of our system. All parameters shown in the block diagram of Figure 18 are taken as for the system discussed in Chapter 4.

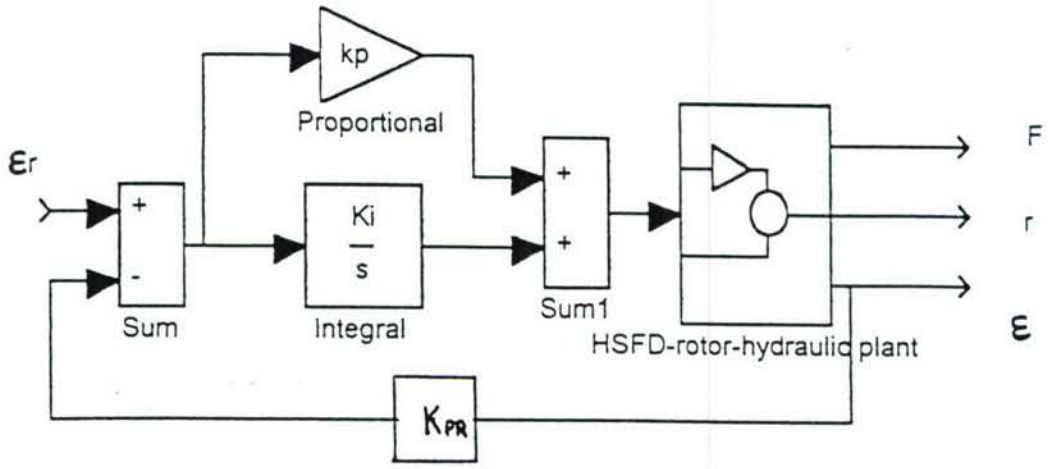

Figure 19 PI Block Diagram

The closed-loop control system with PI controller added to the plant is illustrated in Figure 19. The eccentricity ratio ε at the journal was chosen to be fedback, hence the control input to the servovalve is given by

$$u_c = \left(k_p + \frac{k_i}{s}\right)(\varepsilon_r - \varepsilon) \qquad (21)$$

where u_c is the control input, k_p is the proportional gain, k_i is the integral gain and ε_r is the reference input, and $(\varepsilon_r - \varepsilon)$ is the error to be regulated. K_{PR} in Figure 19 is the

proximity probe gain and was chosen to equal 1 in our simulations. The system shown in Figure 19 is simulated in the next section.

6.2 Simulation of the Behavior of the Closed-Loop Control System

To simulate the behavior of the closed-loop system, the block diagram developed in the previous section describing the dynamics of the complete closed-loop system is implemented on a digital computer. The block diagram is manipulated on SIMULAB™ [25] and MATLAB™ [24] to permit the simulation of a nonlinear system in the Laplace-domain. In order to simulate this model, the most convenient and robust integration technique available on the used softwares was the Adams-Gear method.

As shown from equation (21), the proportional gain k_p and the integral gain k_i have to be tuned to give the performance sought after. Conventional control theory, including the PI regulator, deals predominantly with linear systems having constant coefficients and the controller gains are fixed. However, linear control techniques can be quite efficient in controlling nonlinear systems provided that such systems are regulated at fixed operating conditions. With moderate disturbances and a good control system, the deviations will be so small that the linear approximation is sufficiently good. This requires a thorough study of the plant to be controlled and a careful choice of controller gains. However, the linear coefficient approximation will not always be satisfactory when the operating conditions change largely. Therefore, optimal gains would have to be tuned for different operating conditions ranges. A

solution for such cases would be the construction of a Gain Scheduling technique that will cope with the varying operating conditions in changing controller gains (Gain Scheduling technique will be discussed in the next Chapter as an enhancement for the PI controller behavior). Also, adaptive control techniques (Chapter 9) can be very useful for nonlinear systems with changing parameters and conditions. But, at this moment, the main interest is to study the full capabilities of the closed-loop system with PI control.

The main criteria taken in our approach for controller gain tuning is to find the appropriate gains that would both dampen sudden imbalance and the high amplitudes of vibration at the critical speeds. While running-up through critical speeds the idea is to activate the controlling action (i.e. induce additional damping to the rotor) only at and near criticals where the amplitudes are high. This will induce high damping forces to the bearings to attenuate vibration. Our interest is to minimize the period of time where excessive forces act on the rotor. Controller gains must provide the required damping at criticals, and minimum damping in ranges of mild vibration. On the other hand, while choosing gains to attenuate sudden imbalance, the gains must be chosen to dampen the vibrations of the rotor to a level equal to the permissible vibration level (i.e. the selected reference). The trade-off between selecting controller gains that would accommodate both conditions is the crucial design problem for our controller. The tuning of the regulator gains to give the required performance is quite difficult and time consuming, but the results are quite attractive and show that the effort taken in tuning the PI regulator is worthwhile.

Many trials were done by changing the gains and studying their influence on the roots of the system. Figures 20 (a) and (b) show the pole-zero mapping for both the open-loop and the closed-loop systems respectively. Also, many simulations were performed to check the stability of the system with the change of gains.

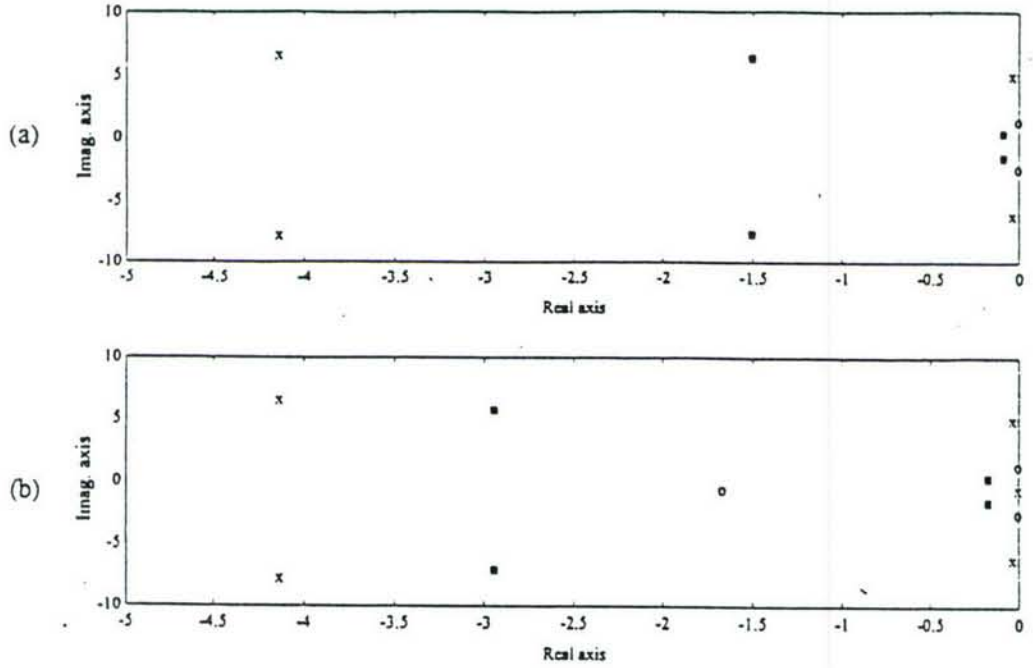

Figure 20 Roots of the Open-Loop (a) and the Closed-Loop (b) System

X pole
O zero

It should be clear that also derivative feedback was first investigated but resulted in severe chattering of the sealing rings. The system would lose its effective control input with the inaccurate positioning and the chattering behavior of the sealing rings which are the means of providing the necessary amount of damping to the system. Thus, we concluded that the behavior of the system is unsatisfactory with the slightest derivative gain. This is because the derivative control component responds to the rate of change of the error, and hence gives a stronger control signal when the

error changes faster and thus it anticipates large errors, and attempt corrective actions before they occur with high control signals [26]. Such high signals cause the chattering of the sealing rings and tend to destabilize the behavior of the system.

On the other hand, the integral control component is commonly used in process control where certain levels must be maintained for the control variables despite disturbances and parameter variations. Integral control tends to reduce steady state error to zero. Our goal is to accurately position the sealing rings with minimum transient oscillations to give zero steady state error of the output controlled variable. The integral action is quite appropriate since its control signals are lower and slower than the derivative signals, hence accurate positioning of the sealing rings without severe chattering is possible. The performance of the PI control is quite adequate for controlling our plant if the reference allowable vibration level to be maintained despite disturbances is selected, thus the controller will reduce the error to zero. The only drawback of a PI controller in our case is that it reacts quite slowly to errors and hence gives quite large overshoots especially in the imbalance control and in attenuating the first critical speed during the rotor run-up.

The optimal gains were chosen to give best control for both suppressing critical speeds and overcoming sudden imbalance. Some well known tuning methods like the Ziegler-Nichols tuning methods [27] were used as a guide to estimate the measure of the PI gains, and this helped in reducing the effort in trial-and-error tuning. The proportional gain k_p and the integral gain k_i were chosen to equal 3 and 5 respectively, and these gains gave quite satisfactory results as shown below.

6.3 PI Control of Transient Run-Up through Critical Speeds

The reference input of the controlled system is chosen to be $\varepsilon_r = 0.3$. The same run-up discussed in section 5.2 is proceeded and the behavior of the controlled system is shown in Figure 21. Figures 21 (a) show that the eccentricity ratio exceeds the reference input at the first critical speed, but still the overall behavior while passing through the critical speed is enhanced. The amplitude of vibration is lowered, the transient oscillations are eliminated. The control action for the first critical speed is slow and the error is quite large. This is caused from the slow reaction of the integral control component to a vibration amplitude peak which builds-up very rapidly; the integral action needs more time to react. This fact is clear while the system overcomes the second peak which is less accentuated and takes quite larger time to build-up; the integral action is more efficient and the reference input is respected. Some transient oscillations persist for about 0.2 seconds then the behavior is improved. These transient oscillations can be explained from Figure 21 (d) which describes the motion of the sealing ring λ. The amount of damping to the system relies on the position of the sealing rings. The controller signal forced the sealing rings to reach a value $\lambda = 0.5$ approximately to dampen the second peak, this finite positioning of the sealing ring between $\lambda = 1$ (short damper mode) and $\lambda = 0$ (long damper mode) requires some time to accurately position the seal at the optimal position that would give the necessary damping to decrease the high peak of vibration, as discussed earlier in Chapter 5. This positioning time results in some oscillations that could be diminished if the damping on the sealing is increased, but because of the uncertainty of the amount of this damping in our test rig as discussed before, we chose it to be quite low. We envision that the

behavior will improve when the controller is experimented on our test rig since the damping at the seals could be greater due to friction effects. Figure 21 (c) shows quite a higher transmitted force in the controlled case than that in the uncontrolled case illustrated in Figure 16 (c), in section 5.2. The increase in force is clear at the criticals' location where higher damping action is needed to attenuate excessive vibration.

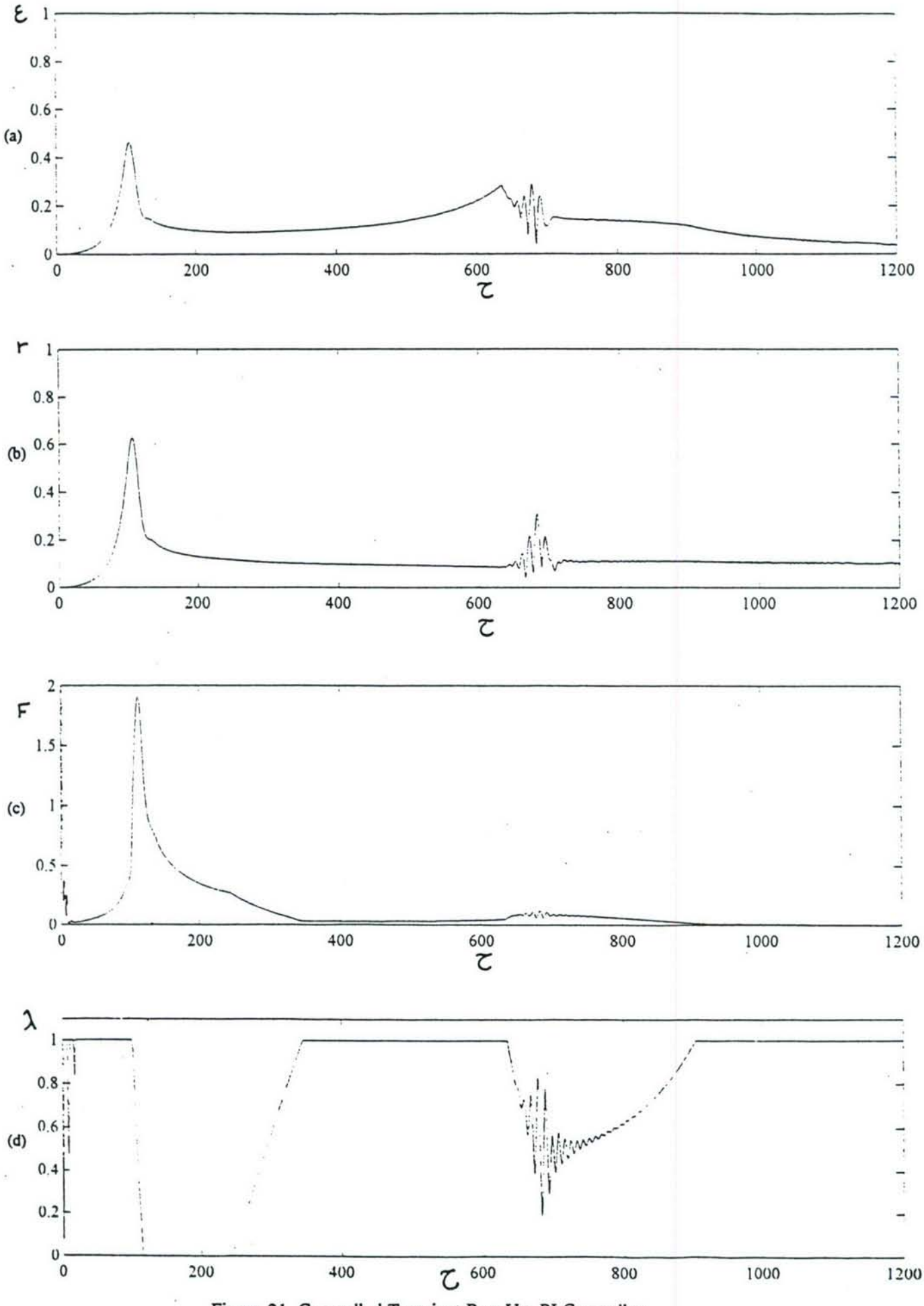

Figure 21 Controlled Transient Run-Up, PI Controller

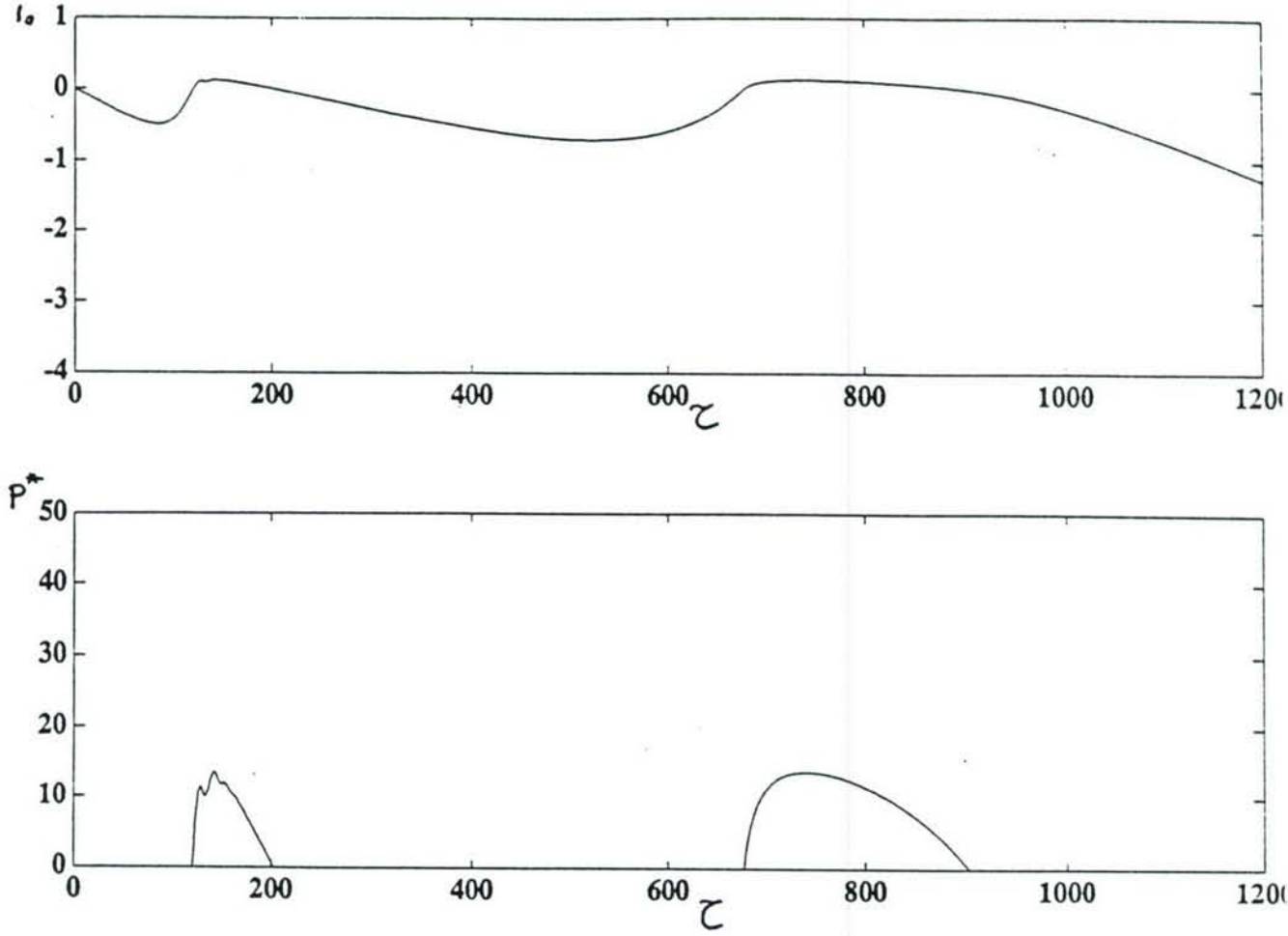

Figure 21 (Cont.) Controlled Transient Run-Up, PI Controller

6.4 PI Control of Sudden Imbalance (e.g. through Blade-Loss)

Rotating machinery may experience dangerously high dynamic loading due to the sudden imbalance associated with blade loss, for instance. Many cases of the destruction of turbomachinery were blamed on excessive bearing loads due to blade-loss. Although considerable efforts are put into the steady state vibration control, there are few methods applicable to transient vibration control of rotor-bearing systems [19] and [35]. The objective of this research is to investigate the capability of the PI controller to suppress rotor vibrations caused by sudden mass imbalance.

The rotor is chosen to rotate at its normal working steady speed with an initial low unbalance of 0.05 at the disk. Then, suddenly at a nondimensional time of τ = 300, the unbalance increases to a higher value equal to 0.1. For this case, we chose the normal working speed to be at $\Omega^* = 1$ which corresponds to the first critical speed of the rotor. This speed was chosen to investigate the performance of the controlled system under severe working conditions: sudden mass imbalance while the working rotational speed coincides with the first critical speed of the rotor. Figure 22 shows the behavior of the uncontrolled system to a sudden imbalance. The amplitudes of vibration of both the journal center ε and the disk center r have nearly doubled in magnitude due to sudden imbalance.

Figure 23 shows the closed-loop behavior. The behavior of the rotor is brought to its normal working condition through a transient overshoot which persists for about 0.18 seconds. We can clearly see from Figure 23 (d), that λ is approximately

positioned at a value of 0.6 which permits the HSFD to give exactly the right amount of damping to the rotor to return to its initial working condition. This implies that for higher imbalances, higher damping forces are needed to reach closer behaviors to the required working condition. This compensation is done with a higher signal from the controller to the servovalve, hence the sealing ring moves closer to the long damper mode (at $\lambda = 0$), with the penalty of increasing the transmitted damping force to the rotor as shown in Figure 24. This Figure illustrates the behavior of the system to higher imbalances of 0.15 and 0.2 compared with the previous case where an imbalance of 0.1 was simulated. As discussed above, λ moves closer to $\lambda = 0$ (Figure 24 (d)) with higher unbalance forces acting on the rotor, and hence the HSFD produces higher damping forces (Figure 24 (c)) to attenuate excessive vibration and return its level as close as possible to the initial working condition of unbalance 0.05.

In conclusion, The controller reacted well with different sudden imbalances, and the damping induced by the HSFD to the rotor bearing system was directly proportional to the intensity of the sudden unbalance force. This is a very attractive issue since the control system is very sensitive to the severe forces produced by sudden unbalance change and produces the appropriate amount of damping necessary to improve the rotor behavior.

In addition, it was shown that while running-up through critical speeds, the PI controller showed some delayed behavior while overcoming the first critical due to the very rapid build-up of the vibration peak, nevertheless, the controller gave an overall enhanced behavior since it attenuated undesirable transient oscillations and reduced the

peak. Moreover, the second vibration peak was well damped by the PI controller. Furthermore, the gain scheduling technique will be incorporated to the closed-loop system with the PI regulator. This resulted in an improvement of the closed-loop system through run-up while maintaining the efficient control of the PI regulator to sudden imbalance, as will be shown later in Chapter 7. The most attractive issues of this control strategy are both the simplicity and the efficiency it provides.

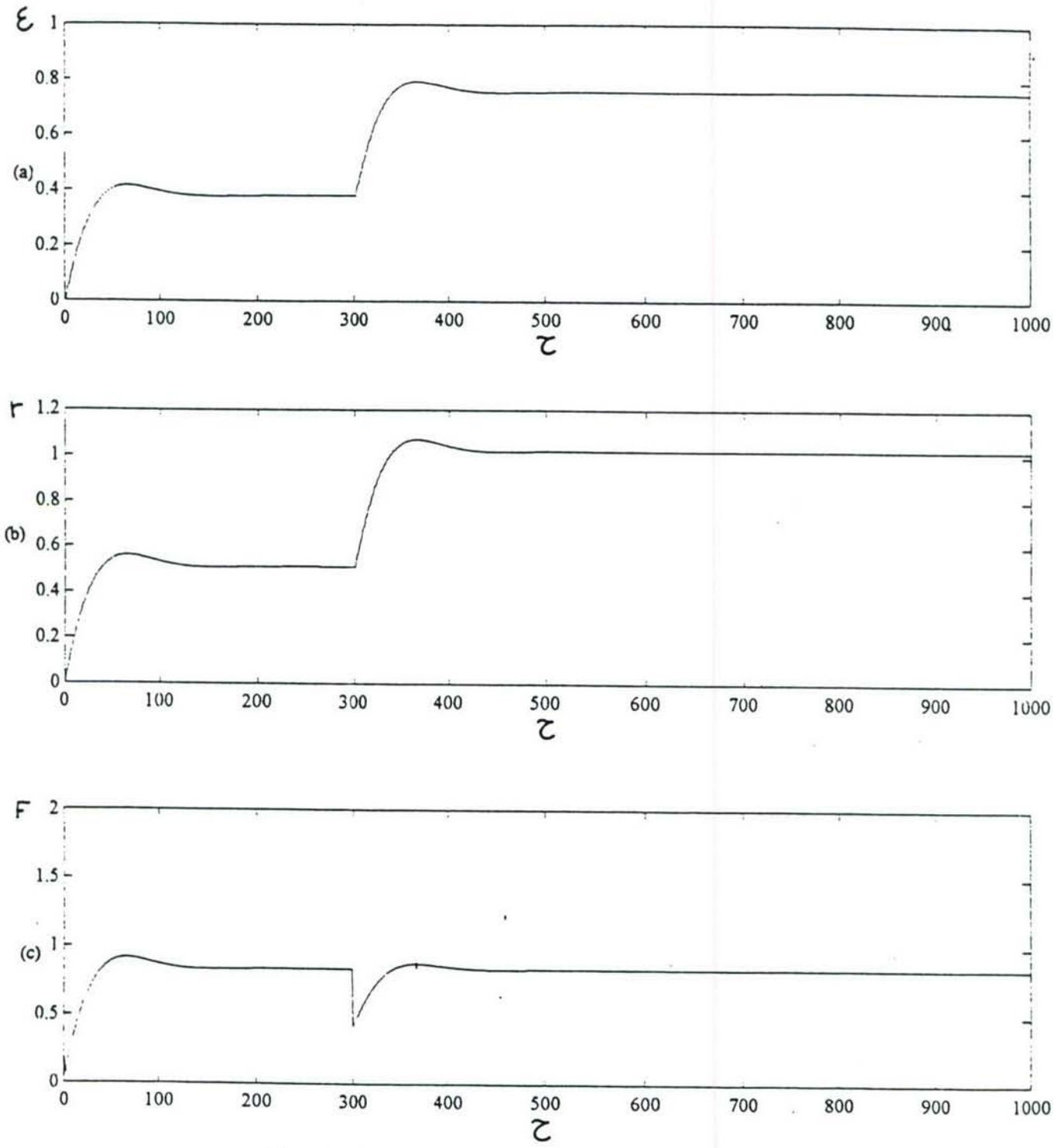

Figure 22 Uncontrolled Response to Sudden Imbalance

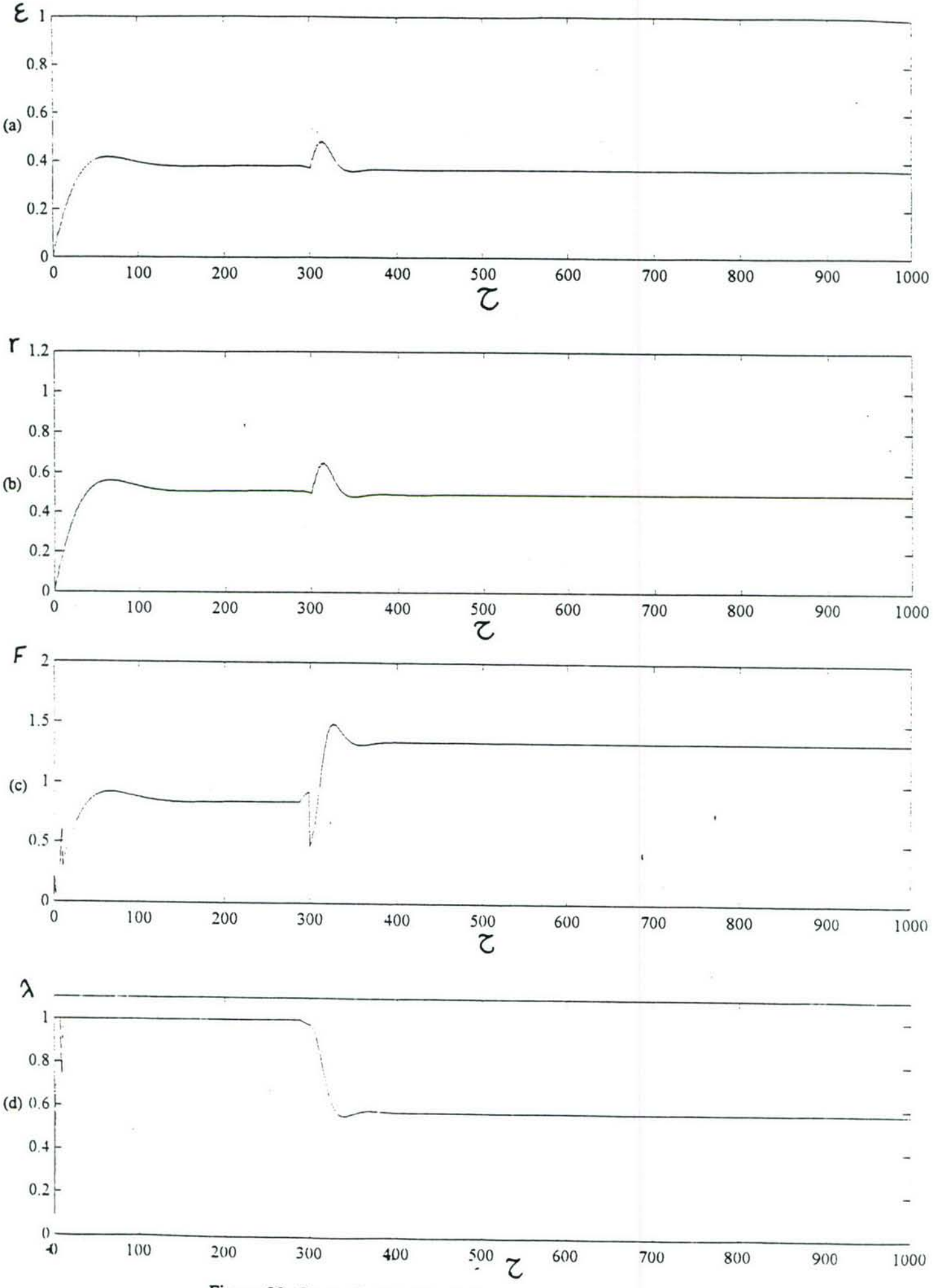

Figure 23 Controlled Sudden Imbalance, PI Controller

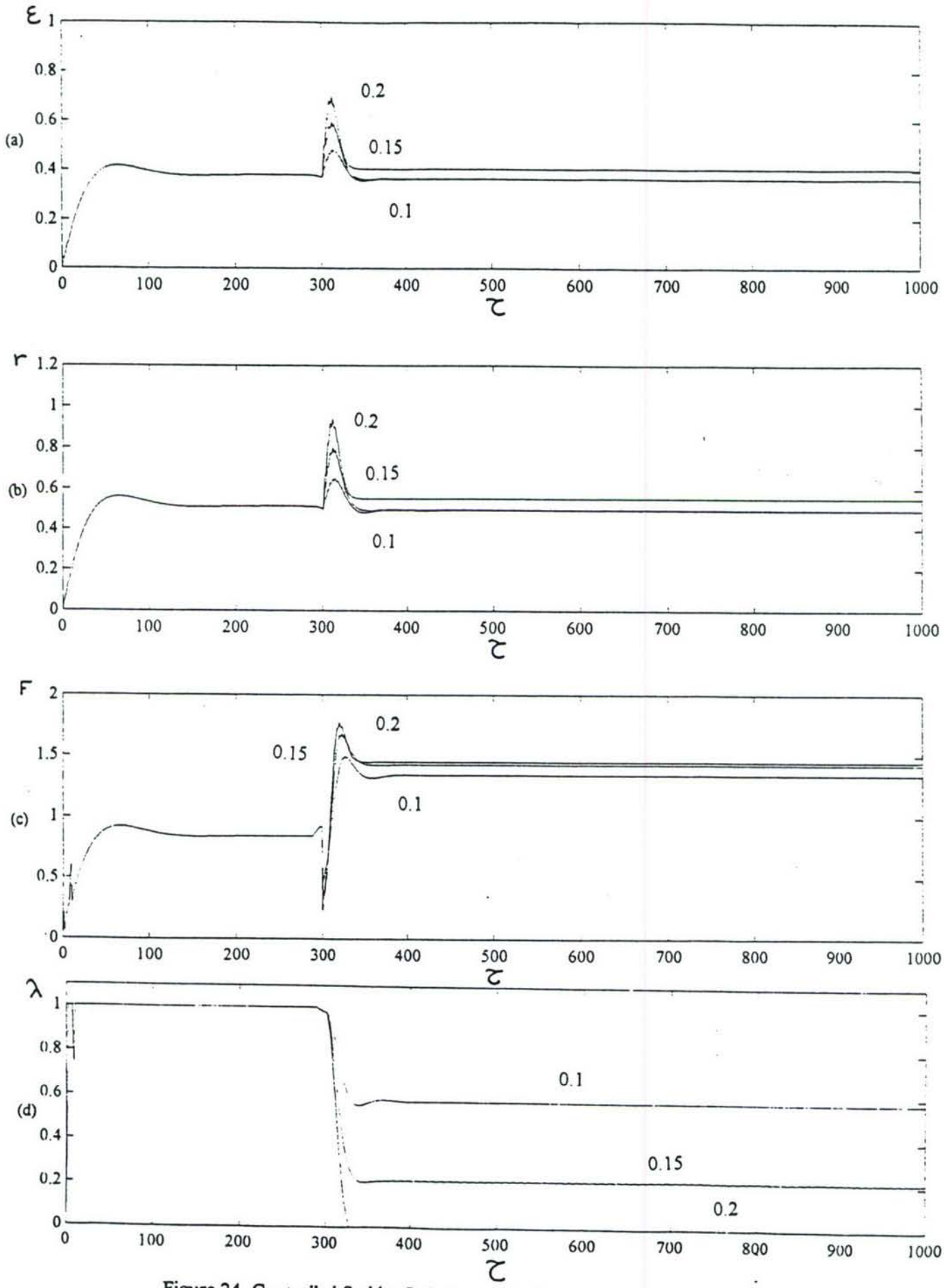

Figure 24 Controlled Sudden Imbalance, U = 0.1, 0.15 and 0.2, PI Controller

CHAPTER 7

GAIN SCHEDULING TECHNIQUE FOR ENHANCING THE PI CONTROLLER BEHAVIOR

The PI controller is efficient in controlling the behavior of the system during run-up through critical speeds and sudden imbalance due to blade-loss. However, the behavior of the closed-loop system while speeding up through critical speeds shows delayed control behavior while passing the first critical speed. To improve the control action through the first critical speed, we chose to incorporate the gain scheduling technique to the closed-loop system with the PI regulator.

7.1 Theory and Model

The gain scheduling technique (GS) is viewed as a nonlinear feedback of special type: it has a linear regulator whose parameters are changed as a function of operating conditions in a pre-programmed way. GS is an open-loop compensation and can be considered as a system with feedback control in which the feedback gains are adjusted by feedforward compensation. The GS technique originated in connection with the development of process control and flight control systems and became a standard method in such applications. For example in some flight control systems for supersonic aircrafts, the Mach number affects largely the response of the controller, therefore it is taken as an auxiliary variable which is measured and used as the

scheduling variable for varying the controller gains [27]. This example is very close to our case, since we can clearly notice that the characteristics of the system are related to the behavior of the rotational rotor speed, as illustrated before in Figure 12. Hence, the rotational speed which can be easily measured in our test rig with a tachometer or a keyphasor, can be considered as the appropriate scheduling variable for changing the regulator gains.

Figure 25 shows the closed loop system with GS-PI controller incorporated. We chose to schedule the integral gain k_i only for the PI regulator since it is the most effective in controlling the run-up through critical speeds. Moreover, k_i has a major influence in decreasing the error and giving a well behaved response. The proportional gain k_p taken equal to 3 all over the speed range results in satisfactory behavior of the closed-loop system. The scheduling of k_i with respect to the speed Ω^* is illustrated in Figure 26. The choice of this schedule for k_i was designed by extensive trial and error simulations until a satisfactory behavior was reached. It can be noticed that the gain is chosen negative from zero speed until overcoming the first critical, this showed to be effective in forcing the HSFD to give maximum damping in this region of severe vibration. This can be explained from the fact that the corrective control action of the integral gain is slow towards the first peak of vibration, as explained before. This is because for a certain time at the beginning of the run-up the control input u_c is slightly negative due to a transient time delay caused by the integral action, this delay is known as integral windup [26]. Integral windup causes the control input u_c (see Figure 27 (a)) to accumulate a large control signal with the same sign (negative in our case) of the error at regions of high disturbances, i.e. at the first critical which is quite high.

After the error becomes positive, and hence the controller is expected to activate the servovalve, the negative signal accumulated retards the wind-down to a value where the servovalve could be actuated. Hence, the negative value of the control input u_c is not capable of powering up the servovalve as soon as the peak arises, thus the HSFD is not activated. Gain scheduling of the integral gain in a manner that prevents this delay may be a good solution [27]. Therefore, assigning a negative value to k_i for the region of the first peak rectifies the signal and this activates the servovalve. Figures 27 (a) and (b) show the transient behavior of the control signal u_c for the PI controller alone and for the GS-PI controller respectively. Also, it can be noted from Figure 27 (a) that u_c is undergoing integral windup in the negative direction after overcoming the second critical. GS of k_i corrected this behavior (Figure 27 (b)) by assigning lower values to the integral gain.

A scheduling was also necessary for the reference input ε_r. For ε_r the scheduling variable is also taken as Ω^* since the reference input is affected by the speed of rotation. The relation between ε_r and Ω^* is shown in Figure 28. The need of scheduling ε_r can be explained that for each speed range a certain value for the reference ε_r is the desired output. The schedule of ε_r with respect to Ω^* is designed to give the desired behavior for the eccentricity ratio ε at the journal. The amplitude of vibration is desired to be attenuated at criticals, hence the reference value ε_r is lowered at criticals. This will increase the error $(\varepsilon_r - \varepsilon)$, and thus the control signal u_c will increase (equation (21)) producing a current signal to the servovalve which will produce the necessary pressure to push the sealing rings towards the long damper configuration and hence the HSFD dampens the vibration at criticals. On the other

of mild vibration where damping action is not needed, thus benefiting from the low transmitted damping force. Therefore, by scheduling the reference input in a manner that describes the behavior sought after, the more the integral action tends to minimize the error (ε_r - ε), the closer the behavior of ε will resemble the behavior of ε_r through speed increase until coinciding with it when the error is minimized to zero which is the advantage of integral control. The idea of ε tending to resemble ε_r can be quite noticed if Figures 28 showing the scheduled ε_r and Figure 29 (a) showing the eccentricity ratio ε transient response through controlled run-up are compared.

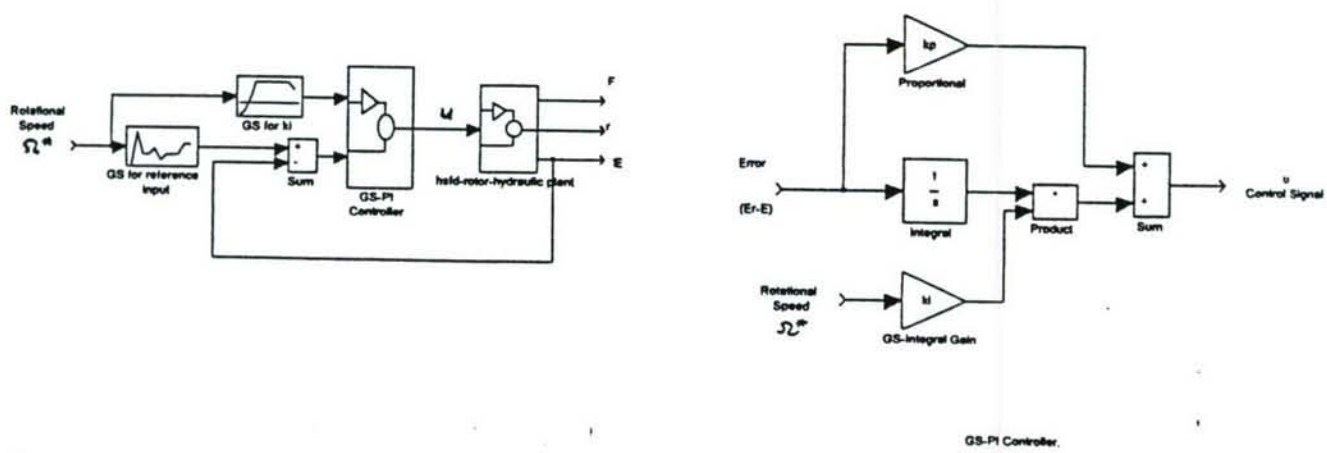

Figure 25 Block diagram of the closed loop system with GS-PI controller.

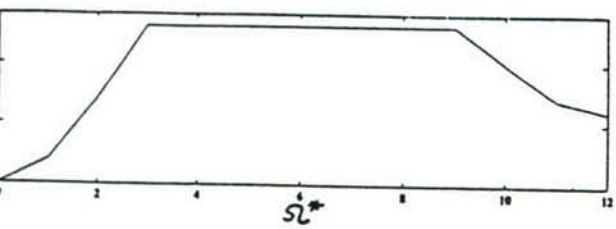

Figure 26. Scheduling of k_i versus Ω^*.

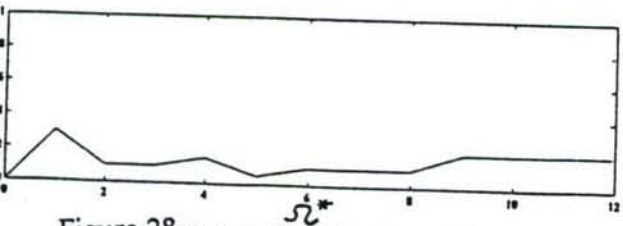

Figure 28 Scheduling of ε_r versus Ω^*.

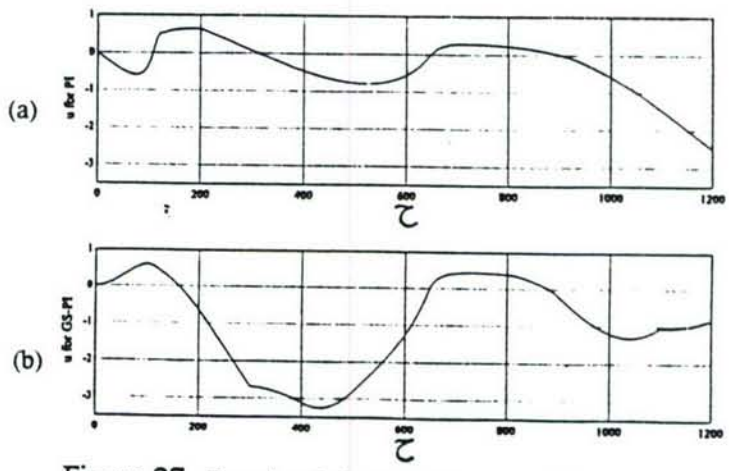

Figure 27 Transient behavior of the control input u for both PI controller case (a). and GS-PI case (b).

7.2 GS-PI Control of Transient Run-Up through Critical Speeds

The transient closed-loop behavior of the system with GS-PI regulator while running-up the rotor through critical speeds is shown in Figure 29. An improvement of the behavior is obvious when compared to Figure 21 which describes the run-up behavior with PI control alone especially in attenuating the amplitude of vibration of the first critical speed. Moreover, the transient chattering at the second critical is reduced. The GS-PI controller has the advantage of giving a well behaved rotor run-up while maintaining the efficient controlled behavior to sudden imbalance of the PI regulator alone.

Gain Scheduling enhanced the behavior of the closed-loop system since it has the advantage of changing the regulator parameters very rapidly in response to changes in the speed of the rotor. One drawback of this method is that the design of schedules may be time-consuming since the gains must be determined for many operating conditions, and the performance and stability of the closed-loop system with GS are typically checked by extensive simulations [27]. Another consideration that must be noted while using GS is that this technique changes the regulator gains in open-loop in response to an auxiliary variable which is the rotor speed in our case. This makes GS impossible to use unless the dynamics of the system are accurately known and the external disturbances well defined. This does not create a serious problem in our system, since usually elaborate study of the rotor dynamics is done beforehand.

Control algorithms which are not based on the pre-knowledge of the rotordynamics of the system are our focus in the next Chapters. Such controllers are investigated through both optimal control theory and adaptive control theory.

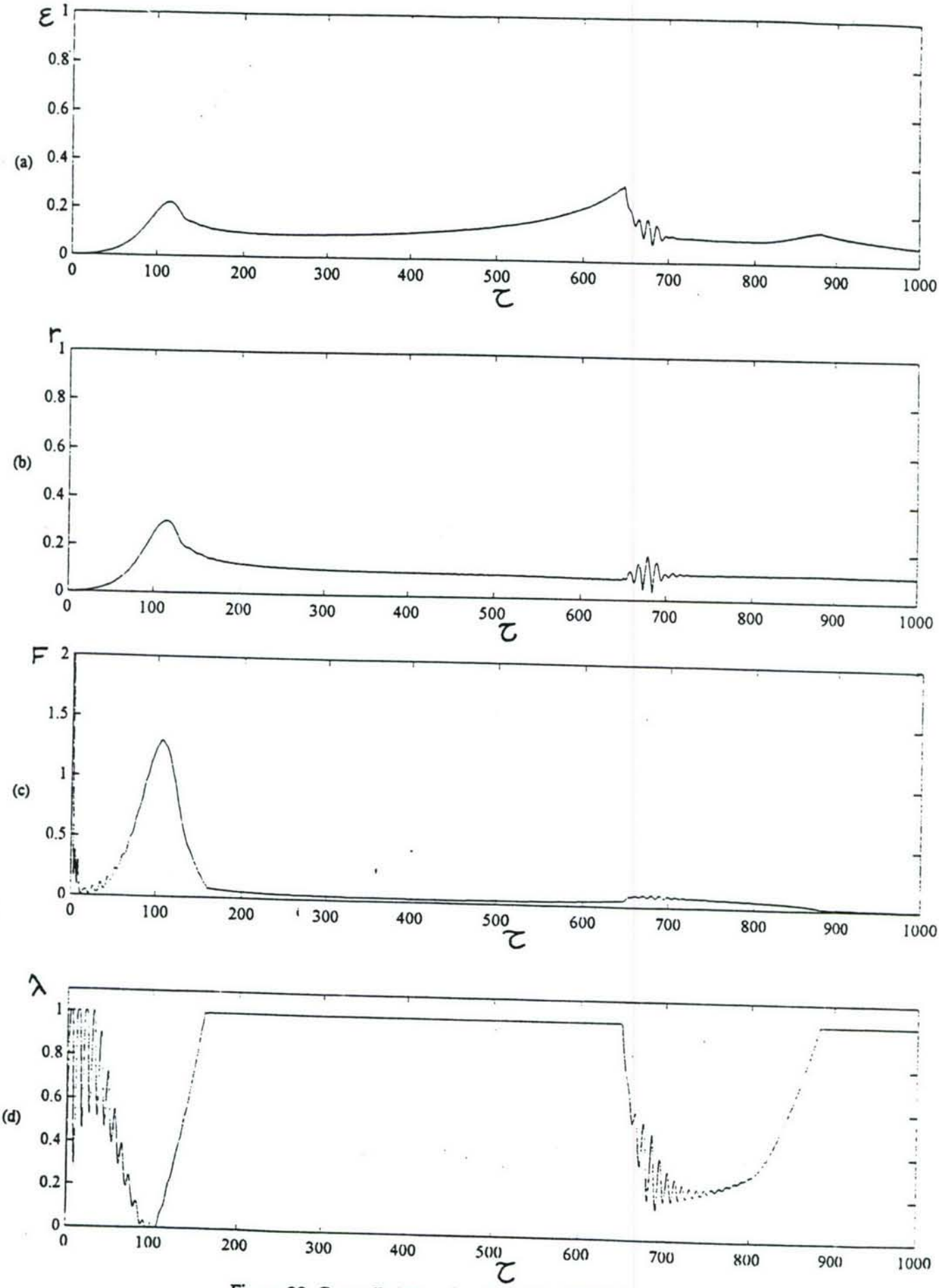

Figure 29 Controlled Transient Run-Up, GS-PI Controller

CHAPTER 8

OPTIMAL CONTROL THEORY THROUGH LINEAR QUADRATIC REGULATOR (LQR)

This chapter presents another trial toward the objective of this thesis which is the active control of the vibration of rotating machinery. An optimal controller is investigated through a Linear Quadratic Regulator (LQR).

Optimal control theory through LQR is very efficient in manipulating multi-input multi-output (MIMO) systems, and also in controlling MIMO systems with lightly damped modes [18]. LQR is also of great aid in handling single-input single-output systems (SISO). This is because optimal control theory depends on the manipulation of the system in the state-space format. State space analysis used instead of transfer functions, can describe large systems in a set of first-order differential equations which are written compactly in a standard matrix form. This standard form has permitted the development of general computer programs, mainly computer aided design programs (CAD), for example MATLAB™ [24] and SIMULAB™ [25], which can be used for the analysis and design of even larger systems.

Our system can be considered as a single-input multiple-output system (SIMO). The single-input consists of the input current signal, while the outputs are taken as states that can be measured and that are important and deserve to be monitored for

best performance of the rotor system. These states are the eccentricity ratio ε, the amplitude of vibration at the disk center r, and the transmitted damping force to the support F.

It should be noted that beforehand we are aware that the LQR will be suitable around design points since the controller is linear. But, if thorough effort is done in tuning the performance can be enhanced also away from design points.

8.1 State-Space Analysis

The derivation of state-space models is no different from that of transfer functions in that the differential equations describing the system dynamics are written first. In transfer function models these equations are transformed and variables are eliminated between them to find the relation between selected input and output variables. For state-space models, instead, the equations are arranged into a set of first-order differential equations in terms of selected state variables, the outputs are expressed in these same state variables. Because the elimination between equations is not an inherent part of this process, state models can be easier to obtain. State-space models are directly derived from the original system equations.

State-space models are usually linear, and hence linearization is necessary for nonlinear systems before tackling the optimal control theory. Our system is nonlinear as discussed before, and linearization of the system equations is indispensable before designing the controller. MATLAB™ [24] offers the possibility of linearizing nonlinear

systems around working conditions specified by the user. The linear system is derived by perturbing the system equations around chosen working conditions (Taylor's series and updated methods for linearization are available in MATLAB™ [24] library). While performing linearization of the system equations, we were able to design an LQR controller for each linearizing point. After numerable simulations the system showed to behave well, for different LQR based on different linearization points. We chose to linearize the system around conditions of mild vibration and with low damping, since LQR is quite efficient in controlling systems with lightly damped modes [18] as discussed before. Linearization under such conditions seemed to be adequate for controlling our rotor system.

Thus, it only remains to put the linearized system in a standard vector-matrix form. The general form of a state-space model is as follows:

$$\dot{x} = Ax + Bu_c \qquad \text{(Set of State Equations)}$$

and $$y = Cx + Du_c \qquad \text{(Set of Output Equations)}$$

where x is the state vector, i.e. the vector of the state variables, u_c is the control vector, and y is the output vector. A is the system matrix, B is the input control vector, C is the output matrix, and D is the vector that connects directly the control input to the output. D will reduce to zero in our case since there is no direct link between the input signal and the output [26].

8.2 The System Controllability and Observability

Before deriving control algorithms for the HSFD, the system controllability and observability have to be addressed. Controllability and observability are important concepts in the theory and design of multivariable systems [26]. Although the HSFD-rotor system is a nonlinear system, the controllability and observability of the system can be carried out on the linearized system since vibration can be assumed to be linear locally around design points.

8.2.1 Controllability

Controllability is generally concerned with the question whether it is at all possible to control all states, disregarding how this might be done. A controllable system is a system where all modes can be controlled. The system showed first some lack of controllability due to its loss of damping at the HSFD which is the primary means of control to the system. To overcome this effect, we had to introduce a linear damping component in our modeling of the A matrix. The system turned out to be controllable and the controllability was checked using the following algebraic equation [26]:

$$rank\,(C^T \left| A^T C^T \right| A^{T^2} C^T \left| \ldots \right| A^{T^{n-1}} C^T) = n$$

where n is the size of the state matrix A.

8.2.2 Observability

Observability is concerned mainly with the question whether it is at all possible to find all states from measured outputs, regardless of the method used [26]. In our case this is possible theoretically, but we are more concerned to design a controller that would be adequate for implementation on our test rig. Since not all states are measured, only ε, r and F are mainly measured, this would not accommodate the Optimal technique which requires full-state feedback. Since, not all states are measured, an additional state estimator is incorporated and will compensate for the lack of observability. With this set-up, the system is observable and the algebraic condition for observability is tested as follows [26]:

$$rank\ (B \mid AB \mid A^2 B \mid \ldots \mid A^{n-1} B) = n$$

Thus, both controllability and observability are addressed and hence the optimal controller design can be performed, and specifically in our case through the Linear Quadratic Regulator (LQR).

8.3 The LQR Block Diagram

The Linear Quadratic Regulator (LQR) algorithm was chosen because of its wide use in active control of vibrations like in the work of Zhu *et al.* [18], Burrows *et al.* [10], and Zaki [36].

The block diagram for the controller is illustrated in Figure 30. It consists of two parts: a state estimator and a regulator.

The LQR controller works as follows: the estimator, in general, takes the system outputs (ε, r and F) and outputs the reconstructed states which will be the input to the controller. This later takes the difference between the desired and the actual states and outputs the control inputs that will bring the system to the desired response.

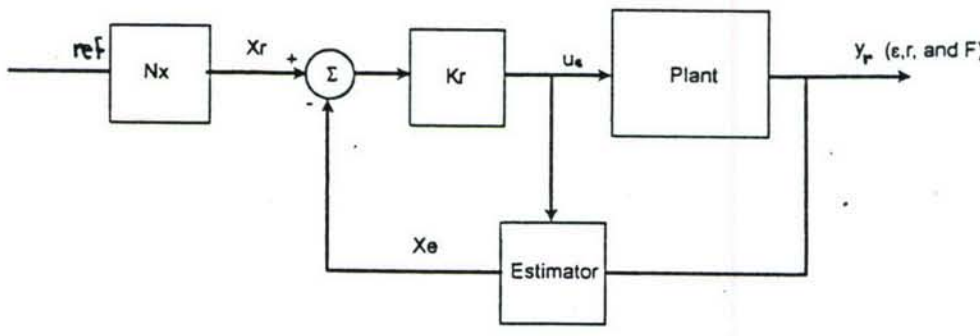

Figure 30 Block Diagram of the LQR

8.4 Optimal Regulator Design

In Linear Quadratic Regulator (LQR), the control sought after is the one which gives the best trade-off between performance (speed of control), and control effort (cost of control).

A standard form of the closed-loop case is to seek the control which minimizes the value of a performance index J, which represents a continuous quadratic cost function given by [26]:

$$J = \frac{1}{2}\int_0^\infty \left(x^T Q x + u_c^T R u_c\right) dt$$

where Q and R_c are weighting matrices and are usually diagonal. Q is the performance measure weighting matrix, while R is the cost of control weighting matrix. The terms $x^T Qx$ and $u_c^T R u_c$ of the integrand are quadratic forms which measure, respectively, the performance and the cost of control.

Thus the optimal control minimizes a weighted sum of areas such that J is minimized. The choice of the elements of Q and R_c allows the relative weighting of individual state variables and individual control inputs, as well as the relative weighting of state variables and control inputs. Therefore, a good choice of Q and R_c from the beginning will facilitate the effort taken in tuning. The important states of our concern (ε, r, and F) are given higher weights since these are the states that require both better

response behavior and better control. Such weights must be chosen carefully to give relatively higher weights to states of more importance to the designer. In our case, all three states (ε, r, and F) are given higher weights than the other states. Moreover, both ε and r are relatively given more importance than F, since a better vibration amplitude response is our primary goal.

Q and R_c are chosen through extensive trial and error and simulations to reach best performance. Tuning aimed primary to result in the best trade-off of getting maximum damping in regions and instances of severe vibrations, and minimum transmitted damping force in regions of mild vibration.

The control weighting matrices were chosen to be

$$Q = diag([100,100,50,50,70,70,50,50,30,30,1,1])$$

and $R_c = [1]$

for the following vector of states

$$x = \{x_E, y_E, \dot{x}_E, \dot{y}_E, x_S, y_S, \dot{x}_S, \dot{y}_S, \lambda, \dot{\lambda}, p, \dot{p}\}$$

It can be noted that x_E and y_E , x_S and y_S are given the higher weights since ε and r are required to be better controlled. Note that ε is given relatively more weight than r since all the control effect is primarily to the journals through the HSFDs. F represented in the vector by mainly $\dot{x}_E$ and $\dot{y}_E$ which are multiplied to the damping

coefficients as shown in Chapter 4, is given relatively lower weight than ε and r. It should be emphasized that λ and $\dot{\lambda}$ are given quite low weights despite they are the main controller for the system, i.e. a stable and accurate positioning of the sealing rings will garantee well-behaved active control. This is because high gains assigned to the sealing ring motion resulted in severe chattering of the seals.

The solution of the LQR problem stated above is to use a linear controller of gain K_{opt} in the form:

$$u = -R^{-1}B^{T}Px = -K_{opt.}x$$

where P is a positive definite matrix obtained from the solution of the Riccati equation which gets a stable optimal solution for the closed-loop system

$$\dot{x} = (A - BK_{opt.})x$$

The Riccati equation with respect to the pair (A,B) is given by [37]

$$PA + A^{T}P - PBR^{-1}B^{T}P + Q = 0$$

Hence, K_{opt} is calculated for optimal constant feedback.

The regulator gain K_{opt} is found to be

$$K_{opt.} = [24.67, 24.67, -17.93, -17.93, -15.83, -15.83, -12.11, -12.11, 4.15, 4.15, 40.94, 143]$$

8.5 Estimator Design

As stated above, LQR requires full-state feedback, but typically not all states are measured (ε, r, and F only in our case). Hence, an estimator is proposed to be added to the system in a manner that the estimator reconstructs all states before entering them to the regulator.

A Kalman Filter Continuous Estimator is proposed since it is the most widely used observer when full-states need to be estimated [37]. The Kalman Estimator observes the output states (ε, r, and F), and estimates the remainder states.

The principium of the Kalman estimator is simple and has been subject of extensive literature ([26] and[37]). It would appear that an estimate $\hat{x}$ of the state x can be obtained by digital simulation $\dot{\hat{x}} = A\hat{x} + Bu_c$ of the plant dynamics $\dot{x} = Ax + Bu_c$. But $\hat{x}$ cannot match x for all time t, because this requires $\hat{x}(0) = x(0)$, and x(0) is not known. However, by subtracting the two equations, the error x_e of the estimate is seen to satisfy

$$x_e = x - \hat{x}, \quad \dot{x}_e = Ax_e, \quad \text{and} \quad x_e(0) = x(0) - \hat{x}(0)$$

If A is stable, $x_e(t)$ will tend to zero, so the estimate $\hat{x}$ will approach x. This is as desired, except that the dynamics of this estimate are those of A; that is, the estimator has the same speed of response as the plant. Because the estimates are to be used to control the plant, the observer dynamics should really be faster than the controller

dynamics. This can be achieved by adding to the model equation a forcing term proportional to the difference between the actual output y = Cx and the estimated output $C\hat{x}$, hence

$$\dot{\hat{x}} = A\hat{x} + Bu_c + L(y - C\hat{x})$$

The Kalman filter observer solves the problem [37]

$$\dot{\hat{x}} = (A - LC)\hat{x} + Bu_c + Ly$$

which is the manipulation of the previous equation and $\hat{x}$ is the vector of estimated states, y is the vector of observed states, and L-matrix is the estimator dynamics matrix.

To show that the estimate $\hat{x}$ approaches x, subtract the last equation from the state model $\dot{x} = Ax + Bu_c$, y = Cx. This yields to the error

$$x_e = x - \hat{x}, \text{ and } \dot{x}_e = (A - LC)x_e$$

If (A-LC) is stable, x_e indeed approaches zero, so $\hat{x}$ approaches x. Moreover, through L the opportunity exists to speed up the dynamics of the estimator.

The problem resolves in getting the best design for the L-matrix which will diminish the estimator error and accelerate the dynamics of the estimator, and stabilize the system.

To design an L-matrix that would result in a speed-up of the dynamics of the systems for correct and fast state estimation, L is calculated with the same optimal technique that is used to evaluate the regulator gain K_{opt}. Hence, the Riccati Equation is solved for the pair (A,C) instead of the pair (A,B) as done before and same weighting matrices are used [37]. Thorough tuning through extensive simulations were indispensable to reach an acceptable response as will be shown later in sections 8.7 and 8.8.

8.6 Reference Input for Full-State Feedback

The LQR has the goal to drive all states to zero [37] to minimize as much as possible the coast function J. This will force the system to behave all along in the long damper mode. This is because the system will be trying to minimize ε and r which have the greatest weights in our design. This requires a maximum damping through the HSFD, and thus the system will all the way be switched to long damper mode. No compromise will be possible between minimizing ε and r at regions of high vibrations, and minimizing F at normal running conditions. The facts discussed above were proven right when we first simulated the controlled system without reference input incorporated.

At this stage it was obvious that a reference input combining all the desired states would have to be introduced since zero output is impossible to achieve in our plant especially for all three states (ε, r and F) which do not have the same trend, i.e. increase of F will decrease both ε and r with different ratios.

Thus, the state command matrices N_x and N_u, shown in Figure 31, which define the desired steady state output are introduced [37]. The values of N_x and N_u are calculated to emulate the steady state behavior required from the controlled plant.

The evaluation of N_x and N_u comes from the required behavior the designer needs at steady state. Hence, beginning on then, the steady state requirements for the system are that

$N_x\, ref = x_r = x_{ss}$,

and $C\, x_{ss} = y_r = ref$,

where x_r is the reference input, x_{ss} is the steady state behavior of the system, y_r is the desired output, and *ref* is the reference input. This equation reduces to

$C\, N_x\, ref = ref$, and hence $C\, N_x = I$

where I is the unity matrix.

Furthermore, we are assuming the system is at steady state; therefore,

$x_{ss} = A\, x_{ss} + B\, u_{css}$

where u_{css} is the steady state control input which can be assumed to equal

$u_{css} = N_u\, ref$

Hence, $(A\text{-}I)\, N_x\, ref + B\, N_u\, ref = 0$

which reduces to $(A\text{-}I)\, N_x + B\, N_u = 0$, and yields to the form [37]:

$$\begin{bmatrix} N_x \\ N_u \end{bmatrix} = \begin{bmatrix} (A-I) & B \\ C & 0 \end{bmatrix}^{-1} \begin{bmatrix} 0 \\ I \end{bmatrix}$$

N_u is taken equal to zero in our system since no feedforward steady state control input is needed for the system to be in equilibrium. This allows all the regulator action to be regulated solely by feedback. The block diagram with the incorporated reference input is shown in Figure 31.

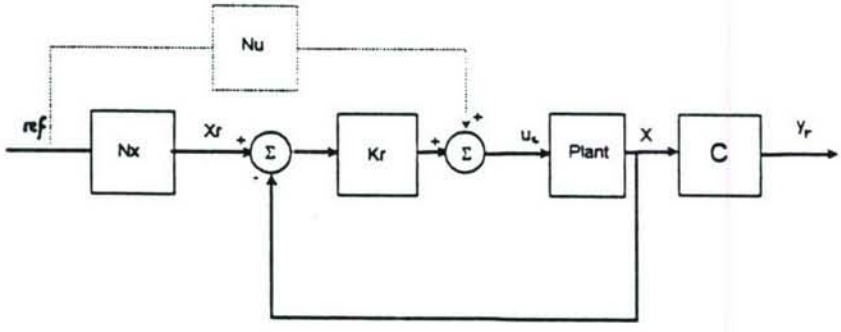

Figure 31 Reference Input Introduced to LQR

9.7 LQR Control of Transient Run-Up through Critical Speeds

The same run-up discussed in section 5.2 for the On-Off controller, and in sections 6.3 and 7.2 for the PI controller and the PI plus GS controller is proceeded with the LQR and the behavior of the controlled system is shown in Figure 32. Figure 32 (a) shows that the eccentricity ratio ε has, an enhanced behavior while passing through the first critical speed; the first peak is adequately damped. Also, the amplitude of vibration of the second critical is also lowered but slightly. Figure 32 (b) illustrates that the amplitude at the rotor disk r is also well damped for the first critical speed. Some chattering occurs in the sealing rings (Figure 32 (d)), while entering the second peak at $\tau = 600$ approximately. This causes some transient oscillations for both ε and r at the beginning of the second peak.

The chattering at the sealing rings is understood to be from the inability of the controller to make a fast decision whether to induce damping to system or not. The controller of the LQR has 3 weighted criteria (ε, r and F) that would help it decide whether to induce damping or not. A dramatic increase in the amplitude of vibration, which is the case for the first critical speed as illustrated in Figures 16 (a) and (b) for both ε and r respectively, will make the controller take the decision to induce as much damping as possible disregarding the transmitted damping force F level. This is what happens when running-up through the first critical speed which is highly damped as shown in Figure 32. On the other hand, the second critical is less accentuated than the first and there is no sudden increase in amplitude of vibration like the first peak. This makes the controller quite undecided whether to increase the damping to the system by moving the sealing rings towards the long damper configuration (i.e. towards $\lambda = 0$) or to keep the initial level of damping. This indecision causes the chattering clearly seen in Figure 32, but it remains for only 0.4 seconds and then the controller is capable of forcing the sealing ring to move to the long damper mode direction and hence giving some damping to the rotor system.

The behavior shown in Figure 32 is the optimal behavior reached with the use of the Linear Quadratic Regulator (LQR). Many other trials have been done through extensive simulations, among them considering only ε and/or r to be weighted; this caused the HSFD to act in the long damper all the way since the LQR has the goal to minimize the output. Also, we tried to consider F alone and this in the contrary drove the HSFD to act almost always in the short damper configuration. This made us think that the best LQR design for controlling our specific system is the one that trades-off

between the amplitude of vibration and the transmitted damping force. This is the conclusion that we used in the design of the regulator and it shows to be the best solution for controlling our system with the LQR. Other trials were performed to try to decrease the chattering of the sealing rings by an increase or decrease of certain gains in the Q matrix. The best choice of gains is proposed in this work and the best response reached is shown in Figure 32.

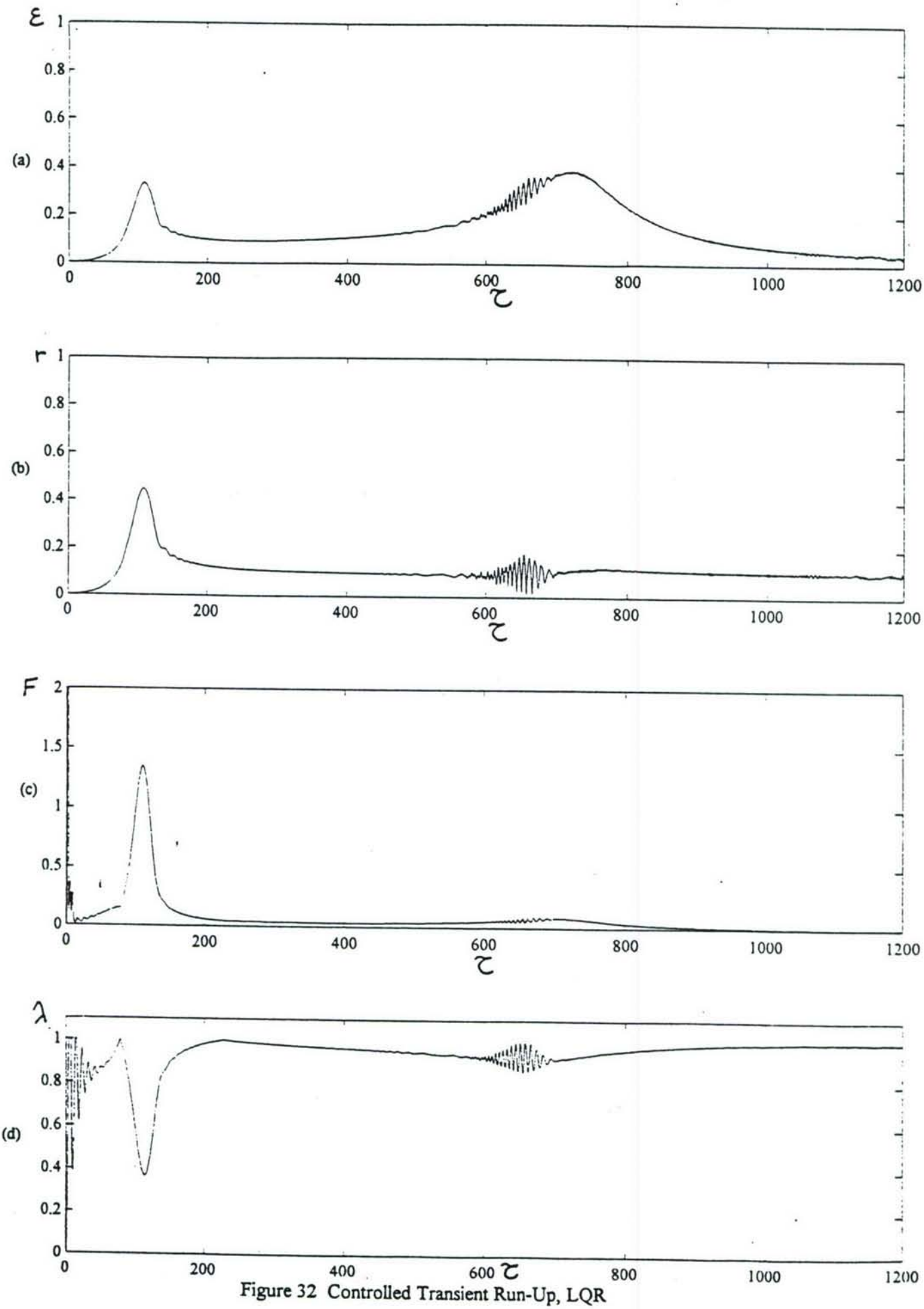

Figure 32 Controlled Transient Run-Up, LQR

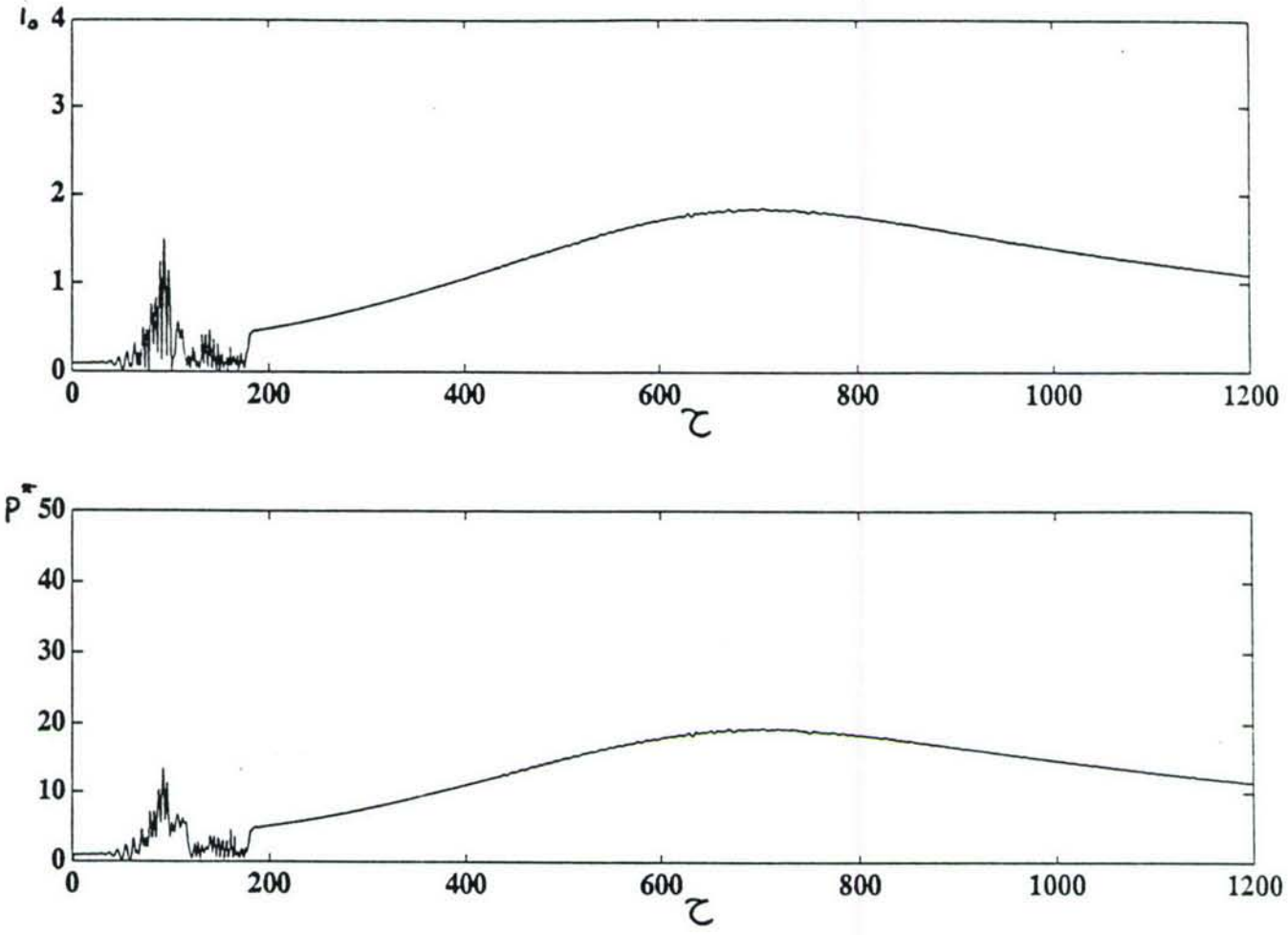

Figure 32 (Cont.) Controlled Transient Run-Up, LQR

8.8 LQR Control of Sudden Imbalance

The rotor is chosen to rotate at its normal working steady speed with an initial low unbalance of 0.05 at the disk as discussed above for the PI controller in section 6.4. Then, suddenly at a nondimensional time of $\tau = 300$, the unbalance increases to a higher value equal to 0.1. For this case also, we chose the normal working speed to be at $\Omega^* = 1$ which corresponds to the first critical speed of the rotor to investigate the performance of the controlled system under severe working conditions: sudden mass imbalance while the working rotational speed coincides with the first critical speed of the rotor.

Figure 33 shows the closed-loop behavior of the rotor system to a sudden unbalance of U = 0.1 with LQR control. The response of the closed-loop system shows an overall enhanced behavior if compared to the uncontrolled case in Figure 22. The controller reacts fast through a small transient spike that remains for about 0.1 second. We can clearly notice that the controller is unable to drive the HSFD to give maximum damping so that the amplitude reaches the initial vibration set point (for U = 0.05). This is caused, as discussed previously, by the conflict that arises in the controller to both minimize F on one hand, and ε and r on the other hand. It is concluded that the LQR is capable of damping the system to a sudden unbalance increase but with keeping some steady state error. It should be noted that the controlled behavior has an momentary input signal at $\tau = 0$ approximately which implies the sealing ring to be positioned initially at $\lambda = 0.6$ approximately. This is caused by the high gains of the regulator matrix K_{opt} which amplify the initial small

transient signal to the controller. But, with a time of 180 nondimensional, i.e. 0.95 seconds approximately, the sealing ring reaches the initial required position, the short mode configuration.

Moreover, the controller is examined with higher sudden unbalances to check if the controller is capable of compensating for higher imbalances with higher inducement of damping from the HSFD. This implies that for higher imbalances, higher damping forces are needed to reach closer behaviors to the required working condition. This compensation is done with a higher signal from the controller to the servovalve, hence the sealing ring moves closer to the long damper mode (at $\lambda = 0$), with the penalty of increasing the transmitted damping force to the rotor as shown in Figure 34. This Figure illustrates the behavior of the system to higher imbalances of 0.15 and 0.2 compared with the previous case where an imbalance of 0.1 was simulated. As discussed above, λ moves closer to $\lambda = 0$ (Figure 34 (d)) with higher unbalance forces acting on the rotor, and hence the HSFD produces higher damping forces (Figure 34 (c)) to attenuate excessive vibration and return its level as close as possible to the initial working condition of unbalance 0.05.

The controller in the case of LQR cannot eliminate all the induced vibration due to the new sudden unbalance; the level of the amplitude of vibration for both ε and r is still quite higher than the initial amplitude of vibration at $U = 0.05$. This is caused by the fact that the LQR is majorly a proportional constant controller that would react proportionally to the change of output controlled variables. Proportional gains in most cases are unable to drive the system to zero steady state error. Zero steady state error

would require the signal from the controller to the plant to change faster and to keep changing without a sensitive change in the steady state of the output variables, this is mainly an integral gain property and the LQR is primarily a proportional gain [26]. Hence, as shown from the behavior of our LQR controlled system, although the response still has a steady state error the overall response is highly enhanced for both the transient run-up and the sudden imbalance.

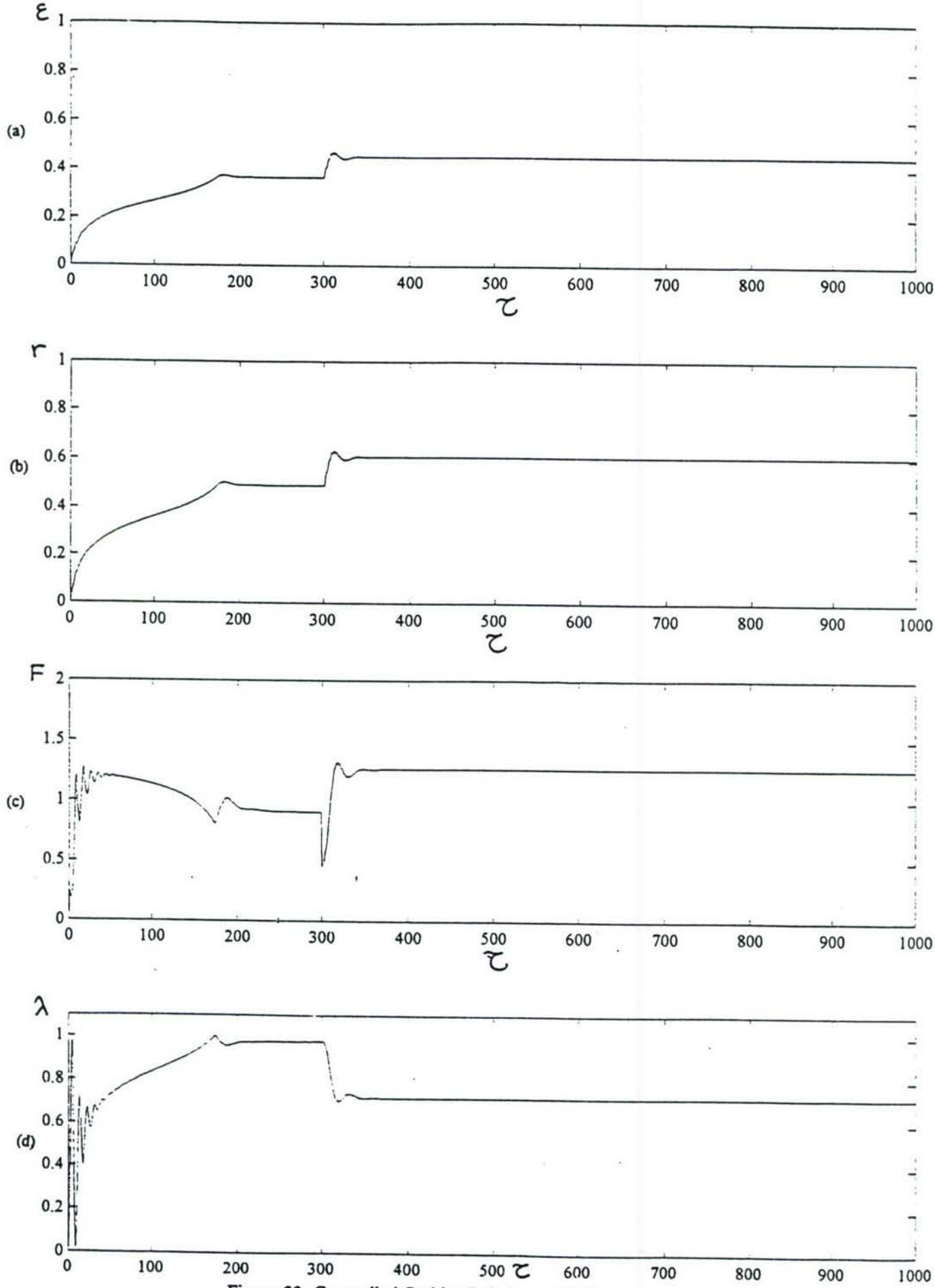

Figure 33 Controlled Sudden Imbalance, LQR

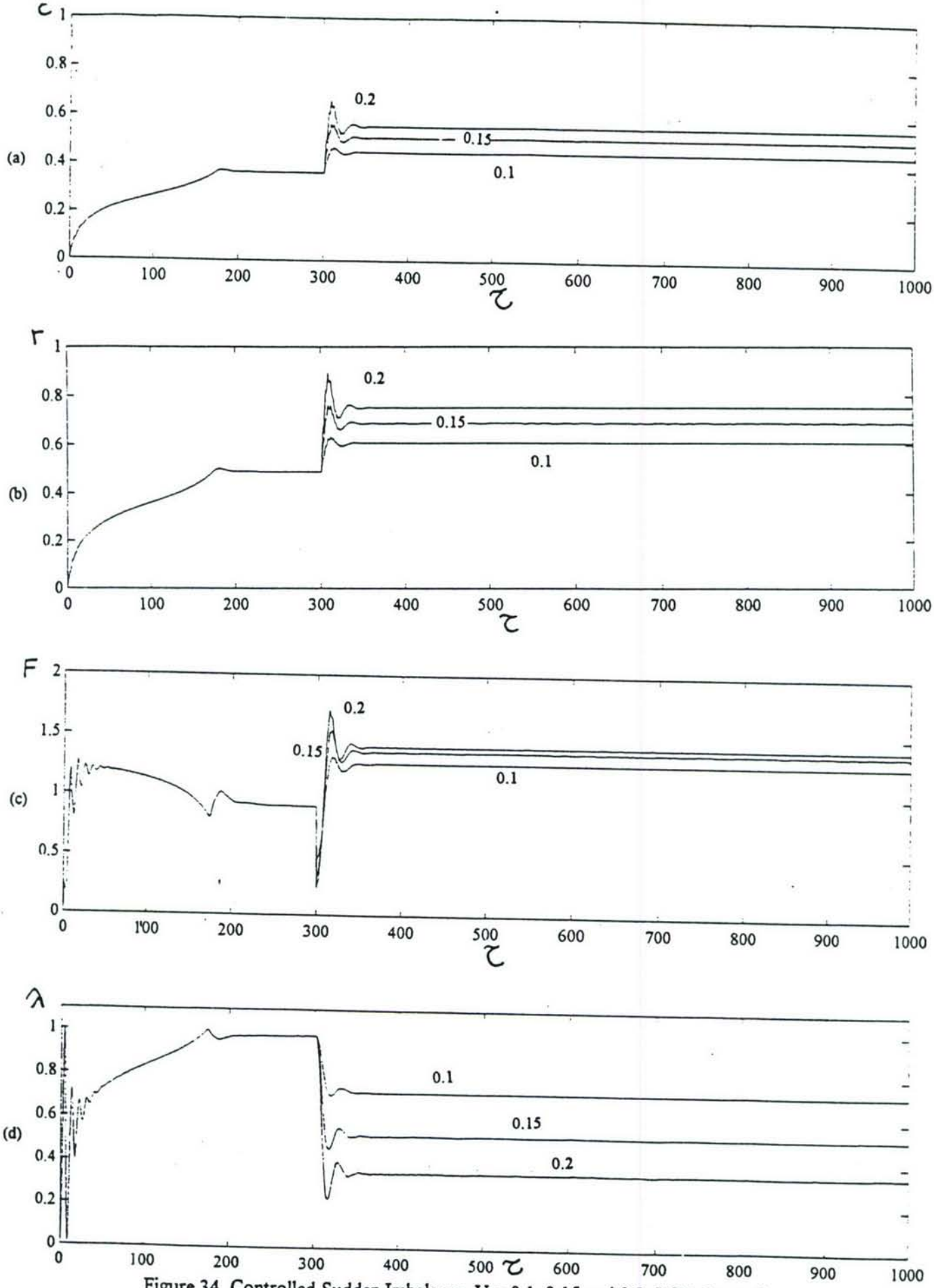

Figure 34 Controlled Sudden Imbalance, U = 0.1, 0.15 and 0.2, LQR Controller

CHAPTER 9

MODEL REFERENCE ADAPTIVE CONTROLLER (MRAC)

In this chapter, a general nonlinear controller is designed for the control of the HSFD for controlling our rotor system. The controller is based on the model reference approach. The adaptation technique was selected to be in the integral form, as the integral approach showed to be quite a success in the application of the PI and the PI plus GS technique controllers investigated before (Chapters 6 and 7 respectively). The gains were chosen to garantee the stability of the system using the gradient approach better known as the MIT rule [27]. Also, a novel way to handle the reference model is proposed: the reference model is designed nonlinear.

The Model Reference Adaptive Control (MRAC) is not new as a basic principle [27]. In the early 1950s there was extensive research on adaptive control, in connection with the design of autopilots for high performance aircraft. Such aircrafts operate over a wide range of speeds and altitudes. It was found that ordinary constant-gain, linear feedback control could work well only at operating conditions, but that changed operating conditions led to difficulties. A more sophisticated regulator, which could work well over a wide range of operating conditions, was therefore needed, and thus MRAC was proposed for the first time.

In everyday language, to "adapt" means to change a behavior to conform to new circumstances. Intuitively, an adaptive regulator is a regulator that can modify its gains in response to changes in the dynamics of the process and the disturbances. Since ordinary feedback has been introduced for the same purpose, the question of the difference between feedback control and adaptive control immediately arises. The clear difference is that the MRAC is nonlinear and has mainly two loops: one similar to that of the normal feedback system, i.e. feedback from the output to the controller and is normally faster, the second loop is the adaptive loop which is usually slower and is concerned with the update of the controller gains.

At a symposium in 1961 a long discussion ended with the following suggested definition for the Model Reference Adaptive Systems (MRAS): "An adaptive system is any physical system that has been designed with an adaptive view point" [27]. The HSFD in its enhanced design with the spring added to counteract the pressure in the sealing chamber (Figure 2), and hence accurately position the sealing rings in finite positions all through the range between the long and short damper modes ($\lambda = 0$ and $\lambda = 1$, respectively), is in itself an adaptive device capable of giving the appropriate amount of damping according to the level of vibration needed to be suppressed as discussed previously in Chapter 2. The adaptability of the HSFD makes it capable of controlling the rotor vibrations for a myriad of operating conditions and for innumerable kinds of disturbances. The belief that the HSFD is primarily an adaptive device incited us to investigate an adaptive regulator for the control of our rotor system as will be shown further in this Chapter.

9.1 The Closed-Loop Structure

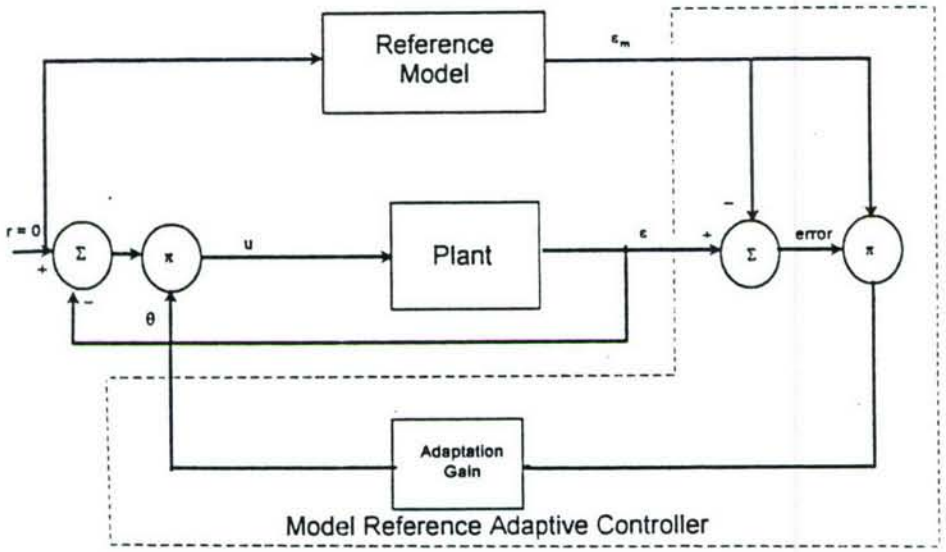

Figure 35 MRAC Block Diagram

The complete MRAC strategy is shown in the block diagram in the Figure 35. We chose only to control one output which is the eccentricity ratio ε and this showed to be sufficient in controlling all other outputs. The MRAC deals predominantly with the *model-following* problem. The desired performance is expressed in terms of a reference model, which outputs the desired output ε_m which is the desired eccentricity ratio. The system also has an ordinary feedback loop composed of the process and the regulator. The error is the difference between the output of the plant and the desired output of the reference model. The regulator has parameters that are changed based on the error. There are thus two loops in Figure 35: an inner loop, which provides the ordinary control feedback, and an outer loop which adjusts the parameters of the inner

loop. The inner loop is reacting normally faster than the outer loop which is designed in the integral form thus slower [27]. It is also noted that the reference model is enough for controlling our system and no reference input is needed. This is quite an advantage since no reference input will be changed for each working condition.

9.2 The Controller Design

The Model Reference Adaptive System (MRAS) gives a general approach for adjusting the parameters so that the closed-loop transfer function will be close to the prescribed reference model. This is called *model-following* problem. One important question is how small we can make the error. This depends on the model, the system, and the regulating rule. The regulating rule, which is the gradient approach, chosen for controlling our system is among the most widely used for its simplicity. The gradient approach is the fundamental idea in the MRAS approach [27]. The parameter adjustment scheme or the adaptation gain is usually called the *MIT rule* because the work was done at the Draper Laboratory at MIT.

The MIT rule [27] chosen for the adaptive regulator is given by

$$\frac{d\theta}{d\tau} = -\gamma(\varepsilon - \varepsilon_m)\frac{\partial(\varepsilon - \varepsilon_m)}{\partial\theta}$$

where θ is the adaptation parameter, $\frac{d\theta}{d\tau}$ is the gradient of the adaptation parameter with respect to τ, and γ is the adaptation gain rate. $\frac{\partial(\varepsilon-\varepsilon_m)}{\partial\theta}$ is the sensitivity derivative of the error with respect to the adaptation parameter θ. The gradient is negative to minimize a certain cost criterion $J_m(\theta)$ given by

$$J_m(\theta)=\frac{1}{2}(\varepsilon-\varepsilon_m)^2$$

which minimizes the error square of the error $(\varepsilon-\varepsilon_m)$. The MIT rule can be explained as follows: assume that the parameter θ change much slower than the other system variables. To make the square of the error smaller, it seems reasonable to change the parameter in the direction of the negative gradient of the error. The parameter adjustment mechanism proposed by the MIT rule can be regarded as composed of a linear filter for computing the sensitivity derivative from the error between the plant and the reference model outputs, a multiplier, and an integrator. The parameter change is then introduced in the control law using a second multiplier as shown in Figure 35. Notice that the MRAS attempts to adjust parameters so that the correlation between the error and the sensitivity derivative becomes zero.

Another approach is made in the MIT rule to solve the problem of adjusting a feedforward gain which is necessary to our case. Let the reference model have the transfer function $G_m(s) = \theta^\circ G(s)$, G(s) is function of the plant transfer function and the relation is through an assumed known constant θ°. The error hence is

$$error = \varepsilon - \varepsilon_m = G(p)\theta u_c - G_m(p)u_c = G(p)(\theta - \theta^*)u_c$$

where p = d/dt the differentiation operator. The sensitivity derivative hence becomes

$$\frac{d(\varepsilon - \varepsilon_m)}{d\theta} = G(p)u_c = \varepsilon_m / \theta^*$$

And thus the MIT rule gives [27]

$$\frac{d\theta}{d\tau} = -\gamma(\varepsilon - \varepsilon_m)\varepsilon_m$$

where θ° has been included in γ. Thus to construct a functional MRAC the rate of change of the gain parameter should be made proportional to the product of the error and the reference model output. By this approach, it should be noted that in the MIT rule, the error $(\varepsilon - \varepsilon_m)$ is multiplied to the ideal output ε_m. and thus the more the error is large, the more the adaptation of the parameter is fast and vice-versa. γ is the adaptation gain rate, it is usually chosen to minimize the error and stabilize the system. The choice of γ is done by trial and error through several simulations until the behavior of the system is enhanced although it is preferable to chose a low value for γ to garantee stability [27]. γ was chosen to equal 5 and showed well-behaved overall response of the closed-loop system. Some of the characteristics of the MIT rule stated in the literature are that the MIT rule can be successful with nonlinear systems, and can be used to handle partially known systems.

9.3 The Choice of the Reference Model

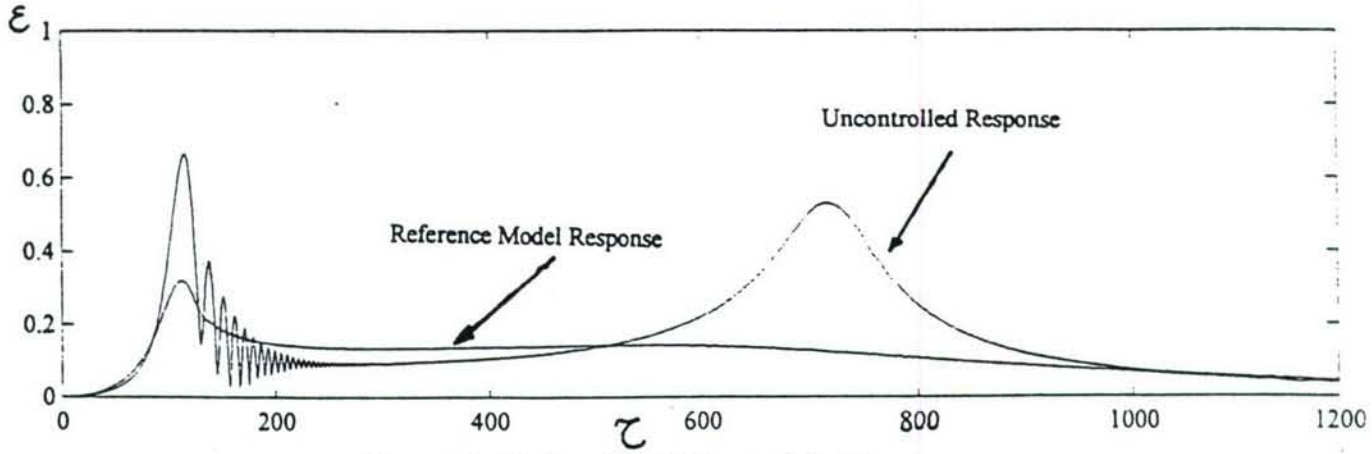

Figure 36 Choice of the Reference Model

We chose the reference model to be exactly as the plant model but working at different conditions and with different disturbances. Usually, reference models which are commonly used in MRAS are either linear or reduced order models for simplicity in modeling (for example[27] and [36]). We thought of using the nonlinear model as a reference since it did not show any difficulty while modeling, and since the nonlinear model will give a more realistic output than the linearized one. The reference model is the model that will give the ideal behavior sought after and which the plant should follow with the help of the adaptive controller.

As a first attempt, we chose the reference model to behave all the way in the short damper configuration with a smaller unbalance than the plant. Model following dictated the HSFD to behave continuously in the long damper mode, since the plant output will be always greater than the reference model output and hence the controller will always give a signal to dampen the higher amplitude of vibration. Many other attempts were made by changing the unbalance but were quite unsuccessful.

The best choice of the reference model was to run it in the long damper with a specific higher unbalance than that of the plant (which was found to equal 0.2 approximately). This produced a system that when compared to the uncontrolled one in the ε sense will give the perfect model following and both the reference model eccentricity ratio and the uncontrolled plant eccentricity ratio are compared in Figure 36. The reference model eccentricity ratio ε_m has its criticals highly attenuated and thus the controller based on model following will enforce the HSFD to give more damping to follow the reference model behavior. In regions of mild vibration, we can see that ε_m is slightly larger in amplitude than ε. Thus, the controller will try to lessen the damping through the HSFD and hence the short damper behavior will be reached which is the minimum damping possible in our system. Therefore, the compromise between giving adequate damping in regions of high vibration and minimum transmitted force in regions of less vibration can be reached successfully. The envisioned control discussed in this section will be investigated in the coming sections and will be shown effective.

9.4 MRAC Control of Run-Up through Critical Speeds

The behavior of the MRAC controlled system is shown in Figure 37 through run-up through critical speeds. The Figure shows an overall enhanced behavior if compared with the uncontrolled run-up in Figure 16. Figure 37 (a) shows that the eccentricity ratio ε has an enhanced behavior while passing through the first critical speed; the first peak is adequately damped. Moreover, ε at the second critical is also attenuated. Figure 37 (b) illustrates that the amplitude at the rotor disk r is also

adequately damped. Figure 37 (c) shows an increase of the transmitted force only at criticals where the peaks have to be attenuated in response to the movement of the sealing rings towards the long damper configuration ($\lambda = 0$). Some low transient oscillations persist while positioning the seals at the required position but since these oscillations are low, they are of very little effect on the behavior of the system as shown in Figure.

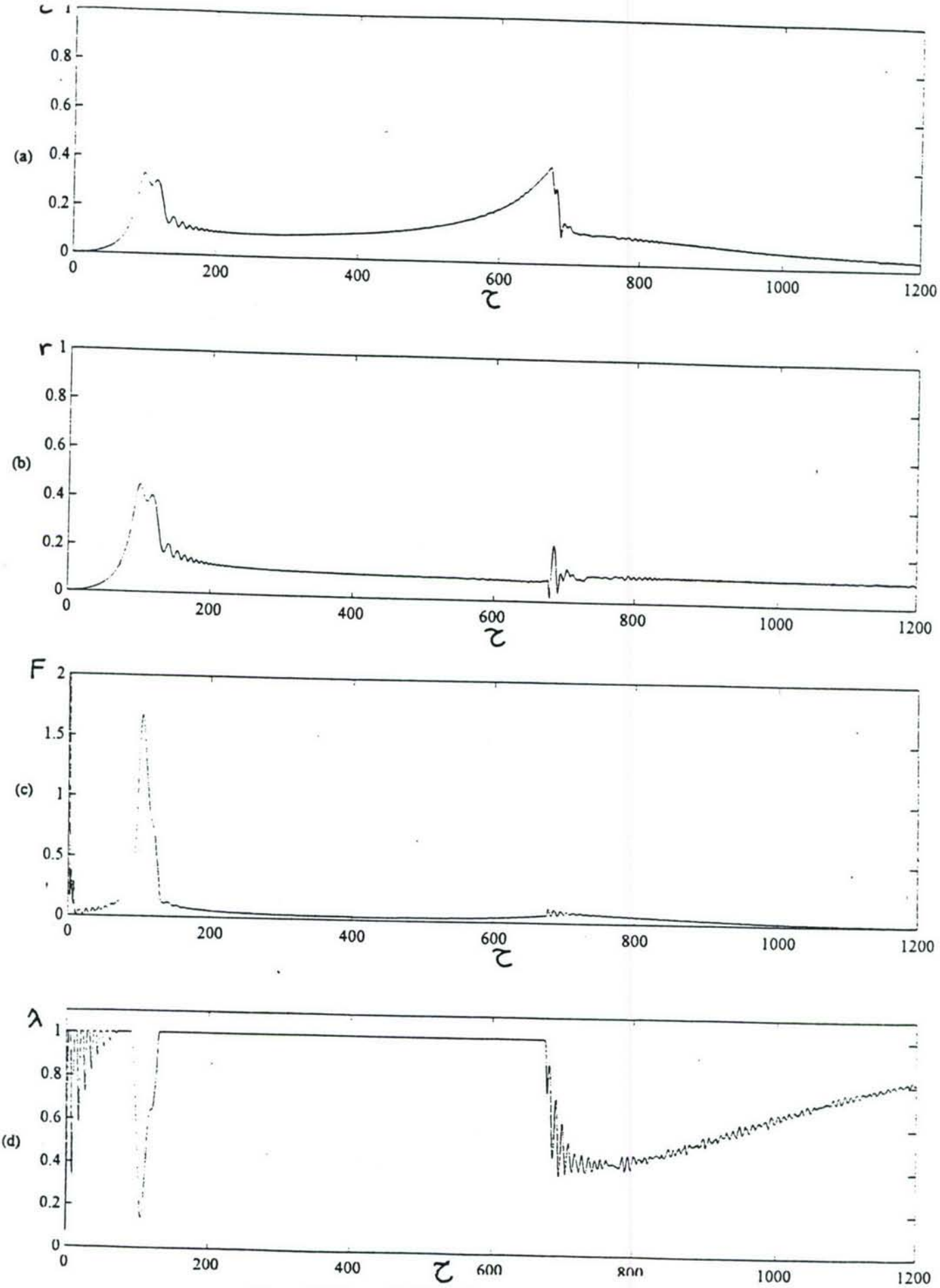

Figure 37 Controlled Transient Run-Up, MRAC

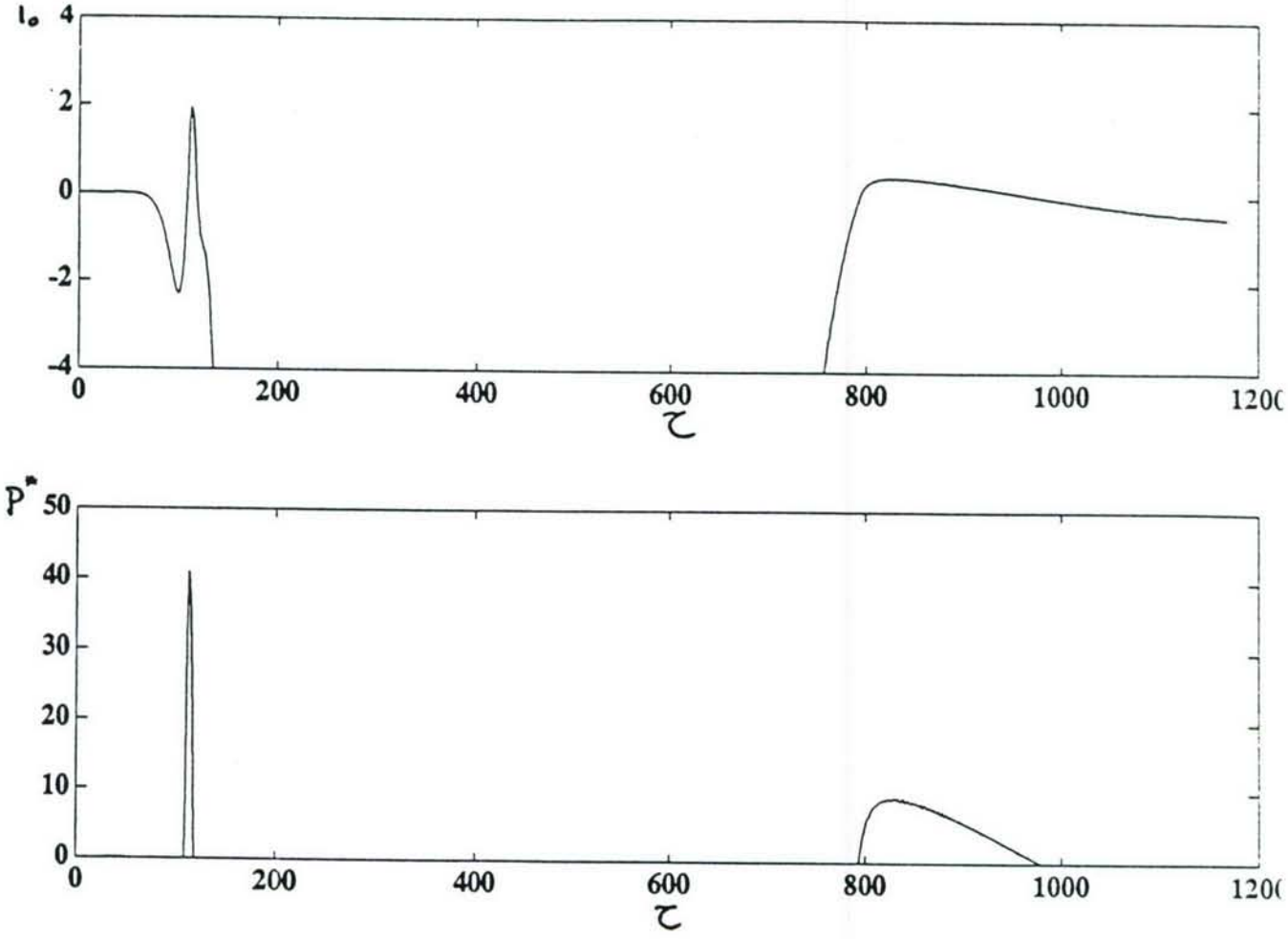

Figure 37 (Cont.) Controlled Transient Run-Up, MRAC

9.5 MRAC Control of Sudden Imbalance

For the same conditions discussed before for both the PI and LQR controllers, the imbalance step change is performed for the closed-loop system with MRAC.

Figure 38 shows the closed-loop behavior of the rotor system to a step sudden unbalance from an initial value of U = 0.05 to U = 0.1 with MRAC control. The response of the closed-loop system shows an overall enhanced behavior if compared to the uncontrolled case in Figure 22. The MRAC reacts fast through a small transient spike that remains for about 0.15 second. The MRAC is capable of inducing the right amount of damping through the HSFD and return the response to its initial state, i.e. with zero steady state error. This is mainly because of the MIT rule which has an inherent integral form, and the integral action tends to produce zero steady state error.

Furthermore, the controller is investigated with higher sudden unbalances. This implies that for higher imbalances, higher damping forces from the HSFDs are needed to reach closer behaviors to the required working condition. Figure 39 illustrates the behavior of the system to higher imbalances of 0.15 and 0.2 compared with the previous case where an imbalance of 0.1 was suggested. Figure 39 (d) shows that the sealing ring motion λ moves closer to the long damper configuration ($\lambda = 0$) with the increase of the magnitude of the sudden unbalance. This compensation is done with a higher signal from the controller to the servovalve, hence the sealing rings move closer to the long damper mode (at $\lambda = 0$), with the penalty of increasing the transmitted damping force to the rotor as shown in Figure 39 (c). Figures 39 (a) and (b) show

both the responses of ε and r. The response of MRAC is very impressive since the system returns to its normal running conditions in very little time for the case of U = 0.1 and 0.15. At U = 0.2, the controller induces the maximum possible damping of the HSFD which is the long damper mode and the behavior of ε and r is very close to the normal running condition; no more damping is possible afterward.

Hence, as shown from the behavior of our MRAC controlled system enforces the system to give zero steady state error, and the overall response is dramatically enhanced for both the transient run-up and the sudden imbalance.

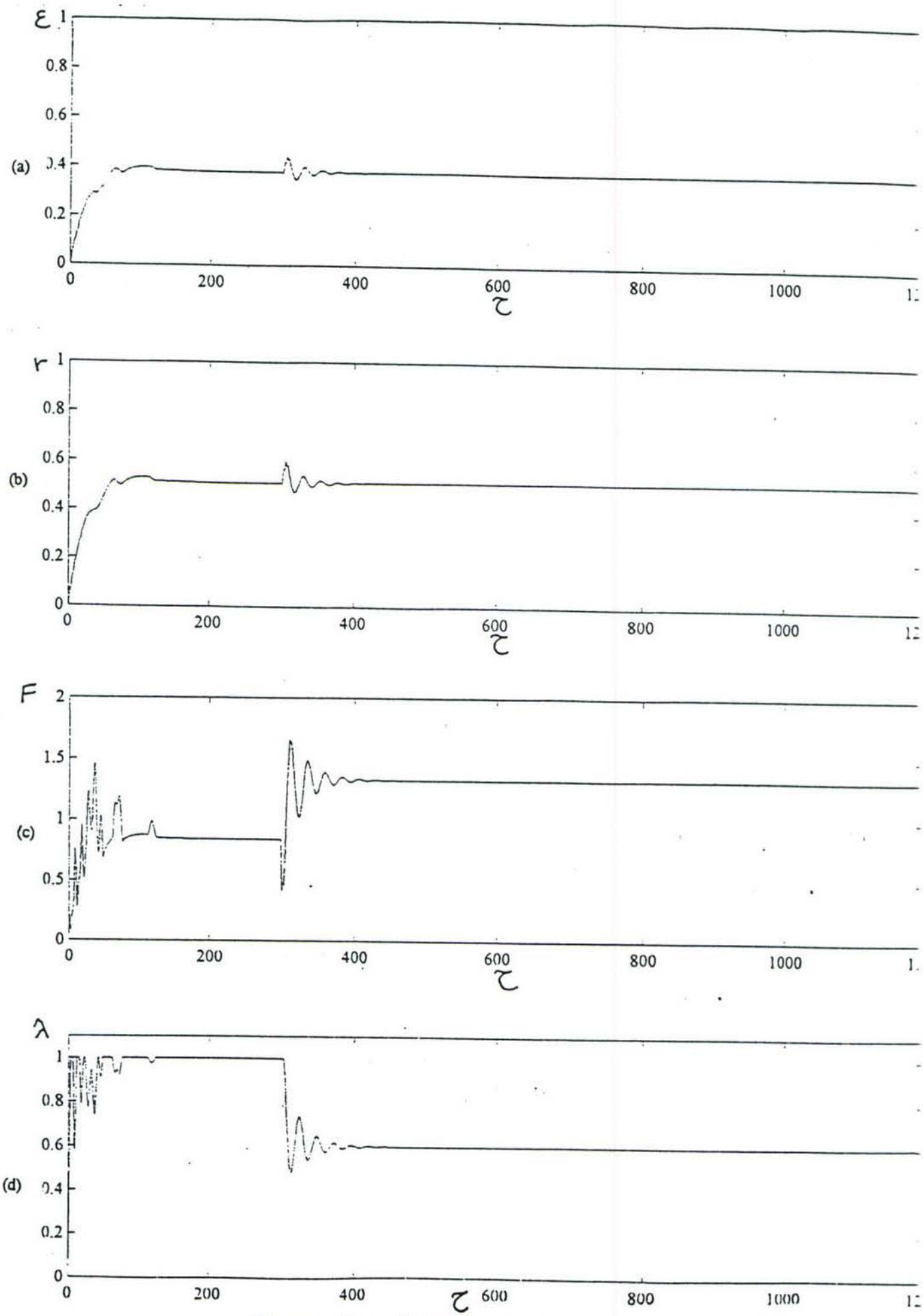

Figure 38 Controlled Sudden Imbalance, MRAC

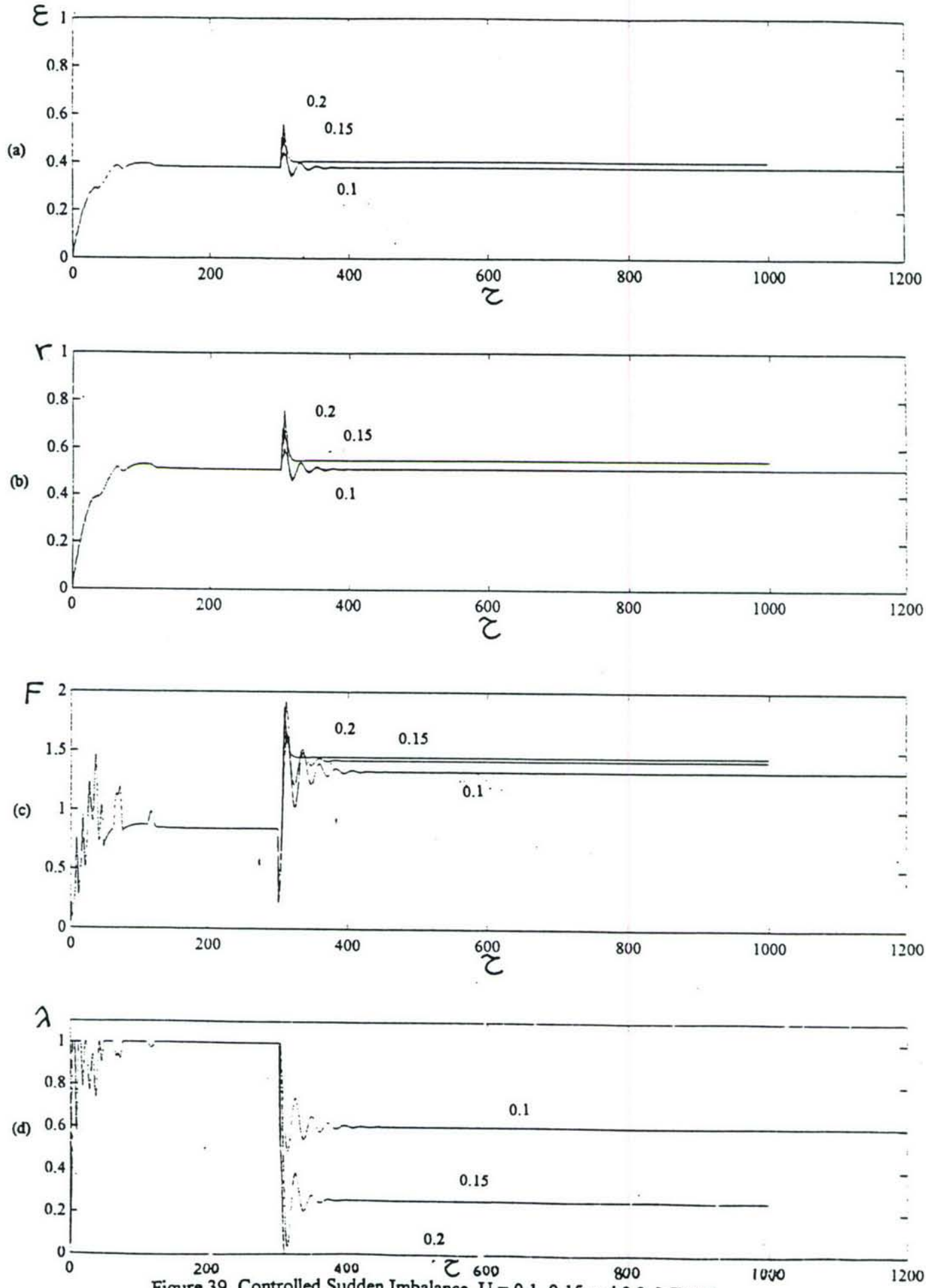

Figure 39 Controlled Sudden Imbalance, U = 0.1, 0.15 and 0.2, MRAC

CHAPTER 10

INSIGHTS INTO THE PROPOSED CONTROLLERS

In this Chapter, the controllers designed for the application of controlling HSFDs for actively controlling rotor-bearing systems are compared and the author recommendation on which controller to use for this specific application is stated with the reasons taking into account the robustness of the controller, the speed of control and the steady state error of the response.

In the control work done in this thesis, five main controllers are successfully designed and implemented numerically, namely: the On-Off (bang-bang) controller with speed feedback, the PI (proportional, integral) controller, the GS-PI (the gain scheduling proportional integral) controller, the LQR (the linear quadratic regulator), and finally the MRAC (Model reference adaptive controller). The study of these controllers made us tackle several control branches namely: the conventional control with the On-Off and PI controllers, the nonlinear control theory with the GS-PI, the optimal control theory through the LQR, and finally the adaptive control theory through the MRAC.

The main purpose of investigating so many controllers in several different branches was to reach a conclusion on the most appropriate controller that would suit our special application. First, we used the on-off controller since it seemed the most

simple to begin with and as acknowledged by Burrows et al. [10], only two levels of damping would secure the control of some kinds of rotor systems. Then, although the bang-bang controller gave satisfactory results, we aimed to control also sudden unpredictable change of unbalance. The on-off controller could not compensate for such a case since it is a pre-programmed controller. Hence, we decided to tackle other more complicated areas of modern control that would compensate for sudden unpredictable vibrations due to blade-loss for example. The vision was not clear which controller to use since we are the pioneers in designing controllers for the Hybrid Squeeze Film Dampers (HSFDs). Thus, we had to investigate several control theories for our special system that would both control the vibrations while running-up the rotor and compensate for sudden disturbances. Insights into the controllers used in this work are presented in summary in this Chapter with a comparative point of view to try to select the most appropriate controller for our system.

10.1 Run-Up through Critical Speeds

The investigated controllers in this thesis give an overall well-behaved response during the run-up through critical speeds.

The On-Off Controller based on rotor speed attained shows excellent results while running-up the rotor as illustrated in Chapter 5. The only drawback is that the system rotordynamics should be studied before designing the control algorithm, this is not considered a serious drawback since usually a meticulous study of the system's natural frequencies and mode shapes is done beforehand. The On-Off controller is

majorly working between two specific ranges of damping and does not exploit the adaptability of the HSFD which can use a myriad of finite damping configurations. Hence it gives maximum damping, i.e. long damper configuration, at peaks which increases the transmitted damping force to the bearings dramatically. The transient switches are stable, well-behaved and very fast.

The PI controller, investigated in Chapter 6, is not as efficient as the previous On-Off controller in controlling the first peak. The second peak is attenuated through quite a high transient and some severe oscillations in the sealing rings. Also, the PI controller requires meticulous tuning for its gains and the obtained PI controller behaves well at and only around the design points. Furthermore, a system input reference must be known at each operating point from the controller, and this requests a good knowledge of the open-loop system behavior. The PI reveals some lack of robustness and some chattering of the seals. In addition, the PI regulator caused wind-up of the control signal and this could make the controller quite lazy in its response, as shown in Chapter 6. Hence, it was proposed to use scheduling of both the gains and the reference for a better use of the PI controller.

In Chapter 7, the Gain Scheduling technique is incorporated to the PI controller. The system behaves better than the PI controller alone. Chattering of the seals is decreased, and the first mode of vibration is better attenuated. The gain scheduling requires a lot of tuning and a good knowledge of the behavior of the open-loop system versus the speed of rotation which is the scheduling parameter. Also, lots of simulations are required to build an efficient schedule of the gains. The GS-PI

controller is robust, its only disadvantages are: the requirement of a good knowledge of the system rotordynamics and the hectic tuning of the gains.

The LQR behavior during run-up, discussed in Chapter 7, shows to damp well the first peak of vibration, but on the other hand the sealing rings show some chattering while controlling the second mode. The chattering of the seals, which are the primary means of controlling of the behavior of the HSFD, causes some transient undesirable vibration at the second mode. Despite the overall well-behaved response of the output, to reach such good results extensive tuning of the gains is required, and this demands thorough simulations. The run-up shown for the LQR was done at specific conditions and disturbances. The LQR is the most sensitive controller to changing working conditions and disturbances, and tends to destabilize the closed-loop behavior if the conditions deviate from the design working conditions; the LQR designed in our work is only robust at and around the design working conditions. This is because the LQR is a linear regulator which requires linearization of the system equations around a specific operating condition. It is thus obvious that there are conditions where the system would be unstable especially if no thorough tuning is done beforehand. The LQR requires also specific reference inputs to be entered to give successful results in the trading-off between the minimum vibration minimum transmitted damping force required from the regulator, since the LQR without reference input tends to drive all states to zero [37]. Moreover the design of the reference input for LQR is based on a steady state formulation as shown in Chapter 8, we intend to use the controller for controlling transient vibration, thus this is expected to create some problems for our closed-loop system. Also, the LQR needs a state

estimator (observer) since not all states are observed, and again the observer is based on the linearized system at certain operating conditions. Hence, the LQR needs extensive tuning at each operating condition and lacks robustness.

The MRAC shows to be the easiest controller to manipulate together with the On-Off controller discussed above, since it is based on model following and thus may be very efficient if a good choice is made for the reference model (ideal desired behavior). Once a good model following technique is achieved, MRAC does not need any reference input since the regulator job is to drive the plant response as close as possible to the reference model response. The simulations during run-up show a very fast, well-behaved and accurate response of the controller. Since the reference model is accurately chosen, no further tuning is needed when the system is operated at different operating points; the MRAC has the job to decrease the error between both the reference model output and the plant output to zero.

10.2 Imbalance through Sudden Blade-Loss

Although most of the research done in active vibration control and stated in the literature is only concerned with the control of the steady-state or the transient run-up and shut-down through critical speeds, only very few papers [19] and [35] have tackled the problem of controlling sudden unexpected disturbances that could be caused by sudden blade-loss from the rotating machinery and thus could cause a disaster.

Despite some decisions on which controller is more robust, accurate and fast can be made from the previous section dealing with the control of the rotor run-up, the controller is also required to compensate for sudden unpredictable vibration, which could be caused by blade-loss and causes sudden imbalance in the rotor. This produces excessive increase in the amplitude of vibration of the rotor, which cause excessive forces on the bearings that would lead to failure. One of many examples stated in the literature is the recent destruction of a 300-MW turbine generator which was set in Texas and the disaster was blamed on excessive bearing loads due to loss of a blade from the final rows of the LP turbine [19].

From our study of the On-Off controller in Chapter 5, it is obvious that the On-Off controller cannot make up for sudden imbalance since it is a pre-programmed algorithm that requires the preknowledge of the system behavior.

The PI regulator and GS-PI regulator have the same ability in couteracting for sudden blade-loss and this is due to the integral gain that drives the steady-state error to zero. The response is fast but with quite a high transient overshoot that persists for a maximum value of 0.4 seconds approximately for an unbalance U of 0.2. The sealing ring behavior shows a very small transient spike, and the overall behavior is good.

The LQR is an optimal constant feedback regulator, hence it does not have the same ability of the integral gain to reduce the steady state error to zero. Hence, some steady state error exists even though the controller reacts fast to the sudden unbalance increase. The time of the transient spike till the behavior reaches steady state is of a

maximum value of about 0.3 seconds approximately for U = 0.2. The LQR is fast, stable but inaccurate in returning the system to the initial operating condition.

The MRAC does not need a reference input like the other regulators discussed above. The reference model is enough for model following compensation. Moreover, it has the fastest response since the maximum transient time until the response reaches steady state for U = 0.2 is less than 0.1 seconds approximately. In addition, the controller, based on integral gains (MIT rule, [27]) as discussed in Chapter 9, is accurate and accomplishes zero steady state error.

For both cases of active control of run-up through critical speeds and control of sudden rotor imbalance, the MRAC seems the most accurate, robust and fast controller. The behavior of the MRAC for both cases is stable and generally well-behaved. The MRAC manipulation is easy, no extensive tuning is required, the control law is easy to use, and above all the adaptive control depends on the model following problem, hence the choice of a reference model that would accommodate our needs and would result in an ideal behavior is the only requirement for good results.

CHAPTER 11

DISCUSSIONS AND CONCLUSIONS

The development of hybrid squeeze film dampers (HSFDs) for active control of rotor vibrations is studied in this thesis.

11.1 Summary of the Thesis Contents

The main emphasis of the work was: (1) enhancing the design of the HSFD for improving it in a adaptive device that would give several aspects of dampers depending on the amount of vibration to be attenuated. Also, (2) the automation of the hydraulic circuit for electrically controlling the HSFD. (3) Modeling of the nonlinear system in a format that could be easily used for (4) simulation of both the open-loop and the closed-loop system behaviors. Finally, (5) investigating all the control theories that could apply to our case in controlling transient run-up and sudden imbalance of rotor system. In this research an On-Off controller based on speed feedback, a Proportional Integral (PI) controller, a nonlinear Gain Scheduling PI regulator (GS-PI), an optimal Linear Quadratic Regulator(LQR), and finally a Model Reference Adaptive Controller (MRAC) are studied.

11.2 Conclusions

The following conclusions can be extracted from the thesis:

1 - We managed to design an HSFD capable of giving several damper configurations between the short damper mode in one extreme and the long damper mode in the other extreme. This represents an adaptive damper that is capable of acting as a finite damper giving the right amount of damping when needed.

2 - An automatically controlled circuit, including an electrohydraulic pressure control servovalve that could be easily interfaced to a digital computer control, was developed and hence complete computer control of the HSFD through controlling the pressure in the sealing chambers is possible.

3 - A complete mathematical model for the finite HSFD-rotor-control system is developed and simulated in the open-loop sense for both the steady-state and transient behaviors. The simulation results illustrate that the automatically controlled HSFD can be a very useful device for the active control of rotors, which can improve the performance of rotating machinery.

4 - Control development is proceeded for both controlling the run-up of the rotor through its critical speeds (i.e. speed-up and coast-down of rotating machinery) and for compensating for sudden rotor imbalance (i.e. through blade-loss). The anticipated basic strategy for the controllers to be investigated is proposed: the goals are to

minimize both the amplitude of vibration and the transmitted damping force to the structure. Only a trade-off between these restrictions is possible: inducing the adequate damping at regions of high vibration, and turning the system to the short damper mode which is the least level of damping in the HSFD in regions of mild vibrations.

5 - Among the controllers investigated (On-Off with speed feedback, PI, GS-PI, LQR, and MRAC), the Model Reference Adaptive Controller showed an overall improved, stable, well-behaved, fast, accurate, robust and reliable performance. MRAC is easy to design, use and handle. MRAC criteria is the good choice of the reference model for perfect model following.

Because of the variable damping properties achieved by the hybrid squeeze film damper, it is anticipated that the actively controlled HSFD can

(1) improve the vibration isolation capability of the support,

(2) reduce amplitude of rotor vibration,

(3) enhance the stability of the rotating machines,

(4) allow the rotor and the damper to operate at high loads,

(5) result in a rotating machine that is capable of operating at wide speed ranges, and

(6) compensate for sudden disturbances, e.g. blade-loss, and thus the rotating machine is capable to operate under varying and adverse conditions,

this should lead to overall improved performance and safety of rotating machinery, particularly for variable speed machinery.

11.3 Suggestions for Future Research

A model of the rotor-bearing system exhibiting two modes of vibration is presented in this thesis. Modeling the system for exhibiting multiple modes and testing the proposed control theories on the new model would be very useful for checking the robustness of the controllers. In this thesis, a model of the HSFD without cavitation and fluid inertia effects is handled for simplicity while tackling for he first time controllers for the HSFD. Future research much take such nonlinearities into account as they may influence the controller behavior.

Several control algorithms have been presented in this work. Experimental investigation of all control theories is needed. The On-Off controller has already been investigated on the experimental test rig at Cairo University and showed impressive results [22].

LIST OF REFERENCES

[1]. El-Shafei, A., 1993, "Experimental and Analytical Investigation of Hybrid Squeeze Film Dampers", Journal of Engineering for Gas Turbine and Power, Trans. ASME, Vol. 115, No.2, pp. 353-359.

[2]. El-Shafei, A., 1991b, "Hybrid Squeeze Film Damper for Active Control for Active Control of Rotors", U.S. Patent number 5,058,452, October.

[3]. Schweitzer, G., and Ulbricht, H., 1980, "Magnetic Bearings - A Novel Type of Suspension", Procedings of the Second International Conference on Vibrations in Rotating Machinery, I. Mech. E., pp. 151-156.

[4]. Bradfield, C.D., Roberts, J.B., and Karunendiran, S., 1989, "A Programmable Electromagnetic Bearing for Vibration Control of Flexible Shaft", in Rotating Machinery Dynamics, T.S. Sankar *et al.* editors, ASME publication DE Vol. 18-1, pp 335-343.

[5]. Palazzolo, A.B., Lin, R.R., Kascak, A.F., Montague, J., and Alexander, R.M., 1989a, "Test and Theory for Piezoelectric Actuator-Active Vibration Control of Rotating Machinery", DE-Vol. 18-1, Rotating Machinery Dynamics, ASME 1989.

[6]. Nonami, K., DiRusso, E., and Fleming, D.P., 1989, "Active Vibration Control for Flexible Rotor by Optimal Direct-Output Feedback Control", in Rotating Machinery Dynamics, T.S. Sankar *et al.* editors, ASME publication DE Vol. 18-1, pp 327-334.

[7]. White, D.C., 1972, "The Dynamics of a Rigid Rotor Supported on Squeeze Film Dampers", Conference on Vibrations of Rotating Machinery, Proc. I. Mech. E., pp. 213-229.

[8]. Gunter, E.J., Barrett, L.E., and Allaire, P.E., 1977, "Design of Nonlinear Squeeze Film Dampers for Aircraft Engines", Journal of Lubrication Technology, Trans. ASME, Vol. 99, No. 1, pp. 57-64.

[9]. Holmes, R., and Dogan, M., 1985, "The Performance of a Sealed Squeeze-Film Bearing in a Flexible Support Structure", Proc. I. Mech. E., Vol.199, No. C1.

[10]. Burrows, C.R., Sahinkaya, M.N., and Turkay, O.S., 1983, "An Adaptive Squeeze-Film Bearing", ASME paper No. 83-Lub-23.

[11]. Adams, M.L., and Zahloul, H., 1987, "Attenuation of Rotor Vibration Using Controlled-Pressure Hydrostatic Squeeze-Film Dampers", presented at the Eleventh Biennial ASME Vibrations Conference, Boston, MA, September 1987.

[12]. Mu, C., Darling, J., and Burrows, C.R., 1991, "An Appraisal of a Proposed Active Squeeze Film Damper", Journal of Tribology, Trans. ASME, Vol. 113, No. 4, pp. 750-754.

[13]. Schweitzer, G., 1985, "Magnetic Bearings for Vibration Control", Bently Nevada Instability Seminar, Minden Nevada.

[14]. Ulbricht, H. and Anton, E., 1984, "Theory and Application of Magnetic Bearing with Integrated Displacement and Velocity Sensors", I. Mech. E. Conf. on Rotordynamics, Paper C 299/84.

[15]. Weise, D., 1985, "Active Magnetic Bearings Provide Closed Loop Servo Control for Enhanced Dynamic Response", Proc. 27th IEEE Machine Tool Conf., October.

[16]. Keith, F.J., Williams, R.D., Allaire, P.E., and Schafer, R.M., 1988, "Digital Control of Magnetic Bearings Supporting a Multimass Flexible Rotor", Presented at NASA Conference on Magnetic Suspension technology, NASA Langley.

[17]. Allaire, P.E., Mikula, A., Benerjee, B., Lewis, D.W., and Imlach, J., 1988, "Design and Test of Magnetic Thrust Bearing", Presented at NASA Conference on Magnetic Suspension technology, NASA Langley.

[18]. Zhu, W., Castelazo, I., and Nelson, H.D., 1989, " An Active Optimal Control Strategy of Rotor Vibrations Using External Forces", DE-Vol. 18-1, Rotating Machinery Dynamics, ASME 1989.

[19]. Palazzolo, A.B., Lin, R.R., Kascak, A.F., and Alexander, R.M., 1989b, " Active Control of Transient Rotordynamic Vibration by Optimal Control Methods", ASME paper No. 88-GT-73.

[20]. Palazzolo, A.B., Jagannathan, S., Kascak, A.F., Montague, G.T., and Kiraly, L.J., 1991, "Hybrid Active Vibration Control of Rotorbearing Systems Using Piezoelectric Actuators", DE-Vol. 38-1, Modal Analysis, Modeling, Diagnostics, and Control - Analytical and Experimental, ASME 1991.

[21]. El-Shafei, A., and Hathout, J.-P., 1994, "Modelling and Control of HSFDs for Active Control of Rotor-Bearing Systems", presented at the International Gas Turbine and Aeroengine Congress and Exposition, The Hague, Netherlands, June, ASME paper 94-GT-52.

[22]. El-Shafei, A., and El-Hakim, M., 1995, "Development of a Test Rig and Experimental Verification of the Performance of HSFDs for Active Control of Rotors", submitted to the ASME Journal of Engineering for Gas Turbine and Power and the IGTI Conference.

[23]. Hathout, J.-P., El-Shafei, A., and Youssef, R., 1995, " Active Control of Multi-Mode Rotor-Bearing Systems Using HSFDs", submitted to the ASME Journal of Tribology and the Tribology Conference.

[24]. MATLAB™ for Windows, User's Guide, The MathWorks, Inc., 1991

[25]. SIMULAB™ for Windows, User's Guide, The MathWorks, Inc., 1991

[26]. Van de Vegte, J., 1990, Feedback Control Systems, Second Edition, Prentice Hall Inc.

[27]. Astrom, K.J., and Wittenmark, B., 1989, Adaptive Control, Addison-Wesley Publishing Company.

[28]. El-Shafei, A., 1989, "Long and Short Bearing Approximations for Squeeze Film Dampers", Proceedings of the Vibration Institute, pp. 145-151.

[29]. El-Shafei, A., 1990, "Unbalance Response of a Jeffcott Rotor Incorporating Short Squeeze Film Dampers", Journal of Engineering for Gas Turbine and Power, Trans. ASME, Vol. 112, No.4, pp. 445-453.

[30]. El-Shafei, A., 1991a, "Unbalance Response of Jeffcott Rotor Incorporating Long Squeeze Film Dampers", Journal of Vibration and Acoustics, Trans. ASME, Vol. 113, No.1, pp. 85-94.

[31]. El-Shafei, A., and Crandall, S.H., 1991, " Fluid Inertia Forces in Squeeze Film Dampers", presented at the 13th Biennial ASME Vibration Conference, Miami, FL, September, published in Rotating Machinery and Vehicle Dynamics, T.C. Huang *et al.* editors, ASME DE-Vol. 35, pp. 219-228.

[32]. El-Shafei, A., and Eranki, R.V., 1993, "Dynamic Analysis of Squeeze Film Damper Supported Rotors Using Equivalent Linearization", presented at the 38th International Gas Turbine Conference, Cincinnati, OH, ASME paper 93-GT-30.

[33]. Trumpler, P.R., 1966, Design of Film Bearings, MacMillan, NY.

[34]. Thayer, W.J, 1965, "Transfer Functions For Moog Servovalves", Moog Technical Bulletin 103.

[35]. Walton II, J.F., and Heshmat, H., 1993, "Rotordynamic Evaluation of an Advanced Multisqueeze Film Damper- Imbalance Response and Blade-Loss Simulation", Journal of Engineering for Gas Turbine and Power, Trans. ASME, Vol. 115, No.2, pp. 347-352.

[36]. Zaki, A., 1994, "Modelling and Experimental Vibration Control of a Two-Link 3D Manipulator with Flexible Links", The University of Western Ontario, London, Ontario, Canada.

[37]. Franklin, G.F., Powell, J.D., Workman, M.L., 1989, Digital Control of Dynamic Systems, Second Edition, Addison-Wesley Publishing Company.

[38]. El-Shafei, A., El-Hakim, M., and Hathout, J.-P., 1993, "Control of Rotor Vibrations Using Hybrid Squeeze Film Dampers", Report MDP-EOARD-1/93, Cairo University.

[39]. El-Shafei, A., El-Hakim, M., Hathout, J.-P., and Youssef, R., 1994, "Control of Rotor Vibrations Using Hybrid Squeeze Film Dampers", Report MDP-EOARD-2/94, Cairo University.

[40]. Stanway, R. And O'Reilly, C., 1984, "State Variable Feedback Control of Rotor Bearing Suspension Systems," IMechE Rotordynamics Conference, C274/84, pp.515-524

PART III

EXPERIMENTAL CONTROL OF HSFDs

CONTENTS

CHAPTER 1
REDESIGN OF TEST ROTOR

The objective of this research work was to control multi-mode rotors. However, as discussed in Chapter 2 of Part I, the rotor that was designed exhibited only one mode during dynamical testing. We attributed this to inappropriate selection of support stiffness. The dynamical testing of the one mode rotor is reported in detail in chapter 2 of Part I, however the objective of this project is to study the behavior of the HSFD as a controlling element for multi-mode rotors. Thus, it was decided to completely redesign the rotor system, rather than working in a trial and error procedure to experimentally obtain different support stiffnesses for the single mode rotor. The trial and error procedure would have required arbitrarily selecting different support stiffnesses, and a major effort in experimentally determining the appropriate selection. The redesigned rotor was decided to exhibit several modes in the speed range under consideration, and to be suitable for use with the previously manufactured HSFD.

This chapter discusses the design of the multi-mode rotor, and the experimental verification of the behavior of this multi-mode rotor and its suitability for HSFD control.

3.1.1 NEW TEST ROTOR

The design criteria for the new test rotor were set as follows:

a - Three critical speeds to be attained in speed range.
b - Speed range to be up to 15000 rpm.
c - Manufactured HSFDs to be used with new test rotor.

Based on these design criteria, it was decided to reinvestigate a three mass rotor with more extensive design effort to obtain sufficient modal activity at the bearings locations, to allow the HSFD to efficiently damp the various modes.

The results of the extensive design effort is illustrated in Figure 1, where a three mass rotor is selected. The three mass rotor exhibits three critical speeds at 3260 rpm,

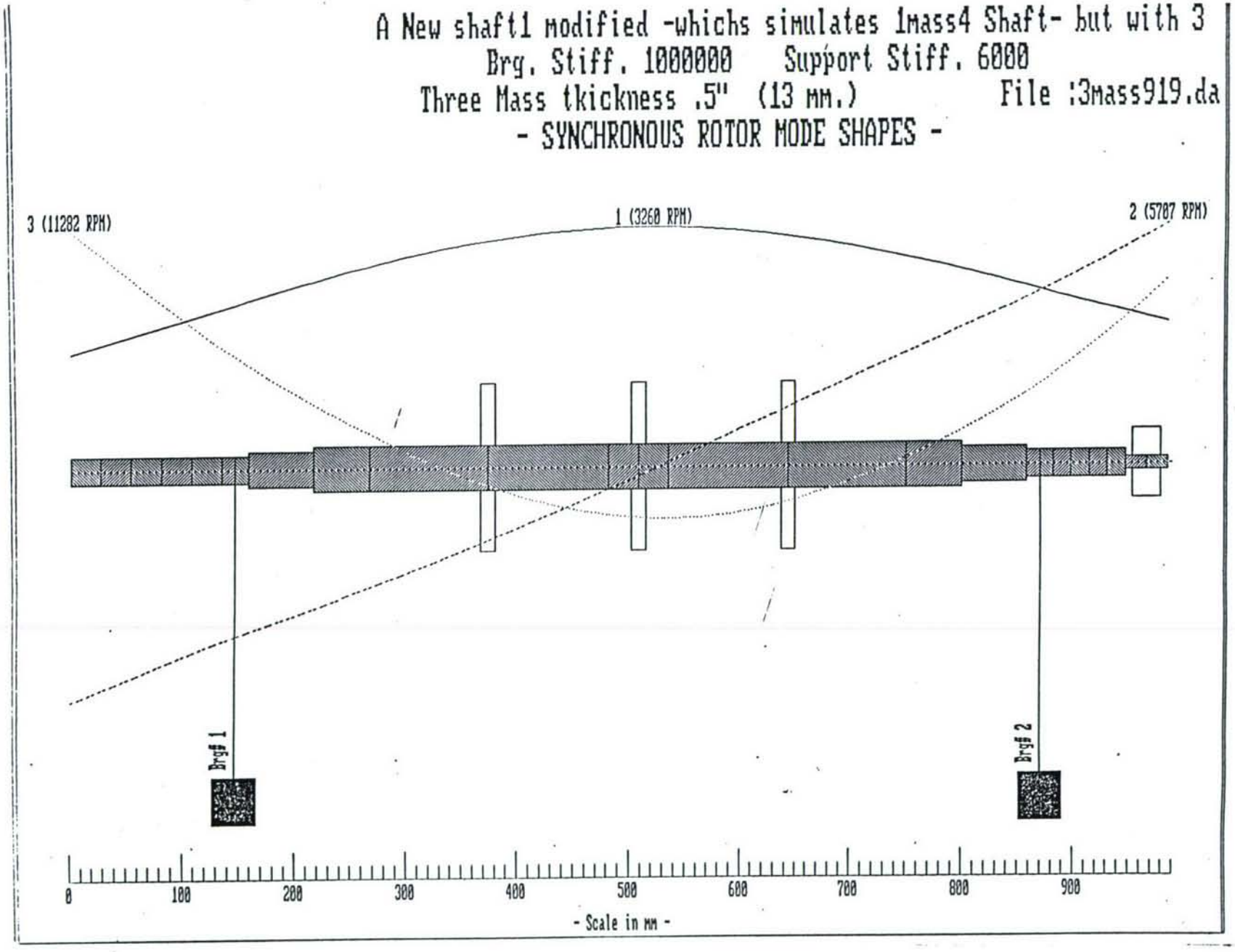

Figure 1 New Test Rig

5707rpm, and 11282 rpm. These critical speeds, as shown in Figure 1, can be classified as bouncing mode, conical mode, and first bending mode, respectively.

Moreover, all three modes exhibit significant modal activity at the bearing location thus allowing the HSFD to adequately control all three modes. The first two modes can be classified as rigid modes, where most of the deflection (and thus potential energy) occurs in the support, while the third mode represents a flexible mode, where most of the deflection (and thus potential energy) occurs in the shaft.

The complete detailed analysis and data of the new test rotor are included in the following pages, which represent the output file from the critical speed analysis.

One more point is that to obtain the third critical speed at 11282 rpm, the motor speed had to be increased. Thus, to use the available motor a belt drive with speed ratio 2:1 was used to drive the rotor, instead of the direct coupling previously reported. A sprocket was used to reduce the tension in the belt, and the effect of the sprocket is included in the critical speed model of Figure 1. The complete setup of the new test rotor with its modified drive is shown in Figure 2.

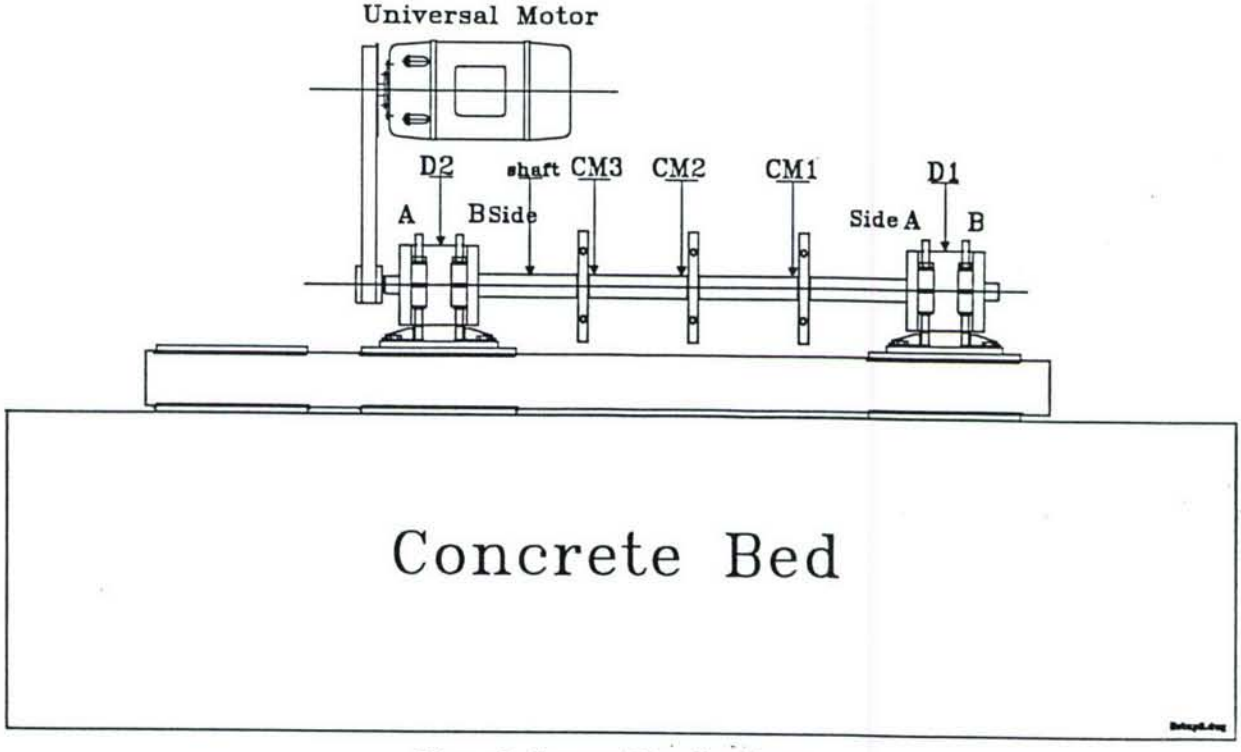

Figure 2 Set-up of New Test Rotor
with Modified Drive

Undamped, Rotor Critical Speed Analysis Program

A New shaft1 modified -whichs simulates 1mass4 Shaft- but with 3 Small Disks
Brg. Stiff. 1000000 Support Stiff. 6000
Three Mass tkickness .5" (13 mm.) File :3mass919.dat

Number of MASS STATIONS = 26
Number of BEARINGS = 2
Number of ATTACHED DISCS = 4
Number of OFFSET FLEXIBLE DISCS = 0
Number of MODES TO CALCULATE = 5
Default Density = 7.90E-06 Kg/mm^3
Default Young's Modulus = 2.11E+04 Kg/mm^2

Distributive Shaft Gyroscopics ARE INCLUDED in Model.
Transverse Shear Deformation IS INCLUDED in Shaft Calculations.
Input data are in ENGLISH units.
Output data are in SI units.

---- ATTACHED DISC DATA ----

ST #	DISC WEIGHT Kg	DISC DIAMETER mm	DISC THICKNESS mm	DISC DENSITY Kg/mm^3	POLAR MOMENT Kg-mm^2	TRANS MOMENT Kg-mm^2	DISC ORIENTATION
11	1.70	152.40	12.70	7.90E-06	5.29E+03	2.67E+03	Centered
13	1.70	152.40	12.70	7.90E-06	5.29E+03	2.67E+03	Centered
15	1.70	152.40	12.70	7.90E-06	5.29E+03	2.67E+03	Centered
25	0.58	62.00	25.40	7.90E-06	2.91E+02	1.77E+02	Centered

-- COMPLETE ROTOR MODEL --

ST #	ST LENGTH mm	ST WEIGHT Kg	EXT DIA mm	INT DIA mm	ST DENSITY Kg-mm^3	EI Kg-mm^2	POLAR MOMENT Kg-mm^2	TRANS MOMENT Kg-mm^2	Z Pos mm
1	27.00	0.05	25.00	0.00	7.90E-06	4.05E+08	4.09E+00	5.22E+00	0.0
2	27.00	0.10	25.00	0.00	7.90E-06	4.05E+08	8.18E+00	1.04E+01	27.0
3	27.00	0.10	25.00	0.00	7.90E-06	4.05E+08	8.18E+00	1.04E+01	54.0
4	27.00	0.10	25.00	0.00	7.90E-06	4.05E+08	8.18E+00	1.04E+01	81.0
5	27.00	0.10	25.00	0.00	7.90E-06	4.05E+08	8.18E+00	1.04E+01	108.0
6	11.90	0.08	25.00	0.00	7.90E-06	4.05E+08	5.89E+00	6.40E+00	135.0
7	11.90	0.05	25.00	0.00	7.90E-06	4.05E+08	3.60E+00	2.35E+00	146.9
8	58.00	0.21	32.00	0.00	7.90E-06	1.09E+09	2.54E+01	6.46E+01	158.8
9	50.18	0.43	40.01	0.00	7.90E-06	2.65E+09	7.34E+01	1.41E+02	216.8
10	106.68	0.78	40.01	0.00	7.90E-06	2.65E+09	1.56E+02	6.32E+02	267.0
11	108.14	2.77	40.01	0.00	7.90E-06	2.65E+09	5.50E+03	3.80E+03	373.7
12	27.00	0.67	40.01	0.00	7.90E-06	2.65E+09	1.34E+02	5.98E+02	481.8
13	27.00	1.97	40.01	0.00	7.90E-06	2.65E+09	5.34E+03	2.71E+03	508.8
14	108.14	0.67	40.01	0.00	7.90E-06	2.65E+09	1.34E+02	5.98E+02	535.8
15	106.68	2.77	40.01	0.00	7.90E-06	2.65E+09	5.50E+03	3.80E+03	643.9
16	50.18	0.78	40.01	0.00	7.90E-06	2.65E+09	1.56E+02	6.32E+02	750.6

17	58.00	0.43	32.00	0.00	7.90E-06	1.09E+09	7.34E+01	1.41E+02	800.8
18	11.90	0.21	25.00	0.00	7.90E-06	4.05E+08	2.54E+01	6.46E+01	858.8
19	11.90	0.05	25.00	0.00	7.90E-06	4.05E+08	3.60E+00	2.35E+00	870.7
20	16.25	0.05	25.00	0.00	7.90E-06	4.05E+08	4.26E+00	3.10E+00	882.6
21	16.25	0.06	25.00	0.00	7.90E-06	4.05E+08	4.92E+00	3.85E+00	898.9
22	16.25	0.06	25.00	0.00	7.90E-06	4.05E+08	4.92E+00	3.85E+00	915.1
23	16.25	0.06	25.00	0.00	7.90E-06	4.05E+08	4.92E+00	3.85E+00	931.4
24	19.00	0.04	12.00	0.00	7.90E-06	2.15E+07	2.61E+00	2.26E+00	947.6
25	19.00	0.60	12.00	0.00	7.90E-06	2.15E+07	2.91E+02	1.77E+02	966.6
26	0.00	0.01	12.00	0.00	7.90E-06	2.15E+07			985.6

TOTALS: Length = 985.60 mm Trans Moment (about cg) = 6.22E+05 Kg-mm^2
Weight = 13.22 Kg Polar Moment = 1.75E+04 Kg-mm^2

Center of Gravity is 520.44 mm from left end

Average Diameter = 28.66 mm Average Length = 39.42 mm
Average Weight = 0.53 Kg Average EI = 1.10E+09 Kg-mm^2

L1avg = 1.13E-07 L2avg = 1.51E-06 L3avg = 2.27E-05 (Internal Scale Factors)

-- BEARING and FLEXIBLE PEDESTAL DATA --

BRG LOC (ST #)	BEARING STIFFNESS (N /mm)	SUPPORT STIFFNESS (N /mm)	SUPPORT WEIGHT (Kg)	-- RESONANT FREQUENCIES -- SUPPORT ONLY (RPM)	SUPPORT/BRG (RPM)
7	175127	1051	0.57	12998	168310
19	175127	1051	0.57	12998	168310

Rotor End Conditions Are : LEFT = FREE RIGHT = FREE

Critical Speeds Generated Are : SYNCHRONOUS

Initial RPM = 100 Delta RPM = 300 Final RPM = 20000

--- CRITICAL SPEED SUMMARY ---

A New shaft1 modified -whichs simulates 1mass4 Shaft- but with 3 Small Disks
Brg. Stiff. 1000000 Support Stiff. 6000
Three Mass tkickness .5" (13 mm.) File :3mass919.dat

SYNCHRONOUS CRITICAL SPEED ANALYSIS

-- BEARING and FLEXIBLE PEDESTAL DATA --

BRG LOC (ST #)	BEARING STIFFNESS (N /mm)	SUPPORT STIFFNESS (N /mm)	SUPPORT WEIGHT (Kg)	-- RESONANT FREQUENCIES -- SUPPORT ONLY (RPM)	SUPPORT/BRG (RPM)
7	175127	1051	0.57	12998	168310
19	175127	1051	0.57	12998	168310

#	CRITICAL SPEED RPM (HZ)	Wmode Kg	Imode Kg-mm^2 It-v/w*Ip	WTmode Kg	Kmode N /mm	Ushft DIM %	Ubrg Strn %	KEtrn DIM %	KErot Kinetic %
1	3260 (54)	10.8	-0.0	10.8	1258	21.6	0.4	95.1	-0.0
2	5707 (95)	2.5	-0.0	2.4	873	2.0	0.4	81.7	-0.6
3	11282 (188)	1.0	-0.0	1.0	1416	79.3	0.0	84.6	-0.2

A New shaft1 modified -whichs simulates 1mass4 Shaft- but with 3 Small Disks
Brg. Stiff. 1000000 Support Stiff. 6000
Three Mass tkickness .5" (13 mm.) File :3mass919.dat

UNDAMPED ROTOR MODESHAPE & ENERGY DISTRIBUTION
SYNCHRONOUS CRITICAL SPEED ANALYSIS

FIRST CRITICAL SPEED = 3259.57 RPM (54.33 HZ) Delta = -4.89e-07

ST. #	X DIM	THETA SLOPE	M MOMENT	V SHEAR	Ushaft STRAIN ENERGY %	Ubrg ENERGY %	KeTran KINETIC ENERGY %	KeRot ENERGY %
1	0.485	0.00	0.0	0.0			0.1	0.0
2	0.521	0.00	0.0	0.0			0.3	0.0
3	0.557	0.00	0.0	0.0			0.3	0.0
4	0.594	0.00	0.1	0.0			0.3	0.0
5	0.630	0.00	0.1	0.0			0.4	0.0
6	0.667	0.00	0.2	0.0			0.3	0.0
7	0.683	0.00	0.3	0.0	0.0	0.2	0.2	-0.0
8	0.700	0.00	-0.5	-0.1			0.9	0.0
9	0.778	0.00	-4.1	-0.1			2.3	0.0
10	0.839	0.00	-7.0	-0.1	2.9		4.8	0.0
11	0.943	0.00	-12.4	-0.1	5.5		21.7	-0.0
12	0.996	0.00	-14.5	-0.0	1.6		5.9	0.0
13	1.000	0.00	-14.9	-0.0	1.6		17.4	-0.0
14	0.999	-0.00	-14.5	0.0	5.5		5.9	0.0
15	0.958	-0.00	-12.4	0.0	2.9		22.4	-0.0
16	0.866	-0.00	-6.9	0.1			5.1	0.0
17	0.811	-0.00	-3.9	0.1			2.5	0.0
18	0.740	-0.00	-0.3	0.1			1.0	0.0
19	0.725	-0.00	0.5	0.1	0.0	0.2	0.2	-0.0
20	0.710	-0.00	0.4	-0.0			0.2	-0.0
21	0.690	-0.00	0.3	-0.0			0.3	-0.0
22	0.671	-0.00	0.2	-0.0			0.2	-0.0
23	0.651	-0.00	0.2	-0.0			0.2	-0.0
24	0.632	-0.00	0.1	-0.0			0.1	-0.0
25	0.610	-0.00	0.0	-0.0			2.0	-0.0
26	0.588	-0.00	-0.0	-0.0			0.0	0.0
Total Rotor Energy					21.64%	0.41%	95.10%	-0.00%

Brg #	St. #	K Brg N /mm	K Eff N /mm	Xbrg DIM	Xsup DIM	Ubrg %	Usup %	KE Sup %
1	7	17858	100	0.68	0.68	0.19	36.68	2.31
2	19	17858	100	0.72	0.72	0.22	41.27	2.60

U Total = 6.74e+01 KE Total = 6.75e+01 Energy Balance = -0.02 % Error

A New shaft1 modified -whichs simulates 1mass4 Shaft- but with 3 Small Disks
Brg. Stiff. 1000000 Support Stiff. 6000
Three Mass tkickness .5" (13 mm.) File :3mass919.dat

UNDAMPED ROTOR MODESHAPE & ENERGY DISTRIBUTION
SYNCHRONOUS CRITICAL SPEED ANALYSIS

SECOND CRITICAL SPEED = 5706.75 RPM (95.11 HZ) Delta = -5.09e-06

ST. #	X DIM	THETA SLOPE	M MOMENT	V SHEAR	Ushaft STRAIN ENERGY %	Ubrg ENERGY %	KeTran KINETIC ENERGY %	KeRot ENERGY %
1	-0.978	0.00	0.0	0.0			1.7	0.0
2	-0.926	0.00	-0.1	-0.0			3.0	0.0
3	-0.875	0.00	-0.2	-0.0			2.7	0.0
4	-0.824	0.00	-0.4	-0.0			2.4	0.0
5	-0.774	0.00	-0.8	-0.0			2.1	0.0
6	-0.725	0.00	-1.2	-0.0			1.3	0.0
7	-0.704	0.00	-1.4	-0.0	0.0	0.2	0.8	-0.0
8	-0.684	0.00	-0.8	0.0			3.2	0.0
9	-0.586	0.00	1.3	0.0			4.9	0.0
10	-0.499	0.00	2.7	0.0			6.4	0.0
11	-0.305	0.00	4.2	0.0			8.6	-0.2
12	-0.092	0.00	2.5	-0.0			0.2	0.1
13	-0.037	0.00	2.0	-0.0			0.1	-0.4
14	0.019	0.00	1.6	-0.0			0.0	0.1
15	0.245	0.00	-0.8	-0.0			5.5	-0.2
16	0.467	0.00	-0.3	0.0			5.6	0.1
17	0.570	0.00	0.5	0.0			4.7	0.0
18	0.692	0.00	2.0	0.0			3.3	0.0
19	0.717	0.00	2.4	0.0	0.1	0.2	0.8	-0.0
20	0.744	0.00	2.0	-0.0			1.0	-0.0
21	0.782	0.00	1.6	-0.0			1.3	-0.0
22	0.821	0.00	1.2	-0.0			1.4	-0.0
23	0.860	0.00	0.8	-0.0			1.5	-0.0
24	0.900	0.00	0.4	-0.0			1.1	-0.0
25	0.950	0.00	-0.0	-0.0			18.0	-0.0
26	1.000	0.00	0.0	-0.0			0.3	0.0
Total Rotor Energy					1.99%	0.38%	81.74%	-0.57%

Brg #	St. #	K Brg N /mm	K Eff N /mm	Xbrg DIM	Xsup DIM	Ubrg %	Usup %	KE Sup %
1	7	17858	86	-0.70	-0.70	0.19	47.87	9.24
2	19	17858	86	0.72	0.71	0.19	49.75	9.60

U Total = 5.49e+01 KE Total = 5.48e+01 Energy Balance = 0.08 % Error

A New shaft1 modified -whichs simulates 1mass4 Shaft- but with 3 Small Disks
Brg. Stiff. 1000000 Support Stiff. 6000
hree Mass tkickness .5" (13 mm.) File :3mass919.dat

UNDAMPED ROTOR MODESHAPE & ENERGY DISTRIBUTION
SYNCHRONOUS CRITICAL SPEED ANALYSIS

THIRD CRITICAL SPEED = 11282.05 RPM (188.03 HZ) Delta = 3.35e-05

T. #	X DIM	THETA SLOPE	M MOMENT	V SHEAR	Ushaft STRAIN	Ubrg ENERGY %	KeTran KINETIC	KeRot ENERGY %
1	1.000	-0.00	0.0	0.0			4.4	0.0
2	0.898	-0.00	0.2	0.0			7.0	0.0
3	0.797	-0.00	0.8	0.0			5.5	0.0
4	0.697	-0.00	1.7	0.0			4.2	0.0
5	0.600	-0.00	2.8	0.0	0.5		3.1	0.0
6	0.508	-0.00	4.2	0.1			1.6	0.0
7	0.469	-0.00	4.9	0.1	0.5	0.0	0.8	-0.0
8	0.433	-0.00	5.5	0.0	1.7		3.2	0.0
9	0.270	-0.00	9.0	0.1	1.4		2.6	0.0
10	0.144	-0.00	12.9	0.1	8.0		1.3	0.2
11	-0.076	-0.00	23.1	0.1	16.4		1.3	-0.4
12	-0.200	-0.00	29.6	0.1	5.4		2.2	0.0
13	-0.212	-0.00	30.8	0.0	5.5		7.4	-0.0
14	.215	0.00	30.3	-0.0	19.3		2.6	0.0
15	0.147	0.00	26.5	-0.0	11.4		5.0	-0.2
16	0.032	0.00	16.8	-0.1	2.4		0.1	0.2
17	0.144	0.00	12.1	-0.1	3.1		0.7	0.0
18	0.297	0.00	7.4	-0.1	0.9		1.5	0.0
19	0.333	0.00	6.5	-0.1	0.7	0.0	0.4	-0.0
20	0.371	0.00	5.6	-0.1	0.6		0.6	-0.0
21	0.426	0.00	4.4	-0.1			1.0	-0.0
22	0.484	0.00	3.2	-0.1			1.2	-0.0
23	0.544	0.00	2.1	-0.1			1.6	-0.0
24	0.605	0.00	1.1	-0.1			1.2	-0.0
25	0.685	0.00	-0.0	-0.1			23.4	-0.2
26	0.765	0.00	0.0	-0.0			0.4	0.0
Total Rotor Energy					79.30%	0.01%	84.64%	-0.24%

Brg #	St. #	K Brg N /mm	K Eff N /mm	Xbrg DIM	Xsup DIM	Ubrg %	Usup %	KE Sup %
1	7	17858	26	0.47	0.47	0.01	13.76	10.37
2	19	17858	26	0.33	0.33	0.00	6.93	5.22

U Total = 8.55e+01 KE Total = 8.55e+01 Energy Balance = 0.03 % Error

RODYN Vibration, Inc. 22 Nov 97 - 15:41:53

3.1.2 CRITICAL SPEED TESTING

The procedure for critical speed testing was to run-up the rotor at above the third critical speed, and to manually remove the belt using a special tool, and to collect data (two channels at a time) using the tracking filter DVF3 during coast-down.

The results of the critical speed testing are illustrated in Figures 3, 4 and 5, where the shaft displacements are presented during coast-down at the mass-locations CM1, CM2, and CM3 of Figure 2. The tests were repeatedly performed and the results indicated consistent repeatability of the critical speed data.

Analysis of the coast-down data illustrated in Figures 3, 4 and 5, indicate that the critical speeds occur at 2950 rpm, 5400 rpm, and 11000 rpm. Table 1 represents a comparison between the theoretical critical speed data obtained from the CRITSPD program, and the experimental critical speed data. Good agreement is observed, and this experimental verification confirmed the suitability of the design of the new rotor shown in Figure 1, for the application of the HSFD.

Table 1 Comparison between Design & Experimental Critical Speeds of New Test Rotor

Critical Speed	Design Value (RPM)	Experimental Value (RPM)	Difference %
1st Critical	3260	2950	9.5 %
2nd Critical	5707	5400	5.4 %
3rd Critical	11282	11000	2.5 %

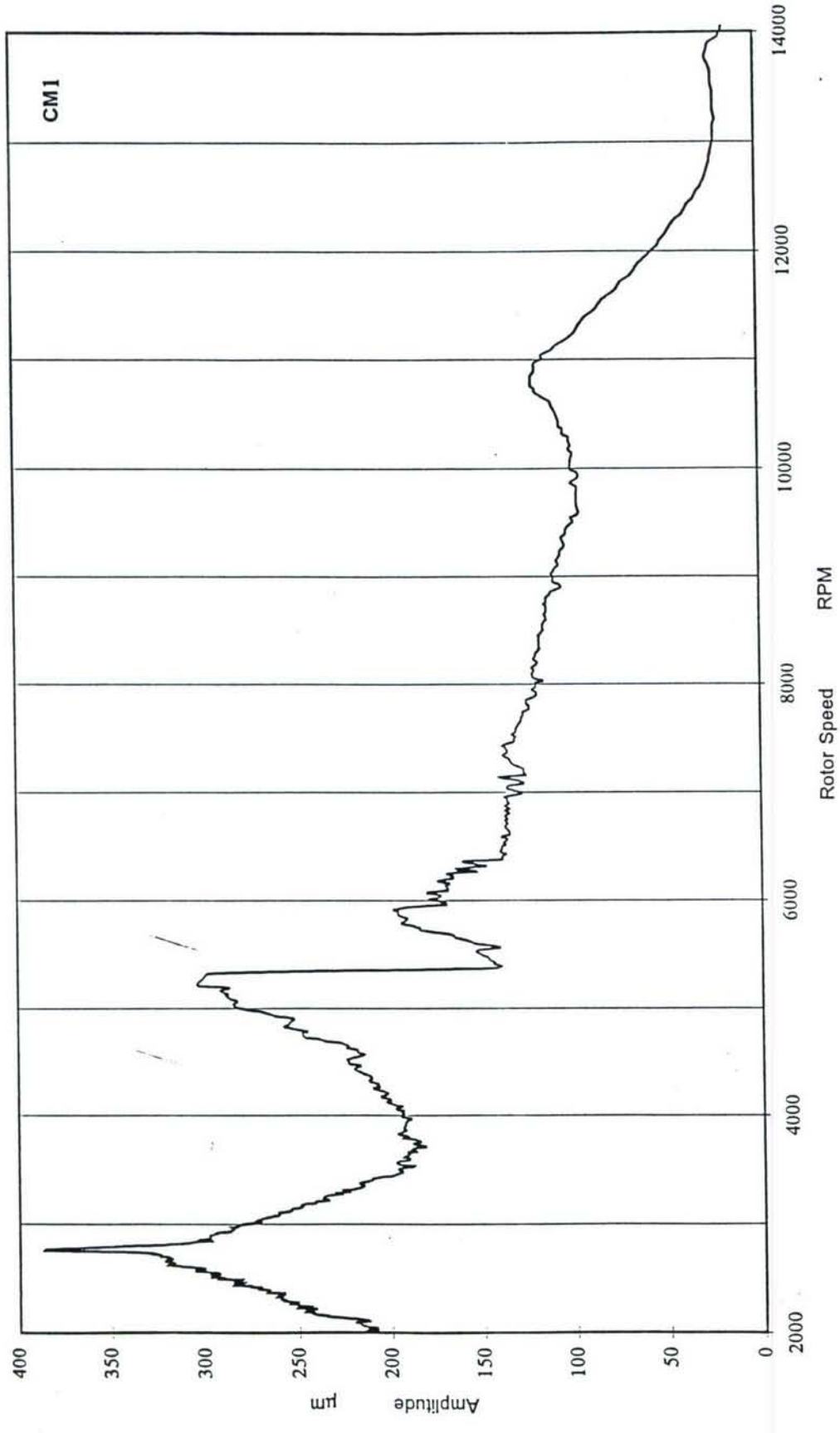

Figure 3 Coast Down Test at CM1

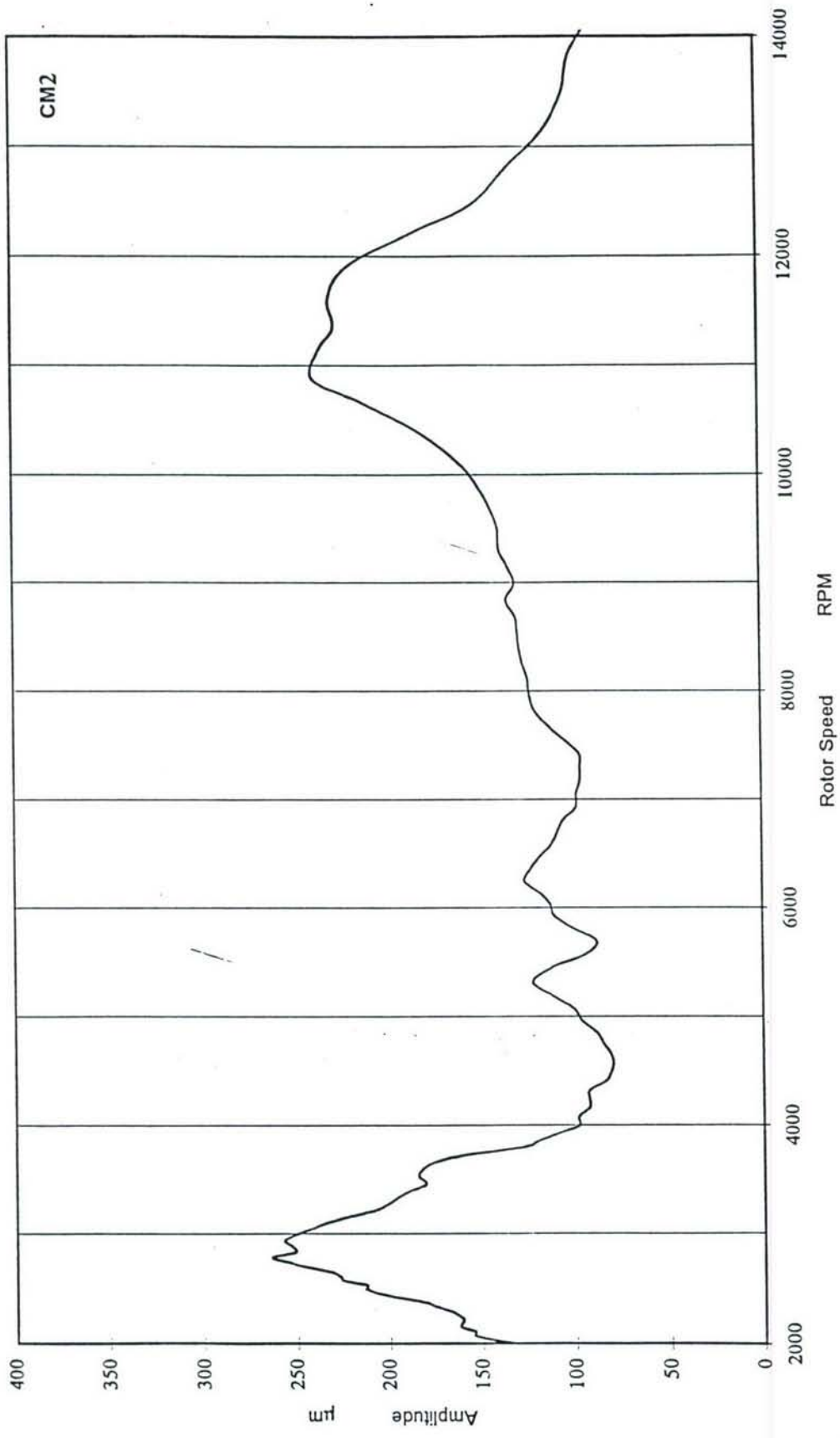

Figure 4 Coast Down Test at CM2

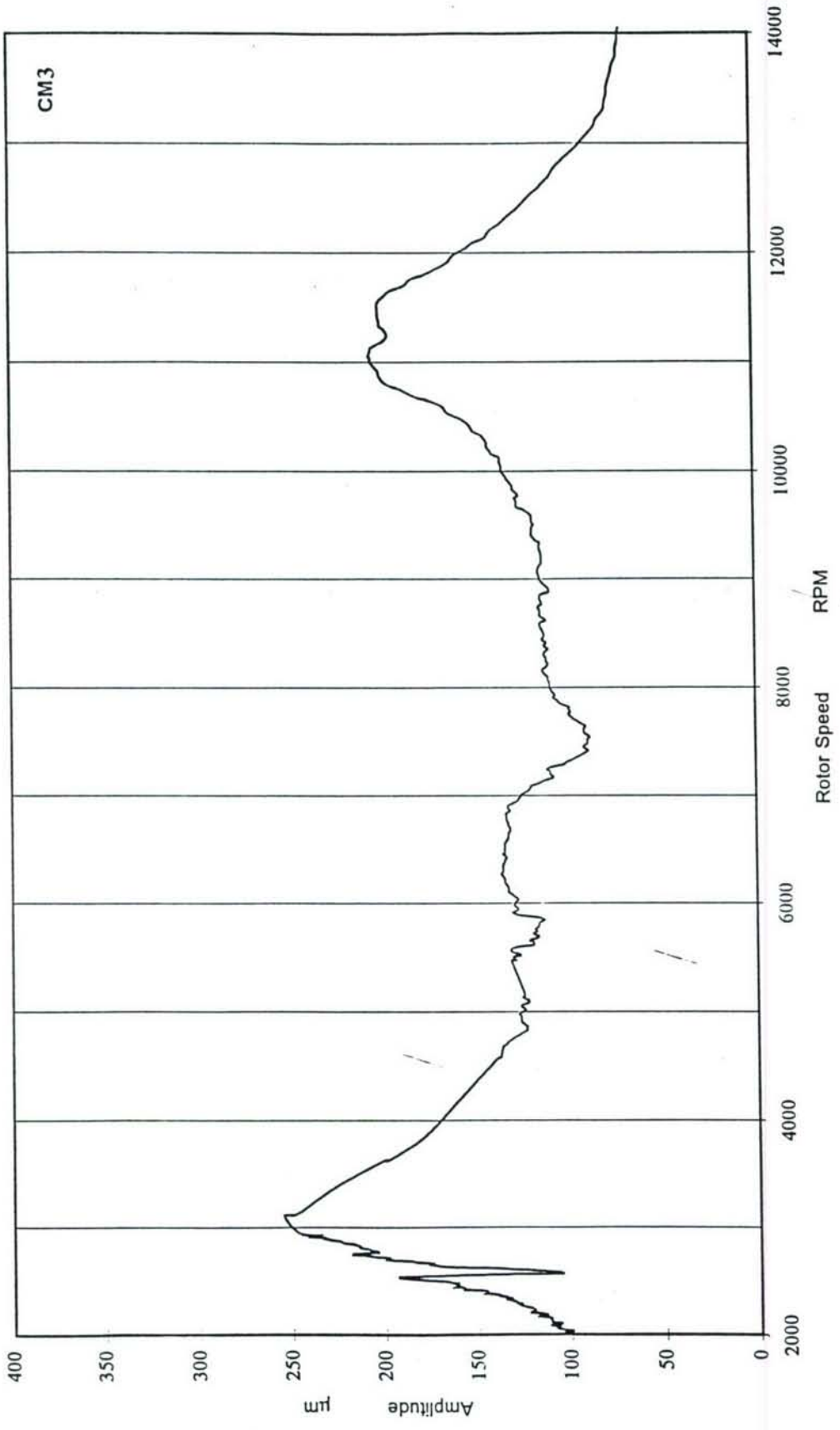

Figure 5 Coast Down Test at CM3

CHAPTER 2

THE REAL TIME CONTROL SYSTEM

This chapter details the implementation of the real time control system on the laboratory computer using data acquisition and control cards and the LABVIEW programming environment. This development was necessary before the implementation of the control algorithms and represents the initial set-up of the instrumentation and the supervisory action of the computer.

3.2.1 COMPUTER-CONTROLLED TEST RIG

Figure 6 shows the complete computer controlled test rig. The test rig consists of the rotor of Figure 1 supported on two HSFDs driven by a high speed DC motor through a belt drive. The oil feed and drain into and out of the dampers are controlled by the hydraulic circuit which is controlled by the pressure control valve signal generated from the computer.

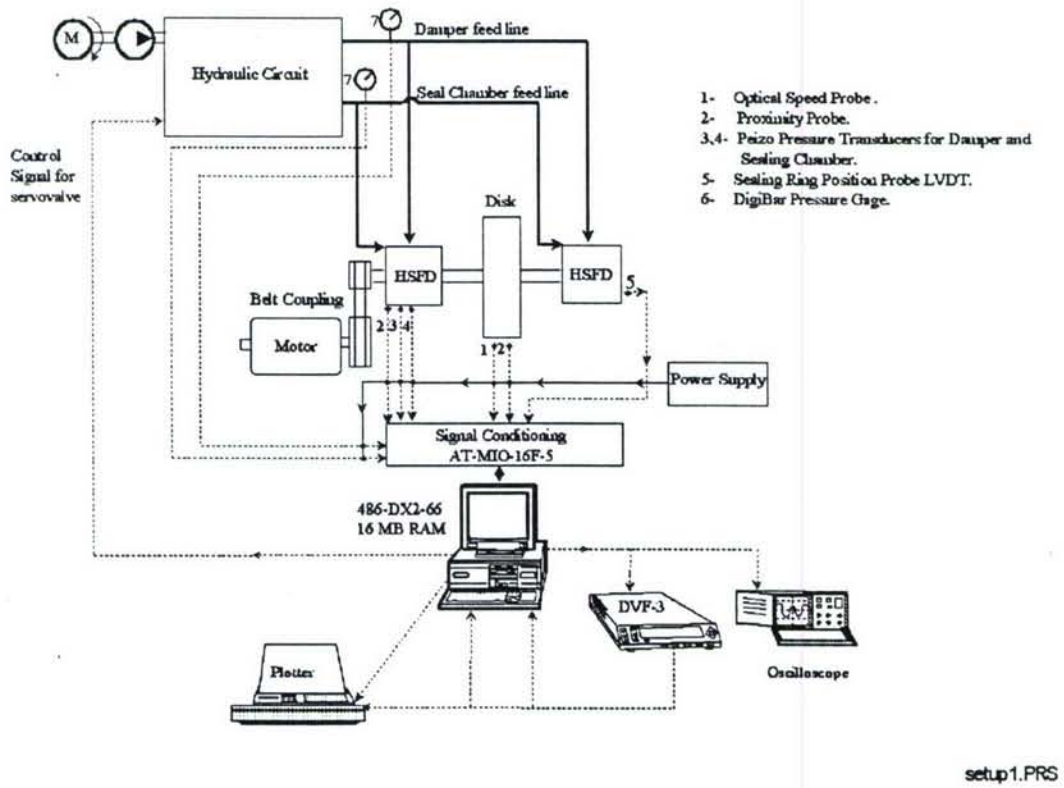

Figure 6 Data Acquisition System

The computer is a 486 DX2-66 PC compatible with 16 MB RAM and 660 MB hard disk. Two cards are installed into the computer. A GPIB card based on the IEEE 488.2 standard is used to control the instruments in the test rig. The other card is a 16 channel 12-bit data acquisition card with two channel control. Both cards are from National Instruments.

The GPIB card is a National Instruments PC II/IIA, and is used to control and acquire data from the Bently Nevada DVF-3 tracking filter and the Brüel & Kjær 2033 single channel spectrum analyzer. The DVF-3 is a two channel tracking filter to which the signal from two of the proximity probes are routed and filtered according to the speed of the shaft, which is also fed into the DVF-3 by another proximity probe monitoring a key-way or a photoelectric probe. The spectrum analyzer is used to view both the time and frequency domain signals from the pressure transducers, or the acceleration signal measured on the damper housing. Both the DVF-3 and the B&K 2033 can either download the data into the computer or directly onto a plotter. Two plotters are available: a Tektronix HC-100 and a Brüel & Kjær 2308.

The data acquisition card is a National Instruments AT-MIO-16F-5 card with 200 KHz sampling rate. The card is 16 channels Analog-to-Digital conversions for data acquisition and 2 channels Digital-to-Analog conversions for control. All channels are 12-bit. Both the GPIB and data acquisition and control cards are controlled by the National Instruments LabView software, which is a versatile and powerful software system that is capable of performing a wealth of functions including a variety of signal processing functions.

In addition to the proximity probe monitoring the key-way for speed information, each of the HSFDs and the central disk are monitored by two proximity probes each, 90° apart, for a total of seven eddy current proximity probes (Bently Nevada series 7200,5mm) monitoring the rotor. The proximity probes within the dampers are located in a very tight space. In order to avoid interference from adjacent material, and to reduce the possibility of disturbing the flow within the damper, a Teflon adapter was manufactured to isolate the probes and allowing them only to view the journal motion.

Each of the dampers is monitored by two Kulite XT-190 pressure transducers for monitoring the dynamic pressure in the damper and the pressure in the sealing chambers. These signals are either fed to the spectrum analyzer or directly to the computer or both. The hydraulic circuit lines are also monitored by Digital Pressure Gages HBM Digibar type PE200/20 bar and are also fed into the computer.

3.2.2 INSTRUMENTATION BUILDUP

Measurements on the test rig were implemented using different types of transducers in accordance with the measured variable. Transducer electrical output signal is either routed to an indicator to give the corresponding variable reading or connected to the data acquisition card to be used by LabView software for monitoring or control tasks. Some variables have the two alternatives. For some critical variables, an indicator is used as a signal processing and the amplified analog output volt from it is routed to the data acquisition card, thus the electrical information is immune to noise in the test rig caused by the incorporated electrical motors.

The main variables measured are:

1 - Journal bearing displacement, in one of the HSFDs namely D2.
2 - Center mass or mid rotor displacement (C.M.2).
3 - Rotor Speed.

These group of variables are connected directly to the Bently Nevada DVF3 digital tracking filter. Bently Nevada proximity probes (type 7200,5 mm) are used to measure displacements of the rotor. The proximity probes within the dampers are located in a very tight space. In order to avoid interference from adjacent material, and to reduce the possibility of disturbing the flow within the damper, a Teflon adapter was manufactured to isolate the probes and allowing them only to view the journal motion. The DVF3 is a two channel tracking filter to which the signals from the proximity probes are routed and filtered according to the speed of the shaft, which is also fed into the DVF3 by a SCHENCK optical reference pickup with integrated amplifier type

P-84. At start of research, a proximity probe, located at the far end of rotor, was used for speed sensing through a key-way in the rotor, but it was damaged due to rotor vibrations. The optical probe was placed at a distance of 50 mm from the rotor, so it was insensitive to rotor vibrations. The filtered output (D2 & C.M.2 amplitudes) are indicated on the instrument and at the same time, are transferred to the controller PC through IEEE 488.2 data bus (section 3.2.3). A DC power supply is used to power all the probes. Squeeze film damper displacement is considered the setup variable (e) to be controlled.

Other variables measured are:

4 - Sealing ring (SR) displacement.
5 - Sealing ring actuating oil pressure.
6 - Squeeze film oil pressure.
7 - Actuating volt applied to the oil pressure regulating valve.

A displacement potentiometer was used to measure sealing ring position at first. But its readings were very sensitive to rotor vibrations and inaccurate, as its full stroke was 200 mm, while the sealing ring displacement is within 6 mm only. Later, a Linear Voltage Differential Transformer LVDT type W100 with 100 mm stroke from Hottinger Baldwin Messtechnik (HBM) was used with its frequency carrier indicator type MVD 2406 A. Analog volt from indicator was connected to the data acquisition card.

Oil pressures for both sealing ring actuation and squeeze film are measured and monitored using two Pressure indicators (Digibar, Hottinger type PE 200/ 20 bar) with built-in transducer. They are mounted in the hydraulic feed lines before inlet to the HSFD. At the same time, to obtain the pressure transients, small Piezo transducers (from Kulite Semiconductor Products, model XT-190M-300g) are mounted onto the HSFD near the oil application ports. To shield the piezo transducer measuring the sealing ring pressure readings from the test rig noise, it was connected to a BECKMANN indicator type 621 with its analog output connected to the acquisition

card. This second parameter group is introduced to the PC by the data acquisition card which is explained in the next section.

3.2.3 REAL TIME ACQUISITION & CONTROL SYSTEM

The data acquisition card National Instruments AT-MIO-16F-5 with 200KHZ sampling rate is used to collect measuring transducer analog outputs and introduce them to the controller PC. The card has 16 analog input channels configured as single ended or 8 differential channels. There are also 2 analog output channels with ± 5 volt or 0-10 volts, used for control. All channels are 12-bit width. The analog input channels were used in the differential mode. Piezo pressure transducers were connected to input channels number 1 and 2 respectively. Channel number 0 in the card was used to obtain the sealing ring position through analog output of Hottinger indicator (section 3.2.2). Acting control signal for the sealing ring pressure regulating valve is generated in output channel number 0 and monitored by input channel number 3. The action of both acquisition and control during test is accomplished by National Instruments LabVIEW as explained in section 3.2.4.

The General Purpose Interface Bus GPIB IEEE 488.2 was used to get data from the DVF3 tracking filter instrument. This bus is one of the standard buses used to interface and exchange data among measuring instruments (up to 16 devices) to PCs. It is introduced into the PC through a National Instrument GPIB PC IIA Card. The card is inserted into internal PC I/O Channel Bus and a software driver is installed during PC startup. This Bus is used also to connect an HC plotter which was used in the first stages of research to plot the DVF3 outputs. One device in the Bus has the responsibility to be the active bus controller. Devices can act as a talker or listener according to controller assignment (Murray and Richard, 1984) and according to each device capabilities.

3.2.4 LABVIEW PROGRAMMING ENVIRONMENT

LabVIEW software was used extensively in this research. It is a graphical programming language used to create programs in diagram form. It has extensive

libraries of functions and subroutines for many tasks. LabVIEW also contains application-specific libraries for data acquisition, GPIB and serial instrument control, data analysis, data presentation and data storage. LabVIEW programs are called Virtual Instruments (VIs), as their appearance and operation imitate actual instruments appearances. VIs can be used in stand alone mode or as modules in other VIs.

VIs have the following three features:

1- Interactive user interface, called front panel. It contains different types of input data supplied by the user. Also, tasks output are presented in graph forms, tables and Boolean indicators.

2- The VI receives instructions to be carried out from a block diagram. It is a pictorial solution to a programming problem. The block diagram is thus the source code for the VI.

3- VIs are hierarchical and modular. They can be used as top-level programs, or as subprograms within others. A VI is represented by an icon and connector. Connectors represent the data passed and supplied by the VI.

Although it is a new programming concept which may be troublesome (to some extent) for the ordinary programmers, yet it has powerful libraries for handling data acquisition tasks and flexible output enhancement. National Instruments is a famous producer of PC acquisition and bus cards, so good supporting routines for these cards are available within LabVIEW.

Signal control flow is done through the LabView Programming environment as follows:

1- The monitored variables are collected either through the GPIB card or the data acquisition card. All data are recorded in the computer.

2- A decision making algorithm is implemented based on the different control strategies, and through the LabView programming environment, the algorithm provides control data to be transferred to the data acquisition/control card.

3- The control signal is generated through the control channels of the data acquisition/control card, and is fed to the pressure reducing valve control module. This module generates the actuating volt to obtain the required valve control.

3.2.5 CALIBRATION OF SETUP MEASUREMENTS

To ensure the accuracy and repeatability of the setup measured parameters, high level Lab standards were used to calibrate the setup instruments. These standards are correlated to National Standards.

It is worth mentioning that all used instruments are of class 1% accuracy or better. They are products of well established firms in the field.

Setup variables measuring systems were calibrated in two steps. The details of the calibration are included in M. El-Hakim's doctoral thesis, and are not reproduced here for brevity. However, the calibration procedures are sketched in the following. First, pressure transducers and indicators were calibrated using dead weight balance as a standard for pressure probes and indicators (DigiBar and piezo transducers). For optical speed probe, a simple comparison test was made using a tacho-generator test rig. In the second step, calibration for all used data acquisition channels were made using the previously calibrated indicators. For the sealing ring position calibration, a Lab mechanical 0.01 mm resolution dial indicator was used as a reference. For pressure channels, the DigiBar indicators were used. Output and input control signal were calibrated against a Digital AVOmeter. For proximity probes, calibration sheets from the supplier were used to introduce their data into DVF3 tracking filter.

Also, a sample of position springs were measured to determine their stiffnesses. A characteristic curve for a sample of position springs was obtained. The deflection of

the spring under different loads was measured. From these characteristics curves, position spring stiffness was calculated.

3.2.6 FUNCTION TESTING OF HSFD

After finishing the static testing (see Part I), the rotor system was assembled with the two HSFDs. fixed to the test rig. Oil supply and drain lines were connected. Pressure regulating valve electrical input was wired to the data acquisition card output channel number 0. A set of programs were developed in LabVIEW environment to control the positioning of the sealing rings during rotor startup and coast down as described in section 3.2.4. The DVF3 two channels (e.g. journal vibrations in one plane and center mass) could be plotted against rotor speed during test and data obtained are saved in a file for later reference. Another program was developed to combine data files for comparison between different modes of operation.

A set of runs were made with short, long and mixed configurations to evaluate the setup operation. The set of runs were repeated in different days to check the repeatability of the results. The data obtained pointed out that they were sound and repeatable with small differences that could be tolerated. For each control algorithm, a short and long mode runs were made before trying the control run and the data files for the three runs are plotted together. Thus in all testing, the short and long damper modes were measured in two reference runs, and the controlled algorithm was then applied in a third run of the coast down test.

CHAPTER 3
VERIFICATION AND IDENTIFICATION

In this chapter, the steps for obtaining the setup dynamic characteristics are discussed. The system checking and verification made before implementing the control algorithms is presented. The rotor response in the short and long modes is presented. This is shown in section 3.3.1. The Open-Loop system is presented in section 3.3.2 as implemented for this experimental work. The reference was adapted from Hathout's Thesis. Scan rate for DVF3 tracking Filter was determined as discussed in section 3.3.3. This parameter was missed in the available device manual. Section 3.3.4 details the step response of the hydraulic control system which is the main control component in the overall setup.

3.3.1 MODEL VERIFICATION, SHORT AND LONG BEHAVIOR

Before implementing any of the proposed control algorithms, it is necessary to understand the dynamic behavior of the system. In particular, it is necessary to analyze the response of the rotor in the short and long damper modes. This is a fundamental issue because any proposed controller aims at infinitely positioning the sealing ring between the long and the short damper modes. As a result, these two modes of control or operation are physical limiting conditions. Moreover, the response, in the steady state, can be a combination of these two limiting modes. The behavior of the rotor vibrations in the short and long modes is presented in Figure 7 for a coast-down from 15500 to 2000 rpm. It should be noted in Figure 7 that due to the nonlinear damping in SFDs the location of the critical speeds has shifted resulting in a much stiffer system with higher critical speeds. This was expected from the study of SFD characteristics. In addition, it is clear in Figure 7 the major difference in behavior between the short and long modes.

The distinguished behavior of the long and short modes is clear while passing through the three critical speeds in the speed range indicated. This clearly shows that the added damping in the long damper mode changes the dynamics of the system significantly.

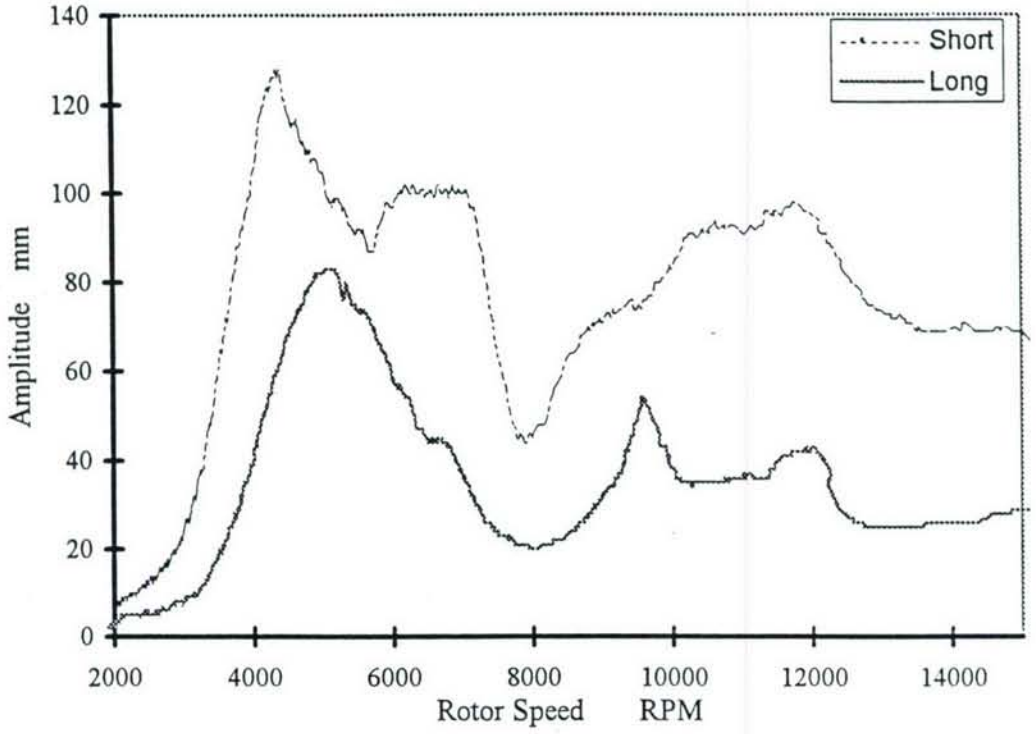

Figure 7 (a) Experimental response of rotor at Damper 2 for short and long damper modes

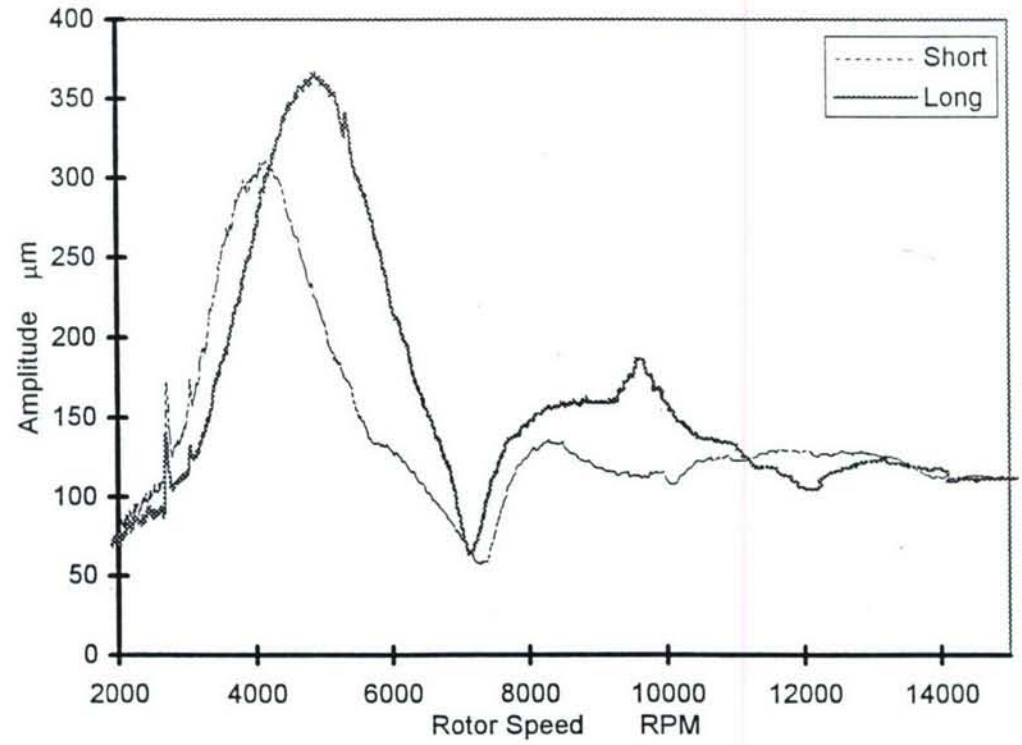

Figure 7 (b) Experimental response of rotor at CM2 for short and long damper modes

Moreover, this clear distinguished difference in behavior supports the principle of controlling the rotor system vibrations by controlling the damping added to the system. One expects that by accurately controlling the damping, a specific response between the two extreme modes of operation can be achieved. In general, the long damper mode attains minimum value of the bearing vibration amplitude throughout the speed range.

The test rig was subjected to severe vibrations during the experimental phase of this project. Actually, most of the testing was concentrated around resonant conditions. As time went on, this abuse of the test rig became significant and the characteristics in Figure 7 were changed appreciably. This change in characteristics was noticed during the testing of the control algorithms, and the different characteristics are shown in Figure 8. Comparison between Figures 7 and 8, not only shows a structural change in the shape of the figures, but also a significant increase in amplitude from maximum 130 μm in Figure 7 to 220 μm in Figure 8. Both these changes, the structural change and the amplitude change may indicate either a change in balance quality or a bent rotor.

Rather than manufacturing a new rotor, we decided to continue investigating the control algorithms on this same rotor with changed characteristics. The reasoning being two fold. First, there is no direct relationship between testing using one control algorithm or the other. What is important is the performance of the controller with the rotor system. Second, and more importantly, it is quite instructive to view the ability of the HSFD in controlling the rotor with changed characteristics. The successful implementation of the HSFD on the rotor at adverse conditions is one of the major advantages of HSFDs. Continuation of testing illustrates the strength and adaptability of the HSFD in controlling rotor vibrations under adverse conditions.

From Figure 8, it can be seen that no significant distinguished difference exists for the phase of the long and short modes. From the control point of view, the difficulty of designing a controller and its performance are the same, since in theory and

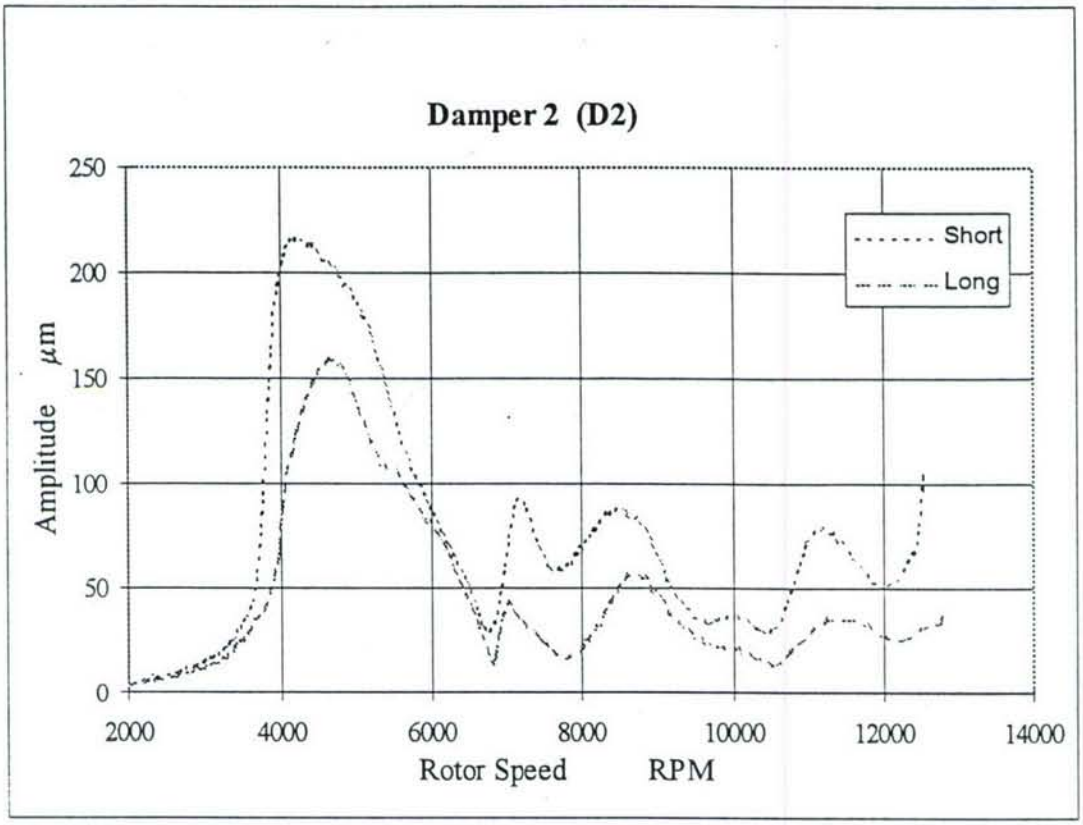

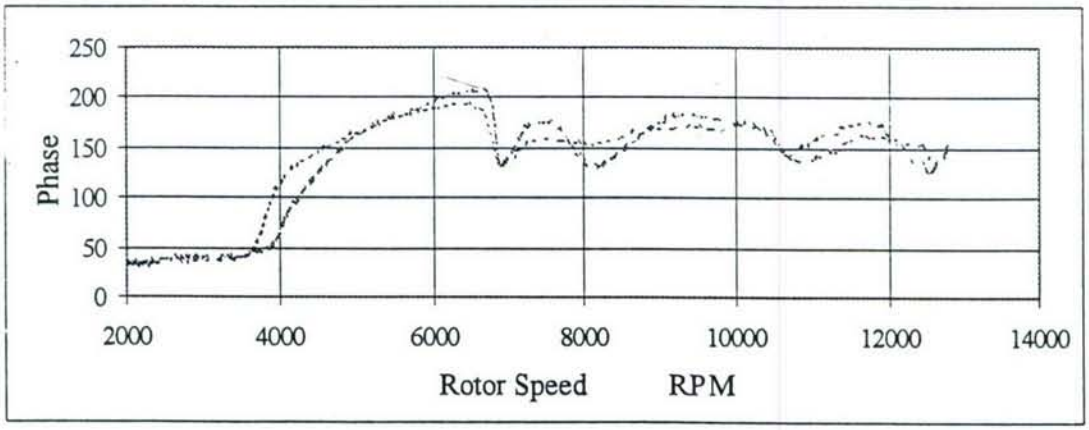

Figure 8 Experimental Response of Rotor at Damper 2 for Short and Long Modes

experiment, the controller sees the similar response characteristics of three critical speeds in the bandwidth of interest.

3.3.2 OPEN-LOOP SYSTEM

The open-loop setup mathematical model was given in detail in Hathout's thesis. The open-loop system consists of control servovalve, the HSFD and the rotor. The system functions as follows, first, a volt is chosen from PC controller and is supplied to the servovalve conditioning board. The board in turn supplies a current i which actuates the servovalve to output a controlled pressure p in the sealing chamber. The amount of the pressure p positions the sealing ring between the short and long modes, and hence controls the amount of damping supplied to the rotor. Figure 9 shows the block diagram of the system.

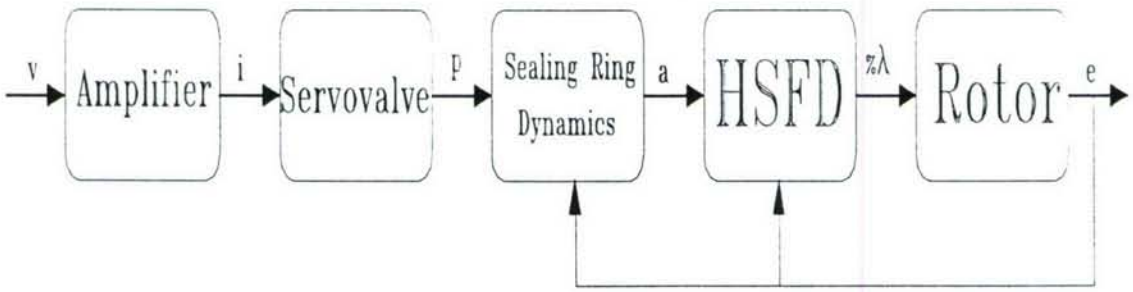

Figure 9 The Open-Loop System

In the existing experimental setup there is a sensor for measuring the vibration amplitude of the output variable to be controlled. In addition, in the work of Hathout, it became evident that the feedback on the eccentricity ratio is enough for controlling the system and achieving the required objectives. Thus, most of the presented control algorithms aim at damping the vibration amplitude through feedback of the eccentricity ratio. Dealing with the transmitted force is tackled in the Gain Scheduling of Proportional-Integral controller only.

If one is to consider controlling the transmitted forces as well as the vibration amplitude then the trade-off between these two output variables, from the control point of view, must be considered. However, most of the presented control algorithms can easily be modified to control the transmitted forces instead of the vibration amplitude if the transmitted forces are of more interest, although the work of Hathout showed that only feedback of the eccentricity is enough as discussed earlier. It should be mentioned that further investigation is required to establish a criterion for the trade-off between these two output variables, in the regions where conflict is identified.

3.3.3 CHARACTERISTICS OF DVF3 FILTER

The DVF3 tracking filter is the main device which monitors the setup control parameter, namely D2 displacement, and filters the data at the rotor speed and transfers the filtered data to the PC controller through the GPIB card. The device manual, did not contain the scan rate of measurement which is a fatal parameter for control of the rotor vibration. The DVF3 is a GPIB Bus talk only device as mentioned in the manual. The data are ready for the bus only after a triggering signal is sent. To determine the scan rate, an executable basic program was made. It consists of a loop with triggering and reading for certain cycles without any data processing. Time stamps are taken at start and end of the cycles, and the scan rate is calculated. This procedure is repeated several times for different number of cycles. An average of 3 scans/second was obtained. This is the maximum scan rate for DFV3 instrument. However, in the control algorithms experiments conducted, this scan rate is reduced as some time was consumed in processing data obtained from DVF3, which led to data acquisition rate less than 3 readings/second according to the complexity of calculations. To overcome this situation, time stamps were taken at start and end of acquisition, and counts of parameters readings were recorded and scan rate was calculated for each run.

3.3.4 STEP RESPONSE OF HYDRAULIC CONTROL SYSTEM

The analysis and study of the time and frequency responses of the control system are used to gain understanding of the dynamics of the system. The control block for the

setup contains the pressure regulating valve, piping system and the damper sealing ring. A step function in the control volt was applied to the pressure regulating valve input. The sealing ring displacement, sealing room pressure and the control volt data were recorded and plotted as shown in Figure 10 by a developed LabVIEW program. Two cases were considered, switching from short mode to long mode and switching from long mode to short. During the test, scan rate was found to be 2 Hz. It was noticed that the control response for second change (i.e. from long to short) is faster than the first one, because of the need to build up pressure in the short to long case.

For Short to Long change, the sealing chamber pressure started to increase after buildup of control signal as indicated in Figure 10. It took 7 seconds to reach its final value. On the other hand, movement of the sealing ring lagged 3 seconds after control signal buildup, and reached the Long mode position after 5 seconds. It is worth to note that the squeeze film oil pressure fluctuated within 5 seconds before returning to its original value. This is due to the sealing ring movement and indicated that the effect of the oil accumulator is not sufficient enough and needs to be considered for future work. The sealing ring O-ring seals have remarkable effects in its movement and the acting pressure accordingly.

For the case of Long to Short control action, sealing chamber pressure and sealing ring movement started directly after control action start. The pressure dropped to zero within 7 seconds while the end of the sealing ring motion was after 4 seconds, with the same effect of O-ring and squeeze film pressure fluctuation recorded. The difference between the two actions' responses was related to the effect of the positioning springs mounted on the damper end cap, while in the first case they opposed the movement, in the second one they enhanced it.

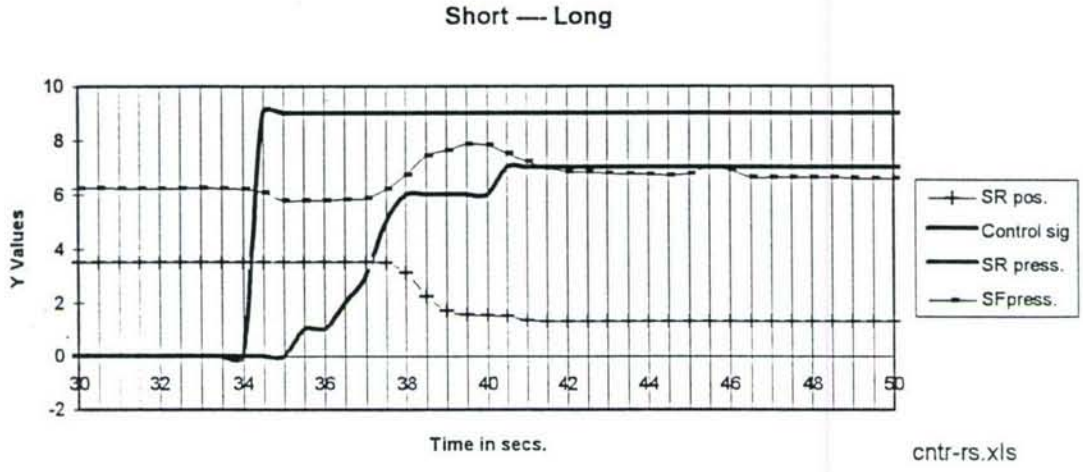

(a) Short to Long

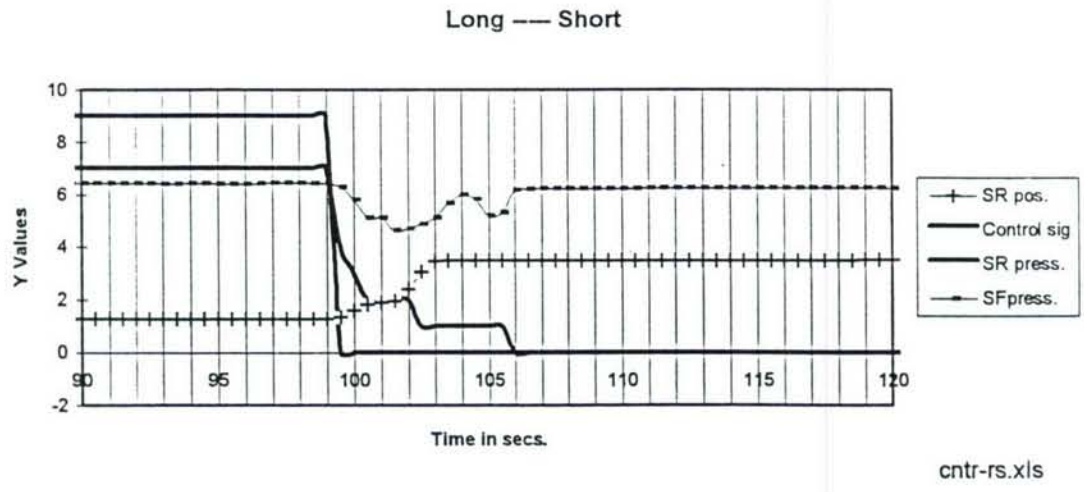

(b) Long to Short

Figure 10 Step Response of Control System for Two Control Actions

CHAPTER 4

APPLICATION OF ELEMENTARY CONTROL ALGORITHMS

In this chapter, the experimental verification and application of the control algorithms developed by Hathout, are applied to the test rig. The application is limited in this chapter to the on-off controller, the proportional controller, and the proportional-integral (PI) controller, as these represent the basic control algorithms. The experimental application of the advanced control algorithms is presented in the next chapter. The reasoning for the separation between the basic and advanced controllers is for presentation purposes and for illustrating the escalating degrees of complexity.

As discussed in the previous chapters, the test rig was controlled through the computer by using the LabView software. All of the control algorithms are adapted to LabView instructions, and these instructions are used to control the National Instruments data acquisition/control card. The measured variables are fed through the card, to the computer, as well as the data measured through the DVF3 tracking filter, which are fed to the computer via the GPIB bus. These measured data are processed as feedback variables in the algorithm implemented in LabVIEW. The algorithm reaches a set of instructions based on the feedback variables which are sent to the control channels of the data acquisition/control card. These instructions are then used through the card to generate the control signal as discussed in Chapter 2 of Part III.

Thus, the computer, LabView Software, Data Acquisition/Control Card, and the GPIB Card, together represent the controlling logic in the control loop. All developed algorithms were implemented through this technique.

Also as discussed in Chapter 2, all the tests were repeatedly performed to assure repeatability, and in particular, a run-down test is performed for the short damper mode and another for the long damper mode, every time a control algorithm is applied in a run-down test. This allows the conformity of the data at the same set of environmental conditions, and presents the analyst with limits of the controller under investigation. This facilitates tremendously the analysis of each of the controllers, as a

visual correlation is always available with the limiting conditions of short damper and long damper.

3.4.1 ON-OFF CONTROL

The basic concept of the typical On-Off controller (see Figure 11) is to switch between two modes of operation based on the error signal. In the active vibration control of the rotor system, the two modes of operations are the short and long damper modes. The criterion for tuning of the controller between its two modes is the major design implication. It is not quite straight forward to design the on-off controller based on the error signal. However, since the steady-state operation of the system in both the short and long modes are available at hand, a speed range can be chosen to be the switching criterion. This can easily be implemented as an on-off design. In summary, the controller is switched to either mode in a particular speed range as defined by the designer off-line. It was shown by Burrows et al. (1983), that for some rotor systems only two levels of damping are required to control the behavior of the rotor-bearing system. The same design principle was adopted by Hathout, the on-off active controller is actuated at specific rotational speeds to achieve the desired damping level for particular speed ranges.

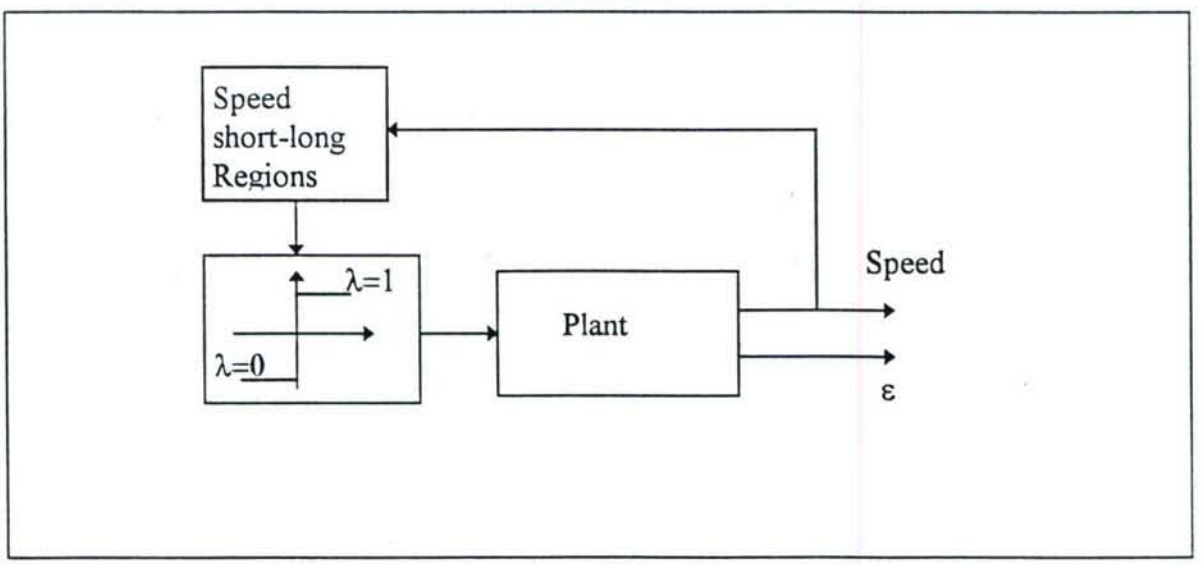

Figure 11 Block Diagram of the On-Off Controller

Neglecting the dynamics of the controller which is composed of the servovalve and the sealing ring, one can assume that the HSFD attains any of the two modes instantaneously as requested by the control action. Thus, a particular mode can be achieved for a particular speed range. The selection of the switching instants was based on the operation in hand of the two modes as identified in Figure 7.

The speed range 2000 to 15500 rpm is divided into five regions. The criterion of using a short or a long damper in each region is based on the vibration amplitude of the bearing and the center mass. Table 2 lists the five regions constituting the speed range of operation with the desired mode of operation and the critical speed in each region if any exists. It is clear from the Table that the controller is to assume the long damper mode while passing through the first two critical speeds. This choice of the switching speeds is based on the fact that the long damper mode has smaller vibration amplitude at the critical speeds. However, the third mode is to be passed while in the short mode as this critical speed has the smallest amplitude. This is a selected schedule, but other schedules can be chosen based on system requirements.

Table 2 Speed ranges for the on-off controller

Speed Range in rpm	Damper Mode	Critical Speed
rest to 3000	short	none
3000 to 5800	long	first critical speed
5800 to 9000	short	none
9000-9400	long	second critical speed
9400-15500	short	third critical speed

Figures 12, 13 and 14 show the experimental results of implementing the on-off controller. It is clear from the figures that the controller succeeded in attaining the desired mode of operation in the given speed region. Switching between the two modes is not instantaneous and a time delay is observed in the response. However, this

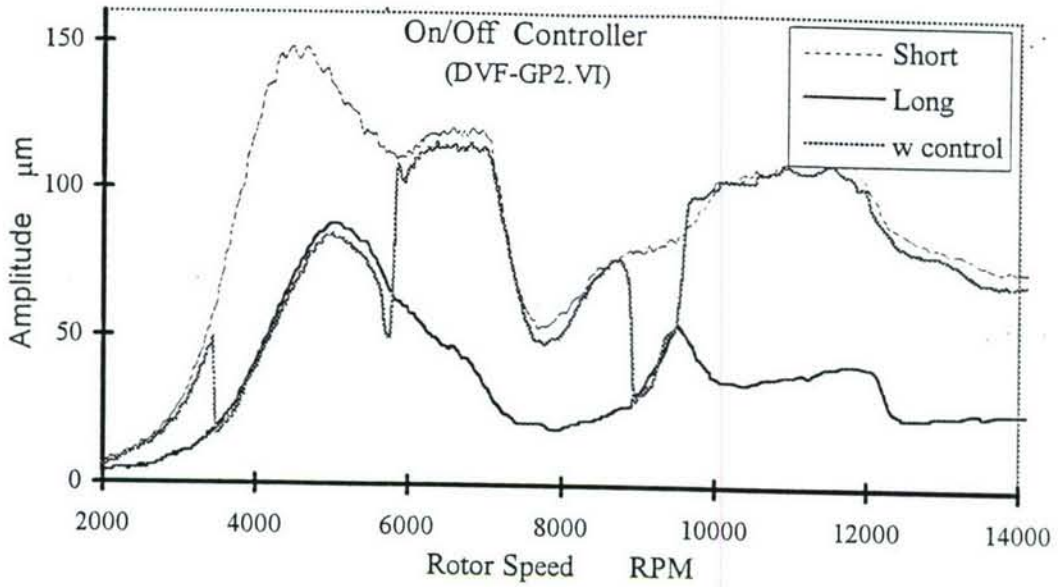

Figure 12 Experimental response of rotor at Damper 2 for On/Off Controller

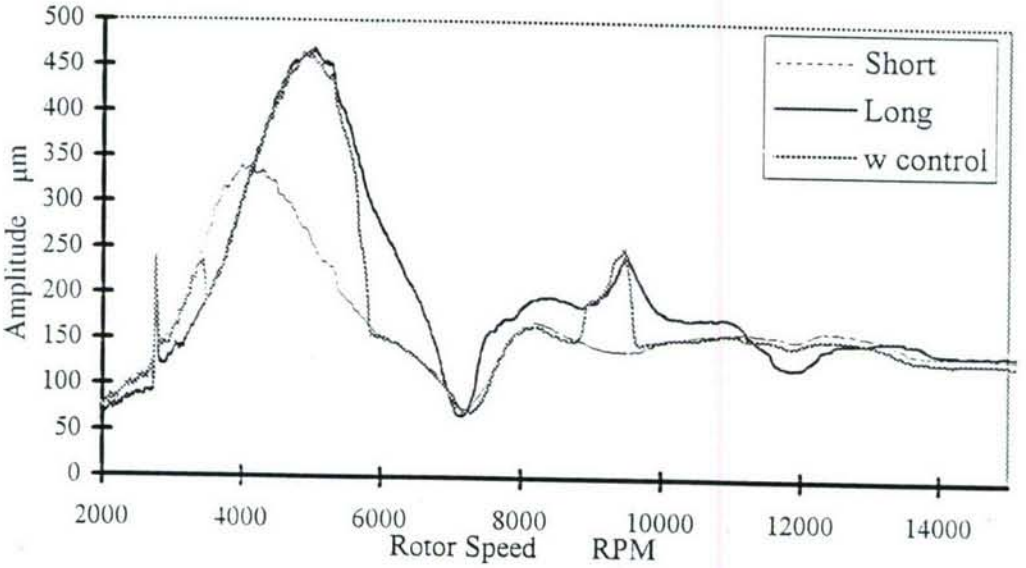

Figure 13 Experimental response of rotor at CM2 for On/Off Controller

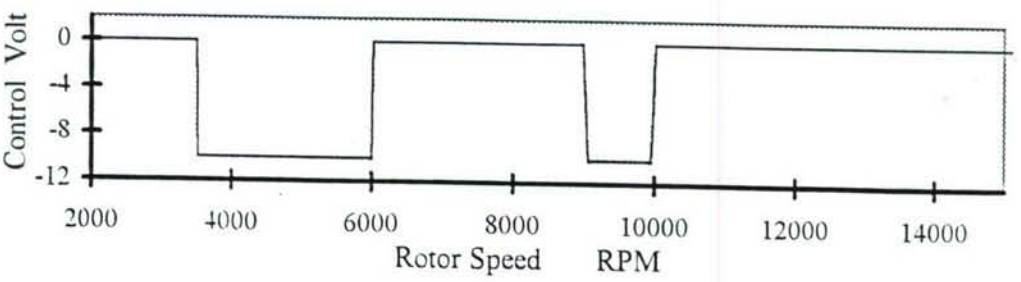

Figure 14 Actuating signal for On/Off controller

is not significant as the switching is designed off-line, and as a result one can include the delay in the design of the different regions.

Comparison of the theoretical results with the experimental results indicated the capability of both modes of operation in controlling the rotor vibrations. However, switching between the modes is slower in the experimental than in the theoretical studies. This was expected based on the delay characterization discussed in Chapter 3, Part III, which can be included in the design of the controller.

The reasoning for choosing the above schedule for speed control is as follows:

1 - In the short damper mode a smaller force is transmitted to the support, thus it is advantageous to operate the rotor as much as possible in this mode of smaller force.

2 - The long damper provides more damping, thus it is advantageous to operate in the long damper mode at the critical speeds.

3 - Notice that in the long damper mode in Figures 12 and 13, the deflection at the rotor center CM2 is larger than in the short damper mode, thus it may be advantageous that in the bending mode of the rotor (the third mode) to try to minimize the deflection between the damper D2 and the center of the rotor CM2. Comparison of Figures 12 and 13 indicates that at high speeds operating in the short damper mode allows only a deflection of about 50 μm between D2 and CM2 although the third critical exhibits a node between CM2 and D2. Thus depending on the objective one can operate around the third critical either in the short damper mode to reduce deflection as in Figures 12 and 13, or in the long damper mode to reduce the amplitude of vibration.

3.4.2 PROPORTIONAL CONTROL

Figure 15 shows a block diagram of the proportional controller. This is a simple control approach in which the control activity is proportional to the error signal. As a result, one expects that the actuating signal instantuously changes with the value and the sign of the error. In the time domain, the controller is defined as:

$$u = K_p e$$

where

u	is the control action	
K_p	is the proportional gain	
e	is the error signal	$e = R - \varepsilon$
R	is the reference input	
ε	is the vibration amplitude at the bearing	

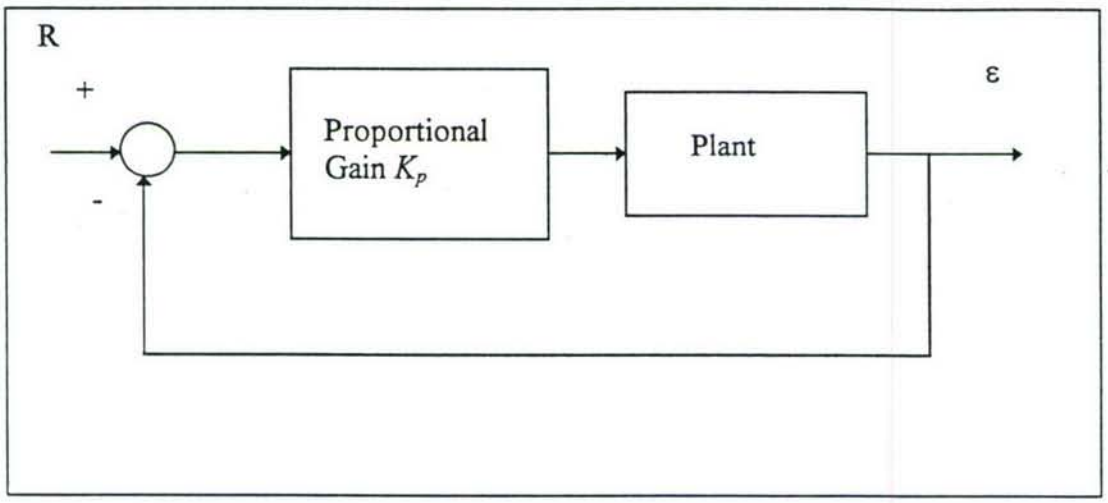

Figure 15 Block Diagram of the Proportional Controller

The error signal is the difference between the reference input and the measured output. The reference input is chosen to be 50μm. This choice is based on a value between the two extreme modes of the short and long dampers. This helps to evaluate and demonstrate the regulation ability of the different control algorithms. Hathout chose the reference input to be 0.3 times the eccentricity c where c = 750μm for the test rig.

The choice of 50 μm for the reference value is also based on finding a reference value between the short and long modes of operation to investigate the capabilities of the controller in achieving a constant vibration amplitude. The output is the same as defined earlier to be the vibration amplitude at the bearing center. This is the first step in investigating the capability of a controller in accurately regulating the vibration amplitude. Tuning of the proportional gain is performed experimentally. It is found that acceptable regulation performance is achieved for a proportional gain of 0.5. The

effect of closing the loop with a proportional controller is twofold, first increasing the speed of response by increasing the control bandwidth and second decreasing the effective damping of the system. This can simply be shown when applying the proportional controller to a second order plant of the form:

$$\frac{U}{R} = G_p(s) = \frac{K}{s^2 + 2\zeta\omega_n s + \omega_n^2}$$

with the proportional control as above applied the following closed loop results in:

$$\frac{C}{R} = \frac{G_p(s)}{1 + G_p(s)} = \frac{K_p K}{s^2 + 2\zeta\omega_n s + (\omega_n^2 + K_p K)}$$

Thus, the effective bandwidth of the controlled system is $\sqrt{(\omega_n^2 + K_p K)}$ which is greater than ω_n and the effective damping ratio is $\frac{\zeta\omega_n}{\sqrt{(\omega_n^2 + K_p K)}}$ which is smaller than ζ. A similar conclusion can be reached for higher order systems.

The experimental results are shown in Figures 16, 17, and 18. Figure 16 shows the response of the vibration amplitude at the bearing. Figure 17 shows the response of the vibration amplitude of the center mass. Figure 18 shows the actuating signal in volts. It is clear from the response figures that the controller managed to some extent in regulating the vibration amplitude, however, chattering is observed in two regions of the speed range. This suggested decreasing the proportional gain which results in a much slower response than that obtained for the proportional gain value of 0.5. It is obvious from the actuating signal of Figure 18 that the response chattering is a direct consequence of the fast changes in the actuating signal. These results were indicative measure of the insufficiency of the proportional controller.

3.4.3 PROPORTIONAL INTEGRAL CONTROL

Figure 19 shows a block diagram of the basic proportional-integral controller. The actuating signal is based on the summation of a proportional activity and an integral activity. Thus, in the time domain the controller is defined by:

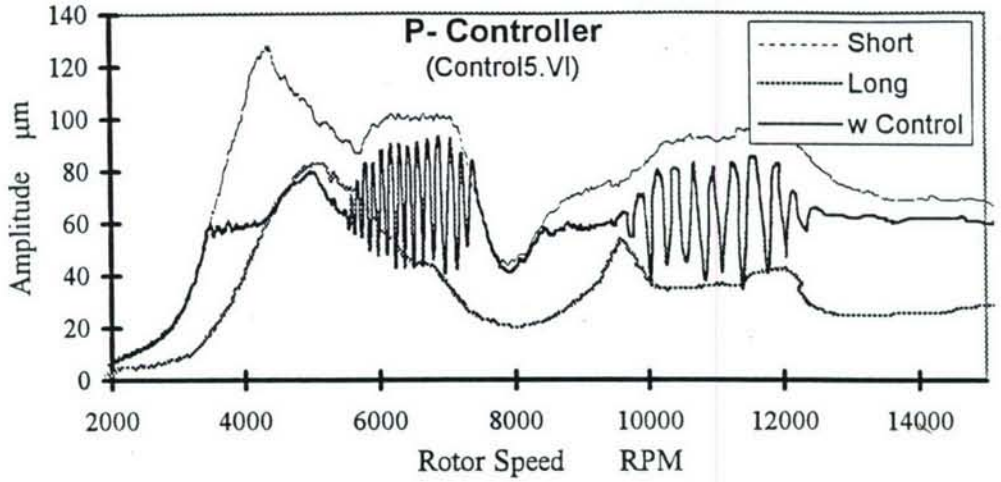

Figure 16 Experimental response of rotor at Damper 2 for P-Controller

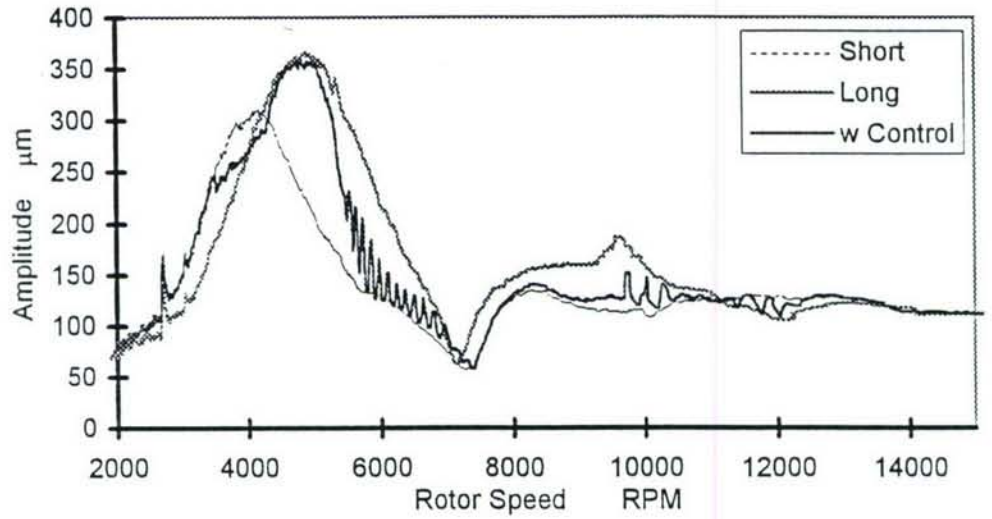

Figure 17 Experimental response of rotor at CM2 for P-Controller

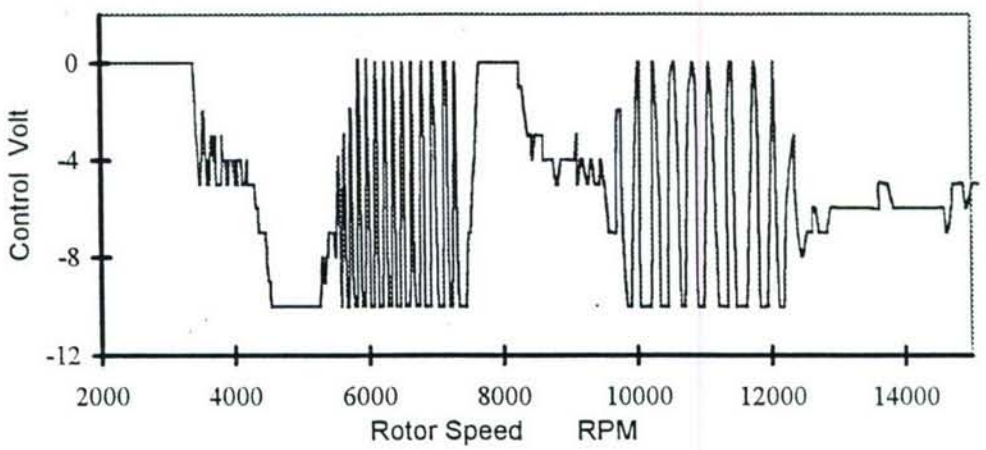

Figure 18 Actuating signal for P-Controller.

$$u = K_p e + Ki \int_0^t e \, dt$$

where

u	is the control action
K_p	is the proportional gain
K_i	is the integral gain
e	is the error signal

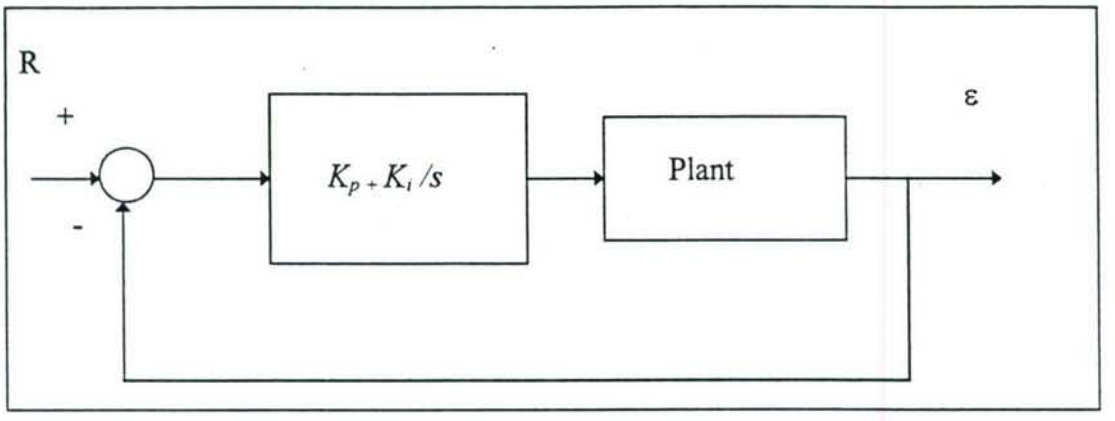

Figure 19 Block Diagram of the Proportional-Integral Controller

In the s domain the controller is given by:

$$U(s) = \left(K_p + \frac{K_i}{s} \right) E(s) = \left(\frac{K_p s + K_i}{s} \right) E(s)$$

Thus, the proportional-integral controller adds a zero and a pole to the system dynamics. In case where the plant model is known, the controller can be designed based on many very well known and developed techniques. However, in the general case, the system is either partially or fully unknown. A practical tuning principle is usually applied in this case.

The proportional-integral controller consists of a proportional activity and an integral activity. The effect of the proportional activity is to increase the speed of response as described for the proportional controller. The integral activity tends to eliminate the stead-state error. It increases the order of the system by one. Hathout studied using

different approaches in designing the proportional integral controller for the rotor system. First, by trial and error to find suitable gains associated with an acceptable location of the roots of the open loop system. Secondly, he used the Zeigler-Nicolos tuning method in selecting the controller gains. In the experimental investigation, the two steps were adopted. However, for the first trial and error approach, no measure of the location of the roots was available and hence this tuning of the gains was entirely based on the observation of the response of the system. The values of the gains based on the trial and error approach are 0.5 and 0.05 for the proportional and integral gains, respectively.

In the rotor dynamic model, tuning of the controller gains was based on the practical technique proposed by Ziegler and Nicolos. It should be noted that the generated control actuating signal aims at infinitely positioning the sealing ring between the short and long damper modes based on the error signal. Thus, starting from a particular position of the sealing ring, the controller aims at repositioning the sealing ring infinitely to achieve the control objective which is regulating the vibration amplitude at the bearing. Therefore, one can think of the controller as changing the damping seen by the rotor between two extreme positions of the short and long damper modes based on the error signal.

Figure 20 shows the response of the vibration amplitude at the bearing. Figure 21 shows the response of the vibration amplitude of the center mass. Figure 22 shows the actuating signal in volts. The response of the vibration at the bearing shows a similar response to that of the proportional control. The chattering is due to the attempt to zero the error. The integration of the error was reset to zero in the beginning of the coast down to avoid build-up. The actuating signal shown in Figure 22 indicated that the output channel is not saturated in most of the speed range as the case in the proportional control. It is clear from the response figures that the proportional-integral controller attempted to regulate the bearing vibration amplitude to the reference value by infinitely positioning the sealing ring to attain a specific damping. The chattering is dominating in the speed range of 6500 to 15500 rpm. Although, the average value of the vibration would approach the reference input value, the vibration did not remain steady close to the reference. In the speed range of 2000 to 6500 rpm, the controller

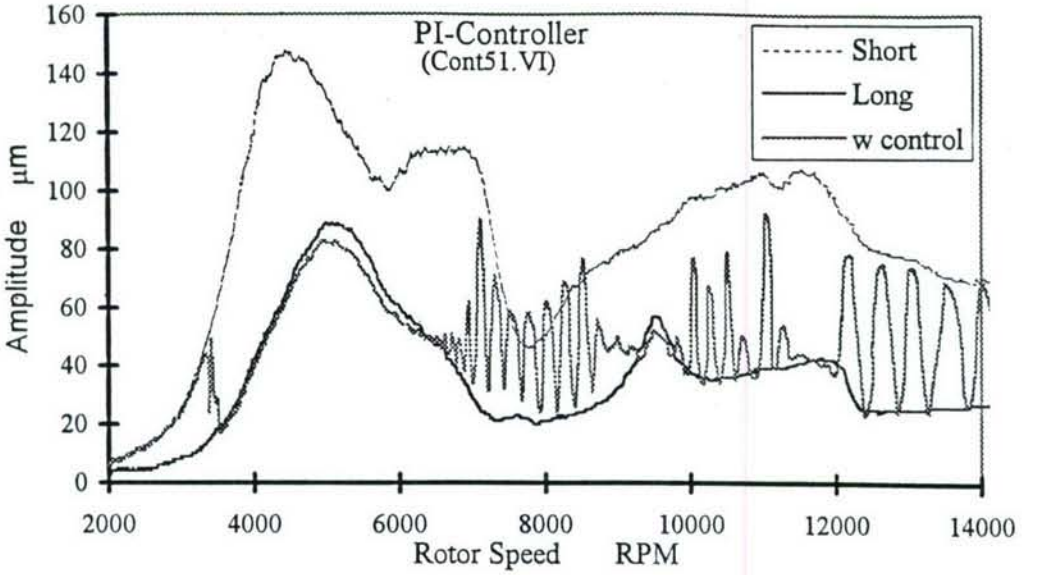

Figure 20 Experimental response of rotor at Damper 2 for Pl-Controller

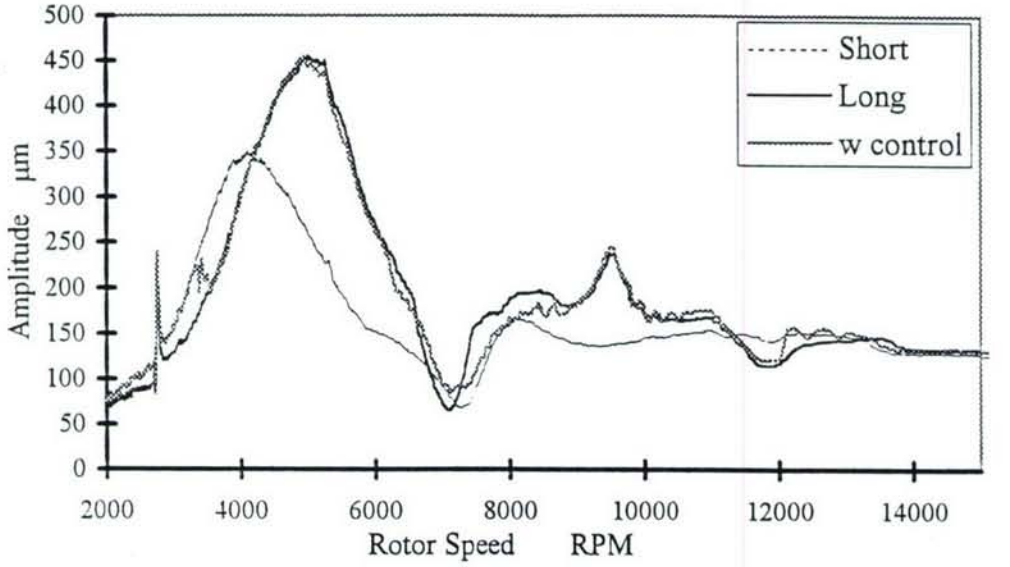

Figure 21 Experimental response of rotor at CM2 for Pl-Controller

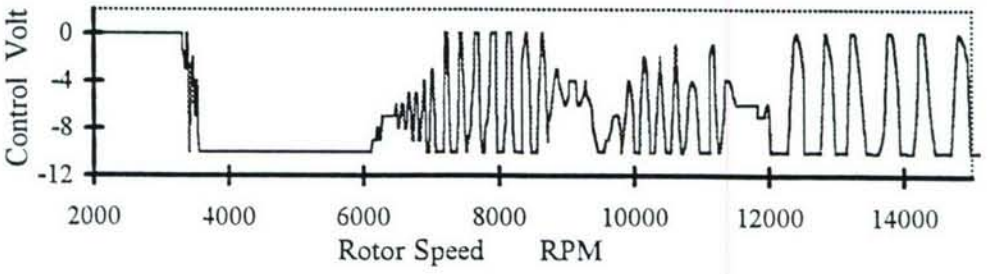

Figure 22 Actuating signal for PI-controller

was saturated and preferred the short mode before crossing the first critical speed then immediately afterward assumed the long damper mode. For the center mass, the behavior of the controller appears to be more steady in attaining a position between the two extreme modes.

3.4.4 CONCLUSION

The experimental results of the application of the elementary control algorithms to the HSFD-rotor test rig give mixed indications. First, the on-off controller based on feedback of speed was successful in attaining the required objectives, but as expected requires pre-knowledge of the critical speeds, and does not accommodate varying operating conditions. Second the P-controller and the PI controller, both based on feedback of eccentricity in the damper, and both exhibited significant chattering which can adversely affect the performance of the rotor. Eventhough the application of these controllers is simple, does not require pre-knowledge of the critical speeds, and can accommodate varying operating conditions, yet the chattering that occurred, was not eliminated by extensive tuning. This lead us to the conclusion that these control algorithms are not adequate for the control of the rotor-HSFD system. In fact, given the shortcomings of both the on-off controller and the P- or PI-controller, one would choose the on-off controller to avoid the chattering problem.

The results of this chapter help in focusing the attention to the advanced control algorithms and present the justification for the introduction of the advanced control algorithms.

CHAPTER 5

APPLICATION OF ADVANCED CONTROL ALGORITHMS

The results of chapter 4 provide enough justification to consider more complicated controllers to the HSFD-rotor test rig. The chattering problem encountered with the P- and PI-controllers preclude their use, and the drawback of inadaptability to varying operating conditions preclude the use of the on-off controller except in special cases.

In this chapter, three advanced controllers are applied to the test rig, namely: the gain scheduling controller, the nonlinear P controller and the MRAC adaptive controller. The theoretical results presented in Hathout's thesis guide the choice of the controllers, although experimental modifications were necessary. The LQR controller studied by Hathout was not investigated because it did not achieve good results with Hathout's theory, as well as requiring extensive design effort. The nonlinear P controller is introduced, although it was not studied by Hathout, yet its promising characteristics lured us into experimentally investigating its potential as a possible controller of the HSFD-rotor test rig.

As before with the elementary controllers, the control for the test rig was performed through the computer, and the various controllers were applied in the LabView software. Feedback was provided through the data acquisition/control card, and the GPIB card, while the control was applied through the control channels of the data acquisition/control card.

Also, as before, each of the test runs with the advanced control algorithms was preceded by coast-down tests of the test rig once in the short damper mode, and another time in the long damper mode. Thus measured data provided limiting conditions of the controller, and allowed visual evaluation of the controller performance. It should be noted that the deterioration in the test rig described in Chapter 3, as evidenced by the coast-down tests of Figures 7 and 8, can be seen clearly here in Chapter 5. Actually the characteristics of Figure 7 apply to all of Chapter 4 testing plus the nonlinear P controller presented here in Chapter 5. While the change

in test rig characteristics shown in Figure 8 is the case of the gain scheduling controller and the MRAC controller. This thus gives the reader an indication of the historical experimental development of the project: the elementary control algorithms were first implemented followed by the nonlinear P controller. The gain scheduling controller and the MRAC controller were later tested after the change of characteristics of the test rig. As discussed before, it was decided to continue testing although the test rig characteristics changed either to a bent shaft or reduced balance quality, because this demonstrates the adaptability of the HSFD in controlling varying operating conditions, and also because there is no direct relationship between each of the proposed control algorithms that can inhibit the development of the controllers.

3.5.1 GAIN-SCHEDULING PROPORTIONAL-INTEGRAL CONTROLLER

Applying linear control techniques to nonlinear systems can work efficiently at specific operating conditions. This is because a linear equivalent system to the original nonlinear system can be constructed at that particular operating condition. However, away from the linearization operating point, the linear controller with constant coefficients results in unacceptable performance and may lead to instability. Therefore, if for each linearized operating point of the nonlinear system a specific linear controller gives desired performance characteristics then one can achieve the required performance for all operating regions by applying different controller gains for different operating regions.

The basic principle of the gain scheduling technique is that a linear controller (such as the proportional-integral controller) is designed, tuned, and tested for a particular region of the operating range. Then, the gain scheduler is to apply a particular set of the controller gains for a particular region of operation. The results obtained from experimental implementation of the proportional-integral controller encouraged using it in the gain scheduling technique (Astrom and Wittenmark, 1989). The basic performance parameter is chosen to be the reference input value for particular speed ranges. It was decided to only schedule the integral gain for the proportional-integral controller since it is the most effective parameter in controlling the run-up through critical speeds as tested in Hathout's simulations. The scheduling of the reference

input and the integral gain is based on similar reasoning as in the work of Hathout. However, as Hathout used nondimensional quantities in his analysis, it was necessary to match the operating speed ranges to his scheduling. This was achieved by matching the first critical speed. Figures 23 and 24 show the speed regions and the corresponding scheduled variables: the reference input and the integral gain. The value of the scheduled reference input is chosen in accordance with the behavior of the rotor system in the short and long modes as discussed earlier.

Figures 25, 26, and 27 show the experimental vibration amplitude at the bearing and at the center mass and the corresponding actuating signal, respectively. Investigating the vibration at the bearing in correlation with scheduled reference input of Figure 23 indicates that the controller managed to regulate the vibration in different regions of the speed range. The response is smoother and does not have the chattering resulted from the proportional and the proportional-integral controllers. No significant changes appeared in the response of the center mass. The actuating signal shown in Figure 27 indicates saturation of the output channel in most of the speed range. This is confirmed by the sealing ring which assumed the short and long damper positions in those speed ranges.

3.5.2 NONLINEAR PROPORTIONAL CONTROLLER

The idea in proposing this controller is to gain the advantages of this controller because of its capabilities in high disturbance rejection and robustness to time delay. The original idea was proposed by Xu et al. (1995) to design a nonlinear proportional-derivative controller to control the contact transients in robot systems. In the design and development reported here, only a proportional controller is suggested, mainly to improve the performance of the proportional controller presented in Chapter 4. The derivative action was excluded from being used in the feedback because it responds to the rate of change of the error, and hence generates strong control actuating signal. Thus, it anticipates large errors and attempts corrective actions before they occur with high control signals. Moreover, the gain scheduling of the proportional-integral control resulted in enhanced performance compared to the proportional-integral controller alone. It is anticipated for the nonlinear proportional controller to have

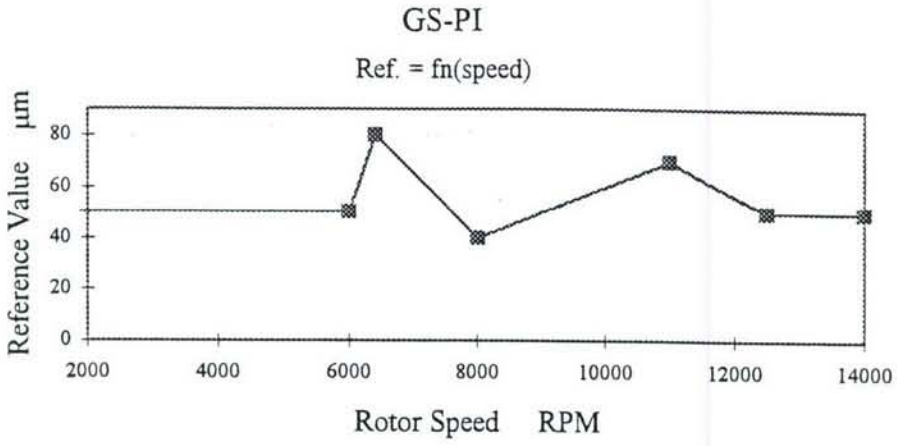

Figure 23 Reference value versus rotor speed

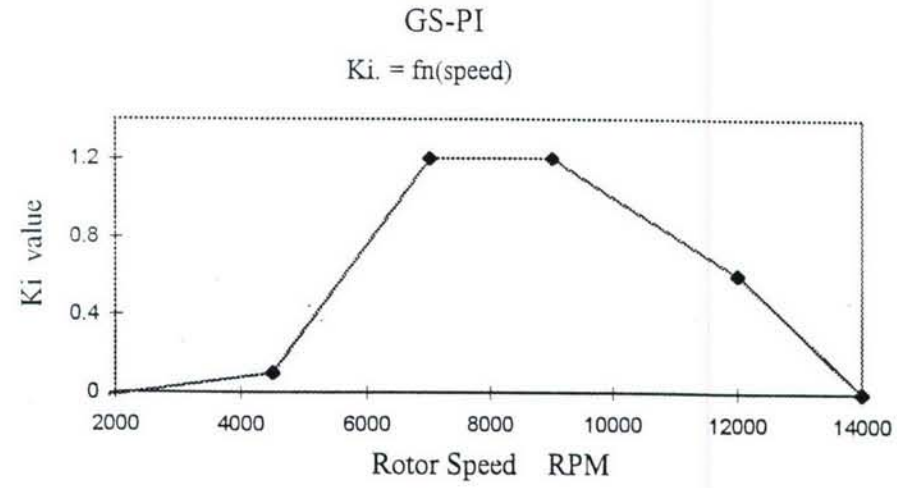

Figure 24 Ki value versus rotor speed

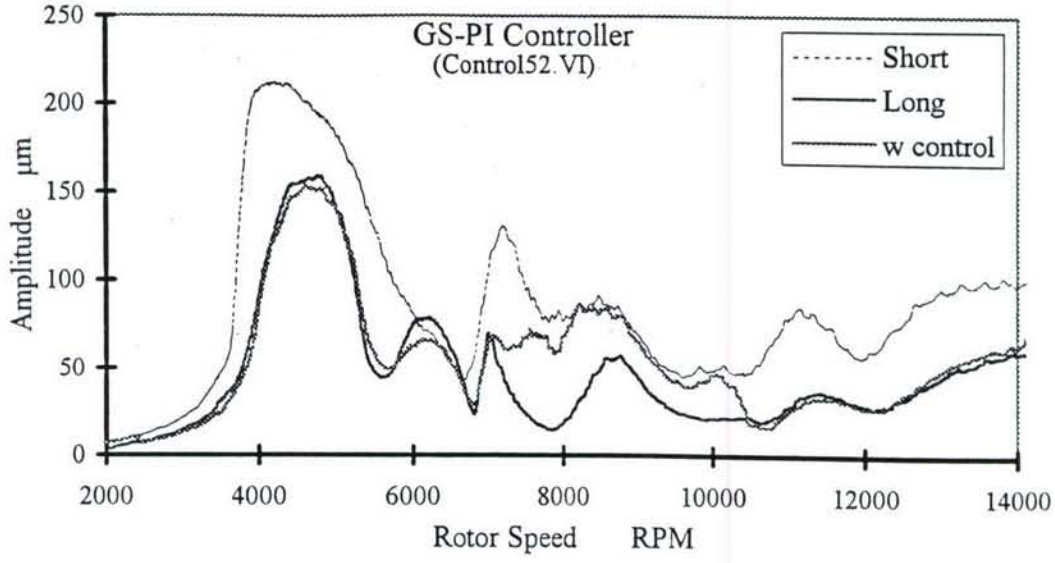

Figure 25 Experimental response of rotor at Damper 2 for GS- Pl Controller

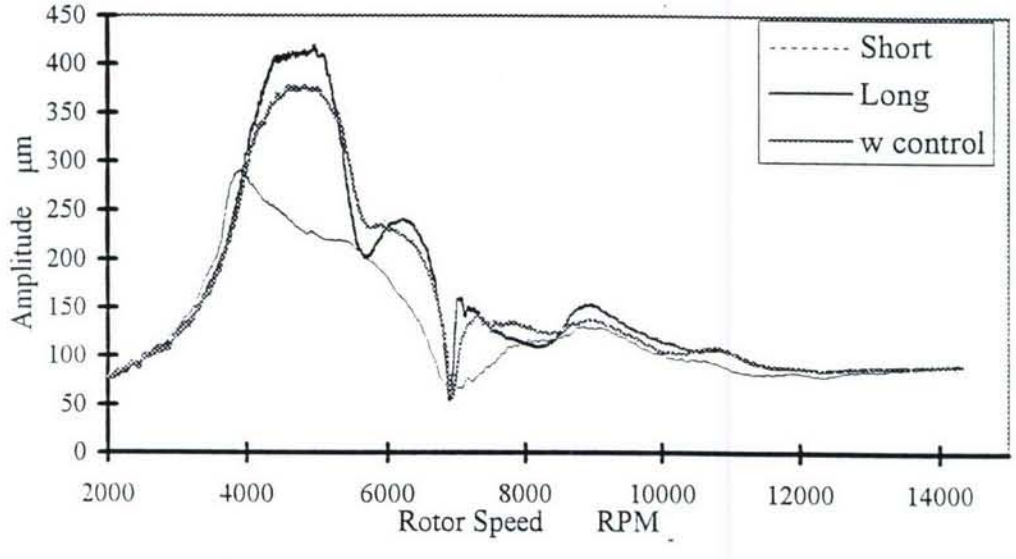

Figure 26 Experimental response of rotor at CM2 for GS-PI Controller

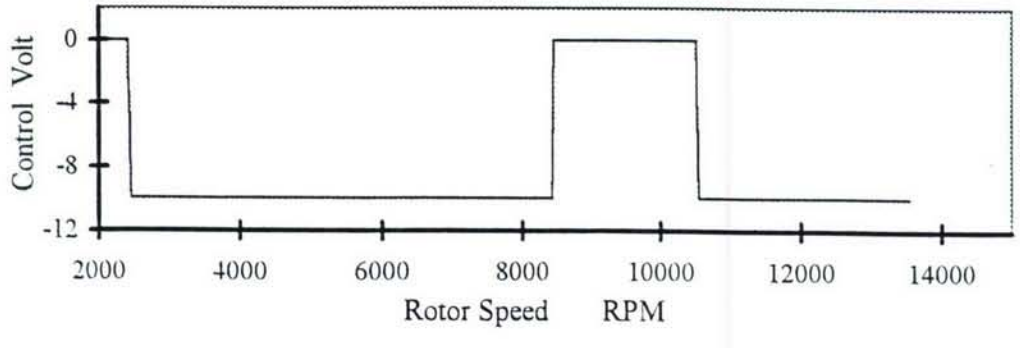

Figure 27 Actuating signal for GS-PI controller

similar influence. This is because it modifies the gain with the operating conditions. In summary, the control law is defined as:

$$u = K_p e$$

The proportional gain is defined based on the formula (Xu et al., 1993):

$$K_p = \frac{K_1}{1 + \beta \exp[\alpha \sin(\dot{e})e]} + K_0$$

In principle the controller changes the gain nonlinearly based on value, sign, and rate of the error. When the error of the system increases, the gains are increased and vice versa. Thus, not only the error is used to modify the gains but also its rate of change. The gains are chosen based on two criteria. First, implementation and tuning the proportional controller guided the selection of the initial values of the proportional gain. Second, the factors characterizing the modification of the nonlinear gain were adopted from the work of Xu et al., (1993). Thus, the experiment was conducted with the following constants $K_1 = 0.7$, $K_0 = 0.2$, $\beta = 1$, $\alpha = 100$.

Figures 28, 29 and 30 show the experimental vibration of the rotor bearing and of the center mass and the actuating signal, respectively. These responses indicate that the updating of the proportional gain according to the nonlinear design presented managed to extensively reduce the chattering resulted from the implementation of the constant gain proportional control. Moreover, the actuation signal remained within its saturation limits. Thus, the nonlinear proportional controller achieved the least control activity and never saturated the output channel. This is a significant improvement over the previous controllers.

3.5.3 MODEL REFERENCE ADAPTABLE CONTROLLER (MRAC)

Adaptive control has a unique feature that distinguishes it from constant linear feedback control. An adaptive controller is usually composed of a controller and an adaptation mechanism. The adaptation mechanism is continuously updating the controller gains or parameters such that a specific performance criterion is maintained or achieved. As a result, the controller is able to perform in a wide range of operating

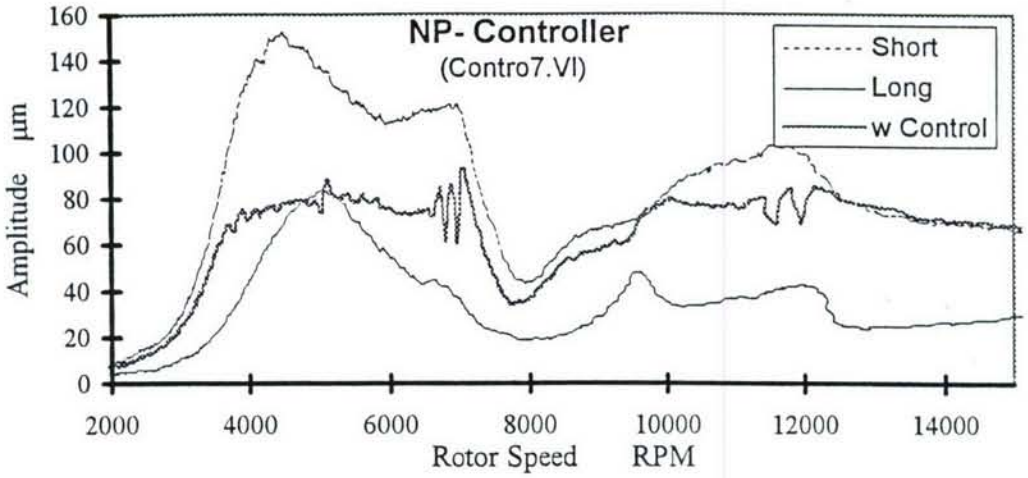

Figure 28 Experimental response of rotor at damper 2 for NP-Controller

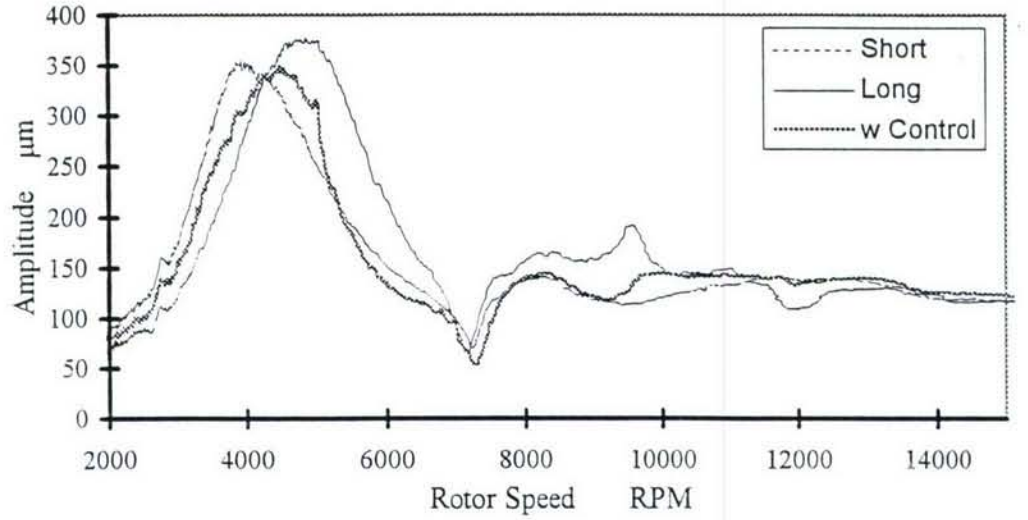

Figure 29 Experimental response of rotor at CM2 for NP-Controller

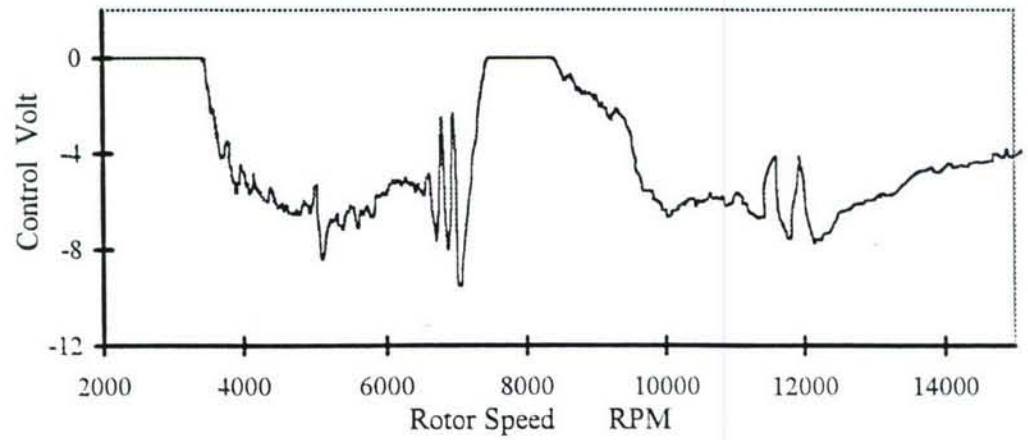

Figure 30 Actuating signal for NP-Controller

conditions for which a constant gain controller either is unstable or does not perform satisfactorily. Another feature of adaptive control encouraged its application for the rotor system is that it can perform quite exceptionally even when the dynamic model parameters of the plant to be controlled are partially known. This is particularly true for the rotor system, since extensive identification is required to construct the full accurate dynamic model.

The principal of operation of the Model Reference Adaptive Control (MRAC) is that a reference model having the same order and structure of the plant is designed to achieve the desired performance. The adaptation mechanism compares the difference between the output of the plant and the output of the reference model then computes and updates the controller parameters in such a way that in the steady state the regulation error approaches zero. In other words, the output of the controller plant can track the output of the reference model.

3.5.3.1 Design of the MRAC for the Rotor System

The complete MRAC strategy is based on the basic structure shown in Figure 31. The output is chosen to be the amplitude of vibration at the bearing center. The desired performance is expressed in terms of the reference model. The three fundamental components that constitute the MRAC are the linear controller, the reference model, and the adaptation mechanism. Once these three components are designed then the MRAC can be tested.

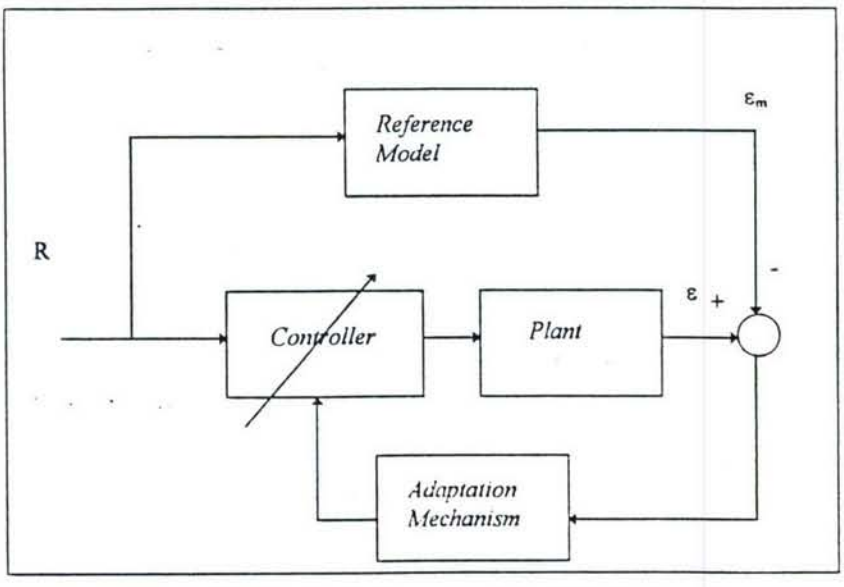

Figure 31 The Basic Structure of the MRAC algorithm

3.5.3.1.1 The Controller

The controller is a simple proportional controller that aims at positioning the sealing ring infinitely between the short and long damper mode positions such that the vibration amplitude is regulated to the reference input. The controller is given by

$$u = K_p e$$

where K_p is a varying proportional gain. This proportional gain is updated according to the adaptation mechanism. The reason a proportional controller is chosen to be the linear regulator are its simplicity and the remarkable enhancement the nonlinear proportional controller achieved over the constant proportional controller. According to the analysis of the proportional controller and the definition of the model reference adaptive controller, one expects that the MRAC is continuously changing the dynamics of the system by changing the proportional gain. Thus, the closed loop response is changing in such a way that the rotor vibration follows the reference model output.

3.5.3.1.2 The Reference model

The choice and design of the reference model reflect the desired performance and the structure of the system. The basic principle that the reference model must satisfy is that it must have the same structure of the plant to be controlled. For the rotor system, the order and structure of the model is dependent of the number of modes represented. In other words, if a single mode of vibration is chosen to model the rotor resonance in a particular speed range then it is sufficient to model the rotor as a second order system. In the speed range of interest, the rotor used has three dominant resonance frequencies and a reasonable model is of order 6. However, since the amplitude of vibration of the first mode is greater than those of the second and third modes, the first mode is of more interest for the control purpose. Thus, the plant during the range containing the first mode can be approximated by a second order system. In fact, according to Ewins (1984), one can construct a particular second order model for each mode and the response of the system is the summation of the responses of the second order systems of all modes. Hathout used the full nonlinear model of the rotor system as the reference model. This is not the usual case in choosing the reference model. It

is common to choose the reference model which reflects a desired performance. The reference models for the MRAC are usually linear reduced order models of the true plant. Based on the above discussion and reasoning, the reference model is chosen to be a second order linear system. It is given by:

$$\frac{\varepsilon_m}{R} = \frac{\omega_v^2}{s^2 + 2\zeta\omega_v s + \omega_v^2}$$

The damping ratio is chosen to be that of a critically damped system. The natural frequency is chosen to be equal to that of the first vibration mode of the rotor. Thus, the reference model is as fast as the first mode. In other words, the desired bandwidth is equal to the bandwidth of a system dominated by the first mode.

3.5.3.1.3 The Adaptation Mechanism

A simple adaptation mechanism is chosen to update the controller gain K_p. The adaptation mechanism is based on the gradient search approach that is usually called the MIT rule. The final form of adaptation mechanism is given by:

$$\frac{d\theta}{dt} = -\nu(\varepsilon - \varepsilon_m)\varepsilon_m$$

where θ is the adaptation parameter and ν is the adaptation gain.

3.5.3.2 Implementation and Experimental Results

The detailed MRAC is implemented in the time domain. Two main issues enabled accurate implementation of the MRAC. The first issue is related to reference model. The solution of the second order reference model to a step input is chosen to replace its function. This eases implementation and saves execution time. The output of the reference ε_m model for a step input R is given by:

$$\frac{1}{R}\left(1 - e^{-\omega_n t}\left(1 + \omega_n t\right)\right)$$

For the adaptation mechanism, integration of the adaptation gain is implemented using the Euler form for its simplicity. Three forms are chosen to update the controller gains

once a new value is computed by the adaptation mechanism. These three forms are meant to give conservative action by relying on previously tested proportional gain. The three forms are:

$$K_p = \theta \qquad \text{(a)}$$

$$K_p = K_{p0} + \theta \qquad \text{(b)}$$

$$K_p = K_{p0}\,\theta \qquad \text{(c)}$$

where K_{p0} is a fixed proportional gain. Hathout used the form (a). The other two forms were proposed so that the effective proportional gain is not entirely dependent on the adaptation parameter θ. This is a usual approach to avoid vast changes by the adaptation mechanism which might cause instability. In the form (b), however, the effective proportional gain is the summation of a test constant proportional controller and the adaptation gain θ. Thus in the dangerous and/or unexpected regions of operation, the controller can safely be switched to the nonadaptive mode. As a result, a previously tested valid performance can be achieved. Based on experimentation with the proportional control, a value of 0.5 gave the most satisfacting performance. The adaptation gain is tuned experimentally to a value of 0.0008. A satisfactory performance is usually obtained for the summation type (b) over the other multiplicative types (a) and (c). This is due to the fact that the summation type is less aggressive than the multiplicative types in changing the proportional gain.

The experimental results of implementing the MRAC are shown in Figure 32. It is clear from Figure 32 that the adaptive controller succeeded in regulating the vibration amplitude at the bearing system to the reference value. Passing over the resonance, the adaptive controller preferred the short mode which results in a smaller error in this range. The response of the center mass is shown in Figure 33. As the vibration of the center mass is not a directly controlled variable, its response is complementing the regulation of the bearing vibration. During the whole range the center mass amplitude remained between the short and long modes with less chattering than that of the bearing vibration. Investigation of the actuation signal shown in Figure 34 clearly indicates that the controller saturated the output channel in a wide range.

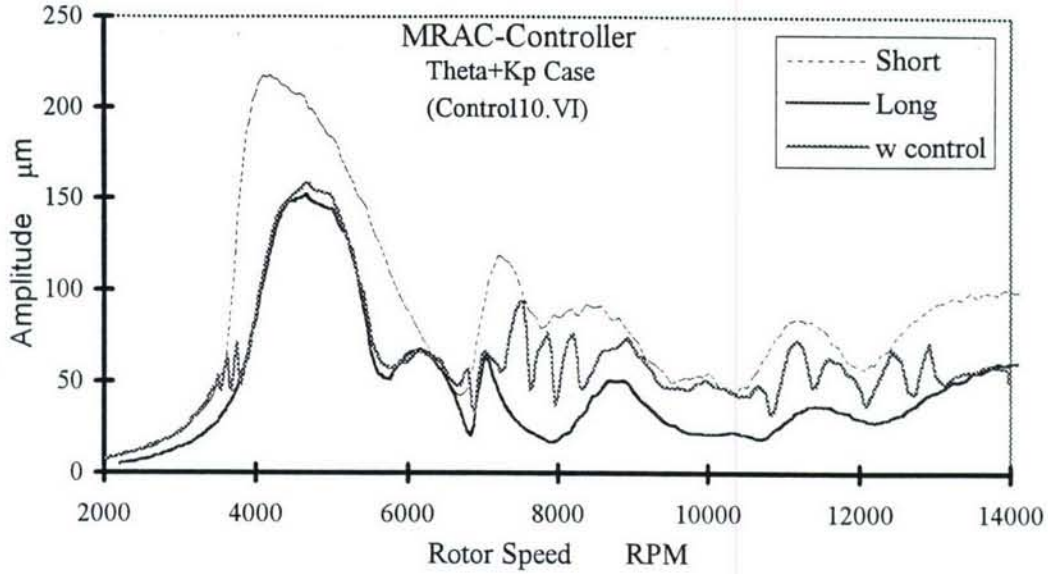

Figure 32 Experimental response of rotor at Damper 2 for MRAC-Controller (Theta + Kp)

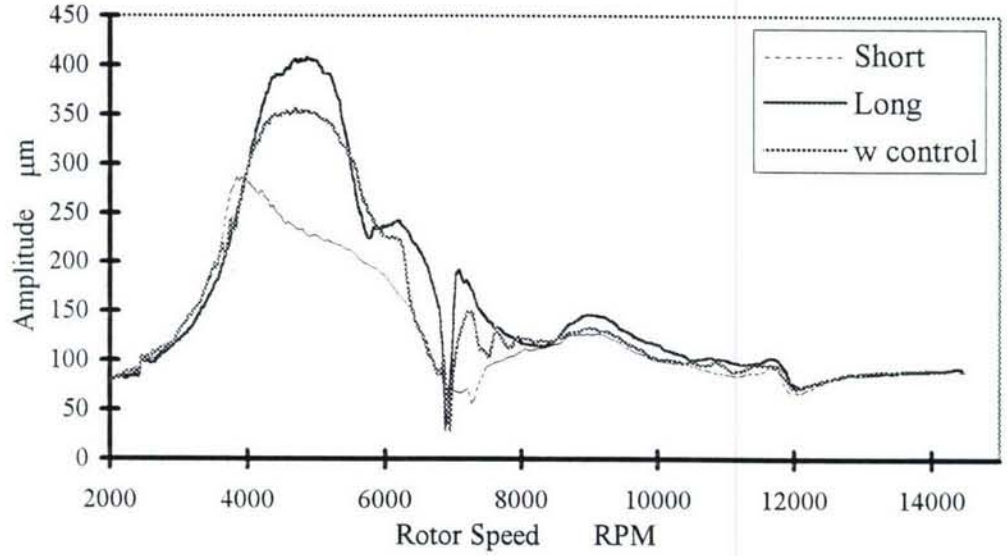

Figure 33 Experimental response of rotor at CM2 for MRAC-Controller (Theta + Kp)

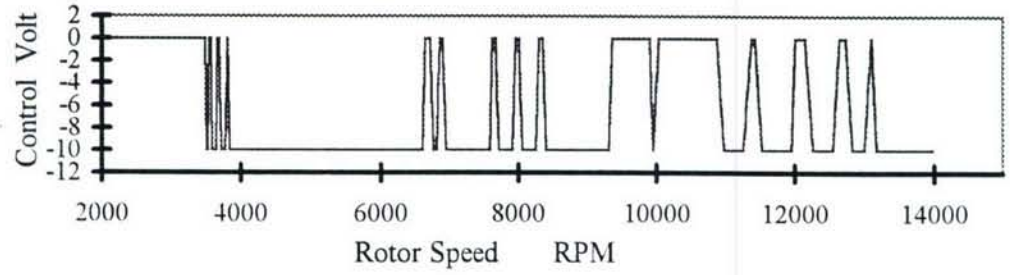

Figure 34 Actuating signal for MRAC-Controller Theta+Kp case

The experimental results of implementing the MRAC in the (a) structure are shown in Figures 35, 36 and 37. Those for (c) structure are shown in Figures 38, 39 and 40, and show similar behavior to those of the additive rule. Experimentally, there is no great difference between the three forms of updating the controller gains.

3.5.4 CONCLUSION

All of the advanced control algorithms provided significantly better performance than the elementary control algorithms of Chapter 4. No chattering was observed using any of the three proposed advanced controllers.

The gain-scheduling controller requires a significant design effort in selecting the gain schedules, and resulted in a controller that resorted to extreme conditions often and saturated the control voltage. This controller resembled the on-off controller, possibly because both have speed dependent schedules, but the gain-scheduling controller has the advantage of its adaptability to varying operating conditions.

The nonlinear proportional controller was a surprise controller by all means. It provided the best qualitative response of avoiding long dampers at operating speeds, and avoiding short dampers at critical speeds. In addition, the controller never saturated which means it was always in control with additional control effort available, if needed. The only disadvantage that we can see is that it does not have a well structured design procedure, and is actually designed in an ad-hoc manner. However, it did not cause any problems in the design procedure and was relatively straightforward in its implementation. We believe that this is the best controller studied.

The MRAC controller was an excellent controller and provided good response, although it saturated sometimes and showed some indecisiveness at instances, changing frequently between the two extreme control signals. The theoretical controller developed by Hathout was a better controller because it used a nonlinear

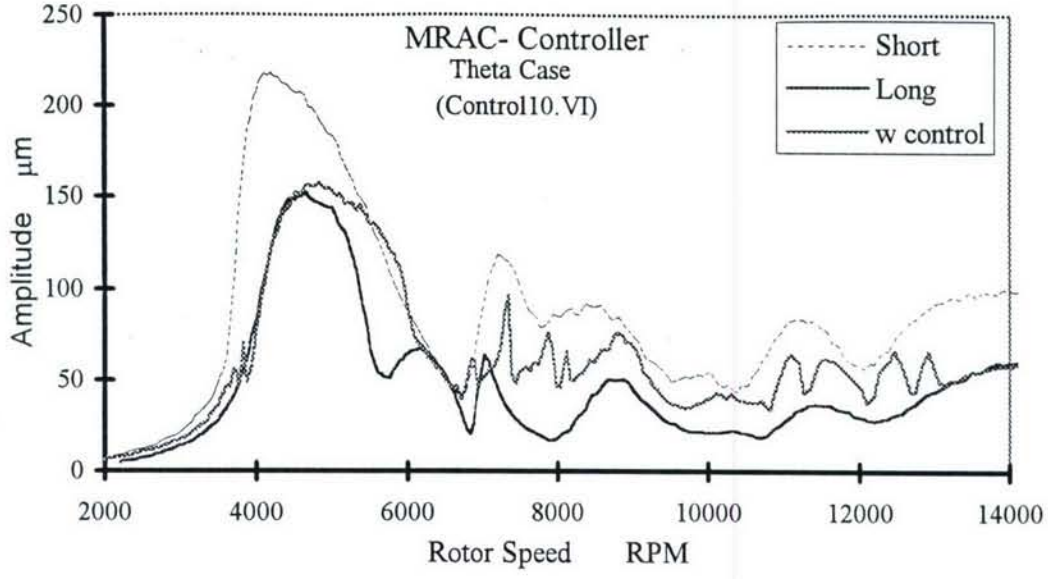

Figure 35 Experimental response of rotor at Damper 2 for MRAC-Controller Theta case

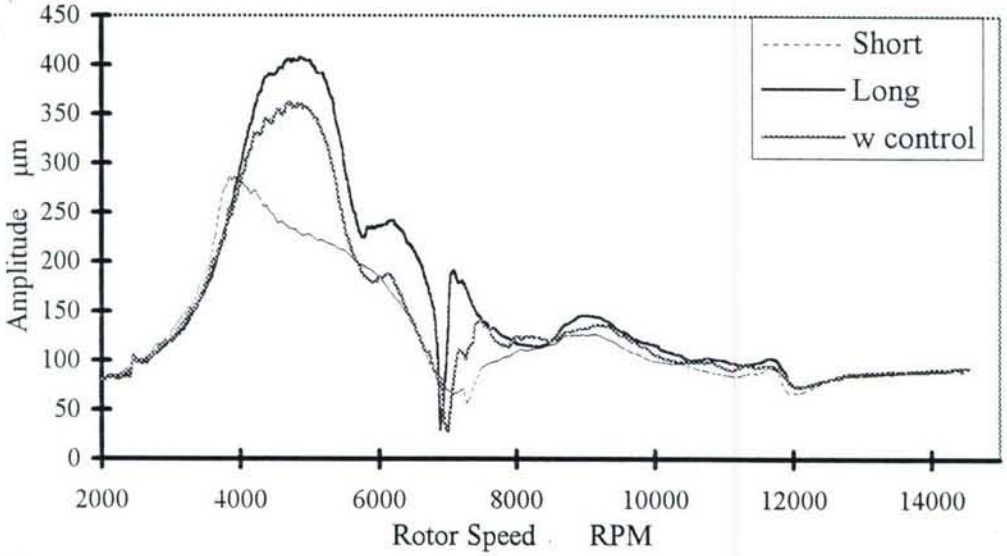

Figure 36 Experimental response of rotor at CM2 for MRAC-Controller Theta case

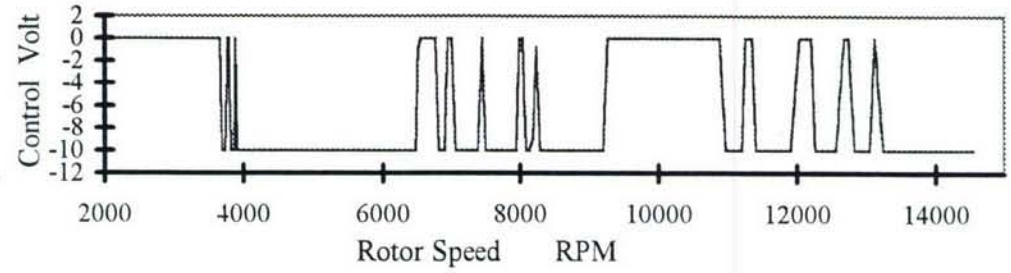

Figure 37 Actuating signal for MRAC-Controller Theta case

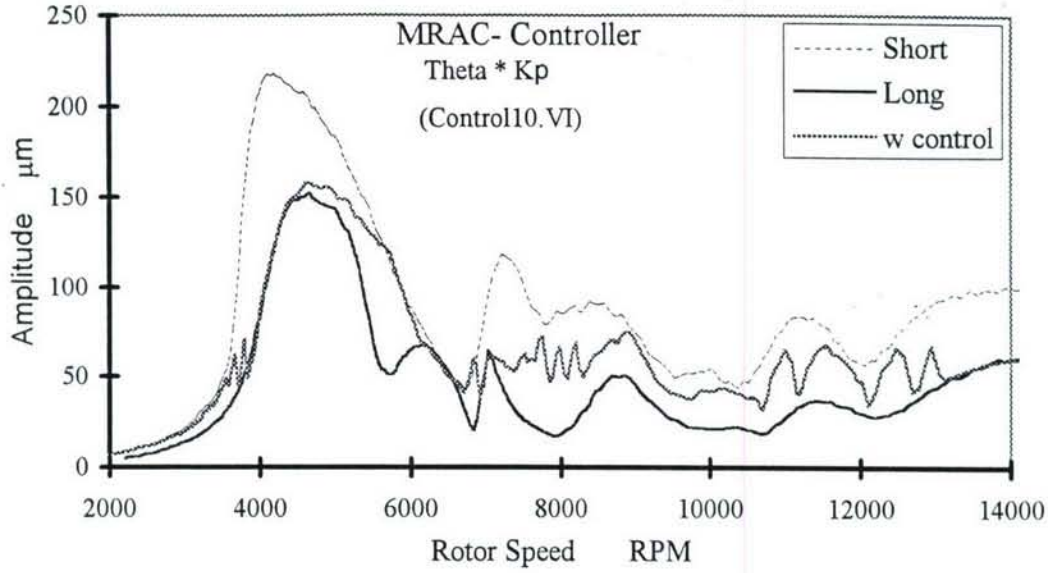

Figure 38 Experimental response of rotor at Damper 2 for MRAC-Controller (Theta * Kp)

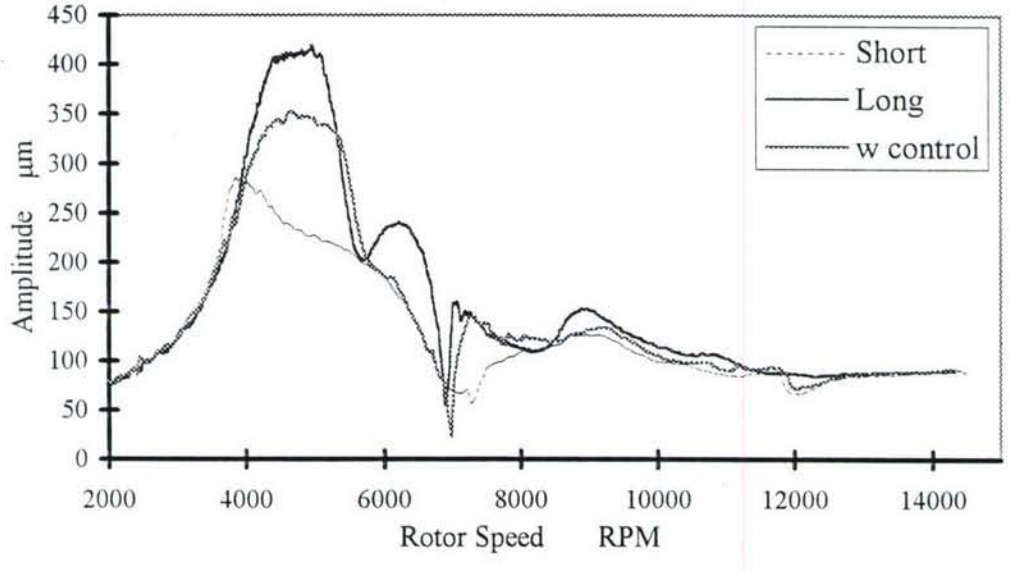

Figure 39 Experimental response of rotor at CM2 for MRAC-Controller (Theta * Kp)

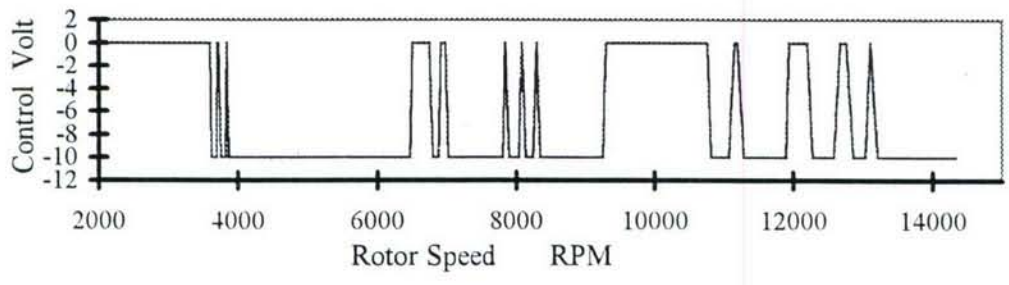

Figure 40 Actuating signal for MRAC-Controller Theta * Kp case

reference model. However, during experimentation, we found that this is an unnecessary complication that presented difficulties in implementation, and we used a reduced order linear reference model. This resulted in good response, but we presume that a nonlinear reference model will provide better response.

CHAPTER 6

COMPARISON OF CONTROL ALGORITHMS

A qualitative and quantitative comparison is warranted for all control algorithms developed theoretically and experimentally in this project. A recommendation of the most appropriate control algorithm is sought.

3.6.1 QUALITATIVE COMPARISON

Qualitatively all of the advanced control algorithms behaved well, although the test rig changed its behavior due to the bent shaft. The nonlinear proportional controller was exceptional in that it never saturated which translates to available control effort to be used when needed. This also resulted in the rotor neither behaving as a short damper or a long damper for considerable time, but rather the controller tried to obey the reference value as much as possible. It was successful in avoiding the short damper mode at critical speeds, and avoiding the long damper mode away for critical speeds.

The gain scheduling controller also behaved extremely well although it was saturated most of the time and preferred the large damping capacity provided by the long damper mode. It is believed that more design effort could yield whatever required behavior because of the scheduling capabilities. Theoretically, the gain schedule controller behaved qualitatively as in the experiments.

The MRAC controller also behaved relatively well, although there was a bit of indecisiveness at higher speeds, changing frequently between the two extreme control signals. This could have happened because the reference model is only based on a single degree of freedom system and does not contain any information on the higher modes. However, the MRAC controller was successful in avoiding either the long damper mode or the short damper modes for a long time except for crossing the first critical speed. Theoretically, the MRAC controller behaved much better than in experimentation, but there was the added complication of a nonlinear reference model. We believe that a reference model with at least as many degrees of freedom as the

rotor exhibits critical speeds is necessary to obtain perfect performance from the MRAC controller.

Both the P and PI controllers exhibited significant chattering both theoretically and experimentally. The Nonlinear P controller is an extension over the P controller and performs much better but has the disadvantage of ad hoc design. The gain scheduling controller is an extension over the PI controller and also performs much better but also requires a significant design effort in selecting the gain schedule.

Finally, the on-off controller behaved very much as expected. This controller has the advantage in that it precisely behaves as the designer wishes, and performs experimentally exactly as theoretically predicted. The only disadvantage that is worth mentioning is the inability of the on-off controller to accommodate varying operating conditions.

3.6.2 QUANTITATIVE COMPARISON BASED ON INDICES

In this section a quantitative comparison among the five feedback controllers is presented. It is necessary and deserves effort to compare the performance of the developed and tested control algorithms. The basic criterion for evaluating the performance of a controller can be its regulation error and associated control effort. For the rotor system, the regulating error indicates how close the controller succeeded in regulating the vibration amplitude to the reference desired level. Thus, the measure of the regulation performance is chosen to be the average integral square root of the error norm:

$$I_e = \frac{\sqrt{\sum_{i=1}^{N} |e|^2}}{N}$$

This normalized index can be used to compare the different control algorithms. Thus, controllers can be differentiated based on one single number.

The measure of the control effort reflects the energy the controller injected into the system. The index is also chosen to be the average integral square root of the control signal:

$$I_c = \frac{\sqrt{\sum_{i=1}^{N} |v|^2}}{N}$$

Table 3 lists the error and control indices for the five feedback control algorithms developed and tested in this research work. From this table one can conclude that the proportional controller achieved the minimum error index followed by the proportional integral controller. While the nonlinear proportional controller has the minimum control effort followed by the MRAC controller. For instance, if one chose a controller based on the error index, one would choose one of the elementary control algorithms which would lead to the undesirable chattering, while if one chose the controller based on the minimum control effort one would definitely choose the nonlinear proportional controller.

Table 3 Indices of five control algorithms

The Controller	I_e	I_c	Comments
Proportional Controller	0.95	0.48	Chattering
Proportional-Integral Controller	0.96	0.36	Chattering
Gain Scheduling Controller	1.29	0.29	Saturation
Nonlinear Proportional Controller	1.05	0.23	
MRAC Controller	1.11	0.26	

Correlating the qualitative and the quantitative comparisons, one finds that both lead to nearly the same conclusions in ranking the controllers. The Nonlinear-Proportional controller passes with high colors both the qualitative and quantitative analyses. A comprehensive comparison of the control algorithms is illustrated in Table 4 and represents the summary of the abilities of each controller.

Table 4 Comparison Between Control Algorithms

Controller	On-Off	P	PI	Nonlinear P	GS-PI	MRAC	LQR
Qualitative	- Follows design objectives - Effective	- Chattering - Saturation	- Chattering - Saturation	- Excellent behavior - Available control effort	- Well behaved - Problem with saturation	- Well behaved - Reference model determines behavior	- Well behaved - Problem with estimator
Error Index	—	Good	Good	Good	Fair	Good	—
Control Effort Index	—	High	High	Good	Good	Good	—
Robustness	- Unable to accommodate any changes - Preselected	Sensitive to gain changes	Sensitive to gain changes	Good	Good	Good, but sensitive to the selection of reference model	Sensitive to design changes and operating conditions
Disturbance Rejection	Unable to reject disturbance	Possible but chattering problem	Possible but chattering problem	Excellent	Excellent	Excellent	Sensitive
Varying Operating Conditions	Unable to accommodate	Possible but chattering problem	Possible but chattering problem	Excellent	- Good - Needs redesign of schedule if changes are large	Excellent	Sensitive to changes
Sudden Unbalance	Unable to accommodate	—	Good	—	Good	Good	Fair
Design Effort	Minimal	Extensive tuning required	Extensive tuning required	Ad Hoc	Extensive design effort in selecting gain schedule	Effort in selection of reference model but simple design	Extensive effort in selecting gains and tuning

CHAPTER 7
CONCLUSION

The conclusion of the effort expended and the results achieved from the project "Control of Rotor Vibrations Using Hybrid Squeeze Film Dampers", grant no. F49620-92-J-0512, are presented herein. The objective of the work done was to investigate the active control of rotating machinery vibration using the newly developed hybrid squeeze film dampers (HSFDs). In particular, the work done included the automation of the hybrid damper, the development of the design of the hybrid damper, the elaborate modeling of the hybrid damper, the development of the control algorithms for the hybrid damper, and finally the experimental verification of the performance and control of the HSFD.

The work in this project was successful in attaining all of these objectives. The hybrid damper control circuit was automated by an electronically controlled proportional pressure control valve with the associated hydraulic circuit. Computer control of the HSFD was achieved. The hybrid damper was completely redesigned to allow for its automation, including instrumenting the damper, adding retainer springs, adding feedback springs and redesigning for compactness. A complete mathematical model was developed for the damper and its control elements. The λ-model was used for finite damper modeling. Simulation of the behavior of the open-loop control system was performed.

A complete test rig was designed with multi-modes. The test rig was well-instrumented and computer-controlled. The test rig consisted of the rotor supported by two HSFDs and driven by a variable speed electric motor.

Simulation of the behavior of the open-loop and closed-loop control system of the test rig was performed for the multi-mode rotor. Several control algorithms were developed and applied to the rotor system. The on-off basic control algorithm with feedback on speed was developed to act as long damper at critical speeds and short damper away from critical speeds. It was shown that this control algorithm is quite

effective but requires pre-knowledge of the behavior of the rotor system and is not able to accommodate variable operating conditions. A PI control algorithm was developed and also shown to be effective. The enhancement of the PI-controller by gain scheduling provides one of the best control alternatives, both in controlling resonant conditions and sudden unbalance. The LQR controller was not as effective as the PI-controller because of its sensitivity. The developed adaptive controller, with a unique nonlinear reference model, was also extremely effective both for controlling resonant conditions and sudden unbalance.

Experimentally, the on-off controller, the PI-controller (with and without gain scheduling), and the model reference adaptive controller were all applied. In addition a nonlinear-proportional controller was also developed and applied, and was shown to be the best overall controller of the HSFD. The experimental results, which involved elaborate set-up and verification and identification, confirmed the results of the theory and simulation and illustrated the power and utility of the developed algorithms, and of the HSFD itself as a robust controlling element of rotor vibrations. A comparison of the theoretical and experimental results of each of the developed controllers allows the designer to select the most appropriate algorithm for the desired application.

It is the opinion of the research team that this extensive research project confirmed the capabilities of the Hybrid Squeeze Film Damper, as an efficient and powerful controlling element for high speed rotors, particularly of aircraft engines and rocket turbopumps. Specifically the results of this research project establish that the HSFD:

1) improves the vibration isolation capability of the rotor support,
2) reduces the amplitude of vibration of the rotor at all speeds,
3) enhances the stability of the rotating machine,
4) allows the rotor and damper to operate at high loads, and
5) results in a rotating machine that is capable of operating under varying and adverse conditions.

These results can be inferred from the various simulations and experiments conducted during this project that illustrate the adaptability of the HSFD.

It is also the opinion of the research team that the HSFD is now ready for engine testing. The control algorithms are sufficiently developed, the laboratory experimentation and verification were extensive and illustrate the strengths and adaptability of HSFDs. In addition, the concept of HSFDs relies on a reliable and robust device that has been used extensively in aircraft engines for over than thirty years as a passive vibration controller. It is thus the belief of the research team that the results of this work should lead to full-scale engine testing for the active control of rotor vibrations using HSFDs.

REFERENCES

Astrom, K.J., and Wittenmark, B., 1989, "Adaptive Control", Addison-Wesley Publishing Co., Massachusetts.

Burrows, C.R., Sahinkaya, M.N., and Turkay, O.S., 1983, "An Adaptive Squeeze-Film Bearing", ASME Paper No. 83-Lub-23.

El-Shafei, A., El-Hakim, M.M., and Hathout, J.P., "Control of Rotor Vibrations Using Hybrid Squeeze Film Dampers", Report No. MDP-EOARD-1/93, Cairo University.

El-Shafei, A., El-Hakim, M.M., Hathout, J.P., and Youssef, R.Y., "Development of Hybrid Squeeze Film Damper for Active Control of Rotor Vibrations", Report No. MDP-EOARD-1/94, Cairo University.

Ewins, D.J., 1984, "Modal Testing: Theory and Practice", Research Studies Press, Somerset, England.

Hathout, J.P., and El-Shafei, A., 1997, "PI Control of HSFDs for Active Control of Rotor-Bearing Systems", ASME Journal of Engineering for Gas Turbine and Power, Vol. 119, No. 3, pp. 658-667.

Hathout, J.P., and El-Shafei, A., 1996, "Adaptive Control of Rotor-Bearing Systems Using Hybrid Squeeze Film Dampers", Proceedings of Sixth Int. Conf. On Vibration in Rotating Machinery, Oxford, England, I. Mech. E., pp. 671-690.

Murray, S., and Richard, L.S., 1984, "IBM Personal Computer from the Inside Out", Addison-Wesley Publishing Company, pp. 389-395.

National Instrument LabVIEW software version 3.0.1, August, 1993.

Ogata, K., 1990, "Modern Control Engineering", 2nd Edition, Prentice Hall Inc., New York.

Xu, Y., Hollerbach, J.M., and Ma, D., 1995, "A Nonlinear PD Controller for Force and Contact Transient Control", IEEE Journal of Control Systems, pp. 15-21, Feb.

Xu, Y., Hollerbach, J.M., and Ma, D., 1993, "Nonlinear Proportional and Derivative Control for High Disturbance Rejection and High Gain Force Control", Proc. IEEE Int. Conf. Robotics and Automation, San Diego, pp. 924-930, May.